

# Monday Morning, October 31, 2011

## Electron Transport in Low Dimensional Materials Focus Topic

Room: 209 - Session ET+EM+SS-MoM

### Quantum Transport: From 0- to 2-Dimensions

Moderator: A.-P. Li, Oak Ridge National Laboratory, K. Varga, Vanderbilt University

8:20am **ET+EM+SS-MoM1 Charge and Spin Transports at Surfaces of Strong Spin-Orbit-Coupling Materials.** *S. Hasegawa, T. Hirahara,* University of Tokyo, Japan **INVITED**

Transports of charge as well as spin at crystal surfaces are now intensively studied by various kinds of experiments. Surface electronic states are generally decoupled from the bulk states and therefore intrinsically low-dimensional. Furthermore, space-inversion symmetry is broken down at crystal surfaces; one side of the surface is empty vacuum while other side is full of electrons in the crystal. These effects provide rich physics of transport, especially on surfaces of strong spin-orbit-coupling (SOC) materials. The surface-state bands are known to be spin-split of such strong SOC crystals such as Bi and Bi alloys, which is called by Rashba effect [1-4]. Similar effect is observed on a special kind of materials called topological insulators such as BiSb, BiSe, and BiTe alloys. Some of them have spin-split Dirac-cone type surface-state bands. This implies that spin-polarized current will flow at the surfaces of such materials.

In my presentation, by using samples of pure Bi [1-4], BiSb [5], BiSe [6,7], and BiTe, I will show that the surface-state bands are really spin-split and the Dirac-cone conductivity is directly measured by microscopic four-point probe method. An on-going project to detect the spin-polarization of surface current by using magnetic tips in a four-tip STM will be also introduced.

[1] T. Hirahara, et al., Phys. Rev. Lett. 97, 146803 (2006).

[2] T. Hirahara, et al., Phys. Rev. B 76,153305 (2007).

[3] T. Hirahara, et al., Appl. Phys. Lett. 91, 202106 (2007).

[4] T. Hirahara, et al., New J. Phys. 10, 083038 (2008).

[5] T. Hirahara, et al., Phys. Rev. B81, 165422 (2010).

[6] Y. Sakamoto, et al., Phys. Rev. B81, 165432 (2010).

[7] T. Hirahara, et al., Phys. Rev. B82, 155309 (2010).

9:00am **ET+EM+SS-MoM3 Electron Transport in Ferroelectric Domains and Walls.** *A. Baddorf,* Oak Ridge National Laboratory **INVITED**

Ferroelectric tunneling, where electron transport is controlled by the polarization state, has recently been realized in a number of experiments. Polarization-controlled transport effects have been detected in tunnel junctions, thin films, single crystals and at domain walls. Yet, little analysis of data has undertaken to determine the transport mechanisms and their interaction with ferroelectric fields and domain boundaries involved in switching. We present seminal experimental observations of transport in thin films of  $\text{Pb}(\text{Zr}_{0.2}\text{Ti}_{0.8})\text{O}_3$  (PZT) and  $\text{BiFeO}_3$  (BFO). Earlier we have shown that both materials exhibit pronounced polarization-controlled electroresistance [1]. Temperature and voltage dependence of currents are not well fit by any one standard model. Instead a transition between surface and bulk limiting effects is observed. Upon close inspection, I-V curves exhibit a reproducible region of negative differential conductance associated with ferroelectric switching. Although this anomaly may originate from extrinsic processes, e.g. due to oxygen vacancies or charge injection, we have carried out a series of control experiments on PZT films that unequivocally connect variation of conductance with the size of the polarization domain in the plane of the surface. The I-V anomaly therefore originates from significant conductivity of the domain wall and a relatively slow expansion of the domain following polarization switching. However, our results do not imply simply that transport is through domain walls, but further that nanoscale domains formed by switching have fundamentally different conduction behavior [2]. We suggest that domains formed by tip-applied bias have curved walls and are consequently charged, modifying adjacent material much as charge accumulation modifies a semiconductor. Engineering the ferroelectric domain size produces a tunable conductance reminiscent of analogue memristors, providing a quasi-continuous spectrum of non-volatile resistive states, even though the PZT polarization itself is bistable. Ferroic memristive behavior, which based on our measurements is likely to be universal to ferroic semiconductors, is a striking departure from the conventional picture of discrete electron transport states in ferroelectrics.

Research was conducted at the Center for Nanophase Materials Sciences and sponsored by the Division of Scientific User Facilities, U.S. Department of Energy.

[1] P. Maksymovych et al., Science 324 (1421) 2009.

[2] P. Maksymovych et al., submitted.

9:40am **ET+EM+SS-MoM5 Electronic Instabilities, Fluctuations, and Transport in Epitaxial Nanowires.** *H.H. Weitering,* University of Tennessee and Oak Ridge National Laboratory **INVITED**

Quantum transport is at the heart of nanoscience and marries a fundamental law of nature — quantum mechanics — with applied electrical engineering and emerging materials technologies. Ultimately, nanoscale electronic devices will contain networks of wires whose cross sections will be so small as to represent one-dimensional conductors with novel transport properties. We have fabricated exceptionally long and uniform  $\text{YSi}_2$  nanowires via self-assembly of yttrium atoms on Si(001). The wire widths are quantized in odd multiples of the Si substrate lattice constant. The thinnest wires represent one of the closest realizations of the isolated Peierls chain, exhibiting van Hove type singularities in the one-dimensional density of states and charge order fluctuations below 150 K. Conduction through individual nanowires follows an inverse Arrhenius behavior, indicative of thermally-assisted tunneling of small polarons between defect centers. Quantitative analysis of individual wire resistances, probe resistances, and negative differential resistances of nanowire networks indicates significant electronic interwire coupling below 150 K. The long-range coupling mechanism involves the dielectric polarization of the substrate, which induces current blockades in neighboring conduction channels.

This work is sponsored by the NIH/NHGRI and was partially conducted at the Center for Nanophase Materials Sciences, which is sponsored at Oak Ridge National Laboratory by the Office of Basic Energy Sciences, U.S. Department of Energy

10:40am **ET+EM+SS-MoM8 Grain Boundary Resistivity in Copper Nanowires.** *T.H. Kim,* POSTECH, South Korea **INVITED**

The reliable choice of the interconnect materials in current integrated circuits is copper because of its higher electrical conductivity and improved stability against electromigration among all possible candidates. However, as the width of interconnects is approaching a mean free path of the electrons, the resistivity of copper interconnects is known to increase dramatically. Typically, this increase in the resistivity of the narrow interconnect is attributed to enhanced sequential scattering of electrons from defect planes such as either grain boundaries (GB) or other surfaces/interfaces. But, it is very challenging to distinguish which scattering factor is dominant over others in such a small scale.

To answer such a fundamental question, theorists developed semi-empirical methods and the relative contribution of various electron scattering mechanisms has been understood largely by relying on the semi-empirical methods based on the theories of Fuchs-Sondheimer and Mayadas-Shatzkes. The direct measurements of the resistance of individual GBs have been surprisingly lacking mainly due to technical difficulty to access single GBs in a nanowire that could not be realized by conventional fabrication methods using a fixed electrical contacts. Recently, Y. Kitaoka *et al.* have observed a resistance change along a damascene Cu interconnect wire with four-probe scanning microscope. They successfully separated the GB scattering effect from other scattering sources; however, the direct correlation between the GB structure and the specific GB resistivity remained unclear.

Here we present the direct measurement of individual GB resistances and the critical role of GB structure in the increased resistivity in copper nanowires with a four-probe scanning tunneling microscope. The resistances of high symmetry coincidence GBs are then calculated using a first-principle method, which confirms that the coincidence GBs have orders of magnitude smaller resistance than those measured at the high-angle random GBs. As well, to explain high resistivity of random GBs, we used free-electron-with-random-point-scatterer (FERPS) model. In the FERPS model, we derived that the specific GB resistivity of random GB is independent of the specific structures of random GB such as orientation and is determined entirely by the Fermi wavelength of the bulk.

This research was conducted at the Center for Nanophase Materials Sciences, which is sponsored at Oak Ridge National Laboratory by the Office of Basic Energy Sciences, U.S. Department of Energy.

11:20am **ET+EM+SS-MoM10 Tunable Coulomb Blockade and Giant Coulomb Blockade Magnetoresistance in a Double Quantum Dot System**, *X.-G. Zhang*, Oak Ridge National Laboratory, *T. Xiang*, Chinese Academy of Sciences

We propose a Hubbard model to describe the tunneling effect of electrons in a double quantum dot system connected in the parallel circuit configuration to electrodes. The change in the interdot coupling is shown to dramatically influence the Coulomb blockade properties. For magnetic double dots, the interdot coupling can be tuned by the external magnetic field, leading to a giant Coulomb blockade magnetoresistance. Possible detection of this effect in organic systems is discussed.

This research was conducted at the Center for Nanophase Materials Sciences, which is sponsored at Oak Ridge National Laboratory by the Office of Basic Energy Sciences, U.S. Department of Energy.

11:40am **ET+EM+SS-MoM11 Quantum Transport in Crossbar Devices**, *B. Cook*, *P. Dignard*, *K. Varga*, Vanderbilt University

Electronic devices with crossbar geometries have recently been fabricated with nanoscale features (Zhong, et al, Science Vol. 302). Consisting of a two dimensional grid, devices have been formed with a variety of components including carbon nanotubes and semiconductor nanowires. These devices are assumed to operate classically, but as the dimensions of the device shrink consideration of quantum effects becomes necessary. We consider a single junction between two wires up to a four by four grid of wires. Through a series of calculations with atomistic first-principles, tight-binding and analytic models of multi-terminal devices we demonstrate the presence of unique behavior, such as interference effects, not present in classical models. It is expected that exploitation of these effects will be useful in the creation of circuit components.

## In Situ Spectroscopy and Microscopy Focus Topic

Room: 106 - Session IS+AS+SS-MoM

## In Situ Studies of Catalysis and Gas-Solid Reactions

Moderator: G. Rijnders, University of Twente, the Netherlands

8:20am **IS+AS+SS-MoM1 In Situ X-ray Studies of Model and Real Catalysts: Bridging the Complexity Gap**, *A.I. Frenkel*, Yeshiva University **INVITED**

In the last decade, there was a surge in advanced characterization methods to study catalytic materials at work. Most notable innovations in synchrotron-based techniques include the coupling of in situ/operando x-ray absorption and scattering methods to vibrational spectroscopies, empowered by improved time and energy resolutions. For example, in situ XAFS-XRD combination enables complementary studies of short and long range order in the same system, a great tool when multiple spatial dimensions evolve in a certain process, such as: modifications of both the catalyst and the support during catalytic reaction, the nucleation and growth of a nano-catalyst, oxidation/reduction of a bulk oxide. Combining in situ XAS or XRD with infrared or Raman spectroscopy is critical for understanding how the structural and electronic properties of a catalyst relate to its reactivity.

Although these are important new improvements in the way we currently study, and understand, processes in nanomaterials, they are done by methods that are not sensitive to local fluctuations in size, shape, structure of nanomaterials, that are present even in well-defined, model catalysts. Thus, in addition to the ensemble averaging that these and other commonly used methods provide, local information, such as one provided by electron microscopy, is needed. In this talk, I will focus on the new efforts in combining the local and average information by coupling the in situ x-ray absorption spectroscopy to in situ environmental transmission electron microscopy (E-TEM) for in situ investigations. Such experiments, done in two separate facilities (NSLS and CFN) at Brookhaven National Laboratory, revealed anomalous, mesoscopic phenomena in the electronic, structural and thermal properties of supported Pt nanoparticles. These systems have long been excellent model systems in catalysis research, yet, at a closer look, as our in situ measurements demonstrated, they turned out to be much more unstable and complex than previously perceived. These clusters exhibited unique physical properties, such as negative thermal expansion, increase in the Debye temperature, broad amorphous-to-crystalline transition zone, large surface strain, as well as charge exchange with support and adsorbates.

I will review recent works showing how such complex behaviors can be, in the case of Pt on  $\gamma$ -alumina and carbon supports, theoretically understood by separately studying the effects of their size, shape, support and adsorbates.

9:00am **IS+AS+SS-MoM3 Communicating Nanostructures: Spillover Processes Studied on Ceria-supported Platinum Nanoparticles**, *M. Happel*, Friedrich-Alexander-Univ., Germany, *Y. Lykhach*, *T. Staudt*, Friedrich-Alexander-Univ., Germany, *N. Tsud*, Charles Univ., Czech Republic, *T. Skála*, *K.C. Prince*, Sincrotrone Trieste, Italy, *V. Matolin*, Charles Univ., Czech Republic, *A. Migani*, Univ. de Barcelona, Spain, *G.P. Petrova*, Univ. of Sofia, Bulgaria, *A. Bruix*, *F. Illas*, *K.M. Neyman*, Univ. de Barcelona, Spain, *G.N. Vayssilov*, Univ. of Sofia, Bulgaria, *J. Libuda*, Friedrich-Alexander-Univ. Erlangen-Nuremberg, Germany

Ceria-based catalysts are technologically important for various applications, including automotive catalysis,  $\text{SO}_x$  scrubbers, and hydrocarbon transformation reactions. The complex surface chemistry and reaction kinetics in these systems are assumed to be strongly influenced by so-called metal-oxide (MO) interactions. We use a surface science-based model approach to obtain detailed insight into the origins of such effects at the microscopic level.

The model catalysts are based on ordered  $\text{CeO}_2(111)$  films on  $\text{Cu}(111)$ , on which noble metal nanoparticles (e.g. Pt) are grown by PVD under UHV conditions. The growth and geometric structure of the model catalysts are characterized by STM. Adsorption and reaction are followed by XPS, synchrotron radiation photoelectron spectroscopy (SR-PES), IRAS, and molecular beam (MB) methods, in combination with DFT calculations. Resonant PES (RPES) is used to monitor the changes in the cerium oxidation state with high sensitivity.

Two types of MO interaction are identified, electron transfer from the Pt nanoparticle to the support, and oxygen transfer (spillover) from ceria to Pt. Whereas electron transfer occurs on ceria supports irrespective of their morphology, oxygen transfer shows a pronounced structure dependency, i.e. it requires the presence of nanostructured ceria aggregates in close contact with Pt.[1]

Not only oxygen spillover, which is a key step in oxidative-self cleaning of carbon-poisoned catalysts, but also spillover and reverse-spillover of hydrogen and hydrocarbon fragments can be followed in detail by RPES. A particularly complex behavior is expected for  $\text{SO}_x$ , for which strong MO effects and spillover have been suggested in previous studies on powder catalysts. On the Pt-free model support we identify different sulfur species forming upon  $\text{SO}_2$  exposure even at 150 K (sulfites, atomic sulfur, and potentially sulfates), formed via different adsorption, decomposition and disproportionation pathways. At higher temperature, these species transform into a bulk-like cerium oxysulfide. For interpretation of the sulfur-chemistry on  $\text{Pt/CeO}_2$ , reference experiments on  $\text{Pt}(111)$  were performed and numerous  $\text{SO}_x$  species were identified by IRAS and SR-PES. RPES for  $\text{SO}_2$  adsorption on  $\text{Pt/CeO}_2$  provides direct evidence for spillover of  $\text{SO}_x$  to the Pt nanoparticles above 300 K. Between 300 K and 600 K Pt acts as a "sulfur-collector", before at even higher temperatures sulfur is finally transformed into a cerium oxysulfide species.

[1] G. Vayssilov, Y. Lykhach, A. Migani, T. Staudt, G.P. Petrova, N. Tsud, T. Skála, A. Bruix, F. Illas, K.C. Prince, V. Matolin, K.M. Neyman, J. Libuda, *Nat. Mater.* **2011**, 10, 310.

9:20am **IS+AS+SS-MoM4 HPXPS Study of the Oxidation of 10 nm PdAg Nanoparticles**, *S. Blomberg*, *J. Gustafson*, *N.M. Martin*, *M.E. Messing*, *K. Deppert*, *J.N. Andersen*, Lund University, Sweden, *L.E. Walle*, *A. Borg*, Norwegian University of Science and Technology, Norway, *H. Grönbeck*, Chalmers University of Technology, Sweden, *M.E. Grass*, *Z. Liu*, Lawrence Berkeley National Laboratory, *E. Lundgren*, Lund University, Sweden

Due to the economic and environmental rewards, one goal in catalysis related research is to create cheaper catalysts. One way to realize this is to dilute the more expensive active catalyst material with a less costly one. This requires that the active material stays at the surface. This could be achieved by using a material which is less prone to interact with the reactant gases, such as a noble metal. In most catalysts, the active material is dispersed in a high area complex oxide support as nanoparticles. In order to maintain the high activity, it would be necessary to ensure that the active material is at the surface of the nanoparticle.

In the present contribution we report on our initial findings from attempts to produce PdAg alloy particles using an aerosol deposition technique [1]. The particles have a diameter of 10 nm distributed over a  $\text{SiO}_x$  wafer. The samples were characterized by high pressure XPS, SEM and TEM as was done previously for aerosol Pd particles [2,3]. By comparing to XPS data from a single crystal  $\text{Pd}_{75}\text{Ag}_{25}(100)$  and from The X-ray Energy Dispersive Spectroscopy (XEDS) analysis we show that the PdAg particles have a similar alloy composition.

The *in-situ* high pressure XPS data from the 10 nm PdAg particles demonstrates that the Pd segregates to the surface in an oxygen rich environment and that the core of the particles are rich in Ag. Although a thin PdOx shell is formed, bulk oxidation is inhibited. The limited oxide formation is promising for the full oxidation of methane, since recent

investigations [4] suggest that the PdO is less active for methane oxidation than the metallic Pd.

[1] M. E. Messing, K. A. Dick, L. R. Wallenberg, K. Deppert, *Gold Bull.* **42** (2009) 20.

[2] M. E. Messing *et al.*, *J. Phys. Chem. C.* **114** (2010) 9257.

[3] R. Westerström *et al.*, *Phys. Rev. B.* **83**, (2011) 115440.

[4] A. Hellman *et al.*, submitted.

9:40am **IS+AS+SS-MoM5 New Assignment for Ag(III) from In Situ XPS of Highly Oxidized Silver Films.** *T.C. Kaspar, T. Droubay, S.A. Chambers*, Pacific Northwest National Laboratory, *P.S. Bagus*, University of North Texas

For decades, it has been a goal to elucidate the mechanisms behind the unique chemistry of both oxygen-exposed silver metal and silver oxides. Silver compounds in bulk, thin film, and nanoparticle form are widely investigated for applications including industrially-relevant catalysis, electrochemistry, transparent conducting oxides, and antimicrobial coatings. Determining the chemical state of both silver and oxygen is critical to developing a mechanistic understanding of the remarkable properties of these materials. *Ex situ* x-ray photoelectron spectroscopy (XPS) has been applied, starting in the 1970's, to determine the chemical state of Ag in various silver metal and silver oxide compounds. In contrast to most elements,  $Ag^{x+}$  ( $x > 0$ ) cations exhibit a negative binding energy (BE) shift relative to metallic Ag(0); thus, the lowest XPS core level binding energy observed for the Ag 3*d* peak, 367.3 eV, has been assigned to Ag(III) in AgO [Ag(I)Ag(III)O<sub>2</sub>]. However, the XPS analysis has been hindered by the ease with which silver oxides form carbonate species upon atmospheric exposure, as well as the instability of silver oxides in vacuum. In this work, silver oxide films have been formed under very oxidizing conditions, by molecular beam epitaxy (MBE) deposition of silver metal in the presence of activated oxygen. *In situ* XPS was then collected in an appended chamber. For the most highly oxidizing deposition conditions, a substantially lower BE, 366.8 eV, was found for the Ag 3*d* peak, with an associated satellite located at 368.2 eV. This oxide species proved unstable in vacuum over several days, but could be recovered by further exposure to activated oxygen. Based on the decomposition behavior of the Ag 3*d* and O 1*s* spectra, the low BE species was assigned as Ag(III), while the previous peak position for Ag(III) was re-assigned as Ag(I). These assignments are supported in part by electronic structure calculations predicting the photoemission spectra of Ag(III). The combination of highly oxidizing deposition conditions and *in situ* characterization allowed identification of the true Ag(III) XPS spectrum for the first time.[1]

[1] T.C. Kaspar, T. Droubay, S.A. Chambers, and P.S. Bagus. *J. Phys. Chem. C* **114** 21562 (2010).

10:00am **IS+AS+SS-MoM6 The Oxidation of Methane Over Pd.** *A. Hellman*, Chalmers Univ. of Tech., Sweden, *A. Resta*, European Synch. Rad. Fac., France, *J. Gustafson, N.M. Martin*, Lund Univ., Sweden, *A. Trinchero, P.-A. Carlsson*, Chalmers Univ. of Tech., Sweden, *O. Balmes*, European Synch. Rad. Fac., France, *J.N. Andersen*, Lund Univ., Sweden, *R. Feici*, European Synch. Rad. Fac., France, *E. Lundgren*, Lund Univ., Sweden, *H. Grönbeck*, Chalmers Univ. of Tech., Sweden

An important goal in surface science is to provide fundamental information on gas-surface interactions for the design of cheaper and more efficient catalysts. For this purpose, the required minimum knowledge is the composition of a catalyst for a certain reaction under realistic reaction conditions. Although this information seems trivial it is surprisingly difficult to obtain due to the complex structural nature of a real catalyst and the sometimes high temperatures and pressures under reaction conditions.

In the case of the complete oxidation of methane using Pd as the catalyst, pure Pd metal, Pd surface oxides and bulk PdO have all been reported to be most efficient to convert CH<sub>4</sub> into CO<sub>2</sub> and H<sub>2</sub>O [1-5]. This highlights the complexity of catalysis even for a relatively simple catalytic reaction.

In order to shed some light on the state of Pd during complete methane oxidation, we have performed *in-situ* Surface X-Ray Diffraction (SXRD) over a Pd(100) surface in a realistic reaction environment combined with DFT calculations. Our study demonstrates that significant roughening of the surface occur during the reaction, which increases the active surface area and thus affects the overall reactivity. Nevertheless, our study strongly suggests that the Pd metal is the most active phase for the full oxidation of methane.

[1] R. Burch, P. K. Loader, and F. J. Urbano, *Catalysis Today* **27** (1996) 243.

[2] R. F. Hicks, H. H. Qi, M. L. Young, and R. G. Lee, *J. Catal.* **122** (1990) 280.

[3] M. Lyubovsky and L. Pfefferle, *Catalysis Today* **47** (1999) 29.

[4] S. Oh, P. J. Mitchell, and R. Siewert, *J. Catal.* **123** (1991) 287.

[5] J. G. McCarthy, *Catalysis Today* **26** (1995) 283.

11:00am **IS+AS+SS-MoM9 The New Ambient Pressure X-ray Photoelectron Spectroscopy Instrument at MAX-lab - An Instrument also for Ultrahigh Vacuum Studies.** *J. Schnadt, J. Knudsen, A. Pietzsch, N. Johansson, A. Olsson, F. Hennies*, Lund University, Sweden, *N. Mårtensson, H. Siegbahn*, Uppsala University, Sweden, *J.N. Andersen*, Lund University, Sweden

Ambient pressure x-ray photoelectron spectroscopy (APXPS) is a technique, which dates back to the 1970s and 1980s, but which only during the past ten years has developed a very significant impact, driven forward especially by groups at the Advanced Light Source and BESSY. APXPS makes possible x-ray photoelectron spectroscopy (XPS) measurements under realistic or close-to realistic conditions, while conventional XPS is limited to vacuum conditions of 10<sup>-6</sup> mbar or better. APXPS thus contributes to closing the "pressure gap" of surface science, which has inhibited the understanding of processes and chemical reactions, for which the chemical potential of the gas atmosphere plays a decisive role. It also renders possible experiments on samples with a large vapour pressure, such as liquids or solid samples with a high degassing rate. Today, there exist a number of APXPS instruments around the world, including a small number of systems at synchrotrons. Common to these instruments is that they perform well at elevated pressures, but none of them is specifically designed to also allow studies under ultrahigh vacuum conditions. This complicates the connection to results from ultrahigh vacuum studies.

A new instrument for APXPS has just been installed at beamline I511 of the Swedish Synchrotron Radiation Facility MAX-lab. This instrument, which has been delivered by SPECS GmbH, Berlin, Germany, and which makes use of a PHOIBOS 150 NAP analyser, has been developed with the particular aim of building a strong link between ultrahigh vacuum and ambient pressure experiments and science. The instrument is capable of performing XPS measurements on the same sample in both types of environment. This is made possible by a unique design, which is based on the use of a retractable ambient pressure cell. For ambient pressure measurements at pressures of around 0.1 to 10 mbar the cell is docked to the electron energy analyser. Once the sample is loaded the cell is locked, and the only leak to the vacuum is through the nozzle of the analyser's lens system. Hence, even during ambient pressure measurements the vacuum remains intact in the analysis chamber. For UHV measurements the cell together with the nozzle is retracted into a separate chamber, and UHV XPS measurements can be performed normally. This entails also another attractive feature of the instrument, namely, that the high pressure cell easily can be replaced by dedicated cells for other sample environments.

In this contribution the design and concept of the APXPS instrument at MAX-lab will be discussed and first results shown. Also plans for an upgraded and dedicated new beamline at MAX-lab will be presented.

11:20am **IS+AS+SS-MoM10 In Situ XPS and STM Studies of Ge<sub>2</sub>H<sub>6</sub> Interactions with the Si(100) Surface.** *S. McDonnell, J.F. Veyan*, University of Texas at Dallas, *J. Ballard, J.H.G. Owen, J.N. Randall*, Zyvex Labs, *Y.J. Chabal, R.M. Wallace*, University of Texas at Dallas

We present a study of the reactions between Ge<sub>2</sub>H<sub>6</sub> and Si(100) surfaces. Ge<sub>2</sub>H<sub>6</sub> is a potential precursor that could allow atomic layer epitaxy (ALE) on Ge(100) and Si(100) surface [1,2] which will be a vital component for atomically precise manufacturing (APM). We investigate the effects of various growth conditions such as substrate temperature, dosing pressure and post deposition annealing. We study the formation of seed layers for ALE along with the reactions on both the atomically clean and the hydrogen passivated surfaces, where we see evidence of Ge<sub>2</sub>H<sub>6</sub> reacting with the dangling bonds.

To facilitate these studies, we utilize a UHV deposition/characterization tool. Chemical analysis of the surfaces is achieved using *in-situ* x-ray and ultraviolet photoelectron spectroscopy. Differences in the chemical states of germanium present on the surface under the various growth conditions are identified. This analysis is supplemented by *in-situ* scanning tunneling microscopy, which allows us to monitor the growth of germanium on silicon and confirm 2D or 3D growth. Comparisons are made with similar experiments carried out in a different UHV chamber where the surface is characterized with Fourier transform infrared spectroscopy (FTIR) and shows evidence of the digermane reacting with the surface at 173K as Ge<sub>2</sub>H<sub>5</sub> rather than GeH<sub>3</sub>.

This material is based upon work supported by the Defense Advanced Research Project Agency (DARPA) and Space and Naval Warfare Center, San Diego (SPAWARSYSCEN-SD) under contract N66001-08-C-2040. It

is also supported by a grant from the Emerging Technology Fund of the State of Texas to the Atomically Precise Manufacturing Consortium.

[1] D.-S. Lin, K.-H. Huang, T.-W. Pi, and R.-T. Wu. Phys. Rev. B, 54 16 (1996) 958

[2] K.-H. Huang, T.-S. Ku, and D.-S. Lin Phys. Rev. B, 56 8 (1997) 4878

## Surface Science Division

Room: 109 - Session SS1-MoM

### Water Films & Environmental Interfaces

Moderator: H. Fairbrother, Johns Hopkins University

8:20am **SS1-MoM1 Surface Science of Acetonitrile on Model Interstellar Ices and Grains**, *A. Abdulgalil, M. Collings, M. McCoustra*, Heriot-Watt University, UK

Physical and chemical processes occurring on the surfaces of icy dust grains in the cold, dense interstellar medium have a crucial role to play in the evolution of the modern Universe. The formation of simple hydrides, e.g. water, on grain surfaces explains the infrared astronomical observations of icy grain mantles and provides a reservoir of coolant molecules during the early stages of star formation that helps maintain the current rate of star formation and favours the formation of small, long-lived stars. Energetic processing of icy mixtures by short wavelength radiation and cosmic rays turns the icy grain mantles into chemical nanofactories producing increasingly complex organic molecules. Nitriles (RCN) represent a potential intermediate on the pathway to forming amino acids in these icy mantles. However, the formation of nitriles in and on icy grain mantles is not understood. Nor is the surface science of these simple species on models of the interstellar grain population. Acetonitrile ( $\text{CH}_3\text{CN}$ ) is the simplest organic nitrile and is amongst the list of chemical species observed in the interstellar medium. This paper will report our recent investigations of the interaction of  $\text{CH}_3\text{CN}$  with model silica and water ice surfaces representative of bare and icy interstellar dust grains. We will report on the nature and strength of the interaction of  $\text{CH}_3\text{CN}$  with these substrates and on the thermal and non-thermal (electron-induced) desorption of  $\text{CH}_3\text{CN}$  from these surfaces as part of our on going programme in solid state and surface astrochemistry.

8:40am **SS1-MoM2 Energetic Xenon Sputtering and Embedding at Ice Surfaces**, *D.R. Killelea, K.D. Gibson, H. Yuan, S.J. Sibener*, University of Chicago

\*\*\*PLEASE NOTE YOU MUST IDENTIFY A DIFFERENT PRESENTER FOR THIS ABSTRACT. YOU MAY PRESENT ONE PAPER ONLY (ORAL OR POSTER) AT THE CONFERENCE. YOU ARE LISTED AS PRESENTER FOR ABSTRACT #278\*\*\*Energetic collisions between gas-phase atoms or molecules and ice surfaces are ubiquitous in nature. Such collisions occur under non-equilibrium conditions given the disparity between the temperature of the substrate and that of the incident species. Moreover, metastable absorption states can be accessed at sufficiently high collision energies, opening up enhanced channels for species collection and concentration. Here, we present results of a study where the energetically accessed absorption states of the network of molecules in an ice surface were probed with translationally activated gas-phase Xe atoms, focusing on sputtering, energy accommodation, and a new mechanism for the incorporation of volatile species into ice surfaces: collisionally activated embedding. Evidence for embedding comes from the observation of Xe desorption at temperatures nearly 100 K above the normal desorption temperature for xenon adsorbed onto an ice surface.

9:00am **SS1-MoM3 Composition and Chemistry at the Liquid/Vapor Interface of Aqueous Solutions: Liquid-Jet XPS Experiments Coupled with MD Simulations**, *J.C. Hemminger*, University of California, Irvine

INVITED

In spite of the importance of liquid/vapor interfaces to many real world problems our understanding of the composition and chemistry of liquid/vapor interfaces is limited. We have employed liquid micro-jet methods to obtain x-ray photoelectron spectra of the liquid/vapor interface of aqueous solutions at the BESSY II synchrotron. The variable photon energy characteristic of synchrotron light sources allows us to carry out experiments over a range of photoelectron kinetic energies—thus varying

the probe depth of the experiment. The result is a depth profile of the composition of the liquid/vapor interface. We have focused our experiments on aqueous solutions. In this talk I will describe results from recent experiments on the following systems: (1) aqueous nitric acid solutions, in which we demonstrate a large difference in the degree of dissociation at the surface compared to bulk solution. We have also been able to determine the degree of dissociation at the interface and in the bulk solution for a range of temperatures sufficient to determine the enthalpy of the dissociation reaction for the interface and the bulk, (2) aqueous solutions of monoethanolamine and monoethanolamine reacted with  $\text{CO}_2$ —aqueous monoethanolamine is widely proposed for  $\text{CO}_2$  capture processes, (3) aqueous solutions of the organosulfur compounds DMS, DMSO,  $\text{DMSO}_2$ ,  $\text{DMSO}_3$ —DMSO is a major source of environmental sulfur compounds including in the atmosphere. In these systems we have been able to determine the relative propensity of each molecule for the liquid/vapor interface, (4) carboxylic acid solutions where we have been able to determine the relative surface activity of the dissociated and undissociated acid. For each of the above systems we have carried out molecular dynamics simulations. These simulations combined with our experimental depth dependent measurements have provided molecular level insight into the behavior of molecular solutes in aqueous solution.

9:40am **SS1-MoM5 In Situ Studies of Sulfuric Acid Aqueous Solutions by X-ray Photoelectron Spectroscopy**, *A. Margarella, T. Lewis*, University of California, Irvine, *M. Faubel*, Max-Planck-Institut für Dynamik und Selbstorganisation, Germany, *B. Winter*, Helmholtz-Zentrum Berlin für Materialien und Energie, Germany, *J.C. Hemminger*, University of California, Irvine

Sulfuric acid is amongst the most widely used acids in the chemical industry, as well as having an important presence in atmospheric aerosols. Using a micro-liquid jet, the chemistry at the liquid-vapor interface of aqueous solutions is explored in-situ by x-ray photoelectron spectroscopy (XPS). Experiments presented were performed at Beamline U41 at the BESSY II synchrotron facility. By tuning the energy of the incoming photons, the kinetic energy of the photoelectrons is varied, allowing measurements from different depths of solution. As a strong diprotic acid, an aqueous solution of sulfuric acid will have  $\text{HSO}_4^-$  and  $\text{SO}_4^{2-}$  present, and at high concentrations, (greater than 16M) undissociated  $\text{H}_2\text{SO}_4$  is present. In XPS, all of these components are distinguishable using their S2p binding energy shifts. A series of sulfuric acid aqueous solutions with concentrations up to 16M is measured and using the peak areas in the XP spectra, the dissociation at the surface relative to the bulk can be determined for different solutions.

Additionally, the effect of solution temperature on the acid dissociation at the surface is explored.

10:00am **SS1-MoM6 Infrared Spectroscopy of Thin Water Films on  $\text{TiO}_2(110)$ : Anisotropy and the Hydrogen-Bonding Network**, *G.A. Kimmel, M. Baer, N.G. Petrik, C.J. Mundy, R.J. Rousseau*, Pacific Northwest National Laboratory

The structure of water at interfaces is crucial for processes ranging from photocatalysis to protein folding. We have investigated the structure of thin water films adsorbed on  $\text{TiO}_2(110)$  using reflection-absorption infrared spectroscopy (RAIRS), temperature programmed desorption and *ab-initio* molecular dynamics simulations. Infrared spectra were obtained for light with the plane of incidence parallel and perpendicular to the [001] azimuth of  $\text{TiO}_2(110)$  for water coverages  $\leq 4$  monolayers (ML). The spectra indicate strong anisotropy in the water structure along the two major azimuths. For both 1 and 2 ML coverages, the water films form “strings” of water molecules parallel to the bridging oxygen rows on the (110) surface. Within the strings, each molecule participates in 4 bonds, such that the films have no dangling hydrogen bonds. The vibrational densities of states predicted by the *ab-initio* simulations for 1 and 2 monolayer coverages agree well with the observations. Despite extensive prior research, the structure of water films on  $\text{TiO}_2(110)$  has remained controversial. Our results provide crucial, molecular-level information about the structure of water films on this benchmark transition metal oxide.

11:20am **SS1-MoM10 Origins of the Molecular Volcano: Dewetting and Crystallization Effects Leading to Rapid Desorption from Amorphous Solid Water Overlayers**, *R.A. May, R.S. Smith, B.D. Kay*, Pacific Northwest National Laboratory

Amorphous solid water (ASW), a metastable phase of water occurring when water is deposited on a substrate cooled below 140K, is of fundamental interest for an array of applications including but not limited to desorption from interstellar ices and investigation of diffusion and solvation processes. When deposited over an immiscible substance, such as  $\text{CCl}_4$ , the underlayer desorption is dictated by the morphology of the ASW overlayer. This desorption process culminates in the rapid release of the underlayer

commensurate with the development of crystallization induced cracks through the ASW. This episodic release is termed the “molecular volcano”. Thus, the desorption event reports on changes in the structure of the ASW overlayer. Infrared spectroscopy combined with programmed desorption elucidates the complex interplay between the dewetting and crystallization processes which dominate the eruption event. The effects of the ASW deposition temperature and overlayer thickness on the CCl<sub>4</sub> desorption process will be presented and discussed.

This work was supported by the U.S. Department of Energy (DOE), Office of Basic Energy Sciences, Division of Chemical Sciences, Geosciences, and Biosciences. The research was performed using EMSL, a national scientific user facility sponsored by DOE's Office of Biological and Environmental Research and located at Pacific Northwest National Laboratory, which is operated by Battelle, operated for the U.S. DOE under Contract DE-AC05-76RL01830.

## Surface Science Division

### Room: 110 - Session SS2-MoM

## Surface Chemical Dynamics

**Moderator:** L. Bartels, University of California, Riverside

8:20am **SS2-MoM1 STM Dynamics Studies of Tip-Induced Reactions of Anthracene Derivatives on TiO<sub>2</sub>(110).** *D.V. Potapenko, R.M. Osgood, Columbia University*

In photocatalysis, reactions are driven by the charges that are generated in the bulk of the catalyst and then are transferred to the adsorbed molecules. Injection of electrons from the STM tip into the adsorbed molecules is a useful tool for surface dynamics studies as the energy the electrons as well as the adsorption state of the molecules could be precisely controlled. We have studied adsorption and tip-induced chemistry of anthracene and its derivatives on the TiO<sub>2</sub>(110) surface. These molecules self-assemble on the rutile(110) surface at room temperature driven by electrostatic interaction. Applying electric pulses from the STM tip to individual molecules causes desorption and in some cases dissociation as indicated by the changes in the STM images. We have observed dissociative electron capture of 2-chloroanthracene molecules that leaves behind a surface chlorine atom. The energy threshold for dissociation found as ~ 3.1 V. We report on the dynamics of this tip-induced chemistry and propose a mechanism for the observed phenomena.

8:40am **SS2-MoM2 Atom Specific Ultrafast Surface Chemistry using Soft X-ray Free Electron Laser: CO on Ru(0001).** *M. Beye, Helmholtz Zentrum Berlin, Germany, R. Coffee, SLAC Nat. Accel. Lab, M. Dell'Angela, Univ. of Hamburg, Germany, A. Foehlich, Helmholtz Zentrum Berlin, Germany, J. Gladh, Stockholm Univ., Sweden, T. Katayama, S. Kaya, O. Krupin, A. Nilsson, D. Nordlund, SLAC Nat. Accel. Lab, H. Oberg, Stockholm Univ., Sweden, H. Ogasawara, SLAC Nat. Accel. Lab, H. Ostrom, L.G.M. Pettersson, Stockholm Univ., Sweden, W.F. Schlott, J.A. Sellberg, SLAC Nat. Accel. Lab, F. Sorgenfrei, Univ. of Hamburg, Germany, J.J. Turner, SLAC Nat. Accel. Lab, M. Wolf, Fritz-Haber-Inst., Germany, W. Wurth, Univ. of Hamburg, Germany*

New possibilities for the study of chemical reactions on surfaces using X-ray free-electron lasers (Linac Coherent Light Source, or LCLS, at SLAC National Accelerator Laboratory) will be presented. We induced the hot electron mediated excitation of CO on Ru(0001) with synchronized excitation by a femtosecond optical laser pulse. We have followed the ultrafast evolution of the bond distortions, weakening and breaking, using x-ray emission spectroscopy resonantly tuned to the oxygen core level with ultrashort x-ray pulses delivered from LCLS. We can directly study the time evolution of the molecular orbitals in an atom-specific way on a subpicosecond timescale. Different adsorption configurations explored have been characterized by comparing the measured time dependent energy shifts of the molecular orbitals in the valence band with theoretical results.

This research was carried out on the SXR Instrument on the Linac Coherent Light Source (LCLS) at the SLAC National Accelerator Laboratory. The SXR Instrument is funded by a consortium whose membership include the LCLS, Stanford University through the Stanford Institute for Materials Energy Sciences (SIMES), Lawrence Berkeley National Laboratory (LBNL), University of Hamburg through the BMBF priority program FSP 301, and the Center for Free Electron Laser Science (CFEL). The LCLS is funded by the U.S. Department of Energy's Office of Basic Energy Sciences.

9:00am **SS2-MoM3 The Oxidation of Benzyl Alcohol on Gold and its Implications Towards a Gold-Mediated Conversion of Hydrocarbons.** *J.C. Rodriguez-Reyes, C.M. Friend, R.J. Madix, Harvard University*

In order to understand alcohol conversion on gold, we have explored the mechanism of the oxidation of benzyl alcohol (C<sub>6</sub>H<sub>5</sub>-CH<sub>2</sub>OH) on a Au(111) surface - a test reaction commonly used to determine the efficiency and selectivity of novel gold-based catalysts. Using adsorbed atomic oxygen as the active oxidizing species, we find that a high selectivity towards the conversion to aldehyde (benzaldehyde, C<sub>6</sub>H<sub>5</sub>-CHO) is achieved at low oxygen coverages. However, in excess oxygen the selectivity decreases dramatically, and benzaldehyde is readily transformed to adsorbed benzoate, which is eliminated as benzoic acid (C<sub>6</sub>H<sub>5</sub>-COOH) and CO<sub>2</sub>. In addition, we show that the production of the ester produced by self-coupling (benzyl benzoate) does not require the separate presence of acid, as might be expected from acid-alcohol condensation reactions. These surface transformations are extremely facile and exhibit small kinetic barriers of the rate-limiting steps. Lastly, by comparing the mechanism of benzyl alcohol oxidation to that of toluene oxidation, we extract information of a model hydrocarbon-to-alcohol reaction (toluene to benzyl alcohol, C<sub>6</sub>H<sub>5</sub>-CH<sub>3</sub> to C<sub>6</sub>H<sub>5</sub>-CH<sub>2</sub>OH). Our results suggest that due to the relatively large kinetic requirements for toluene conversion, the alcohol cannot be selectively produced on a gold surface; indeed, preliminary TPRS data indicates that the gold-mediated conversion of toluene yields benzoic acid and combustion gases.

9:20am **SS2-MoM4 Determination of the Structure and Vibrational Dynamics of Methyl-Terminated Si(111) Using Helium Atom Scattering.** *R.D. Brown, S.J. Sibener, University of Chicago*

MMethyl-terminated Si(111) interfaces are of great interest in the fields of solar energy, solar fuels, and electronics due to their superior electrochemical stability and device performance. Recent advances in synthetic techniques allow for the fabrication of high-quality, passivated organic-semiconductor hybrid interfaces on single-crystalline silicon substrates. This termination maintains the bulk electronic behavior of the underlying silicon, but eliminates surface trap states which hinder the performance of any device. We directly examined the structural and dynamical characteristics of the CH<sub>3</sub>-Si(111) and CD<sub>3</sub>-Si(111) interfaces using helium atom scattering. Helium atom scattering is a uniquely surface-sensitive technique which probes both atomic structure and dynamics. These results are the first measurements of this nature for an organic-semiconductor hybrid interface. Helium atom diffraction confirmed a high quality (1x1) methyl termination of the Si(111) substrate. We observed unusual dynamical characteristics for these interfaces through Debye-Waller attenuation measurements of helium atom diffraction peaks. These measurements characterized the thermal motion of the interface, and elucidated the surface Debye temperature and gas-surface interaction well depth. The Debye Waller measurements yielded temperature dependencies of the surface mean-square displacements displaying polarization dependence, and were similar to the thermal motion of local molecular vibrational modes. The effective surface Debye temperatures were much higher than expected, and correspond to the local vibrational modes of the C-Si bond. These two unusual results indicate that termination with the simplest monolayer organic film initiates a transition away from phonon dominated surface dynamics to dynamics dominated by local molecular vibrational modes. We also performed a series of high precision inelastic time-of-flight measurements to characterize the phonon band structure of these interfaces. Our measurements have clearly resolved multiple single phonon surface modes on CH<sub>3</sub>-Si(111), and are the first observations of this nature on an organic-semiconductor hybrid interface.

9:40am **SS2-MoM5 STM Insights into Single-Molecule Dynamics.** *K. Morgenstern, Leibniz University of Hannover, Germany* **INVITED**

The development of molecular switches on the single molecule level is a major challenge on the path towards incorporating molecules as building units into nanoelectronic circuits. With a scanning tunneling microscope (STM) it is possible to induce chemical reactions on a single molecule basis by electrons tunneling inelastically from the STM tip into a molecule. The method is based on high-resolution imaging at low-temperature (5K) that allows us to identify different groups within the molecule. Chemical reactions are induced by injecting selectively electrons into specific parts of the molecule. The success of the manipulation is visualized in the recorded tunneling current during the manipulation and in STM images taken afterwards. We investigate isomerization of individual molecules adsorbed on metal surfaces. For chlorobenzene and azobenzene derivatives, the effects of different substitutional groups and different substrates are explored.

10:40am **SS2-MoM8 State-resolved Reactivity of Methane ( $v_2+v_4$ ) on Ni(111)**, *N. Chen, Y. Huang, A. Utz*, Tufts University

Methane dissociation on transition metal surfaces is the rate-limiting step in the steam reforming reaction, which is the principal route for converting  $\text{CH}_4$  to  $\text{H}_2$ . Understanding the dynamics of energy flow during this process has both fundamental and practical impact. Experiments that measure the reactivity of methane prepared in select vibrational states reveal how specific nuclear motions promote methane dissociation. State-resolved measurements for methane reactivity on Ni and Pt surfaces show that molecules prepared in vibrationally excited states are more reactive than those without laser excitation, and the efficacies of vibrational energy in different excited states can differ significantly.

Here, we present state-resolved reactivity measurements of the  $v_2+v_4$  bending combination vibration of  $\text{CH}_4$  on Ni(111) as a function of translational energy. This state is a member of the pentad of vibrational states that can play an important role in the thermal activation of methane. We are able to quantify the state-resolved reactivity of methane in this particular vibrational state over a wide range of translational energies. We compare the efficacy for  $v_2+v_4$  bend with that of the  $v_3$  stretching and  $3v_4$  bending states to gain insight into the ability of  $v_2$  excitation to promote dissociative chemisorption. The result permits a detailed comparison of the role of stretch and bend excitation of methane dissociative chemisorption on Ni(111).

11:00am **SS2-MoM9 Molecular Beam Scattering of CO and  $\text{CO}_2$  on  $\text{Cu}_x$  Nanoclusters Supported on Silica Fabricated by Electron Beam Lithography**, *M. Komarneni, U. Burghaus*, North Dakota State University

Adsorption dynamics of CO and  $\text{CO}_2$  on 12 nm  $\text{Cu}_x$  nanoclusters supported on silica are studied by molecular beam scattering. Samples are fabricated by electron beam lithography. Scanning electron microscopy, auger electron spectroscopy, and x-ray photoelectron spectroscopy are used to characterize the sample. Cu clusters which are nearly metallic, partially oxidized, and fully oxidized are prepared by varying the sample treatment. The initial adsorption probability,  $S_0$ , of both CO and  $\text{CO}_2$  decreased with an increase in impact energy,  $E_i$ , and adsorption temperature,  $T_s$ , which is consistent with non-activated molecular adsorption.  $S_0$  of CO approaches the values obtained for copper single crystals for  $E_i$  of 0.4 eV. This is a result of the so-called capture zone effect, where CO molecules are trapped on the support and subsequently diffuse to the metal clusters.  $S_0$  of  $\text{CO}_2$  is larger than for single crystals. The differences in  $S_0$  for metallic and oxidic clusters can be explained by deviations in the mass matching. In-contrast with  $\text{CO}_2$ ,  $S_0$  of CO on metallic clusters is slightly larger than that of oxidic clusters. At low  $E_i$  and  $T_s$ , coverage dependent adsorption probabilities,  $S(\theta)$ , of CO and  $\text{CO}_2$  on metallic clusters obeyed precursor-mediated Kisliuk-like dynamics. At large  $E_i$ , Langmuirian-like dynamics is seen for CO which is less pronounced for  $\text{CO}_2$  on metallic clusters.

11:20am **SS2-MoM10 Precursor-Mediated Reactivity of Vibrationally Hot Molecules**, *D. DelSesto, E. Peterson, E. Dombrowski, A. Utz*, Tufts University

Methane's dissociative chemisorption is highly activated on a range of transition metal surfaces. Internal-state-averaged and state-resolved beam-surface scattering experiments show that vibrational energy ( $E_{\text{vib}}$ ) can be highly effective in promoting dissociative chemisorption via a direct mechanism, but evidence for  $E_{\text{vib}}$  activation via a precursor-mediated mechanism on a metal surface remains scarce. We will present recent experimental results from our lab that demonstrate the ability of  $E_{\text{vib}}$  to promote methane dissociation via both direct and precursor mechanisms on Ir(111). These results build on prior studies of trapping-mediated reactivity on Ir(111) by exploring how  $E_{\text{vib}}$  in the incident methane molecule promotes reactivity, and they are consistent with the timescales and pathways of vibrational energy flow and damping on these surfaces.

1. Seets, D. C., C. T. Reeves, et al. (1997). "Dissociative chemisorption of methane on Ir(111): Evidence for direct and trapping-mediated mechanisms." *J. Chem. Phys.* **107**(23): 10229-10241.

11:40am **SS2-MoM11 Three-Dimensional Spatial Distribution of Desorbing  $\text{N}_2$  and  $\text{N}_2\text{O}$  from Pd(211)**, *M. Sakurai, T. Kondo, J. Nakamura*, University of Tsukuba, Japan

Spatial distributions of  $\text{N}_2$  and  $\text{N}_2\text{O}$  desorbing from Pd(211), Pd(S)-[3(111) $\times$ (100)], in temperature programmed desorption (TPD) were measured after the  $\text{N}_2\text{O}$  dosing on the surface at 60 K. About one-third of  $\text{N}_2\text{O}$  molecules on the surface are found to desorb as  $\text{N}_2$  by the decomposition with sharp concentration to  $25^\circ$  ( $\theta = -25^\circ$ ) (100) side from the normal direction of (211) plane at 108 K in the parallel plane to [211]

and [-111] directions at  $\text{N}_2\text{O}$  coverage of 1.0 ML. This indicates that  $\text{N}_2$  desorbs without thermal equilibration by  $\text{N}_2\text{O}$  decomposition on Pd(211). From the preferential desorption direction ( $\theta = -25^\circ$ ), the adsorption structure of  $\text{N}_2\text{O}$  just before the desorption is assigned as the bridge-structure at step-site, where O and terminal-N bonded with Pd at atop (100) and 3fold hollow(111), respectively along the [-111] directions. On the other hand, the spatial distribution of desorbing  $\text{N}_2\text{O}$  obeyed cosine distribution directing the normal direction to the (211) plane, suggesting the existence of pre-desorption state on the surface.

# Monday Afternoon, October 31, 2011

**In Situ Spectroscopy and Microscopy Focus Topic**  
**Room: 106 - Session IS+AS+SS-MoA**

**In Situ Characterization of Solids: Film Growth, Defects, and Interfaces**

**Moderator:** M. Salmeron, Lawrence Berkeley National Laboratory

2:00pm **IS+AS+SS-MoA1 A New Approach to Defect Evolution Studies – Combined In Situ Experiments and Electron Tomography.** **I.M. Robertson, J. Kacher, G. Liu,** University of Illinois at Urbana-Champaign **INVITED**

Electron micrographs are two-dimensional images capturing specific instances in the evolution of the microstructure and composition as well as the electronic and magnetic state. As these yields no insight as to how the state evolved, *a posteriori* knowledge is used to determine the most likely pathway. This challenge can be addressed by conducting experiments *in situ* in the transmission electron microscope, which allows direct observation and in some cases quantification of the reactions and interactions responsible for the evolved structure. The information, however, remains two-dimensional and with increasing use of this technique it is becoming apparent that lack of three-dimensional knowledge is hindering interpretation. Information in the beam direction can be recovered by applying electron tomography, but this is a relatively new technique to defect studies and despite its potential it remains a static snapshot. In this talk, I will illustrate how time-resolved deformation studies have improved our understanding of the behavior of dislocations and how this information has informed the development of new models. I will also demonstrate how three-dimensional images yield a better understanding of complex dislocation interactions and configurations. Finally, I will address the challenges faced in combining these two techniques such that three-dimensional snapshots of the evolving microstructure can be acquired periodically.

2:40pm **IS+AS+SS-MoA3 Real-time Oxide Growth Characterization using Atomic Force Microscopy.** **G. Rijnders,** University of Twente, the Netherlands **INVITED**

Complex oxides have attracted great interest since they exhibit a rich spectrum of physical properties such as ferromagnetism, antiferromagnetism, colossal magnetoresistance, ferroelectricity, dielectricity, and superconductivity. Novel heteroepitaxial devices based on these complex oxides, like spin-polarized ferromagnetic tunnel junctions, superconducting devices and piezoelectric devices, have great potential and are currently under investigation in many groups.

The nature of the above-mentioned physical properties in complex oxides is determined by very small characteristic length scales, comparable to the unit cell lattice parameters of complex oxide. Because of these small characteristic length scales, growth control on an atomic level as well as understanding of the different mechanisms affecting the growth mode is essential for the fabrication of epitaxial heterostructures.

Two independent processes, i.e., nucleation and growth of islands, play an important role during vapor-phase epitaxial growth on an atomically flat surface. Here, nucleation causes the formation of surface steps and subsequent growth causes the lateral movement of these steps. Both processes are determined by kinetics, since they take place far from thermodynamic equilibrium. These kinetic processes affect the final surface morphology and are, therefore, extensively studied. I will demonstrate the applicability of high-pressure RHEED as well as Scanning Force Microscopy (SFM) to monitor to the growth of complex oxides during Pulsed Laser Deposition (PLD). Because of recent developments, SFM is nowadays also used to study dynamic processes, such as thin film growth and surface reaction mechanisms.

We have realized a system, in which SFM can be performed during Pulsed Laser Deposition (PLD). Deposition and force microscopy are performed in one vacuum chamber and via a fast transfer (in the order of seconds) the surface of a sample can be scanned. In our system we take advantage of the *pulsed* deposition process, because microscopy measurements can be carried out between the pulses. This provides real-time morphology information on the microscopic scale during growth. The transfer mechanism allows switching between microscopy and deposition with a re-position accuracy of  $\pm 500$  nm which gives new opportunities to study growth processes. Furthermore, it can provide information if RHEED is not possible, for example during amorphous and polycrystalline growth.

In this contribution, I will highlight recent advances in oxide thin film growth as well as the latest equipment developments.

3:40pm **IS+AS+SS-MoA6 An Auger Electron Analyzer System for In Situ MBE Growth Monitoring.** **W.L. Calley,** Georgia Institute of Technology, **P.G. Staib,** Staib Instruments, **J.E. Lowder, J.D. Greenlee, M.W. Moseley, W.E. Henderson, W.A. Doolittle,** Georgia Institute of Technology

Auger Electron Spectroscopy (AES) analysis is a surface sensitive technique for thin film analysis, able to detect nearly all elements [1]. Not only can AES help determine the species present at the surface, but AES can also yield information about the chemical bonding [1]. However, this analysis tool has historically been an *ex situ* technique with a few noted exceptions [2]. Herein we demonstrate the capabilities and usefulness of an Auger probe, the Staib *In situ* Auger Probe (SIAP) that has a sufficient working distance (tested up 82 mm) so as to not shadow beam fluxes allowing use during growth. The probe leverages an existing RHEED gun as an e-beam source for Auger electron excitation.

The configuration and operation of the SIAP has been described in detail [3]. The tool is installed on an MBE system configured for Terfenol growth, a miscible alloy of TbFe<sub>2</sub> and DyFe<sub>2</sub>. Initial growths performed without Auger monitoring exhibited substantial oxidation even after Ar etched to remove surface contamination, figure 1. The SIAP was then employed to determine the sources of oxygen contamination.

Three sources of O were identified. The growth chamber had a high enough partial pressure of oxygen to oxidize the highly reactive rare earth elements. After 30 hours in the chamber, uncapped Tb showed a substantial increase in the ratio of O to Tb, figure 2. The Tb source material also delivered O and the rate of O delivery increased with cell temperature, figure 3. A final oxygen source was identified to be the Tb/SiO<sub>2</sub> interface as shown in the SIMS data in figure 4. Figure 5 shows the Si wafer with C and O present at the surface. After growth is initiated the C is not detected after 40 Å of deposition, however, the O can be detected until 200 Å are deposited, indicating intermixing with the SiO<sub>2</sub> interface.

Further tests were conducted starting with a layer of Dy and depositing part of a monolayer of Tb in 2% increments. Figure 6 shows a clear distinction between bare Dy and 2, 4, 6, 8, and 10% monolayer coverage of Tb on a Dy layer, demonstrating the SIAP's sensitivity is at least 2% of a monolayer for these heavy elements.

The SIAP is complementary to existing RHEED systems. While RHEED gives information about the crystal structure of the growing film, the SIAP provides chemical information. This is especially useful when working with films without line compositions. The SIAP coupled with a future closed loop control system may enhance growth of films with multiple oxidation states or other similar phase/chemical transitions. Finally this technique could give information about transitions between layers in multilayered films grown via MBE.

4:00pm **IS+AS+SS-MoA7 Quantum Size Effect Driven Structure Modifications of Bi-films on Ni(111).** **T.R.J. Bollmann, R. van Gastel, H. Zandvliet, B. Poelsema,** University of Twente, The Netherlands

We have investigated the initial growth of Bi/Ni(111) using Low Energy Electron Microscopy (LEEM) and Selected Area Low Energy Electron Diffraction ( $\mu$ LEED). Bismuth represents an interesting material since 1) it has a tendency for allotropism, 2) it forms several ordered alloys with Ni and 3) with Bi being a neighbor of Pb in the periodic system, one may find evidence for quantum size effects in ultrathin Bi layers. Indeed we obtain ample evidence for Bi/Ni(111) as being a very rich system, even at a fixed substrate temperature of 474 K.

We find first that the deposition of Bi leads to the formation of a surface alloy with a  $(\sqrt{3}\times\sqrt{3})\text{-R}30^\circ$  structure at a Bi-coverage of 1/3. Continued Bi deposition leads to the formation of an incommensurate wetting layer with a continuously decreasing lattice parameter, finally ending in a  $(7\times 7)$  structure. From the variation of the step position at the buried interface, nicely accessible with LEEM, we conclude that the dealloying of the  $\sqrt{3}$  phase is incomplete and that the  $(7\times 7)$  wetting layer in fact involves two layers with a small, but finite Bi content in the second layer. Upon further Bi deposition elongated, 3-4 layers high nanowires emerge, with a  $p(5\times 2)$  structure and a width of about 80 nm, oriented along  $\langle 110 \rangle$  and  $\langle 100 \rangle$ -azimuths. Further deposition of Bi-leads to different (sometimes coexisting) structures:  $(3\times 3)$ -patches with a thickness of three atomic layers and patches with a matrix structure ( $m_{11}=3, m_{12}=1, m_{21}=1, m_{22}=2$ ) and a thickness of five atomic layers. This accurate height assignment is uniquely enabled by the analysis of LEEM-IV data.

The results are fully consistent with quantum size effect driven thin film morphology: the different film structures and their thicknesses nicely fit with integer numbers of nodes in their specific Fermi wave function, even for the seven layers thick (7x7) structure obtained at a lower temperature of 422 K. Tensor LEED calculations of the interlayer spacing of the different structures concur with this assignment.

The influence of the structure and morphology on electronic properties of various materials is well known. The interaction between electronic and crystal structure should be reciprocal. The Bi/Ni(111) system provides a nice and we think first illustration: electronic properties, in particular quantum size effects, actually drive the structure of the thin bismuth films.

4:20pm **IS+AS+SS-MoA8 Growth and Structure of Sm on an Ultrathin Al<sub>2</sub>O<sub>3</sub>/Ni<sub>3</sub>Al(111) Film: A Comprehensive Study, J.F. Zhu, Q. Xu, S. Hu, X. Feng, D. Chen, University of Science and Technology of China**

The growth and electronic structure of vapor-deposited Sm onto a well-ordered Al<sub>2</sub>O<sub>3</sub>/Ni<sub>3</sub>Al(111) ultrathin film under ultrahigh vacuum (UHV) conditions at room-temperature has been studied comprehensively using X-ray photoelectron spectroscopy (XPS), ultraviolet photoelectron spectroscopy (UPS), scanning tunneling microscopy (STM) and low electron energy diffraction (LEED). Our results indicate that at room temperature Sm grows in a layer-by-layer fashion for the first two layers, followed by three-dimensional (3D) growth. The interaction of Sm with Al<sub>2</sub>O<sub>3</sub> thin films is so strong that deposited Sm is immediately oxidized at beginning. Both the oxidation states of Sm<sup>2+</sup> and Sm<sup>3+</sup> are found at low coverages (<1 ML) with the situation that the concentration of Sm<sup>2+</sup> dominates below 0.2 ML and subsequently that of Sm<sup>3+</sup> dominates. With increasing Sm coverage, the metallic state of Sm gradually appears. Annealing the film of 0.2 ML Sm/Al<sub>2</sub>O<sub>3</sub> at T < 500 K results in further oxidation of the Sm species where all the Sm<sup>2+</sup> species converts to Sm<sup>3+</sup>. Further annealing at higher temperatures leads to loss of Sm from the surface via subsurface diffusion.

4:40pm **IS+AS+SS-MoA9 In Situ Study of the Reaction Mechanism Kinetics of Pt ALD from (<sup>109</sup>Cp)PtMe<sub>3</sub> and O<sub>2</sub>, I.J.M. Erkens, A.J.M. Mackus, H.C.M. Knoops, F. Roozeboom, W.M.M. Kessels, Eindhoven University of Technology, Netherlands**

Atomic layer deposition (ALD) of noble metals and noble metal oxides on high-aspect-ratio 3D nanostructures has a wide variety of potential applications in sensing and catalysis. Despite several studies,<sup>1-3</sup> much is still unknown about the reaction mechanism of Pt ALD using (<sup>109</sup>Cp)PtMe<sub>3</sub> and O<sub>2</sub>, which can be considered a model system for noble metal ALD processes. Questions remain regarding the surface species and reactions, and the temperature dependence of the growth per cycle (GPC). In this contribution we expand the understanding of the Pt ALD mechanism by combining quadrupole mass spectrometry (QMS) and spectroscopic ellipsometry (SE). Using these in-situ techniques to study the process as a function of temperature between 100 and 300°C, we have gained a unique perspective, which has led to several new insights. The time-resolved QMS data for CH<sub>4</sub> and CO<sub>2</sub> show that combustion and other ligand reactions at the surface occur in sequence, while competing for the available carbon atoms. Quantification of the data showed that approximately 80% of the C atoms are combusted during the O<sub>2</sub> pulse. By performing the QMS measurements in a temperature series, valuable information was obtained on the rate of combustion of the hydrocarbon ligands at the Pt surface during the O<sub>2</sub> pulse. Using a combination of QMS and SE data, we were able to formulate a mechanism explaining growth inhibition at low temperatures. This mechanism manifests itself through three temperature dependent growth regimes: no growth below 100°C; limited growth between 100 and 250°C; and full growth between 250 and 300°C. Using results from surface science literature a likely explanation for these regimes was given. This involves the cyclopentadienyl ligands at the Pt surface forming reactive intermediates or being thermally decomposed. The mechanism was corroborated by QMS and SE data on post-plasma treatment cycles, by which catalytic activity was temporarily restored. We were therefore able to link the temperature dependence of the GPC to combustion kinetics. A detailed description of our methods and results will be given in our contribution.

1. Aaltonen *et al.*, *Electrochem. Solid-State Lett.* **6**, C130 (2003).
2. Kessels *et al.*, *Appl. Phys. Lett.* **95**, 013114 (2009).
3. Setthapun *et al.*, *J. Phys. Chem. C* **114**, 9758 (2010).

5:00pm **IS+AS+SS-MoA10 In Situ Surface Analytical Characterization of Electronic Devices: Thin Film Solar Cells and Lithium Ion Batteries as Examples, A. Thissen, SPECS Surface Nano Analysis GmbH, Germany**

Electronic devices have revolutionized everyday life in industrial countries over the last decades. Especially devices for energy conversion and storage like thin film solar cells and lithium ion batteries are of importance for the future. Recently two main tasks for research and development are dominant: miniaturization for sophisticated applications targeting at the nanoscale, and designing low cost large scale devices. In both fields the device performance is strongly determined by materials quality, composition, combination and last but not least by processes at materials interfaces. Nanostructures, minimization of material consumption and the need to improve device efficiencies consequently leads to the widespread focussing on thin film preparation. For thin film devices surface and interface analysis like photoelectron spectroscopy and surface (spectro-)microscopies are an important tools for material and device characterization. Classical well defined model experiments already reveal important insights using highly integrated vacuum systems for analysis and preparation. But analysis of materials and devices under near ambient conditions and even in situ during operation is an inevitable future development to improve the significance of data for development and quality management. In this respect the application of techniques like Near Ambient Pressure XPS, XPS from liquids and solid liquid interfaces, hard x-ray PES (HAXPS), Near Ambient Pressure SPM on solar cell and lithium ion battery materials is the challenging tasks for manufacturing companies of surface analytical equipment.

## Surface Science Division

Room: 109 - Session SS1-MoA

### Selectivity and Reactivity of Chemisorbed Species

Moderator: A.J. Gellman, Carnegie Mellon University

2:00pm **SS1-MoA1 Observation and Modeling of Chiral Modifier-Substrate Complexes on Pt(111), B. Hammer, Aarhus University, Denmark, V. Demers-Carpentier, P.H. McBreen, Université Laval, Quebec, Canada**

INVITED

We present a combined density functional theory (DFT) and scanning tunneling microscopy (STM) study of the complex formation between the chiral modifier naphthylethylamine (NEA) and the model substrate trifluoroacetophenone (TFAP) on a Pt(111) surface. The two molecules interact via a hydrogen bond between the amine group on the NEA and the carbonyl on the TFAP. Many different realization of the hydrogen bond exist depending on the relative position and orientation of the two molecules. However, only very few are observed experimentally. These are all among the most stable structures found in DFT. The chemisorbed TFAP is prochiral and hydrogenation of the carbonyl would lead to a chiral product. The prochirality of TFAP when forming a complex with NEA is regiospecific, i.e., it depends on the position at which the TFAP is chemisorbed relative to the NEA. The origin of this regiospecificity is discussed.

2:40pm **SS1-MoA3 Enantiospecific Decomposition of Tartaric Acid on Spherically Curved Copper Single Crystals, B. Holsclaw, P. Kondratyuk, A. De Alwis, A. Reinicker, V. Pushkarev, A.J. Gellman, Carnegie Mellon University**

The kinetics and mechanisms of many catalytic surface reactions depend on the atomic level structure of surfaces. Detailed study and understanding of the influence of surface structure on a given reaction is experimentally arduous. The space of possible surface orientations spans a two-dimensional continuum. A detailed study of structure sensitive surface chemistry requires preparation and study of many different single crystal substrates, each with a different orientation. A new high-throughput methodology has been developed based on the use of Surface Structure Spread Single Crystals (S4C), spherically curved single crystals that expose a continuous distribution of different crystallographic planes across their surfaces. These S4C surfaces are being studied using surface analysis tools capable of spatially-resolved measurements that can sample the continuous space of surface orientations.

Six copper S4C surfaces have been produced in-house: three low Miller index centered surfaces, (100), (110), and (111); and three high Miller index surfaces, (821), (861), and (432). Each surface has been chosen and spherically curved so that the complete set of surfaces spans the entire stereographic triangle. The surfaces have been characterized using laser profilometry and oriented using x-ray diffraction and low energy electron



diffraction. A benefit of the S4C surfaces is that they are naturally chiral, forming regions of either R- or S- chirality. The surface chemistry of a chiral molecule, such as tartaric acid, on a naturally chiral surface can be enantiospecific. Tartaric acid decomposition from copper surfaces shows very high enantioselectivity due to its highly nonlinear surface explosion kinetics. The nature and magnitude of the enantioselectivity of tartaric acid decomposition across the stereographic triangle is not currently well-understood. Copper S4C surfaces provide an opportunity to study tartaric acid decomposition on virtually all possible copper surface structures. This research is the first attempt to map surface enantioselectivity for any compound across the entire stereographic triangle in high detail.

**3:00pm SS1-MoA4 Reaction Pathways of Alcohols with Transition Metal Oxides: A Comparison between  $\text{WO}_3$  and  $\text{MoO}_3$ , Z.J. Li, Y.K. Kim, R.J. Rousseau, B.D. Kay, Z. Dohnálek, Pacific Northwest National Laboratory**

The reactions of C1-C4 aliphatic alcohols over cyclic  $(\text{WO}_3)_3$  and  $(\text{MoO})_n$  (n ranges from 3 to 6) clusters were studied experimentally and theoretically using temperature-programmed desorption, infrared reflection-absorption spectroscopy, and density functional theory. Three reaction channels, dehydration, dehydrogenation, and condensation, have been identified on  $(\text{WO}_3)_3$  clusters while only dehydration and dehydrogenation have been observed on  $(\text{MoO}_3)_n$ . The desorption temperature of reaction products decreases with increasing alkyl chain length. The lack of a condensation channel on  $(\text{MoO}_3)_n$  is attributed to the lower reactivity of alcohols with  $(\text{MoO}_3)_n$  as compared to  $(\text{WO}_3)_3$  and consequently a negligible concentration of the Mo(VI) centers coordinated with two alkoxy species required for this reaction are formed. DFT calculations provide a detailed explanation for the reactivity and relative selectivity among the reaction channels and W(VI) and Mo(VI) metal centers.

This work was supported by the U.S. Department of Energy Office of Basic Energy Sciences, Division of Chemical Sciences, Biosciences and Geosciences, and was performed at EMSL, a national scientific user facility sponsored by the Department of Energy's Office of Biological and Environmental Research located at Pacific Northwest National Laboratory (PNNL). PNNL is operated for the U.S. DOE by Battelle Memorial Institute under contract no. DE-AC06-76RLO 1830. Computational resources were provided at EMSL and the National Energy Research Scientific Computing Center at Lawrence Berkeley National Laboratory.

**3:40pm SS1-MoA6 Molecular Dynamics Simulations of Oligomer Film Stabilization through Ion-Beam Deposition, T. Kemper, University of Florida, D. Lee, Lawrence Livermore National Laboratory, S.R. Phillpot, S.B. Sinnott, University of Florida**

Ion-beam deposition is used to stabilize conducting oligomer films for use in organic photovoltaic devices. The goal is to prevent structural changes caused by chemical attack, disorder, or desorption, that are known to degrade device performance. The second-generation reactive empirical bond-order (REBO) potential has been successfully applied to the irradiation and modification of crystalline, polymer and nanostructures, such as carbon nanotubes. In this work the atomic-level processes involved in selective modification of oligomers for optoelectronic applications through thermal energy particle deposition are explored to identify the mechanisms by which different polyatomic ions and radicals assist in the stabilization of oligomer films. In particular, oligomer films of polythiophene are bombarded with incident  $\text{H}$ ,  $\text{CH}_2$ ,  $\text{C}_2\text{H}$  and thiophene in the hyperthermal regime that involve incident energies of 4-50 eV. The results of classical molecular dynamics simulations with the REBO potential are compared to experimental findings, as well as linearly scaled density-functional theory molecular dynamics results. This work was supported by the NSF (CHE-0809376).

**4:00pm SS1-MoA7 Structure-Reactivity Relationships in the Electron Induced Reactions of Surface Bound Organometallics, H. Fairbrother, S. Rosenberg, J. Wnuk, Johns Hopkins University, C. Hagen, W. vanDorp, K. Landheer, Delft University of Technology, Netherlands**

Electron beam induced deposition (EBID) is a direct-write lithographic technique where volatile organometallic precursors are decomposed by a focused electron beam in a low vacuum environment to create metallic nanostructures. As a tool for nanofabrication, EBID offers an attractive and unique combination of capabilities including high spatial resolution and the flexibility to deposit free-standing three-dimensional structures without the need for resist layers. However, a major limitation of EBID is that nanostructures deposited from organometallic precursors typically possess unacceptable levels of organic contamination. To overcome this limitation it is crucial to develop a more detailed and fundamental understanding of how adsorbed organometallics undergo electron stimulated decomposition. Using a selected suite of organometallic precursors used in EBID ( $\text{CH}_3\text{CpPt}(\text{CH}_3)_3$ ,  $\text{Pt}(\text{PF}_3)_4$  and  $\text{W}(\text{CO})_6$ ) I will describe how a surface

science approach has been used to provide mechanistic and kinetic insights into EBID and to identify key structure-reactivity relationships. Central to our findings is the observation that for many organometallic precursors, EBID is initiated by the cleavage of a single metal-ligand bond and the release of the free ligand into the gas phase. However, subsequent electron stimulated reactions are characterized by decomposition rather than desorption of the residual ligands. Rationale design criteria for new organometallics which will decompose to produce metallic nanostructures with greater metallic purity have also been developed, such as the need to avoid using cyclopentadienyl ligands. In related studies we have also identified and rationalized the often significant effect that substrate temperature exerts on the composition of EBID materials created from organometallic precursors. Specifically, increased purity is expected for EBID films deposited at high substrate temperatures and low electron fluxes; the same conditions that reduce growth rates.

**4:20pm SS1-MoA8 Role of Substituents in Reactivity of Isocyanates Pre-Adsorbed on  $\text{Ge}(100)\text{-}2\times 1$ , K.T. Wong, S.F. Bent, Stanford University**

Direct attachment of organic molecules to semiconductor surfaces offers the ability precisely control interfacial properties through tailoring of the organic molecule. This study focuses specifically on organic functionalization of germanium, as the ability to control its interfacial properties may enable devices to take advantage of its favorable electronic properties, as compared to silicon. Past studies have shown that a number of isocyanate-containing molecules react with the  $\text{Ge}(100)\text{-}2\times 1$  surface in ultra-high vacuum by [2+2] cycloaddition across the C=N bond of the isocyanate. In this study, we use *in situ* Fourier transform infrared spectroscopy and X-ray photoelectron spectroscopy to investigate further reaction following [2+2] cycloaddition. Density functional theory calculations are also used to corroborate and help understand these experimental results. We show that phenyl isocyanate pre-adsorbed on  $\text{Ge}(100)\text{-}2\times 1$  is highly sensitive to subsequent exposure to water vapor. Experimental evidence suggests that water reacts with the adsorbed isocyanates to form a diphenyl urea compound, similar to what is expected for the reaction of phenyl isocyanate and water in solution. Extending the analogy with classic organic chemistry in solution, we find that addition of methyl or methoxy substituents to the phenyl ring of phenyl isocyanate can significantly decrease the adsorbed isocyanate's reactivity towards water. Such ability to easily tune the reactivity of an adsorbate-covered surface using principles from organic chemistry demonstrates the flexibility of organic functionalization and could be of importance when using organic functionalization for various applications.

**4:40pm SS1-MoA9 Investigation of Adsorbed Sodium Dodecyl Sulfate Films Formed on Charged and Hydrophilic Surfaces, S.-H. Song, T. Weidner, National ESCA and Surface Analysis Center for Biomedical Problems, M.S. Wagner, The Procter & Gamble Company, D.G. Castner, National ESCA and Surface Analysis Center for Biomedical Problems**

Surfactants are important compounds used in many industrial applications, with sodium dodecyl sulfate (SDS) being one of the most widely used surfactants. This study uses sum frequency generation (SFG) vibrational spectroscopy and surface plasmon resonance (SPR) sensing to investigate the structure of SDS films formed from the adsorption of SDS onto positively charged and hydrophilic surfaces. The surfaces studied included  $\text{CaF}_2$  as well as RF glow discharge deposited films of allylamine. The SDS films were prepared by adsorption of SDS from water solutions ranging in concentration from 0.067 to 20 mM. Since the water molecules above the SDS layer interact with the films, peaks from both the SDS molecules and water molecules were studied. SFG spectra of SDS adsorbed onto the positively charged  $\text{CaF}_2$  surface exhibits two well resolved  $\text{CH}_3$  peaks at 2877 and 2942  $\text{cm}^{-1}$ , and two OH peaks at  $\sim 3200$  and  $\sim 3400$   $\text{cm}^{-1}$ . At the 0.2 mM SDS concentration on the  $\text{CaF}_2$  surface the intensity of both the  $\text{CH}_3$  and OH peaks decrease to close to background levels and then increase as the SDS concentration is raised. As the SDS solution concentration continues to increase the  $\text{CH}_3$  and OH go through a second intensity minimum. This second intensity minimum occurs between 3-6 mM for the  $\text{CH}_3$  peaks and near 8 mM for the OH peaks. Previous studies have suggested these SFG intensity minima are due to the neutralization of positively charged  $\text{CaF}_2$  surfaces by the anionic charged head group of SDS (1). Since the shape and, thus, the phase of the SFG peaks are affected by the molecular environment, fits of the SFG data were used to quantify the orientation and alignment of the SDS layers across the wide range of SDS solution concentration. Since SFG is sensitive to both orientational order and the amount of material adsorbed we used SPR to determine the SDS coverage for the different solution concentrations in order to separate the two contributions. Combining SFG and SPR results provides a more detailed understanding of the structure and interactions of adsorbed SDS films.

(1) Becraft, K. A.; Moore, F. G.; Richmond, G. L. *Journal of Physical Chemistry B* **2003**, *107*, 3675.

5:00pm **SS1-MoA10 Photon Stimulated Desorption of the Sub-Nanometer Size Clusters of Water, Methane, Ethylene, and Their Mixtures, I. Arakawa, D. Matsumoto, S. Takekuma, R. Tamura, T. Miura, Gakushuin University, Japan**

Photon stimulated dynamics, such as desorption, dissociation, or chemical synthesis, at the water cluster which contains organic molecules have been studied in conjunction with the photochemistry at ice particles in cosmic space and in the atmosphere. In our experimental study, the clusters were prepared on the surface of a solid rare gas, which was condensed on the copper substrate cooled by liquid helium in an ultra high vacuum chamber. Our method has the advantage in controlling the cluster size and of high density of specimens in comparison with a molecular beam experiment. The clusters on the solid rare gas were excited by vacuum ultra-violet light with a photon energy between 12 and 108 eV with a pulse width of 10 ns, which was generated by a laser plasma light source [1]. The mass spectrum of photo-desorbed ions was measured by a time-of-flight (TOF) method. There are variety of species in the photo-desorbed ions from the co-adsorbed system of water and methane; protonated water clusters,  $(\text{H}_2\text{O})_n\text{H}^+$ , methane clusters,  $(\text{CH}_4)_n\text{CH}_k^+$ , hetero-clusters of water and methane,  $(\text{H}_2\text{O})_n(\text{CH}_4)_m\text{CH}_k^+$ , and synthesized species, methanol,  $\text{CH}_3\text{O}^+$ .

It was found that the presence of a water molecule in a cluster substantially enhanced, or was almost essential for, the desorption of any species, even for  $\text{CH}_3^+$  and  $\text{CH}_5^+$ , observed in the spectrum. Dissociation of the water molecule plays a key role in the chemical reaction in the clusters. It was also found that the desorption yield of each species showed strong dependence on the composition and the size of the mother cluster on the substrate, which were controlled by the amount of adsorption of water and methane. Close and systematic investigation of their correlation has revealed the mother cluster which yields the each desorbed ions:  $(\text{H}_2\text{O})(\text{CH}_4)$  clusters yield  $\text{CH}_3^+$ ,  $\text{CH}_4^+$ ,  $(\text{H}_2\text{O})\text{CH}_3^+$ , and  $\text{CH}_3\text{O}^+$  while  $(\text{H}_2\text{O})(\text{CH}_4)_2$  clusters yield  $\text{CH}_3^+$ ,  $(\text{H}_2\text{O})\text{CH}_3^+$ , and  $\text{C}_2\text{H}_4^+$ . These specific behaviors were also the case for the clusters of water and ethylene.

[1] T. Tachibana et al, Surf. Sci., **593**, 264-268 (2005).

5:20pm **SS1-MoA11 Nanobonding between 2-nm  $\beta$ -cristobalite  $\text{SiO}_2$  on OH(1x1)Si(100) and  $\text{SiO}_x$  for Monolithic Electronics by Surface Smoothing via Wet Chemical and Spin Processing: TMAFM Study and Modelling of Interphases, S.D. Whaley, ASU, N.X. Herbots, ASU / SiO2 NanoTech Inc. / SiO2 Associates, LLC, J.D. Bradley, SiO2 Associates LLC / ASU, R.J. Culbertson, M.A. Hart, D.A. Sell, Q.X. Bradley, ASU, R.L. Rhoades, S.N. Drews, Entrepix, Inc., R.B. Bennett-Kennett, ASU**  
 $\beta$ -cristobalite nanofilms, 2-nm thick, are nucleated on OH(1x1)Si(100) via the Herbots-Atluri (H-A) method [1,2] and form ultra-smooth, ordered, interphases that desorb at low temperatures ( $T < \sim 200^\circ\text{C}$ ) [3] These ordered oxide nanophases on OH (1x1)-Si(100) promote oxidation at low temperatures in ambient, when in contact with oxygen-deficient phases of  $\text{SiO}_2$  used in electronics. They can nucleate and grow a cross-bonding interphase between two substrates and achieve "nanobonding" [4] between various combinations Si and silica.

Nanobonding means forming cross-bonding molecules which condense into a continuous macroscopic bonding interphase between 2 smooth surfaces put into mechanical contact. For this to occur, the surfaces need to exhibit wide flat atomic terraces (width  $>10$  nm), low atomic step density ( $< 500$  steps/ $\mu\text{m}$  across atomic terraces direction) and very low particulate density (less than  $1/100 \mu\text{m}^2$ ). This contrasts with the typical density of surface steps ( $\sim 500$  steps/ $\mu\text{m}$  a.a.t.d.) and particulate density  $> \sim 0.1 - 1 \mu\text{m}^2$  in as received wafers or post-processing. A surface step density  $\geq 500$  step/ $\mu\text{m}$  a.a.t.d, typically found on Si(100) with miscuts  $< 0.025^\circ$  and particulates densities  $\geq 0.1 \mu\text{m}^2$  particulates results in 3-dimensional isolated bonding points of contacts as opposed to more uniform, 2-dimensional interphases that grow laterally as well as across is shown to occur in nanobonding. Wet chemical processing and SEZ spin technology are compared and combined to smmoth substrates via the H-A chemistry [1,2] via Tapping Mode Atomic Force Microscopy, before and after nanobonding. Our results show nanobonding can result in bonding strength larger than  $10 \text{ MPa/cm}^2$  as measured by mechanical bond pull tests. Wafers fracture within the bulk of both Si and silicate substrates rather than interfacial delamination.

[1] US Patent 6,613,677, issued 9/2/03 "Long range ordered semiconductor interface phase and oxides," 6,613,677, Herbots, N; Atluri, V. P.; Bradley J.D.; Swati, Banerjee; Hurst, Q.B.; Xiang, J.

[2] US patent 7,851,365 issued 12/14/10, "Methods for preparing semiconductor substrates & interfacial oxides there on" Herbots N., Bradley J.D., Shaw J.M., Culbertson and Atluri V.P.

[3] Patent Filed: 4/30/09, "Low Temperature Wafer Bonding and for Nucleating Bonding Nanophases. N. Herbots, R. J. Culbertson, J.D. Bradley, M. A. Hart, D. A. Sell and S. D. Whaley

[4] N. Herbots, Q. Xing, M. Hart, J. D. Bradley, D. A. Sell, R. J. Culbertson, Barry J. Wilkens; "IBMM of OH Adsorbates and Interphases

on Si-based Materials". Nucl. Instr. and Meth. in Phys. Res., B. IBMM 17<sup>th</sup> International Conference Proceeds (Aug, 2010), accepted

## Surface Science Division

### Room: 110 - Session SS2-MoA

## Molecular Ordering and Electrochemical Interfaces

Moderator: S.L. Tait, Indiana University

2:00pm **SS2-MoA1 Self-assembled Chains of 4,4'-azopyridine on Cu(100) Stabilized by Metal-Organic Coordination Interactions, H. Lim, S.L. Tait, Indiana University**

Understanding self-assembled molecular architectures at surfaces is essential to control and tune low-dimensional nanometer-scale organic structures. 4,4'-azopyridine (APY) has been vapor deposited on the clean Cu(100) surface in ultra-high vacuum and investigated using scanning tunneling microscopy and X-ray photoelectron spectroscopy. APY is chosen as a model building block for metal-organic frameworks, and for its conformational switching by the photoactive azo bridge. At low coverage, APY self-assembles into highly-ordered one-dimensional chains oriented along the low symmetry directions of the surface, many of which grow from the Cu step edges and some of which form tee junctions with other chains. Careful analysis of high resolution STM images points to pyridyl-Cu interactions being responsible for the high chain stability at room temperature. The related molecule, azobenzene, forms 1D chains on Au(111), but these grow side-to-side by hydrogen bonding at the azo bridge nitrogens and are only observed at cryogenic temperatures [1]. At higher coverages, APY chains align in a parallel fashion to form 2D islands, which increase in size with annealing.

[1] A. Kirakosian, M. J. Comstock, J. Cho, M. F. Crommie, *Phys. Rev. B* **71**, 113409 (2005).

2:20pm **SS2-MoA2 Molecular Self-assembly of Terephthalic Acid and Sodium Chloride on the Cu(100) Surface, D. Skomski, S. Abb, S.L. Tait, Indiana University**

To expand the catalogue of available interactions for the efficient self-assembly of highly-ordered nanoscale structures, we have investigated the formation of new supramolecular networks of terephthalic acid (TPA) and sodium chloride (NaCl) on the copper (100) surface. The mixture of this organic species with salt is prepared by vapor deposition in an ultra-high vacuum system and represents a model system for ionic self-assembly in two-dimensions. Several structures have been observed by means of scanning tunneling microscopy molecular resolution imaging. Chemical shifts in the sodium 1s photoelectron peak have been observed by X-ray photoelectron spectroscopy upon addition of TPA to the surface, confirming a direct interaction. Our research indicates that TPA and sodium produce new structures due to favorable ionic interactions between sodium cations and the negatively charged carboxylate groups in TPA's deprotonated form. Interactions with the metal surface and organic molecules appear to be sufficient to break the ionic bonds of the NaCl lattice. The formation of new TPA-Na structures illustrates the interplay between adsorbate-substrate and ionic interactions and opens new possibilities for ionic self-assemblies at surfaces with highly ordered structure and specific chemical function.

2:40pm **SS2-MoA3 Characterization of Azulene-Based Self-Assembled Monolayer Films, C.L. Berric, M. Barybin, B. Neal, A. Dela Rosa, University of Kansas**

Azulene has been predicted to have attractive electronic properties for potential use in molecular electronics applications. However, examples of self-assembled monolayers (SAM) of azulene-based molecules are rare. Characterization of a variety of azulene based SAM films has been carried out using ellipsometry, contact angle, FTIR, and AFM. The role of the functional linker group on the structural properties of the film as well as the electronic properties has been investigated. In addition, the interactions with gold surfaces of azulene-based molecules with different functional groups has been studied. Specifically, the competition between isocyanazulenes and mercaptoazulenes for binding at the Au(111) surface has been examined.

3:00pm **SS2-MoA4 Formation of Closed Shell Quantum Dots as a Driving Force for Molecular Ordering, L. Bartels, J. Wyrick, Z. Cheng, D. Sun, D. Kim, University of California, Riverside, T.L. Einstein, University of Maryland**

Anthraquinone self-assembles on Cu(111) into a giant honeycomb network with exactly three molecules on each side. Here we propose that the exceptional degree of order achieved in this system can be explained as a

consequence of the confinement of substrate electrons in the pores, with the pore size tailored so that the confined electrons can adopt a noble-gas-like two-dimensional quasi-atom configuration with two filled shells. Formation of identical pores in a related adsorption system (at different overall periodicity due to the different molecule size) corroborates this concept. A combination of photoemission spectroscopy with density functional theory computations (including van der Waals interactions) of adsorbate-substrate interactions allows quantum mechanical modeling of the spectra of the resulting quasi atoms and their energetics.

The resultant pores have about 4 nm in diameter. In this study we explore how the behavior of adsorbates inside them differs from that on extended terraces. CO molecules and adlayers exhibit properties under such nanoscale confinement that markedly depart from those of extended adlayers: a) the confinement stabilizes dislocation lines (anti-phase domain boundaries) in the adlayer that affect roughly  $\frac{1}{4}$  of the adsorbed molecules; b) confinement prevents the formation of dense islands of adsorbed molecules, depending on coverage either causing dispersion of vacancies in the adlayer or preventing the growth of molecular islands; c) at a coverage of just a few molecules on the facet, we observe that a molecular shell structure is formed, resembling in its underlying mathematics the atomic model. Confined structures are an ideal test bed for measurement of the coverage dependence of molecular diffusion and in this study we find a reduction of the diffusion barrier at a slope of 57%/ML.

### 3:40pm SS2-MoA6 Redox Activity and Structural Transitions at Electrochemical Interfaces, K.R. Wandelt, University of Bonn, Germany INVITED

Ordered layers of organic molecules play an increasing role in modern material science. Their electrochemical deposition from solution has several important advantages: i) Thermally unstable organic molecules which are not intact volatile may be deposited under mild conditions, ii) unlike vacuum deposition electrochemical adsorption may be performed near equilibrium, and iii) the electrochemical potential is an extra parameter which enables a controlled switching of the redox-state of the adsorbed molecules and, thereby, structural transitions of the layers. This lecture concentrates on the correlation between redox-activity and structural properties of viologen and porphyrin layers at metal – electrolyte interfaces. The selfassembly of the molecules is studied as a function of i) the nature and symmetry of the substrate (Cu(111), Cu(100), Au(111) and Cu/Au(111)), ii) the nature of the accompanying counter ions (Cl, Br, I, SO<sub>4</sub>), iii) the concentration of the solution, and, most importantly, iv) the potential dependent redox state of the adsorbed molecules, by using in-situ ElectroChemical Scanning Tunneling Microscopy (EC-STM), in-situ Infrared Reflection Absorption Spectroscopy (IRRAS) as well as ex-situ Synchrotron X-ray Photoelectron Spectroscopy (SXPS) after air- and contamination-free transfer from the solution into the UHV analysis chamber. The lecture not only provides a deep insight into the properties of the investigated model systems but also demonstrates the status of modern electrochemical surface science.

### 4:20pm SS2-MoA8 Influence of Solvent on the Chiral Resolution of Organic Molecules on Au(111): EC-STM Study of Biphenyl Dicarboxylic Acid on Au (111) in an Aqueous Environment, B.I. Kim, J.A. Hanson, M.W. Turner, L.J. Reeder, Boise State University

Adsorption induced chiral resolution of organic molecules is important due to its potential applications in stereo-selective catalysis. We studied the adsorption induced chiral resolution using a model achiral molecule of 4,4' biphenyl dicarboxylic acid (BPDA) on Au (111) in 0.1 M perchloric acid (HClO<sub>4</sub>) by scanning tunneling microscopy (STM). The BPDA molecules are known to have chiral resolution on Au(111) in an ultrahigh vacuum (UHV). However, our experimental data show that the molecules form island structures with distinctive preferred orientations at the length scale of the molecular size, whereas they have no orientation order at the length scale bigger than the molecular size. We calculated angle dependent binding energy between the substrate and a BPDA molecule, the intermolecular interactions between the BPDA molecules and their interactions with water molecules. The calculation suggests that the absence of chiral resolution in the aqueous environment may originate from the increase of effective rotation energy barrier of the BPDA molecules due to its hydrogen bonding with the surrounding water molecules. The strength hydrogen binding between BPDA molecules is sufficient to overcome the energy barrier for chiral resolution through rotational motion in UHV, but not in an aqueous environment.

### 4:40pm SS2-MoA9 Surface and Interface Forces between Dissimilar Surfaces in Aqueous Solution: The Effect of Electrochemical Surface Potentials, Surface Roughness and Hydration Layers, M. Valtiner, K. Kristiansen, G.W. Greene, J.N. Israelachvili, University of California, Santa Barbara

With the rapid progress in the design and fabrication of micro- and nanometer-scaled devices at smaller and smaller length scales, a fundamental understanding of, and the ability to control the interfacial interactions between materials across ultra small distances plays a critical role in advancing these technologies. The ability to 'tune' the forces in various device components remains a critical hurdle to optimizing device performance and reliability of, for example nanofluidic and lab-on-a-chip systems, aqueous-based MEMS, sensor devices; as well as devices where adhesion and adsorption can be controlled, surface contacts and wetting properties tuned, and single molecules and bi-layer interactions manipulated. Surface morphology (including roughness) and electrostatic potential-dependent interaction forces significantly affect the physical and mechanical properties of surfaces and play a critical role in all of these systems.

We present novel setups for both an improved electrochemical AFM [1] and a newly developed electrochemical surface force apparatus [2], and compare the two techniques. We describe the results of the first surface force measurements under electrochemical potential control between a metal and a ceramic surface across a liquid medium (water). Our experiments also reveal how increasing levels of surface roughness and dissimilarity in the surface potentials of the interacting surfaces influence the strength and range of electric double layer, van der Waals, hydration, and steric forces, and how these contribute to deviations from DLVO theory, particularly at distances less than two Debye lengths, or 2-3 times the rms roughness, whichever is greater.

[1] Markus Valtiner, G. Anka, A. Bashir and F. Renner, *Rev. Sci. Instrum.* **82**, 023703 (2011)

[2] Markus Valtiner, Kai Kristiansen, George W. Greene, Jacob N. Israelachvili, *Advanced Materials*, DOI: 10.1002/adma.201003709 (2011)

### 5:00pm SS2-MoA10 Diffusion of Single Water and Hydrogen Sulfide Molecules on Ag(111): A DFT Study, D.-J. Liu, Ames Laboratory - US DOE

Diffusion of water (H<sub>2</sub>O) and hydrogen sulfide (H<sub>2</sub>S) on metal surfaces can be more complicated than single adatom diffusion, even for simple hopping mechanism. Additional degree of freedom, such as rotation and tilting of the molecule, must be considered. Due to the asymmetry of the molecule, and therefore the potential energy surface, the saddle points generally deviate from any high symmetry adsorption site. We carry out a systematic study based on the density-functional theory for diffusion of H<sub>2</sub>O and H<sub>2</sub>S on Ag(111). For both molecules, the most stable configuration for adsorption is nearly flat and on top of a Ag atom. As it approaches the bridge site, the molecule can tilt, and in the case of H<sub>2</sub>S, also rotate, to lower its energy. We also find that in this case, zero point vibrations contribute significantly to diffusion of the molecule.

### 5:20pm SS2-MoA11 The Structure of Methylthiolate and Ethylthiolate Monolayers on Au(111): Absence of the ( $\sqrt{3}\times\sqrt{3}$ )R30° Phase, L. Tang, University of Birmingham, UK, F. Li, University of Birmingham, UK & Northwestern Polytechnical Univ., P.R. China, W. Zhou, Northwestern Polytechnical Univ., P.R. China, Q. Guo, University of Birmingham, UK

Surface structures of self-assembled methylthiolate and ethylthiolate monolayers on Au(111) have been imaged with STM. For saturation coverage at room temperature, the well-known ( $\sqrt{3}\times\sqrt{3}$ )R30° phase routinely observed for longer chain alkanethiolates does not appear under any conditions for adsorbed methylthiolate and ethylthiolate. Instead, both thiolate species organize themselves into a well-ordered 3×4 structure with a coverage equal to 0.33 ML. We thus conclude that the stable structure for saturation coverage of methylthiolate/ethylthiolate on Au(111) at RT is 3×4, not ( $\sqrt{3}\times\sqrt{3}$ )R30° as generally believed.

We performed experiments by imaging methylthiolate and ethylthiolate monolayers in ultra-high-vacuum (UHV) using high-resolution STM. The methylthiolate monolayer was prepared by exposing a gold single crystal in vacuum to 10<sup>-8</sup> mbar of dimethyl disulfide (DMDS) vapour at RT for 15 minutes. It is known that DMDS adsorb dissociatively on Au(111) at RT by forming methylthiolate. Ethylthiolate monolayer was prepared by exposing a (111) oriented gold film to 5×10<sup>-5</sup> mbar of ethanethiol vapor at room RT for 2 hours. The much higher exposure required for ethanethiol is due to the very low dissociation probability of this molecule.

When the 3×4 phase is subjected to a gentle thermal annealing to 320 K, partial desorption takes place and a striped phase with coverage equal to 0.27 ML appears. The striped phase for ethylthiolate resembles that observed for propylthiolate and other long chain thiolates, but the striped

phase for the methylthiolate takes a unique structure of its own. Our findings suggest that the general belief that all alkanethiols form at least one common structural phase is not true and new theoretical modeling is urgently required to address the chain-length dependent property of alkanethiol monolayers.

# Tuesday Morning, November 1, 2011

## In Situ Spectroscopy and Microscopy Focus Topic Room: 106 - Session IS+AS+SS-TuM

### In Situ Studies of Organic and Soft Materials and Liquid-Solid Interfaces

Moderator: A.I. Frenkel, Yeshiva University

8:00am **IS+AS+SS-TuM1 Solid-Vacuum, Solid-Gas, and Solid-Liquid Interfaces: Structure and Dynamics under Environmentally Relevant Conditions**, *M. Salmeron, C. Escudero*, Lawrence Berkeley National Laboratory **INVITED**

Surfaces play a fundamental role in many of today's frontier topics, such as clean and renewable energies, efficient and highly selective chemical processes (green catalysis), high capacity rechargeable batteries and fuel cells, and also environmental problems. To advance our For this it is imperative to develop new fundamental approaches to the study of the interface of solid materials with gases, liquids and solids, because it is in these environments that crucial processes occur that need to be understood to enable game-changing discoveries.

One way to control the structure of interfaces and their properties is through the design of materials of nanoscale dimensions, with specific shape, size and composition. It is equally imperative to develop and use techniques for in situ atomic level structural and spectroscopic characterization of the interfaces. New advances in instrumentation are fulfilling this need. I will illustrate this with examples from research carried out in my laboratory, which include scanning tunneling microscopy (STM), photoelectron and x-ray absorption spectroscopies (PES) under ambient conditions, for studies of catalyst models, thin films, single crystals and nanoparticles, for applications in catalysis and electrochemistry. The results obtained so far demonstrate that the information obtained with these new techniques is unique and could not have been obtained or extrapolated from other more traditional surface sensitive techniques.

8:40am **IS+AS+SS-TuM3 Imaging Tagged Proteins in Whole Eukaryotic Cells in Liquid with Scanning Transmission Electron Microscopy**, *N. De Jonge, D.B. Peckys*, Vanderbilt University School of Medicine **INVITED**

We have recently introduced a novel electron microscopy technique for the imaging of whole cells in aqueous media using scanning transmission electron microscopy (STEM) [1, 2]. Eukaryotic cells in liquid were placed in a microfluidic chamber with a thickness of 5 - 10  $\mu\text{m}$  contained between two ultra-thin electron-transparent windows. On account of the atomic number (Z) contrast of the STEM, nanoparticles of a high-Z material (e.g., gold) were detected within the background signal produced by a micrometers-thick layer of a low-Z liquid (e.g. water, or cellular material). Nanoparticles specifically attached to proteins can be used to study protein distributions in whole cells in liquid, similar as proteins tagged with fluorescent labels can be used to study protein distributions in cells with fluorescence microscopy.

COS7 fibroblast cells were labeled with gold nanoparticles conjugated with epidermal growth factor (EGF). Intact fixed cells in liquid were imaged with STEM with a spatial resolution of 4 nm and a pixel dwell time of 20 microseconds [1]. In test experiments we demonstrated a maximal spatial resolution of 1.5 nm on gold nanoparticles placed above a water layer of a thickness of 3 micrometer, consistent with theoretical predictions, and with Monte Carlo simulations of the STEM imaging [3]. The use of quantum dots (QDs), which are fluorescent nanoparticles, allowed STEM images to be correlated with fluorescence images [4]. Eukaryotic cells were grown directly on microchips for the microfluidic chamber, fixed, and imaged with fluorescence microscopy. The intact cells were then imaged in liquid with STEM. The STEM images showed individual QDs, and their locations were correlated with the cellular regions, as imaged with fluorescence microscopy. We have also demonstrated the imaging of nanoparticle uptake in live cells [5], and the ultrastructure of pristine yeast cells was studied [6]. Liquid STEM presents an innovative approach for the imaging of whole cells, with significantly improved spatial resolution and imaging speed over existing methods.

URL: <http://www.mc.vanderbilt.edu/labs/dejongelab/>

#### References

- [1] de Jonge, N., Peckys, D.B., Kremers, G.J. & Piston, D.W., Proc. Natl. Acad. Sci. 106, 2159-2164, 2009.
- [2] Peckys, D.B., Veith, G.M., Joy, D.C. & de Jonge, N., PLoS One 4, e8214-1-7, 2009.

[3] Dukes, M.J., Peckys, D.B. & de Jonge, N., ACS Nano 4, 4110-4116, 2010.

[4] de Jonge, N., Poirier-Demers, N., Demers, H., Peckys, D.B. & Drouin, D., Ultramicroscopy 110, 1114-1119, 2010.

[5] Peckys, D.B. & N. de Jonge, Nano Lett. 11, 1733-1738, 2011.

[6] Peckys, D.B., Mazur, P., Gould, K.L. & de Jonge, N., Biophys. J., in press, 2011.

9:20am **IS+AS+SS-TuM5 Imaging Live Cells in Liquid with Scanning Transmission Electron Microscopy**, *D.B. Peckys, N. De Jonge*, Vanderbilt University School of Medicine

We have applied a novel electron microscopy technique, referred to as liquid scanning transmission electron microscopy (liquid STEM) [1, 2] for the imaging of live eukaryotic cells. In two separate experiments, we studied a) nano particle (NP) uptake in COS-7 cells [3], a green monkey kidney fibroblast cell line, and, b) the ultrastructure of *Schizosaccharomyces pombe* cells [4], also known as fission yeast. The cells were confirmed to be alive at the onset of the liquid STEM imaging using specific fluorescent, live indicating dyes and correlative fluorescence microscopy. For the STEM imaging in liquid the cells were placed (in liquid) in a microfluidic chamber. The chamber had two ultra-thin electron-transparent windows allowing the passage of electrons and photons. The dimensions of the COS-7 cells required a thicker liquid filled space in the microfluidic chamber compared to the experiments with the fission yeast cells, and contrast was mainly obtained on the gold NP's. However, the thinner *S. pombe* cells allowed a thinner liquid layer, and images were recorded of the cellular ultrastructure.

Despite the fact, that the cells were not anymore alive after the STEM imaging, we consider the first STEM images taken from a cell or a specific cellular region, to represent the unperturbed and therefore physiological state. We derived this assumption after evaluation of the STEM images for signs of radiation damage at the achieved resolution. Our STEM results were found to be consistent with known data about intracellular NP trafficking and storage in mammalian cells and data about the dimensions and distribution of organelles in fission yeast.

In conclusion, we have demonstrated the feasibility of STEM imaging live eukaryotic cells. The advantages of this approach are a) a several-fold higher resolution than live cell imaging with conventional light microscopy, b) a much faster (hours versus days) sample preparation than needed for conventional transmission electron microscopy (TEM) imaging of cells, c) absence of artifact introduction associated with conventional TEM sample preparation, and d) no need for introducing any kind of labels in order to achieve a similar range of resolution as possible with the new nanoscopic imaging techniques.

#### References

[1] de Jonge, N., Peckys, D.B., Kremers, G.J. & Piston, D.W., Proc. Natl. Acad. Sci. 106, 2159-2164, 2009.

[2] Peckys, D.B., Veith, G.M., Joy, D.C. & de Jonge, N., PLoS One 4, e8214-1-7, 2009.

[3] Peckys, D.B. & N. de Jonge, Nano Lett. 11, 1733-1738, 2011.

[4] Peckys, D.B., Mazur, P., Gould, K.L. & de Jonge, N., Biophys. J., in press, 2011.

9:40am **IS+AS+SS-TuM6 Microscopic Imaging of Biological Samples using Coherent Soft X-rays from Free-Electron Laser and Synchrotron Sources**, *T. Gorniak, T. Senkbeil, M. Beckers, C. Christophis*, University of Heidelberg, Germany, *K. Giewekemeyer*, University of Göttingen, Germany, *M. Grunze*, University of Heidelberg, Germany, *T. Salditt*, University of Göttingen, Germany, *A. Rosenhahn*, University of Heidelberg, Germany

Coherent X-ray microscopy of hydrated biological samples – especially in the so-called water window of 284-540 eV – is of tremendous interest for life sciences due to the high contrast of organic matter with respect to the aqueous background. Especially free-electron lasers can provide highly intense and coherent pulses, which allow single pulse imaging to overcome resolution limits set by radiation damage. We present the first holographic microscopy images of dehydrated biological material acquired in the water window with higher harmonic radiation provided by the free-electron laser FLASH. In order to increase the photon flux we used high efficiency zone plates instead of pinholes to create the divergent light cone for holography. The results pave the way to the vision of holographic imaging of hydrated biological samples with single FEL pulses. We supplement single pulse imaging experiments byptychographic imaging with synchrotron radiation at BESSY II. This method uses coherent diffraction imaging at different

sample positions while maintaining a fixed spatial overlap between the fields of view. By introducing this spatial redundancy to the data an additional constraint for the iterative reconstruction algorithm is achieved. This enhances the convergence of phase retrieval drastically. The spatial resolution of below 50 nm and the imaging properties were characterized using lithographic and biological test samples. We also show results on resonant imaging with chemical contrast caused by both, absorption and phase shifts, in the vicinity of core level absorption edges.

10:40am **IS+AS+SS-TuM9 Surface Chemistry of Amino Acids at Near Ambient Pressure of Water Vapor**, *A. Shavorskiy*, Lawrence Berkeley National Laboratory, *T. Eralp*, The University of Reading, UK, *F. Aksoy*, Nigde University, Turkey, *M.E. Grass*, *Z. Liu*, *H. Bluhm*, Lawrence Berkeley National Laboratory, *G. Held*, The University of Reading, UK

The co-adsorption of water with organic molecules under near-ambient pressure and temperature conditions opens up new reaction pathways on model catalyst surfaces that are not accessible in conventional ultra-high vacuum surface-science experiments. The surface chemistry of glycine and alanine at the water-exposed Cu{110} and Pt{111} interface was studied both in situ and in UHV using ambient-pressure photoemission and X-ray absorption spectroscopy techniques [1,2]. At water pressures above 10<sup>-5</sup> Torr a significant pressure-dependent decrease in the temperature for dissociative desorption was observed for both amino acids on Cu{110}[3]. On Pt{111}, on the other hand, desorption temperature does not depend significantly on the presence of water vapor. The most likely reaction mechanism of decomposition involves dehydrogenation induced by O and/or OH surface species resulting from the dissociative adsorption of water on Cu{110}, but not on Pt{111}.

The linear relationship between the inverse decomposition temperature on Cu{110} and the logarithm of water pressure enables determination of the activation energy for the surface reaction, between 213 and 232 kJ/mol, and a prediction of the decomposition temperature at the solid-liquid interface by extrapolating towards the equilibrium vapour pressure. Such experiments near the equilibrium vapour pressure provide important information about elementary surface processes at the solid-liquid interface, which can neither be retrieved under ultra-high vacuum conditions nor from interfaces immersed in a solution.

[1] H. Bluhm, et al. *J. El. Spec. Rel. Phenomena* 150 (2006) 86.

[2] G. Jones, L. B. Jones, F. Thibault-Starzyk, E.A. Seddon, R. Raval, S. Jenkins, G. Held, *Surf. Sci.* 600 (2006) 1924.

[3] A. Shavorskiy, F. Aksoy, M.E. Grass, Z. Liu, H. Bluhm, G. Held, *J. Am. Chem. Soc.* 133 (2011) 17

11:00am **IS+AS+SS-TuM10 STM Tip Catalyzed Adsorption of Thiol Molecules and Functional Group-Selective Adsorption of Bi-Functional Molecule Using This Catalysis**, *Y.H. Min*, *S. Kim*, *S.J. Jung*, *Y.-S. Youn*, Korea Advanced Institute of Science and Technology, Republic of Korea, *D.H. Kim*, Daegu University, Republic of Korea, *E.H. Park*, Korea Advanced Institute of Science and Technology, Republic of Korea

In this study, in contrast with cases in which Scanning Tunneling Microscopy (STM) tip-induced reactions were instigated by the tunneling electrons, the local electric field, or the mechanical force between a tip and a surface, we found that the tungsten oxide (WO<sub>3</sub>) covered tungsten (W) tip of a STM acted as a chemical catalyst for the S-H dissociative adsorption of phenylthiol and 1-octanethiol onto a Ge(100) surface. By varying the distance between the tip and the surface, the degree of the tip-catalyzed adsorption could be controlled. We have found that the thiol head-group is the critical functional group for this catalysis and the catalytic material is the WO<sub>3</sub> layer of the tip. After removing the WO<sub>3</sub> layer by field emission treatment, the catalytic activity of the tip has been lost.

3-mercapto isobutyric acid is bi-functional molecule which has two functional groups, carboxylic acid group and thiol group, at each end. 3-Mercapto Isobutyric Acid adsorbs at Ge(100) surface only through carboxylic acid group at room temperature and this adsorption was enhanced by the tunneling electrons between a STM tip and the surface. Using this enhancement, it is possible to make thiol group-terminated surface where we desire. On the other hand, surprisingly, the WO<sub>3</sub> covered W tip of STM was found to act as a chemical catalyst to catalyze the adsorption of 3-mercapto isobutyric acid through thiol group at Ge(100) surface. Using this catalysis, it is possible to make carboxylic acid group-terminated surface where we want. This functional group-selective adsorption of bi-functional molecule using the catalysis may be used in positive lithographic methods to produce semiconductor substrate which is terminated by desired functional groups.

Min, Y. H.; Jung, S. J.; Youn, Y. -S.; Kim, D. H.; Kim, S. *J. Am. Chem. Soc.* 2010, 132, 9014.

11:20am **IS+AS+SS-TuM11 CO<sub>2</sub> Capture in Aqueous Monoethanolamine Solutions: Role of the Solution Interface Investigated with X-ray Photoelectron Spectroscopy**, *T. Lewis*, University of California, Irvine, *B. Winter*, Helmholtz-Zentrum Berlin für Materialien und Energie, Germany, *M. Faubel*, Max-Planck-Institut für Dynamik und Selbstorganisation, Germany, *J.C. Hemminger*, University of California, Irvine

Aqueous monoethanolamine (MEA) solutions are commonly used to capture CO<sub>2</sub> emitted into the atmosphere from industrial processes. It is likely that interactions between MEA and CO<sub>2</sub> at the aqueous solution surface are important to this process, yet surprisingly very few studies have explicitly addressed the role of the solution-gas interface. In the present study, interfacial chemistry of CO<sub>2</sub> capture is studied by surface sensitive photoelectron spectroscopy measurements from a liquid microjet of CO<sub>2</sub>-reacted MEA solutions with carbon loadings of 0.1 to 0.9 mol/mol. These experiments determine the spatial distribution of MEA and reaction products into the solution as a function of CO<sub>2</sub> loading. Results show that neutral MEA exhibits a propensity for the solution surface, whereas protonated MEA and reaction products prefer bulk solvation, suggesting enhanced reactivity at the solution interface, especially at high CO<sub>2</sub> loading. These observations indicate that a detailed understanding of the chemistry of CO<sub>2</sub> at the liquid/vapor interface and interface to bulk transport of the products will be important in understanding CO<sub>2</sub> capture.

11:40am **IS+AS+SS-TuM12 Fundamental Aspects of Organic Heterostructure Formation Examined using Supersonic Molecular Techniques and In Situ Real Time X-ray Synchrotron Radiation**, *E.R. Kish*, *T.V. Desai*, *A.R. Woll*, *J.R. Engstrom*, Cornell University

Over the past several years significant advances have been made concerning our understanding of the growth of crystalline small molecule organic thin films consisting of a single component. An important challenge in organic electronics, photonics and photovoltaics is to develop and improve methods to integrate both *p*-type and *n*-type small molecule organic semiconductors into the same device microstructure. Thus, developing an understanding of the molecular scale events that lead to heterojunction formation is essential in these systems consisting of multiple components. Here we report on our examinations of the nucleation, growth, and dynamics of adsorption of a *n*-type organic semiconductor, *N,N*-ditridecylperylene-3,4,9,10-tetracarboxylic diimide (PTCDI-C<sub>13</sub>), on SiO<sub>2</sub> surfaces modified by self-assembled monolayers (SAMs) and on a pre-deposited monolayer of pentacene (a *p*-type semiconductor) using supersonic molecular beam techniques, *in situ* synchrotron x-ray scattering and *ex situ* atomic force microscopy. From real-time x-ray scattering we find that PTCDI-C<sub>13</sub> exhibits prolonged layer-by-layer growth for approximately the first 10 monolayers (MLs) of deposition on all three SAMs examined. Concerning the kinetics of growth we find that the adsorption probability of PTCDI-C<sub>13</sub> on itself is similar to that observed on two SAMs that possess aromatic endgroups, but it differs significantly to that observed on a relatively short, methyl-terminated SAM. These differences could reflect mechanisms such as direct molecular insertion of PTCDI-C<sub>13</sub> into either the existing PTCDI-C<sub>13</sub> film, or the longer chain SAMs with aromatic endgroups. Concerning growth in the submonolayer regime, we find that nucleation is homogeneous, and that the absolute density of islands depends on the nature of the surface, while the relative change of the island density with increasing growth rate is essentially independent of the underlying SAM. From the latter we find that a critical island size of a single molecule of PTCDI-C<sub>13</sub> can describe all the data. Finally, we will discuss our most recent results concerning the growth of heterostructures composed of a few to several monolayer stacks of PTCDI-C<sub>13</sub> and pentacene. In this work we find that PTCDI-C<sub>13</sub> grows in a smooth layer-by-layer fashion on pentacene, but the opposite is not true—pentacene grows in a purely 3D mode when deposited on PTCDI-C<sub>13</sub>. We will discuss the implications of this observation concerning the growth of organic heterostructures for applications in electronics, photonics and photovoltaics.

## Surface Science Division

Room: 109 - Session SS1-TuM

## Chemisorption & Surface Reactions

Moderator: D.A. Chen, University of South Carolina

8:00am **SSI-TuM1 XANES and EXAFS Analysis of the Effects of Cobalt Incorporation Into Silica Supports for Fischer-Tropsch Synthesis**, *B.M. Goundie*, *I.T. Ghampson*, *M.C. Wheeler*, *W.J. DeSisto*, *B.G. Frederick*, *R.W. Meulenberg*, University of Maine

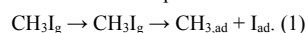
The growing need for non-petroleum based fuel sources has led to an increase in research into Fischer-Tropsch synthesis (FTS), which can be

used to convert biomass into fuels. We have developed several silica supported cobalt catalysts to investigate the role of pore size on phase and reactivity. Cobalt based catalysts produce high molecular weight hydrocarbons in FTS, and there has been increased research into the characterization of such catalysts. The catalysts have been previously characterized using several techniques including x-ray diffraction (XRD), nitrogen porosimetry, and transmission electron microscopy/selected area diffraction (Ghampson IT, et al. Effects of pore diameter on particle size, phase, and turnover frequency in mesoporous silica supported cobalt Fischer-Tropsch catalysts. *Applied Catalysis A – General*. 2010; 388(1-2)).

In this presentation we will discuss x-ray absorption near edge structure (XANES) and extended x-ray absorption fine structure (EXAFS) measurements of three different MCM-41 supported cobalt catalysts. These materials include incorporation of cobalt into the silica framework (Co-MCM-41), and cobalt impregnated catalysts, via wet impregnation, onto the pure (Co/MCM-41) and cobalt in the framework (Co/Co-MCM-41) supports. We analyzed the XANES and EXAFS at three different stages in the catalyst history: after calcination, after temperature programmed reduction, and after Fischer-Tropsch synthesis. Evidence suggests that the presence of cobalt in the framework affects the reducibility of the cobalt species. The data also suggests mixed phases of cobalt metal and cobalt monoxide in the reduced and post FTS samples. The as prepared samples show only the Co<sub>3</sub>O<sub>4</sub> phase, while the post FT and post TPR show both CoO and Co metal. The good agreement between XAS and XRD measurements demonstrates the use of these techniques to quantitatively determine the cobalt phase composition.

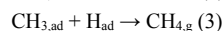
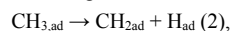
8:20am **SS1-TuM2 Measurement of the C-Pt Bond Energy for Adsorbed Methyl on Pt(111) by Methyl Iodide's Dissociative Adsorption Energy**, E.M. Karp, T.L. Silbaugh, C.T. Campbell, University of Washington

Knowing the bond energies of molecular fragments adsorbed to surfaces is an important ingredient in the fundamental understanding needed for rational design of heterogeneous catalysts. This study utilizes the ultrahigh vacuum technique of single crystal adsorption calorimetry to study the energetics of adsorbed methyl (CH<sub>3,ad</sub>) on Pt(111), using measurements of the dissociative adsorption energy of methyl iodide (CH<sub>3</sub>I) on Pt(111). At temperatures above 250 K, adsorbed CH<sub>3</sub>I on Pt(111) is known to undergo C-I bond scission to form CH<sub>3,ad</sub> and adsorbed iodine (I<sub>ad</sub>). At 270 K, the rate of C-I scission is fast relative to the 100 ms time of calorimetric measurement, so that it provides the enthalpy for the net, two-step dissociative adsorption reaction:



The integral heat of Reaction (1) is -224 kJ/mol at a coverage of 0.05 ML. Through the use of a simple thermodynamic cycle and other known adsorption energies, this provides a heat of formation of CH<sub>3,ad</sub> of -63 kJ/mol and a Pt-CH<sub>3</sub> bond energy of 209 kJ/mol.

Mass spectrometer measurements taken during experiments at 300 K and 320 K indicate that methane is produced. Previous studies indicate that at these temperatures, adsorbed methyl both decomposes to form adsorbed methylene (CH<sub>2,ad</sub>) and hydrogen (H<sub>ad</sub>) and reacts with H<sub>ad</sub> to form methane according to the reactions :



where CH<sub>4,g</sub> is gas phase methane. The microcalorimetric measurements performed at 300 K and 320 K, along with information on the rates of Reactions (2) and (3) available in the literature, allowed for the decoupling of Reactions (1)-(3) and an analysis of the energetics of all three reactions as a function of surface coverage, and the heat of formation of CH<sub>2,ad</sub>.

8:40am **SS1-TuM3 A DFT Study of Methanol Reaction Pathways on the Au<sub>13</sub>/TiO<sub>2</sub>(110) Surface**, S. Hong, University of Central Florida, D.A. Chen, University of South Carolina, T.S. Rahman, University of Central Florida

We have performed density functional theory calculations to understand the reaction pathway selection for methanol decomposition on clean and Au<sub>13</sub> deposited TiO<sub>2</sub>(110) surface. We find that when methanol adsorbs on the *clean* and *reduced* TiO<sub>2</sub>(110) surface, it decomposes spontaneously into methoxy, which adsorbs on the O-vac site and desorbs as methyl leaving behind O-br on the TiO<sub>2</sub>(110) surface. On the *stoichiometric* TiO<sub>2</sub>(110) surface, we find that while methanol decomposition has a small activation energy of 0.2 eV, methoxy decomposition (i.e. formaldehyde formation) is not possible because of high activation energy of 3 eV. Nevertheless, once the surface is oxidized formaldehyde formation becomes *spontaneous*, through C-H bond scission by surface oxygen species. These results confirm the experimental results of methyl formation on the *reduced* and formaldehyde formation on the *oxidized* TiO<sub>2</sub>(110) surface. Turning to the

case of partially reduced Au/TiO<sub>2</sub>(110) surface, our DFT calculations show that the adsorption of methanol and its intermediate methoxy does not occur on gold sites but on TiO<sub>2</sub> sites. Methoxy, in fact, forms at the Au-titania interface as a result of O-H bond scission by lattice oxygen (O-br), and its optimized tilted structure makes C-H bond scission -- through H abstraction by lattice oxygen near the interface site -- much easier than that for a vertical, non-tilted structure of methoxy in a non-interfacial site. Moreover, depending on the reduction level of the TiO<sub>2</sub>(110) surface, the adsorption site preference for methanol and methoxy species on the Au/TiO<sub>2</sub>(110) surface is: O-vac > interfacial Ti-cus > stoichiometric Ti-cus site. This hierarchy implies that the major product will switch from methyl on the fully-reduced surface, to formaldehyde on the partially-reduced or oxidized Au/TiO<sub>2</sub>(110) surface. This conclusion is in full agreement with experiment.

This work is supported in part by US-DOE under Grant No. DEFG02-07ER15842.

9:00am **SS1-TuM4 Turning Aluminum into a Noble-metal like Catalyst for Low Temperature Molecular Hydrogen Activation**, I. Chopra, University of Texas at Dallas, S. Chaudhuri, Washington State University, J.F. Veyan, Y.J. Chabal, University of Texas at Dallas

There has been an ongoing quest to find cheaper hydrogen activation routes based on aluminum. Despite theoretical suggestions<sup>1,2</sup> it has been difficult to obtain unambiguous experimental evidence for such catalytic activity towards hydrogen activation.

We demonstrate here that aluminum doped with very small amounts of Ti can activate molecular hydrogen at temperatures as low as 90K. The method is based on the ability to introduce a high flux of molecular hydrogen seeded with a *guest molecule to probe the catalytic activity and H<sub>2</sub> dissociation*. Once dissociated, hydrogen forms a complex with adsorbed CO (CO-H), characterized by a substantially and uniquely blue-shifted CO internal frequency. This complex is metastable, and is removed at a temperature (115K). We find that CO does not adsorb even weakly on H-covered Al, and use this finding to clearly show that, once dissociated, hydrogen diffuses away from the catalytic site onto Al sites (i.e. spills over). We use this new method to determine the dependence of the catalytic activity of aluminum surfaces on Ti coverage. Finally we show that the complex with activated hydrogen leads to further reactions at remarkably low temperatures (115K), such as formation of formyl (HCO), formaldehyde (HCHO) or methanol. These results provide the first direct evidence that Ti-doped Al can perform the quintessential first step of molecular hydrogen activation under nearly barrier-less conditions, thereby challenging the monopoly of noble metals in hydrogen activation.<sup>3</sup>

References:

- [1] Chaudhuri, S. & Muckerman, J. T. First-principles study of Ti-catalyzed hydrogen chemisorption on an Al surface: A critical first step for reversible hydrogen storage in NaAlH<sub>4</sub>. *Journal of Physical Chemistry B* **109**, 6952-6957 (2005).
- [2] Chaudhuri, S., Graetz, J., Ignatov, A., Reilly, J. J. & Muckerman, J. T. Understanding the role of Ti in reversible hydrogen storage as sodium alanate: A combined experimental and density functional theoretical approach. , 11404-11415 (2006). B. Author, Nano. Bio. Info. Sci. **001**, 1234 (3001).
- [3] Chopra, I. S., Chaudhuri, S., Veyan, J.-F., and Chabal, Y. J., Nature materials ( submitted ) 2011.

9:20am **SS1-TuM5 On the Role of Hydrogen in Heterogeneously Catalyzed Reactions**, M. Mavrikakis, University of Wisconsin Madison

**INVITED**

Hydrogen is a frequent participant in several heterogeneously catalyzed reactions, including Fischer-Tropsch Synthesis (FTS) of fuels, ammonia synthesis, oxygen reduction reaction (ORR), NO reduction, preferential oxidation of CO in the presence of H<sub>2</sub> (PROX), etc. Having analyzed the detailed aspects of the reaction mechanism for a number of these reactions on various transition metal and alloy surfaces using first-principles methods, some common principles governing the role of hydrogen in a wide range of catalytic transformations begin to emerge. In this presentation, we will discuss these common mechanistic principles by examples, including FTS<sup>1,2</sup>, NO-reduction, ORR<sup>3</sup>, PROX<sup>4,5</sup>, through an analysis of the energetics of alternative elementary reaction steps and the resulting potential energy diagrams. Connections to observations from experimental studies provide an invaluable perspective for the evaluation of our theoretical assessments.

References

1. M. Ojeda, R. Nabar, A. U. Nilekar, A. Ishikawa, M. Mavrikakis, E. Iglesia, *Journal of Catalysis* **272**, 287 (2010).
2. M. Ojeda, A. Li, R. Nabar, A. U. Nilekar, M. Mavrikakis, E. Iglesia, *Journal of Physical Chemistry C* **114**, 19761 (2010).

3. D. C. Ford, A. U. Nilekar, Y. Xu, M. Mavrikakis, *Surface Science* **604**, 1565 (2010).
4. A. U. Nilekar, S. Alayoglu, B. Eichhorn, M. Mavrikakis, *Journal of the American Chemical Society* **132**, 7418 (2010).
5. S. Alayoglu, A. U. Nilekar, M. Mavrikakis, B. Eichhorn, *Nature Materials* **7**, 333 (2008).

10:40am **SS1-TuM9 Prediction of Surface Ensembles in Au-based Bimetallic Alloys using Combined DFT and Monte Carlo Simulations**, *J.A. Stephens, H.C. Ham, G.S. Hwang*, University of Texas at Austin

Bimetallic materials have shown great promise for the development of superior catalysts. The recent surge of new interest in catalysis by gold has led researchers to investigate the effects of adding gold to other metals. While mechanisms underlying the alloying effect are still not understood in detail, recent evidence suggests that the enhanced reactivity of bimetallic catalysts can be attributed to a combination of metal-metal interactions (ligand effect) and unique mixed-metal surface sites (ensemble effect). The ability to accurately predict the arrangements of constituent atoms in a surface alloy is indispensable to unraveling the roles played by the ensemble and ligand effects in the performance of bimetallic model catalysts. We have developed a scheme to predict the equilibrium arrangement of atoms in surface alloys in the presence of adsorbates at finite temperatures. It is based on the Ising model and is capable of reproducing DFT-predicted total energies to within no more than a few meV per surface atom. We have used it successfully to predict the populations of monomers, dimers, and other, larger ensembles in Au-Pd and Au-Pt fcc (111) and (100) surface alloys. The scheme will be presented in detail, as well as what we have learned about the effects of temperature, composition, and the presence of adsorbates on ensemble formation in both fcc (111) and (100) surface alloys. We will also discuss how the atomic arrangements affect the reactivity of gold-based alloy surfaces, particularly towards oxygen reduction and carbon monoxide oxidation.

11:00am **SS1-TuM10 Adsorption and Electron-induced Dissociation of CO<sub>2</sub> on TiO<sub>2</sub>(110)**, *J. Lee, X. Deng, D. Sorescu*, National Energy Technology Laboratory

Adsorption and electron-induced reaction of CO<sub>2</sub> on the TiO<sub>2</sub>(110) surface has been investigated using scanning tunneling microscopy (STM) and dispersion corrected density functional theory (DFT). At low coverage the adsorption of CO<sub>2</sub> takes place at the oxygen vacancy defect. At higher coverage the CO<sub>2</sub> starts to adsorb on the Ti rows. The DFT results show that the CO<sub>2</sub> at the oxygen vacancy defect is in a tilted configuration and the molecular axis is perpendicular to the bridging oxygen row. On the Ti row, the DFT results confirm that the CO<sub>2</sub> adsorbs in a flat configuration with its axis parallel to the bridging oxygen row. Electron injection from the STM tip into the CO<sub>2</sub> at the oxygen vacancy defect induces the dissociation of CO<sub>2</sub>. The oxygen vacancy defect is found to be healed by the O atom released during the CO<sub>2</sub> dissociation process. Statistical analysis shows that the dissociation of CO<sub>2</sub> is a one-electron driven process with a threshold voltage of 1.4 eV above the conduction band minimum of TiO<sub>2</sub>. The formation of a transient negative ion by the injected electron is considered to be the key process in the CO<sub>2</sub> dissociation.

11:20am **SS1-TuM11 Adsorption and Dissociation of Propane-1, 3-diol Molecules on Reduced TiO<sub>2</sub>(110) Surface- A Scanning Tunneling Microscopy Study**, *D. Acharya, X. Lin, B.D. Kay, Z. Dohnálek, Z. Zhang*, Pacific Northwest National Laboratory

Rutile TiO<sub>2</sub>(110) surface is one of the most studied model systems for the fundamental investigations of a variety of processes on metal oxide surfaces, including heterogeneous catalysis, greenhouse gas reforming, solar cells, photodecomposition of organic pollutants, and photoinduced water splitting. It is widely accepted that the surface chemistry of the oxide surfaces are mainly influenced by the defects sites, particularly oxygen vacancies. Here we study the adsorption of propane-1,3-diol molecules on partially reduced rutile TiO<sub>2</sub>(110) surface using variable temperature scanning tunneling microscope (STM). STM images obtained before and after in-situ dose of propane-1,3-diol molecules at room temperature shows that the molecule preferentially binds at the bridging oxygen vacancies via bond scission of one of the OH groups. The hindered rotation of the 3-hydroxypropoxide species was seen at room temperature, while the diffusion and dissociation of the species were observed at elevated temperatures. The experiment was carried out at the Environmental Molecular Science Laboratory, a National Scientific user facility supported by the U.S. Department of Energy, Office of Biological and Environmental Research at Pacific Northwest National Laboratory.

11:40am **SS1-TuM12 Oxygen-Vacancy Assisted Formation of Enolate Species on Reduced CeO<sub>2</sub>(111) Surfaces**, *F.C. Calaza, Y. Xu, D.R. Mullins, S.H. Overbury*, Oak Ridge National Laboratory

Enolate species are key intermediates proposed in a number of important organic reactions heterogeneously catalyzed by metals and metal oxides, but enolate has been difficult to identify on active catalytic surfaces due to difficulties of isolating it in the keto-enol equilibrium.

Reflection absorption infrared spectroscopy (RAIRS) was coupled with density functional theory (DFT) to study the adsorption of acetaldehyde, a simple  $\geq C_2$  aldehyde, on CeO<sub>2-x</sub>(111) surfaces of different extent of oxidation (where  $x = 0 - 0.5$ ). It is found experimentally that the molecule adsorbs weakly on the fully oxidized surface ( $x=0$ ) at low temperatures and desorbs without further reaction near 215 K. The molecule bonds to *c.u.s.* Ce<sup>4+</sup> cations through the oxygen lone pair electrons in the carbonyl group with its C-C bond perpendicular to the surface plane and the acyl hydrogen tilted slightly towards one of the lattice oxygen anions of the first layer.

On the reduced surfaces ( $x=0.1 - 0.4$ ), acetaldehyde interacts more strongly with the surface upon adsorption at low temperatures by losing its carbonyl bond character and adsorbing as 1,1-dioxyethane and forming dimers and polymers. Heating the surface to 400 K leads to desorption of some amount of these strongly adsorbed species as acetaldehyde and the appearance of hydroxyl and yet a different organic species.

The identities and structures of the different intermediates on the CeO<sub>2</sub> and CeO<sub>2-x</sub> surfaces have been determined by their characteristic signatures in RAIRS and by DFT calculations. Our observations for the CeO<sub>2-x</sub> surfaces are consistent with the vacancy-promoted dehydrogenation in the original methyl position of acetaldehyde and the formation of enolate (CH<sub>2</sub>=CHO-Ce). Experiments with isotopically labeled acetaldehyde have verified the vibrational assignments for the enolate species and are in excellent agreement with DFT results. The assignment of the enolate species is furthermore consistent with C 1s XPS and C k-edge NEXAFS results.

Research sponsored by the Division of Chemical Sciences, Geosciences, and Biosciences, Office of Basic Energy Sciences, US Department of Energy. Use of the National Synchrotron Light Source, Brookhaven National Laboratory, was supported by the US Department of Energy, Office of Science, Office of Basic Energy Sciences.

## Surface Science Division

### Room: 110 - Session SS2-TuM

#### Self Assembled Monolayers and Networks

**Moderator:** J.E. Reutt-Robey, University of Maryland

8:20am **SS2-TuM2 In Situ UHV Growth and XPS/NEXAFS Characterization of Aromatic Self-Assembled Monolayers on Gold Substrates**, *A. Nefedov*, Karlsruhe Institute of Technology, Germany, *H. Muzik*, University of Bielefeld, Germany, *M. Naboka*, Karlsruhe Institute of Technology, Germany, *A. Turchanin*, *A. Götzhäuser*, University of Bielefeld, Germany, *C. Wöll*, Karlsruhe Institute of Technology, Germany

Aromatic self-assembled monolayers (SAMs) on gold show high potential for applications in nanobiotechnology [1]. Although the SAMs are typically prepared by immersing gold substrates in a solvent, their growth by vapor deposition in vacuum has various advantages both for the technological applications and fundamental studies [2, 3]. Thus, it is possible to characterize in detail the monolayer growth by various UHV compatible surface science techniques such as, e.g., electron spectroscopy. Here, we employ a new endstation of the HESGM beamline at BESSY II to study the *in situ* growth of 4'-nitro-1,1'-biphenyl-4-thiol (NBPT) SAMs on gold/mica substrates by X-ray photoelectron spectroscopy (XPS) and near edge X-ray absorption fine structure spectroscopy (NEXAFS). XPS C1s, N1s, O1s and S2p spectra as well as NEXAFS CK-, NK- and OK-absorption edge spectra were analyzed. These results demonstrate the formation of NBPT SAMs by vapor deposition in UHV with a similar packing density and molecular orientation as usually obtained in solvents. Moreover, we analyze the electron-radiation-induced modification of NBPT SAMs, that is widely employed in chemical nanolithography [4]. By varying the dose of electron irradiation we study two effects: (i) mechanisms of the electron-induced cross-linking [5] and (ii) conversion of the nitro groups into amino groups [6]. We analyze these transformations and compare the experimental NEXAFS data with calculations made by the StoBe software package.

[1] A. Turchanin, A. Tinazli, M. Ei-Desawy, H. Großmann, M. Schnietz, H. H. Solak, R. Tampé and A. Götzhäuser, *Adv. Mater.* **20**, 2008, 471.

[2] L. Kankate, H. Großmann, U. Werner, R. Tampé, A. Turchanin, A. Götzhäuser, *Biointerphases* **5**, 2010, 30.



- [3] L. Kankate, A. Turchanin, and A. Götzhäuser, *Langmuir* **25**, 2009,10435-10438.
- [4] A. Götzhäuser, W. Eck, W. Geyer, V. Stadler, T. Weimann, P. Hinze, M. Grunze, *Adv. Mater.* **13**, 2001, 806.
- [5] A. Turchanin, D. Käfer, M. Ei-Desawy, Ch. Wöll, G. Witte and A. Götzhäuser, *Langmuir*, **25**, 2009, 7342.
- [6] W. Eck, V. Stadler, W. Geyer, M. Zharnikov, A. Götzhäuser, M. Grunze, *Adv. Mater.* **12**, 2000, 805.

**8:40am SS2-TuM3 Structure, Bonding and Electronic Properties of Self-assembled 2D Organic Nanostructures at Surfaces: Negatively Charged TCNQ Networks and Other Systems, S.L. Tait, Indiana University INVITED**

Interfaces between organic materials and inorganic supports are critical for the design and function of new organic-based technologies (e.g., OLEDs, organic photovoltaics, and molecular electronics) as well as novel routes to chemical sensors and catalysts. There are vast opportunities for designing structure-function relationships in these systems due to the immense library of organic compounds and metal-organic chemistries available. Molecular self-assembly at surfaces by covalent, metal-organic, ionic, and weaker interactions are active fields of research, but much remains to be determined with regard to the complex interplay of intermolecular and adsorbate-substrate interactions and how these impact structure and function. TCNQ undergoes a charge transfer from a Cu surface to adopt a bond conformation to the surface that enables stable adsorption and the self-assembly of highly ordered 2D structures via surface-mediated attractive interactions. These structures are stable at room temperature. Addition of Mn triggers a structural transformation to a highly-ordered porous network with Mn centers in a high spin state. These studies have allowed new insight into organic / metal interfaces by collaborative work involving high-resolution scanning tunneling microscopy, photoelectron spectroscopy methods, synchrotron measurements, other UHV surface experiments, and density functional theory calculations. Recent progress on other 2D and multilayer organic systems in our group lends further evidence to the significance of direct organic-surface interactions in such systems, the problems those interactions may pose, and solutions for balancing them at a desired level. We are making progress towards tailored chemical function by rational design of molecular architectures at surfaces and tuning such function through supramolecular design strategies.

**9:20am SS2-TuM5 Ultrafast Self-Assembly of 1-Adamantanethiol and p-Terphenylthiol on Au(111)-surface, V.V. Korolkov, S.A. Allen, C.J. Roberts, S.J.B. Tendler, The University of Nottingham, UK**

Study of organic thiols adsorption on noble metals continues to be a subject of many research papers within the last three decades. Such steady interest arises mainly from the possibility to design metal surfaces with predefined chemical and physical properties that makes them suitable for a whole range of theoretical and applied studies.

Here we propose and investigate an idea that thiols with rigid or spherical hydrocarbon moieties should self-assemble on Au-surface much quicker than those with long-chain moieties. To support this idea we have investigated adsorption dynamics and monolayer structure for 1-adamantanethiol<sup>1</sup> (AdSH) and [1,1':4',1''-terphenyl]-4-thiol (TPT) molecules self-assembled on Au(111)-surface at 393K. We have demonstrated that both thiols form defect free and uniform SAMs almost instantly at elevated temperature. It takes ~1sec for AdSH to self-assemble on gold. In case of TPT ~90% of the monolayer forms within the first ~10 seconds of adsorption, and then it takes ~60 seconds to develop into a well-ordered structure. Both SAMs on Au were characterized with ambient STM up to a single-molecule level, X-ray photoelectron spectroscopy and spectroscopic ellipsometry. We were able to obtain near atomic resolved STM images for AdSH SAM on Au. They clearly showed that all AdSH molecules adsorbed in the same conformation with the molecular tilt and the twist angles being 114° and 0° correspondingly. We have also demonstrated that most AdSH molecules are arranged in a head-to-tail orientation, with some molecules having a head-to-head orientation without forming a disulfide bond.

Molecular resolved STM images of TPT SAM/Au clearly demonstrated that within first seconds of adsorption the Au-surface is equally covered with two different phases ( $\alpha$ - and  $\beta$ -).  $\beta$ -phase dominates on the Au-surface from ~10 sec of exposure and onwards. A closer inspection of the  $\beta$ -phase on a single molecule level allowed us to propose an upright conformation for TPT molecule on Au with the tilt angle of  $0\pm 5^\circ$ . We also estimated the tilt angle for the  $\alpha$ -phase to be within 10-20°. For both systems STM and XPS analysis suggest a high chemical and structural quality of the monolayers.

Overall we have proposed a simple and straightforward protocol for ultrafast fabrication of AdSH and TPT SAMs on Au-surface, which we believe can be readily extended for other similar molecular systems.

*Korolkov et al. J. Phys. Chem. C, Vol. 114, No. 45, 2010*

**9:40am SS2-TuM6 Role of van der Waals Interaction in the Binding of 1,4 diaminebenzene to the Au(111) Surface, D. Le, M. Aminpour, University of Central Florida, A. Kiejna, University of Wroclaw, Poland, T.S. Rahman, University of Central Florida**

The physisorption of 1,4 diaminebenzene (BDA) molecule on Au(111) surface is studied within the generalized gradient approximation of the density functional theory with the PBE [1], vdW-DF [2], and vdW-DF2 [3] exchange correlation functionals. The binding energy of an isolated BDA adsorbed on Au(111) surface calculated from vdW-DF (vdW-DF2) is 0.78 eV (0.84 eV) in better agreement with the experimental value (1.0 eV) [4] than that from PBE (0.37 eV), while the alignment of the molecule along the surface obtained from PBE (20°) is closer to the experimental value of 24° [4] than that of about 5° derived from vdW-DF (or vdW-DF2). On the other hand, when interactions between the BDA molecules is included in the calculations, as would be the case if the molecules were to self-assemble, say in the form of a linear line structure on Au(111), inclusion of vdW interactions gives excellent agreement with experimental observations. In particular vdW-DF and vdW-DF2 predict the BDA tilt angles to be 23° and 21°, respectively. The binding energy of a BDA on Au(111) in this case is 0.70 eV and 0.71 eV, respectively. As is to be expected, PBE does not account for intermolecular interactions and does not give good agreement with the data. We suggest the presence of such alignment of molecules along the surface in the experiments, and that they are governed by hydrogen bonding between N and H atoms of neighboring BDA molecules. We compare our results also with unpublished STM data for the system.

- [1] J. P. Perdew, K. Burke, and M. Ernzerhof, *Phys. Rev. Lett.* **77**, 3865 (1996).
- [2] M. Dion, H. Rydberg, E. Schröder, D. C. Langreth, and B. I. Lundqvist, *Phys. Rev. Lett.* **92**, 246401 (2004)
- [3] K. Lee, É. D. Murray, L. Kong, B. I. Lundqvist, and D. C. Langreth, *Rev. B82*, 081101 (2010).
- [4] M. Dell'Angela, G. Kladnik, A. Cossaro, A. Verdini, M. Kamenetska, I. Tamblyn, S. Y. Quek, J. B. Neaton, D. Cvetko, A. Morgante, and L. Venkataraman, *Nano Lett.* **10**, 2470-2474 (2010)

\*Work supported by DOE Grant DE-FG02-07ER15842.

**10:40am SS2-TuM9 Conformational Chirality, Chiral Switching and Chiral Induction in Self-Assembled Molecular Structures, T.R. Linderth, University of Aarhus, Denmark INVITED**

Chiral self-assembled structures formed from organic molecules have been subject to intense investigation, motivated both by applications such as enantiospecific heterogeneous catalysis as well as by fundamental interest e.g. in relation to the origin of biomolecular homochirality. Chirality on surfaces may arise both for intrinsically chiral molecules and for prochiral molecules that become chiral due to reduced symmetry upon adsorption. However, chiral effects originating from conformational degrees of freedom have received relatively little attention.

Here we use a combination of organic synthesis and UHV-STM experiments to address how rational design of molecular building blocks allows transfer of chirality from the molecular to the supra-molecular level. We investigate a class of custom-designed molecules based on a linear oligo-phenylene-ethynylene backbone and characterize their adsorption structures on the Au(111) surface. Most of these compounds are prochiral and display conformational chirality in the sense that they can adsorb in different chiral conformations distinguished by the positions of two tert-butyl side-groups. A novel chiral switching mechanism, involving a conformational change where the terminal groups rotate around the molecular axis, is directly revealed from time-resolved STM. We demonstrate that it is possible through control of the terminal group functionalization to steer the molecular backbones into surface assemblies that are either mirror symmetric or display pronounced organizational chirality in the form of a characteristic windmill motif. We furthermore achieve control over the absolute chirality of windmill assemblies by synthesizing an intrinsically chiral variant where the tert-butyl side pendant is replaced by a chiral (*S*)-*sec*-butyl group. This intrinsically chiral compound is finally used in co-deposition experiments as an induction seed to control the chirality of assemblies formed from the original prochiral compound.

Chiral switching by spontaneous conformational change in adsorbed organic molecules

S. Weigelt, C. Busse, L. Petersen, E. Rauls, B. Hammer, K.V. Gothelf, F. Besenbacher, and T.R. Linderth, *Nature Materials*, **5** 11 (2006)

Steering organizational and conformational surface chirality by controlling molecular chemical functionality

C. Bombis, S. Weigelt, M. M. Knudsen, M. Nørgaard, C. Busse, E. Lægsgaard, F. Besenbacher,

K. V. Gothelf, and T. R. Linderoth, ACS NANO 4, 297 (2010).

Controlling chiral organization of molecular rods on Au(111) by molecular design

M. Knudsen, N. Kalashnyk, F. Masini, J. Cramer, E. Lægsgaard, F. Besenbacher, T. R. Linderoth, K. Gothelf, Journ. Am. Chem. Soc. 133 4896 (2011).

11:20am **SS2-TuM11 Electronic Structure and Charge Injection Barriers of Self Assembled Peptide Nucleic Acid Monolayers on Au.** *M.A. Wolak*, University of South Florida, *A. Balaeff*, Duke University, *S. Gutmann*, *M.M. Beerbom*, University of South Florida, *E. Wierzbinski*, *D.H. Waldeck*, University of Pittsburgh, *S. Bezer*, *C. Achim*, Carnegie Mellon University, *D.N. Beratan*, Duke University, *R. Schlaf*, University of South Florida

Peptide nucleic acids (PNA) are a promising alternative to DNA for bio-sensing applications as well as for strategies for self assembly based on nucleic acid hybridization. This potential is a result of the PNA's neutral pseudopeptide backbone, which eliminates inter-strand electrostatic repulsion. In recent years charge transfer through PNA molecules has been a focus of research due to potential applications in self-assembled molecular circuits. This makes it interesting to investigate the electronic structure of PNA interfaces to electrode materials. A widely used strategy to 'connect' PNA molecules to metallic electrodes is through thiol-Au bonds using a terminal cysteine appended to PNA oligomers. This motivated the here presented research where the electronic structure of self-assembled PNA monolayers on Au substrates was investigated. Cys-appended PNA 7-mers of thymine (Cys-T7) were incubated on Au substrates in a nitrogen glove box attached to a photoemission spectrometer. Ultraviolet and x-ray photoemission spectroscopy (UPS and XPS) measurements on the resulting SAMs revealed the hole injection barrier at the interface and the interface dipole. Electronic structure calculations based on molecular dynamics sampling of the PNA structure yielded the band gap and the electronic density of states for PNA. Combined with the UPS data, the theoretical calculation enabled the estimate of the electron injection barrier at the interface, as well as the assignment of individual UP spectral features to specific molecular orbitals. Control measurements on Cys-appended, abasic PNA backbone 7-mers allowed the identification of the emissions related to the PNA backbone in the UP spectra. The orbital line-up at the interface between the Au substrate and the Cys-PNA indicates a significant interface dipole resulting in the alignment of the Au Fermi level near the center of the PNA HOMO-LUMO gap. This alignment causes large charge injection barriers for both holes and electrons, and thus impedes charge transfer from Au into the Cys-PNA SAM.

11:40am **SS2-TuM12 Immobilization of Single-Stranded DNA Probe on InAs Surfaces for Biosensor Application.** *E.K. Cho*, University of Wisconsin, *A. Brown*, Duke University, *T.F. Kuech*, University of Wisconsin

We study the immobilization of single-stranded DNA (ssDNA) probe on indium arsenide (InAs) surface and its characterization for diagnostic application. In contrast to other semiconductors, the Fermi level in InAs is typically pinned above the conduction band minimum, resulting two-dimensional electron gas (2DEG) located immediately below the surface. The InAs based system forms the basis of a DNA sensing platform because hybridization of complimentary DNA sequence with the immobilized DNA probes on InAs surface causes the conductivity changes due to negativity charges on the phosphorus backbone of DNA sequences. The DNA immobilization was done using weakly basic solution and characterized by X-ray photoelectron spectroscopy (XPS) and hall measurement. The DNA probe is modified with thiol for 5' end to anchor the DNA probes on InAs surface and fluoro adenosine for 3' end to reveal the existence of DNA on the InAs surface. The XPS spectrum of F 1s and N 1s peaks verify that the DNA is successfully attached on InAs surfaces. The As 3d peak shows that there are considerable amount of As-S observed with no As-Ox after exposing the basic DNA solution. In contrast, In-S is not found in the In 3d core-level. The XPS data suggest that the DNA probes are attached to the InAs surface exclusively via thiolate bonds to As atoms and the DNA functionalization effectively removes InAs oxide as well. This result is not consistent with what has been observed on InAs (100) surfaces, where the thiolate bond is predominantly anchored to Indium atoms. For example, it has been shown a predominance of In-S bonds of alkanethiols and thioacetamide self-assembled monolayer (SAM) on InAs [1, 2]. However, the bonding chemistry of thiolate to III-V surface has been of great debate in literature [3]. The predominance of As-S bonds has been shown with octadecanethiol SAM on GaAs (100) surfaces driven by kinetic competitions [3] even though Ga-S bonds are energetically more favorable than As-S bonds [4]. In addition, the sheet resistivity of initial InAs surface

and DNA immobilized surface is measured, and the response of a DNA functionalized InAs surface with complimentary DNA sequence is monitored.

[1] D. Y. Petrovykh et al., Surf. Interface Anal. 2005, 37, 989-997.

[2] D. Y. Petrovykh et al., Langmuir 2009, 25, 12185-12194.

[3] C. L. McGuinness et al., J. Phys. Chem. C 2007, 111, 4226-4234.

[4] T. Scimeca et al., Phys. Rev. B 1991, 44, 12927-12932.

# Tuesday Afternoon, November 1, 2011

## Surface Science Division

Room: 110 - Session SS+EM-TuA

## Organic Electronic Interfaces

Moderator: J.R. Engstrom, Cornell University

2:00pm SS+EM-TuA1 **The Effect of Structure on Interfacial Energy**, *F. Stellacci*, EPFL, Switzerland **INVITED**

In this talk I will highlight recent result on solid-liquid interfaces where the solid has a nanostructure with a characteristic length scale that is only a few liquid molecule wide. The talk will start with the presentation of a new scanning probe technique able to measure interfacial energy (work of adhesion to be precise) with atomic/molecular resolution. It will then show how surfaces with alternating stripe-like domains a few nanometer thick have a structural component to their work of adhesion that can account for as much as 20% of the total energy. Finally novel self assembly approaches to achieve such surfaces will be discussed.

2:40pm SS+EM-TuA3 **Interfacial Electronic Structure of Dipolar Organic Semiconductors**, *O.L.A. Monti, M.P. Steele, N. Ilyas, L.L. Kelly, D.A. Rucke*, University of Arizona

We present an investigation of the evolution of the electronic structure at the interface of the dipolar organic semiconductor vanadyl naphthalocyanine with both highly oriented pyrolytic graphite and Au (111). Using angle-resolved two-photon photoemission and other photoelectron spectroscopies we observe both excitonic as well as strictly interfacial states in both ground and excited state manifolds, with large differences between the two surfaces. Simple electrostatic considerations provide a chemisorption model that is capable of quantitatively describing long- and short-range interface-mediated intermolecular coupling, significantly altering the molecular electronic structure. Additional insights are available from full-scale first-principles calculations at these interfaces. As a consequence, we show that electrostatic multipoles can significantly influence molecular and interfacial electronic structure, with direct and observable impact on interfacial charge-transfer dynamics. Interfacial electrostatic fields may therefore be used to manipulate in a concrete fashion processes of critical importance to solar energy conversion such as photoinduced interfacial electron transfer.

3:00pm SS+EM-TuA4 **Characterization of Quinonoid Zwitterion Molecular Films on Metal Surfaces**, *L. Routaboul, P. Braunstein*, Lab. de Chimie de Coordination (UMR 7177 CNRS), France, *B. Doudin*, Inst. de Phys. et Chimie des Mat. de Strasbourg, France, *J. Xiao, Z. Zhang*, Nebraska Ctr. for Mat. & Nanosci., *Y.B. Losvyj, O. Kizilkaya*, The J. Bennett Johnston Sr. Ctr. for Adv. Microstructures & Devices, *L.G. Rosa*, Univ. of Puerto Rico-Humacao, *P.A. Dowben*, Nebraska Ctr. for Mat. & Nanosc.

There is considerable interest in the functionalization of metal surfaces by molecules with large dipoles. For this purpose, *p*-benzoquinonemonimine-type zwitterions represent ideal candidates. These zwitterions can be anchored on gold surfaces where they form homogeneous thin films with the dipole preferentially oriented along the surface normal.<sup>[1]</sup> Some zwitterions will selectively adsorb on patterned gold substrates from solution while selective deposition of the zwitterions onto specific ferroelectric domains has been demonstrated. This represents an attractive approach to pattern molecular deposition on optically transparent planar substrates through electrostatic dipolar interactions or orientation dipole controlled surface chemistry. Taking advantage of the high solubility of two zwitterions in both organic solvents and water, we studied the influence of the solvent on the functionalization of surface.<sup>[2]</sup> The goal is to control both packing and selective deposition on a variety of substrates through zwitterion solvent combination.

**Acknowledgement.** This research was supported by the CNRS and the Ministère de la Recherche et des Nouvelles Technologies, the ANR (07-BLAN-0274-04), the National Science Foundation (grants CHE-0909580 and DMR-0851703), and the Nebraska Center for Materials and Nanoscience at the University of Nebraska-Lincoln.

4:00pm SS+EM-TuA7 **Directed Organization of C<sub>70</sub> Kagome Lattice by TiOPc-Monolayer Template**, *J.E. Reutt-Robey, Y. Wei*, University of Maryland

Abrupt molecular semiconductor interfaces between titanyl phthalocyanine (TiOPc) and C<sub>70</sub> were prepared by physical vapor deposition and characterized by UHV-STM. Molecular TiOPc is a highly anisotropic

molecule with a 3.5 dipole moment. Ordered TiOPc monolayer films of the honeycomb phase thus represent a regular 2-d dipolar lattice, which was investigated as an electrostatic template for the growth of the highly polarizable C<sub>70</sub>. Films of C<sub>70</sub> grown layer-by-layer revealed the directed formation of a Kagome lattice. Atomically detailed structural models were obtained for the 0-6 nm C<sub>70</sub> thickness (up to 5 ML) range over which the ordering influence of the TiOPc dipolar substrate persists. Unusually low-density C<sub>70</sub> molecular packing arrangements result from the ellipsoidal shape, curved surfaces and high polarizability of C<sub>70</sub>. While Kagome lattices have been frequently observed in colloidal and magnetic systems, this appears to be the first electrostatically-induced Kagome lattice involving a molecular film.

This work has been supported by the National Science Foundation under Surface Analytical Chemistry grant CHE0750203 and under the University of Maryland MRSEC DMR-05-20471

4:20pm SS+EM-TuA8 **Solvation - Assisted Growth of ZnPc and 4NO<sub>2</sub>-ZnPc Monolayer Films on Au(111)**, *L. Tskipuri, Q. Shao, J.E. Reutt-Robey*, University of Maryland, College Park

The UHV spray-jet molecular beam deposition technique marries the chemical versatility and efficiency of solution-film processing with the atomic-level control and analytical tools of UHV surface science. Here we show how the solvent used in aerosol deposition can be used to fine tune film morphology. Thin films of ZnPc and 4NO<sub>2</sub>-ZnPc are grown on a Au(111) support with a newly developed spray-jet molecular beam deposition source and characterized in situ via UHV-STM. Phthalocyanines are delivered to the Au(111) surface in a series of N<sub>2</sub>-entrained μ-sized solvent droplets of variable surface residence time. The formation of submonolayer films with corresponding density variations demonstrates the impact of the ~nm-thick solvation layers on growth kinetics. Phthalocyanine film registration to the herringbone reconstruction of the Au(111) substrate, indicative of thermodynamically-favored structure, is observed only for aromatic solvents with long residence times. Vacancy cavities in monolayer films from solvent memory are eliminated with mild annealing, yielding film structures that rival PVD grown films. Results are interpreted through solvation-mediated kinetics.

4:40pm SS+EM-TuA9 **Direct Observation of NO<sub>2</sub> Adsorption onto CuPc Monolayers with STM**, *J.H. Park, J. Royer, S. Lee, T. Kent, W. Trogler, A.C. Kummel*, University of California San Diego

Copper phthalocyanine (CuPc) thin film devices have been widely studied for use as chemical vapor sensors; however, the molecular scale sensing mechanism remains undetermined. This study presents molecular scale observation of NO<sub>2</sub> adsorption onto CuPc monolayers using ultra-high vacuum (UHV) scanning tunneling microscopy (STM). CuPc monolayers were deposited on Au (111) surfaces by organic molecular beam epitaxy in ultra-high vacuum (UHV) and subsequently exposed to different NO<sub>2</sub> concentrations at atmospheric pressure. After annealing at 50 °C to improve STM imaging, for low NO<sub>2</sub> doses (1 ppm for 5min) the STM images reveal NO<sub>2</sub> molecules arranged as islands primarily along the domain boundaries. The NO<sub>2</sub> molecules almost completely desorb from the CuPc monolayer after annealing at 100 °C for 1 hr. Conversely, at high NO<sub>2</sub> doses (10 ppm for 5 min), the NO<sub>2</sub> exhibit irreversible reactions with the CuPc surface. After annealing at 50 °C, the domain boundaries act as nucleation centers for semi-ordered NO<sub>2</sub> adsorbates. As the annealing temperature is increased to 150 °C, the islands of NO<sub>2</sub> molecules diffuse from the domain boundaries to the CuPc terraces to form ordered structures on the terraces. After annealing at 250 °C for 1 hr, the CuPc monolayer becomes disordered and has numerous vacancies. The data is consistent with that NO<sub>2</sub> inducing CuPc decomposition. The behavior of NO<sub>2</sub> dosed CuPc monolayers suggests that NO<sub>2</sub> undergoes molecular chemisorption with the CuPc metal center at low exposures. However, at high exposures, NO<sub>2</sub> not only undergoes molecular chemisorption with the metal center, but also induces decomposition of the CuPc. This direct observation for NO<sub>2</sub> dosed CuPc monolayers with STM can give an insight into reversible versus dosimetric sensing in CuPc organic thin film chemical sensors (chemFETs). While nearly all weakly bonding analytes give reversible mobility sensor responses on CuPc chemFETs, some strong oxidants are observed to give reversible mobility responses at short exposures and dosimetric irreversible threshold voltage responses for longer exposures. This is consistent with the larger doses saturating the reversible chemisorption sites and inducing an oxidative decomposition of the CuPc which induces a dosimetric response via formation of uncompensated positive charge in the CuPc film. Therefore, the data is consistent with two chemisorption mechanisms of a strong oxidant on a single molecule given two different classes of sensor response.

5:00pm **SS+EM-TuA10 Tunneling Spectroscopy of Benzoic Acid Monolayers: The Role of the Metal-Molecule Interface**, *J. Kreil, P. LeClair, G.J. Szulczewski*, The University of Alabama

A series of self-assembled monolayers were prepared from para-substituted benzoic acids ( $X-C_6H_5CO_2H$  where  $X = H, F, Cl, Br, I,$  and  $CN$ ) onto oxidized Al films and characterized by x-ray photoelectron spectroscopy and contact angle measurements. The acids adsorb to the oxide as a carboxylate group with the plane of the aromatic ring largely perpendicular to the surface, which places the para-substituent away from the surface. Tunnel junctions were made by vapor deposition of Ag and Pb films as the top electrodes onto the monolayers. Four point probe electrical measurements were made from 4 to 300K. At 4 K the superconducting gap of Pb was observed and unequivocally demonstrates tunneling through a barrier without metallic shorts. When Ag was the top electrode, differential conductance [ $G(V) = dI/dV$ ] measurements at 4 K showed a quadratic dependence on the applied bias voltage and no zero-bias anomalies. These low temperature measurements suggest the monolayers form pin-hole free tunnel barriers. Two trends emerge when comparing  $G(V)$  versus bias voltage for junctions with Ag and Pb top electrodes. When Pb was the top electrode the minimum in  $G(V)$  versus bias voltage is offset from zero bias for each monolayer, which scales in a systematic manner with the polarity of the para C-X bond. However, when Ag was the top electrode there was no offset the tunneling conductance. The origin of the different tunneling behavior observed for Pb and Ag top electrodes will be discussed in detail.

5:20pm **SS+EM-TuA11 Interfacial Engineering of Organic Light Emitting Diodes with Sputter Treated Molybdenum Oxides as Hole Injection Layers**, *C.I. Wu, P. Wang, I. Wu*, National Taiwan University, Republic of China

In this paper, the mechanisms leading to the enhancement of organic light emitting diodes (OLEDs) with molybdenum oxide  $MoO_3$  incorporated in as hole injecting layers (HILs) will be discussed. The first one is the lowering of hole injection barrier between anodes and organic layers when a thin film of  $MoO_3$  is inserted. The high work function of  $MoO_3$  serves as a carrier ladder which decreases misalignment between the Fermi level of electrodes and highest occupied molecular orbital (HOMO) level of hole transport layers, such as  $N,N'$ -di(naphthalene-1-yl)- $N,N'$ -diphenyl-benzidine (NPB). The second model is the formation of gap states above the valence band edge of  $MoO_3$  to the Fermi level of electrodes when NPB molecules are deposited on  $MoO_3$  layers. These gap states enhance the conductivity of  $MoO_3$  and provide transition paths of carrier to assist the injection of hole from indium tin oxide (ITO) anodes to NPB layers. The third mechanism is the p-type doping effect of  $MoO_3$  doped in NPB layers. This p-type doping increases hole concentration in NPB layers and reduces the energy difference between the Fermi level of electrodes and the HOMO of NPB.

We will also demonstrate an effective method to improve the current injection efficiency of OLEDs by modifying the oxidation states of as-deposited  $MoO_3$  as HILs with in-situ argon ion ( $Ar^+$ ) sputtering. The injection current of devices incorporating this method is enhanced by one order of magnitude, as compared to that of devices without sputter treatment. The luminance of the devices is also improved. Beside device characterization, X-ray photoemission spectroscopy (XPS) and ultra-violet photoelectron spectroscopy (UPS) were carried out to obtain the chemical and electronic information of  $MoO_3$  thin films treated with  $Ar^+$  sputter and to unveil the origins of improvement in device performance. It is found that, with slight sputter treatments,  $MoO_3$  layers represent lower oxidation states and show metallic characteristics in energy band structure, which remarkably elevates the carrier injection efficiency from ITO to NPB.

5:40pm **SS+EM-TuA12 Probing Surface Photovoltage Development by Dynamical XPS Measurements**, *S. Suzer*, Bilkent University, Turkey

Various semiconducting, photoactive and insulating materials have been investigated using XPS where the data is collected in a dynamic mode. This is achieved by recording the spectrum while applying an electrical signal in the form of  $\pm 5$  or 10 V d.c. bias, and/or square-wave pulses, without and under photoillumination using different lasers. This method enables us to probe and sort out the effects and contributions of the three fundamental processes operating; **Charging, Photovoltage-Development, and Photoconductivity** in a **chemically specific fashion**. Accordingly, the chemical shift differences between the n- and p-doped semiconductors are amplified due to the effect of the photovoltage operating in the opposite directions. Time and/or frequency dependence of various processes adds a new dimension to XPS for sorting out the effects of external stimuli (electrons, ions, photons, etc.) as well as the chemical nature of the material under investigation. Experimental results and various applications will be presented and discussed.

**Surface Science Division**  
**Room: 109 - Session SS-TuA**

**Catalysis on Metals and Alloys**

**Moderator:** G. Fisher, University of Michigan

2:00pm **SS-TuA1 La<sub>1-x</sub>Ce<sub>x</sub>MnO<sub>3</sub> Perovskites: Structural Features and Performance for Preferential CO Oxidation Reaction**, *S.S. Maluf*, Federal University of Sao Carlos, Brazil, *B.E. Hayden*, University of Southampton, UK, *C.R.M. Afonso*, Federal University of Sao Carlos, Brazil, *E.M. Assaf*, University of Sao Paulo, Brazil, *P.A.P. Nascente*, Federal University of Sao Carlos, Brazil

The perovskite structure is characterized by a large capacity to stabilize unusual valence states of different metal ions and can also accommodate variable amounts of different lattice defects. Several lanthanum transition metal based perovskites, represented as  $La_{1-x}A_xMO_3$ , have been known as very good oxidation catalysts in a variety of reactions. Particularly,  $LaMnO_3$  perovskites have shown to be the most active. The catalytic activity of these compositions in different reactions can be further enhanced by the substitution of lanthanum by cerium. The catalysts were prepared by co-precipitation method, from aqueous solutions of La, Mn, and Ce nitrates with  $Na_2CO_3/NaOH$  solution (pH 10). The prepared samples were  $La_{1-x}Ce_xMnO_3$  ( $x = 0, 0.05,$  and  $0.10$ ) and were characterized by EDS-SEM, surface area-BET method, X-ray diffraction (XRD), and temperature programmed reduction (TPR). The catalytic activity was tested over the temperature range of 130–230°C in a fixed-bed tubular glass micro-reactor, with 200mg of catalyst. The reaction products were analyzed in-line by gas chromatography. The amounts of the constituent metals obtained by EDS were in agreement with expected values; the presence of cerium did not change the surface area of the samples ( $26-27m^2g^{-1}$ ). The X-ray diffraction lines corresponded to cubic  $LaMnO_3$  structure; the replacement of La did not change the diffractograms. Peaks of cerium oxide were not observed, suggesting the incorporation of Ce ions into the  $LaMnO_3$  lattice. The sample with the highest content of cerium presented an increase on thermal stabilization of  $Mn^{3+}$  ions, and  $Mn^{4+}$  species were reduced to lower temperatures. The SEM results indicated that the presence of cerium decreased slightly the grain size (from 56 to 43 nm) and the range of distribution sizes is homogeneous and the most grains are spherical. All samples presented the same catalytic behavior, starting their activities at 130°C, and their activities increased with the temperature. At 150°C, the sample with 5% of Ce presented a slight advantage compared to other samples, and this was more significant at 230°C, indicating that the promoter effect of cerium can be observed for higher reaction temperatures. The results suggested that the replacement of La by Ce caused an increase of cationic/anionic vacancies and also in the  $Mn^{4+}/Mn^{3+}$  ratio change, and consequently the catalytic behavior for CO oxidation changed, facilitating the CO adsorption.

**Acknowledgements**

The authors thank FAPESP for financial assistance, Ilika Technologies and University of Southampton for the XRD analyses.

2:20pm **SS-TuA2 Faceted Metal Surfaces: Surface Chemistry and Growth of Metallic Nanoclusters**, *W. Chen, Q. Shen, R.A. Bartynski*, Rutgers University

In this work, surface faceting is used to prepare a nanoscale model catalyst for surface reactions and a nanoscale template for growth of metallic nanoclusters. Faceting occurs when an initially planar surface converts to a “hill and valley” structure exposing new crystal faces of nanometer scale dimensions. Nanoscale three-sided pyramids exposing (311), (31-1) and (110) faces with tunable facet sizes are formed on an initially planar Ir(210) surface upon annealing in  $O_2$  and a clean faceted Ir(210) surface can routinely be prepared in situ by heating in  $H_2$ . Surface reaction of  $NO+CO$  has been carried out on clean planar Ir(210) and clean faceted Ir(210) with varying facet size (5-14nm). Both planar and faceted Ir(210) favor reduction of NO by CO with high selectivity to  $N_2$ , which is accompanied by simultaneous oxidation of CO. The reaction is not only structure sensitive on faceted Ir(210) versus planar Ir(210) but also exhibits size effects on faceted Ir(210) for average facet size ranging from 5nm to 14nm without change in facet structure. Strong interaction between NO and CO at high NO exposure and 1ML CO pre-coverage results in “explosive” evolution of  $N_2$  and  $CO_2$  on planar Ir(210). Annealing Ru(11-20) in  $NO_2$  leads to formation of ridge-like faceted surface exposing (10-11), (10-1-1), (01-11) and (01-1-1) faces. Faceted O/Ru(11-20) facilitates growth of nanoscale metallic clusters at room temperature which preferentially nucleate within valleys of the faceted surface.

Supported by DOE contract No. DE-FG02-93ER14331

2:40pm **SS-TuA3 Modeling the Complexities of Heterogeneous Catalysts**, *D.W. Goodman, Matt Lundwall*, Texas A & M University  
**INVITED**

In the past several decades, surface science methodologies have contributed significantly to our understanding of reaction mechanisms of heterogeneous catalysts. From fundamental studies on metal single crystals to investigations of metal oxide supported metal clusters, the relative complexities of model catalyst systems have continued to evolve in complexity and likeness to industrial catalysts. Studies on metal single crystals have aided researchers in understanding the effect of surface structure on catalyst reactivity and selectivity for a number of important reactions. More recently model systems consisting of metal clusters deposited on planar oxide surfaces under ultra high vacuum conditions have facilitated the study of metal particle size and support effects. These model systems are useful for carrying out kinetic investigations, yet are amenable to surface spectroscopic techniques, thus enabling investigations under realistic pressures and at working temperatures. This talk will present selected investigations of catalytic reactions on single crystal and model supported catalysts with emphasis on recent work addressing the nature of the active site in structure sensitive reactions.

4:00pm **SS-TuA7 Nanocatalysis: New Developments in Catalytic Performance of Size- and Shape-Controlled Metal Nanoparticles**, *B. Roldán Cuenya*, University of Central Florida

Tailoring the chemical reactivity of nanomaterials at the atomic level is one of the most important challenges in catalysis research. In order to achieve this elusive goal, fundamental understanding of the geometric and electronic structure of these complex systems at the atomic level must be obtained. To study these effects, homogeneous size- and shape-selected Pt nanoparticles (NPs) were synthesized by means of diblock copolymer encapsulation.

The influence of the nanoparticle *shape* on the reactivity of Pt nanocatalysts supported on nanocrystalline  $\gamma$ -Al<sub>2</sub>O<sub>3</sub> will be described. Nanoparticles with similar size distributions (~0.8-1 nm) but with different shapes were found to display distinct reactivities for the oxidation of 2-propanol. A correlation between the number of undercoordinated atoms at the nanoparticle surface and the onset temperature for 2-propanol oxidation was observed, demonstrating that catalytic properties can be controlled through shape-selective synthesis. Furthermore, the complex interaction between catalysts and reactants was investigated under *operando* conditions via X-ray absorption fine-structure spectroscopy. Platinum oxides were found to be the active species for the partial oxidation of 2-propanol (<140°C), while the complete oxidation (>140°C) was catalyzed by oxygen-covered metallic Pt NPs. Our findings highlight the decisive role of the nanoparticle structure and chemical state in oxidation catalytic reactions.

4:20pm **SS-TuA8 Oxidative-Coupling Reactions via Nucleophilic Attack on Gold Surface**, *B. Xu\**, *C.M. Friend, R.J. Madix*, Harvard University

Metallic gold owes its centuries-old mystique and intrinsic value to its chemical inertness toward bulk compound formation. In the past decade, however, it has been discovered that the surface of gold is far from inert, and that gold can catalyze important chemical transformations – particularly with the assistance of molecular oxygen or other oxidizing agents. These processes are of particular significance because they may occur at remarkably low temperatures and pressures, suggesting the possibility of energy efficient and environmentally benign reaction conditions using metallic gold catalysts. Recently, there has been a focus on selective oxidation of alcohols to aldehydes, oxidative self-coupling of alcohols to form esters and, most recently, acylation via amine-formaldehyde coupling. Our work under ultra-high vacuum (UHV) condition on the well defined model system of Au(111) surface has unequivocally proved that surface adsorbed atomic oxygen is critical in facilitating a range of nucleophilic coupling-reactions among alcohols, aldehydes and amines. A general reaction mechanism for this class of coupling-reactions is established: surface alkoxy or amide is formed via the deprotonation of the corresponding alcohol or amine by surface atomic oxygen, which can subsequently nucleophilically attack the aldehydes (formed in situ from alkoxy or introduced directly) and produce the corresponding ester or amide. The product distribution of our low-pressure experiments match remarkably well with gas phase reactions carried out in the ambient condition as well as liquid phase reactions, proves the generality of the mechanism.

4:40pm **SS-TuA9 Understanding the Enhanced Activity for Methanol Reaction on Titania-supported Au Clusters**, *D.A. Chen, S.A. Tenney, B.A. Cagg, M.S. Levine*, University of South Carolina, *S. Hong, T.S. Rahman*, University of Central Florida

The growth and chemical activity of Au clusters deposited on rutile TiO<sub>2</sub>(110) were studied by scanning tunneling microscopy, temperature programmed desorption and density functional theory calculations. Methanol reaction on 0.25 ML Au clusters produces formaldehyde as the major product at 535 K with methanol desorption observed at the same temperature; water and hydrogen evolution are detected below room temperature, as well as methyl radical evolution at 575 K. On the titania surface itself, methanol reaction also produces methyl radical around 600 K. Formaldehyde production reaches its maximum value between 0.25 and 2 ML but decreases dramatically as the coverage is increased to 5 ML. This behavior suggests that formaldehyde is produced at the Au-titania interface since formaldehyde production does not occur at pure Au sites. STM experiments confirm that the 0.25 ML Au coverage has the greatest number of Au-titania interfacial sites at the perimeter of the clusters. For higher coverages of 2 and 5 ML, cluster coalescence diminishes the number of Au-titania sites, and this is consistent with the decreased formaldehyde yield at higher Au coverages. When the titania surface is reoxidized with <sup>18</sup>O prior to Au deposition and exposure to methanol, lattice oxygen is incorporated into the water that is evolved at low temperature. We propose that the role of the titania support is to facilitate the formation of the reactive methoxy intermediate via abstraction of the hydroxyl hydrogen in methanol by lattice oxygen. Density function theory calculations also indicate that methoxy is the intermediate formed at the Au-titania interface after O-H bond scission is induced by lattice oxygen.

5:00pm **SS-TuA10 Oxygen Chemisorption, Formation, and Thermal Stability of Pt Oxides on Pt Nanoparticles Supported on SiO<sub>2</sub>/Si(001): Size-Effects**, *L.K. Ono, J.R. Croy, H. Heinrich, B. Roldan Cuenya*, University of Central Florida

The changes induced in the structure and chemical state of size-selected Pt nanoparticles (NPs) supported on ultrathin SiO<sub>2</sub> films upon exposure to oxygen have been investigated by atomic force microscopy, transmission electron microscopy, in situ X-ray photoelectron spectroscopy (XPS), and temperature-programmed desorption (TPD). For low atomic oxygen dosings, chemisorbed oxygen species were detected on all samples. Exposure to higher atomic oxygen coverages at room temperature lead to the formation and stabilization of PtO<sub>x</sub> species (PtO<sub>2</sub> and PtO). On all samples, a two-step thermal decomposition process was observed: PtO<sub>2</sub> → PtO → Pt. For NPs in the 2-6 nm range, the NP size was found to affect the strength of the O-binding. Contrary to the case of Pt(111), where no oxides were detected above 700 K, 10-20% PtO was detected on the NP samples via XPS at the same temperature, suggesting the presence of strongly bond oxygen species. In addition, for identical atomic oxygen dosings, decreasing the NP size was found to favor their ability to form oxides. Interestingly, regardless of whether the desorption of chemisorbed oxygen species or that of oxygen in PtO<sub>x</sub> species was considered, our TPD data revealed higher O<sub>2</sub> desorption temperatures for the Pt NPs as compared to the Pt(111) surface. Furthermore, a clear size-dependent trend was observed, with an increase in the strength of the oxygen bonding with decreasing NP size.

5:20pm **SS-TuA11 Alloy Surface Reactivity on Cu<sub>x</sub>Au<sub>y</sub>Pd<sub>1-x-y</sub> Composition Spread Alloy Films**, *A.J. Gellman, J.B. Miller, P. Kondratyuk, D. Priyadarshini*, Carnegie Mellon University, *B.D. Morreale*, National Energy Technology Laboratory

The key features of Cu-Au-Pd alloys relevant to their application as hydrogen purification membranes are the ability to dissociatively adsorb H<sub>2</sub> and the ability to transport H atoms through their bulk. We have developed tools for the preparation of Cu<sub>x</sub>Au<sub>y</sub>Pd<sub>1-x-y</sub> composition spread alloy films (CSAFs) as libraries for high throughput study of their catalytic surface properties. These ternary Cu<sub>x</sub>Au<sub>y</sub>Pd<sub>1-x-y</sub> CSAFs expose a broad and continuous distribution of compositions for spatially resolved analysis of their properties. Electron backscatter diffraction has been used to verify the structure of the films across their composition spread and to demonstrate that they have the atomic structure expected on the basis of their phase diagram. LIES has been used to study surface segregation as a continuous function of composition, (x,y), demonstrating that segregation is preferred in the order Au>Cu>Pd at the clean alloy surfaces. A multichannel microreactor array has been used to spatially resolve the surface activity for H<sub>2</sub> dissociation by measuring the kinetics of H<sub>2</sub>-D<sub>2</sub> exchange as a function of alloy composition. This reveals that while both Cu and Au poison surface activity, Cu is more effective than Au at suppressing H-D exchange activity. This work demonstrates the potential value of CSAFs as platforms for study of alloy surface chemistry and for comprehensive study of their properties across composition space.

\* Morton S. Traum Award Finalist

5:40pm **SS-TuA12 Pd Ensemble Effects on Enhancing Low Temperature CO Oxidation and Tolerance on AuPd Alloys: A First Principles Study**, *H.C. Ham, J.A. Stephens, G.S. Hwang*, University of Texas at Austin

In the oxidation reaction of fuels such as CO-contained hydrogen, methanol and formic acid at the low temperature region (300 ~ 400K) at the anode side of polymer electrolyte membrane fuel cell, the precious catalysts such as Pd and Pt have suffered the gradual loss in the catalytic activity due to the blocking of active sites (Pd/Pt) by CO molecules (the so-called CO poisoning effect). To handle this issue, alloying precious catalysts by other transition metals has been suggested as one of solutions since the synergetic alloying effects such as the creation of unique mixed-metal surface sites [ensemble effect] and electronic structure change by metal-metal interactions [ligand effect] can provide an avenue for preventing CO poisoning and enhancing CO oxidation at the low temperature.

In this talk, we will present our recent first-principles results on the role of Pd ensembles on the AuPd alloy in enhancing CO oxidation and tolerance at the low temperature. Using spin-polarized DFT-GGA calculations, for the first time, we elucidate that the reactivity toward CO+O<sub>2</sub> oxidation at the low temperature on various CO-precovered Pd ensembles (such as monomer, dimer, trimers and tetramers) is a strong function of surface Pd arrangements on the AuPd surface. In particular, the small-sized ensembles like dimer or compact trimer are responsible for enhancing the low temperature CO+O<sub>2</sub> oxidation by the increased availability of free Pd sites and facile O<sub>2</sub> activation on CO-precovered Pd ensembles. We will also show the importance of the interplay of ensemble and ligand effects in reducing the CO poisoning of the catalysts through the comparison study on the energetics, charge transfer, geometric and electronic structures of CO between Pd and Pt ensembles. Finally, we will present geometric parameter effects (such as strain and facet) on the CO tolerance of Pd ensembles, which can provide the proper criteria for designing the nano-sized Au-based bimetallic catalysts.

This study hints on how the surface arrangements of atoms and the influence of ensembles on the reaction kinetics and energetics can offer insight to properly tailor CO-tolerant Au-based bimetallic catalysts for fuel cell applications.

## Vacuum Technology Division

**Room: 111 - Session VT+MN+NS+SS+AS-TuA**

### Surface Science for Future Electronic Materials and Accelerator Applications

**Moderator:** M. Wüest, INFICON Ltd, Liechtenstein

2:00pm **VT+MN+NS+SS+AS-TuA1 New UHV Low Temperature Scanning Probe Microscopy Facility for the Study of Future Electronic Materials**, *J.A. Stroscio*, National Institute of Standards and Technology  
**INVITED**

Since the beginning of the last century new frontiers in physics have emerged when advances in instrumentation achieved lower experimental operating temperatures. Notable examples include the discovery of superconductivity and the integer and fractional quantum Hall effects. New experimental techniques are continually adapted in order to meet new experimental challenges. A case in point is scanning tunneling microscopy (STM) which has seen a wealth of new measurements emerge as cryogenic STM instruments have been developed in the last two decades. In this talk I describe the design, development and performance of a scanning probe microscopy facility operating at a base temperature of 10 mK in magnetic fields up to 15 T [1]. The STM system can be connected to, or disconnected from, a network of interconnected auxiliary UHV chambers used for sample and probe tip preparation. Results from current measurements on graphene and topological insulators will be described.

[1] *A 10 mK Scanning Probe Microscopy Facility*, Y. J. Song, A. F. Otte, V. Shvarts, Z. Zhao, Y. Kuk, S. R. Blankenship, A. Band, F. M. Hess, and J. A. Stroscio, *Rev. Sci. Instrum.* **81**, 121101 (2010).

2:40pm **VT+MN+NS+SS+AS-TuA3 Contact Resistance of RF MEMS at a Randomly Rough Surface in the Presence and Absence of Adsorbed Organic Monolayers**, *D. Berman, J. Krim, M.J. Walker*, North Carolina State University

Understanding of current flowing through the asperities is interesting for many applications: in RFMEMS, Molecular electronics, Nanotube tunneling etc.

Previous results [2] suggest that the films are displaced from the contacts themselves, but remain present in nearby regions. The increase in resistance is associated with elimination of vacuum electrical tunneling currents in

those regions. This raises the question of the relative proportions of contact resistance ( $R_c$ ) and effective tunneling resistance ( $R_t$ ).

Measurements on the gold on gold contacts adhered in the closed position, where the contamination film cannot possibly be placed inside the contacts are reported, to investigate vacuum tunneling current contributions to the total current at the contact. Electrical Contact Resistance measurements are reported for RF micro-electromechanical switches with Au/Au and Au/RuO<sub>2</sub> contacts, situated within an ultrahigh vacuum system equipped with *in situ* oxygen plasma cleaning capabilities. Fused Au/Au switch resistance increases by 3-5% (which corresponds to 20W tunneling resistance in parallel) after adding pentane to the switch environment. Moreover, the results are repeated with a different substrate (Ruthenium rather than Au), known for higher resistance, to change the resistance values with almost the same work function. If this is tunneling, the same effective tunneling resistance is expected, because tunneling depends on the work functions of the tip and substrate, which are close for gold and ruthenium oxide. In addition, the results are investigated for two different adsorbates, pentane and dodecane. Measurements have been recorded as the function of film coverage and the same tunneling resistance impact is observed. This is consistent with elimination of vacuum tunneling when adsorbed films are present.

Theoretical analysis of two possible mechanisms of the impact of molecular uptake is performed to interpret the experimental results: a) parallel connection of contact resistance and effective tunneling resistance before molecular adsorption, followed by molecules blocking the tunneling current; b) in series connection of contact resistance and pentane layer after adsorption. The data are more consistent with model a).

This work was supported by US National Science Foundation, AFOSR MURI and DARPA. We are grateful to C. Nordquist at Sandia National Lab and J. Hammond at RF Micro Devices for providing the experimental switches.

[1] D. Berman, M. Walker, C. Nordquist, J. Krim, *in preparation for Journal of Applied Physics*

[2] M. Walker, C. Nordquist, J. Krim, *in preparation for Tribology Letters...*

3:00pm **VT+MN+NS+SS+AS-TuA4 Surface Issues for Solid Niobium SRF Accelerator Cavities**, *M. Kelley*, College of William and Mary

The world-wide physics community looks forward to a slate of accelerator projects of unprecedented magnitude and diversity. Certainly its sheer size makes the International Linear Collider the most visible to the public eye, with 16,000 solid niobium cavities performing at historically high gradient, and built (and operated) for historically low unit cost. Net performance makes superconducting radiofrequency (SRF) technology the approach of choice.

Solid niobium is the material most widely used for construction of SRF cavities because it has the highest critical transition temperature ( $T_c = 9.2$  K) of the pure metals, sufficiently high critical magnetic field ( $H_c > 2$  k Oe) for SRF applications, and metallurgical properties adequate for fabrication and service load. Studies of the SRF performance of niobium cavities began to be reported more than 30 years ago and continue now with the application of improved experimental techniques. Niobium metal superconductivity is a nanoscale, near-surface phenomenon because of the shallow RF penetration. Considerable evidence indicates that cavity interior surface chemistry and topography strongly impact SRF accelerator performance, motivating investigation of how they are affected by post-fabrication treatments.

Current status and prospects are discussed with respect to accelerator needs and opportunities.

4:00pm **VT+MN+NS+SS+AS-TuA7 Examples of Surface Related R&D on Nb Samples and SRF Cavities for Particle Accelerators at JLab**, *A.T. Wu*, Thomas Jefferson National Accelerator Facility

This contribution will review some examples of surface related R&D on small and flat niobium (Nb) samples and single cell Nb superconducting radio frequency (SRF) cavities done at Jefferson Lab in the past few years. Most of the surface measurements were performed via the experimental systems available in the surface science lab that was set up<sup>1</sup> at JLab to study the various problems on the Nb surfaces in the SRF field.

The first topic is about a new Nb surface polished technique called buffered electropolishing (BEP) that was developed at JLab<sup>2</sup>. This technique can produce the smoothest surface finish ever reported in the literature<sup>3</sup>. It was also demonstrated that under a suitable condition, a Nb removal rate higher than 10  $\mu\text{m}/\text{min}$  could be realized. Efforts have been made to try to understand the polishing mechanism through experiments with a well defined experimental geometry on small flat Nb samples. A unique versatile vertical polishing system was constructed to perform BEP on Nb single cell cavities. Small flat samples, Nb dumbbells and Nb single cell cavities were also studied and treated at CEA Saclay in France and Peking University in

China and the cavities were RF tested at JLab. Experimental results will be analyzed and summarized. It is showed that BEP is a very promising candidate for the next generation surface polishing technique for Nb SRF cavities.

A second topic will deal with a new Nb surface cleaning technique employed gas cluster ion beam (GCIB)<sup>4</sup>. This is a result of collaboration with Epion Corporation, Fermi Lab, and Argonne Lab. Beams of Ar, O<sub>2</sub>, N<sub>2</sub>, and NF<sub>3</sub> clusters with accelerating voltages up to 35 kV were employed in this technique to bombard on Nb surfaces. The treated surfaces of Nb flat samples were examined by several surface experimental systems such as SEM, EDX, AFM, SIMS, and 3-D profilometer. The experiments revealed that GCIB technique could not only modify surface morphology of Nb, but also change the surface oxide layer structure of Nb and reduce the number of field emission sites on the surface dramatically. Computer simulation via atomistic molecular dynamics and a phenomenological surface dynamics was employed to help understand the experimental results. A system was set-up at Epion Corporation to do treatments on Nb single cell cavities and then RF-tested at JLab. The experimental results will be summarized and the perspective of this technique for real applications is discussed.

Finally, I will show two typical examples of surface studies of Nb using a high resolution transmission electron microscope<sup>5</sup> and a home-made scanning field emission microscope<sup>6</sup> respectively.

4:20pm **VT+MN+NS+SS+AS-TuA8 Early Stages of Nb Growth on Cu for SRF Accelerator Applications**, *C. Clavero*, The College of William and Mary, *N.P. Guisinger*, Argonne National Laboratory, *R.A. Lukaszew*, The College of William and Mary

Among the large range of possible applications for superconducting Nb thin films, coatings for superconducting radio-frequency (SRF) cavities in linear accelerators have greatly aroused the interest of researchers in the last years[1]. Superconducting thin films and multilayer coatings are expected to increase further the maximum field gradients that SRF cavities can withstand, pushing them above 100 MeV/m [2]. In this regard, Nb coated Cu cavities have been proposed as a prototypical system for this purpose since they combine the better thermal stability of Cu due to its much higher thermal conductivity and the superconducting properties of Nb thin films [3]. Nevertheless, it is well known that structural dislocations and localized surface resistive defects on the thin films have a dramatically negative influence on their superconducting properties and resonator quality. Indeed, the quality of the films is strongly conditioned by the growth mode below the single atomic layer coverage at the very early stages of growth, and thus special attention needs to be devoted to this range. Here we present a complete study on the early stages of growth of Nb on Cu(111). Different growth and annealing temperatures ranging from room temperature (RT) to 600 °C were used in order to investigate the characteristic growth mode of Nb in the sub-monolayer coverage range. Scanning tunneling microscopy (STM) and scanning tunneling spectroscopy (STS) were used to investigate morphology and chemical composition of the surfaces with atomic resolution. Growth of sub-monolayer coverages at RT leads to amorphous Nb islands with 1 and 2 AL heights. Annealing at 350 °C gives rise to crystallization of the islands pseudomorphically with the substrate, *i.e.* Nb(111). Further annealing at 600 °C promotes interdiffusion of Nb atoms into the Cu substrate and alloying of the islands. Growth of higher coverages above 1 AL at 350 °C reveals preferential Volmer-Weber growth mode.

1. H. Padamsee, Annual Review of Nuclear and Particle Science, 635 (1993).
2. A. Gurevich, Applied Physics Letters (1), 012511 (2006).
3. C. Benvenuti, S. Calatroni, I. E. Campisi, P. Darriulat, M. A. Peck, R. Russo and A. M. Valente, Physica C: Superconductivity (3-4), 153-188 (1999).

4:40pm **VT+MN+NS+SS+AS-TuA9 Epitaxial Niobium Thin Films for Accelerator Cavities**, *W.M. Roach*, *D. Beringer*, *C. Clavero*, College of William and Mary, *C. Reece*, Thomas Jefferson National Accelerator Facility, *R.A. Lukaszew*, College of William and Mary

The currently proven superconducting radio frequency (SRF) technology used in linear accelerators is based on bulk niobium cavities. Since this has a high cost and these cavities are approaching the maximum field gradients that they can withstand [1], development of a suitable, reliable, cost effective alternative to bulk niobium SRF cavities is needed. Attempts have been made to replace bulk niobium cavities with niobium-coated copper cavities since the thermal conductivity of a suitable base material such as copper is better than bulk niobium [2]. Coating niobium on SRF cavities is a promising but also challenging path, since there are several difficulties associated with various thin film deposition techniques and a lack of systematic studies pertinent to niobium thin film nucleation and growth leading to surfaces of greatest benefit.

Our systematic studies show that the transport properties, in particular the residual resistance ratio (RRR), are improved when niobium is epitaxially grown on crystalline ceramic substrates such as MgO and Al<sub>2</sub>O<sub>3</sub>, compared to niobium grown on (001) copper templates. Since grain boundaries are typically one of the main obstacles to superconducting transport, we show how the increased number of crystallographic domains that can occur during epitaxial niobium growth onto copper surfaces leading to higher density of grain boundaries can explain our results. We will discuss a route to improved transport properties while maintaining thermal efficiency by using alternative seed-layers grown on copper templates that can limit increased grain boundary density. We will show our correlated studies of microstructure and surface morphology (RHEED and AFM) and the resulting transport/magnetic properties (four point probe and SQUID magnetometry) illustrating possible mechanisms to improve SRF cavity performance of such niobium films.

This work is funded by HDTRA1-10-1-0072 from the Defense Threat Reduction Agency as well as a subcontract from Thomas Jefferson National Accelerator Facility under contract DE-AC05-06OR23177 from the Department of Energy as supplemented by ARRA funds.

References:

- [1] P. Kneisel *et al.*, Proceedings of 2005 Particle Accelerator Conference, Knoxville, TN, TPPT076 (2005).
- [2] S. Calatroni, Physica C **441**, 95 (2006).

5:00pm **VT+MN+NS+SS+AS-TuA10 Development via Energetic Condensation of Niobium Thin Films Tailored for Superconducting RF Applications**, *A.-M. Valente-Feliciano*, Jefferson Lab

For the past three decades, bulk niobium has been the material of choice for SRF cavities applications. In the recent years, RF cavities performances have approached the theoretical limit for bulk niobium. For further improvement of RF cavity performance for future accelerator projects, an interesting alternative has been recently proposed by Alex Gurevich with the Superconductor-Insulator-Superconductor multilayer approach, using the benefit of the higher critical field H<sub>c2</sub> of higher-T<sub>c</sub> superconductors without being limited with their lower H<sub>c1</sub>.

JLab is pursuing this approach with the development of multilayer structures based on NbTiN via magnetron sputtering and High Power Impulse Magnetron Sputtering (HiPIMS). Insulators such as, AlN, Al<sub>2</sub>O<sub>3</sub> and MgO are being investigated as candidates for the insulator layers.

This paper presents the characteristics of NbTiN and insulator layers produced and results on NbTiN-based multilayer structures on bulk Nb and thick Nb films.

5:20pm **VT+MN+NS+SS+AS-TuA11 Evaluation of Secondary Electron Emission Yield Suppression Coatings at CEsrTA**, *Y. Li*, *X. Liu*, *J. Calvey*, *J. Conway*, *J.A. Crittenden*, *M.A. Palmer*, *J.P. Sikora*, Cornell University, *S.De. Santis*, Lawrence Berkeley National Laboratory

The performance of particle accelerators may be significantly limited due to buildup of electron cloud (EC) in the vacuum chambers. The EC buildup intensity is strongly affected by secondary electron emission from interior surfaces of the chambers. Application of coatings with reduced secondary electron yield (SEY) onto vacuum chamber interior surfaces is one of the most economical EC suppression techniques. As a part of the International Linear Collider (ILC) R&D program, the Cornell Electron Storage Ring (CESR) has been successfully reconfigured as a Test Accelerator (CesrTA) to study EC buildup and suppression techniques. During the CesrTA program, various passive SEY-reduction coatings (TiN, amorphous-carbon and diamond-like carbon thin films) have been applied to diagnostic vacuum chambers in CESR in order to evaluate the efficacy of the EC suppression and the vacuum performance of these coatings in an accelerator environment. These chambers are equipped with both vacuum instrumentation (ion gauges and residual gas analyzers), as well as EC diagnostics (retarding field analyzers and RF-shielded pickups). In this paper, we present the results of studies of the vacuum conditioning and EC mitigation performance of these coatings.

5:40pm **VT+MN+NS+SS+AS-TuA12 Electron Cloud Mitigation for the Large Hadron Collider (LHC)**, *V. Baglin*, *G. Bregliozzi*, *P. Chiggiato*, *P. Costa Pinto*, *J.M. Jimenez*, *G. Lanza*, *M. Taborelli*, *C. Yin Vallgren*, CERN, Switzerland

One of the main issues for the vacuum system of the Large Hadron Collider (LHC) is the build-up of electron clouds generated by electron multipacting

in presence of beams. The occurrence of spatially distributed negative charges can lead to beam instabilities and emittance blow-up, pressure rises with a consequent background growth in the experimental areas, and increased thermal load in the cryogenic sections. The development of electron clouds depends on beam intensity and structure, magnetic field, and, in particular, the secondary electron emission of the beam pipe walls. With respect to this latter point, electron clouds can be eradicated whenever the maximum secondary electron yield becomes lower than a critical threshold. In the LHC the problem has already been tackled at the design phase by introducing TiZrV non-evaporable getter thin film coatings as the baseline for most of the room temperature sectors of the ring. After activation by in situ heating, this material provides maximum secondary electron yield lower than 1.1. In addition, during operation, dedicated scrubbing runs are carried out by generating intentionally electron clouds and electron impingement onto the non-coated vacuum chambers, in a way to reduce their secondary electron yield. Recently magnetron sputtered carbon coatings have been also studied because they can reach exceptionally low secondary electron emission without any heating; their application in the LHC injectors and future LHC components is under investigation.

The effect of electron clouds in the pressure variations during the first months of LHC operation will be presented, together with the effects ascribed to the mitigation techniques.



# Tuesday Afternoon Poster Sessions

## In Situ Spectroscopy and Microscopy Focus Topic

Room: East Exhibit Hall - Session IS-TuP

### In Situ Spectroscopy and Microscopy Focus Topic Poster Session

**IS-TuP1 In Situ Infrared Spectroscopy of Oxidation Process of Amorphous Carbon Film, Depending on Substrate Temperatures.** *M. Shinohara, Y. Takaki, K. Hara, Y. Takami, Y. Matsuda, H. Fujiyama*, Nagasaki University, Japan

There has been much interest in amorphous carbon films because they have a lot of useful properties: mechanical hardness, chemical inertness, and changeable electrical properties. The films can be deposited at low temperatures by using plasma process. The films have been used as coating materials for mechanical apparatus. The property of the film surface can be change with the addition of the other atoms on the surface. The addition of oxygen atoms to the surface leads the surface hydrophilic. The hydrophilic property on the surface has advantages to the further surface treatment. Therefore, it is important to understand the oxidation process of amorphous films. One of the effective oxidation methods is oxygen plasma exposure. We investigated the plasma oxidation process with in-situ infrared spectroscopy in multiple internal reflection geometry (MIR-IRAS). In this presentation, we focus on the dependence of oxidation process on the substrate temperatures. Infrared spectroscopic studies indicated that the oxygen plasma exposure induced the generation of OH components in the film. It means that carboxyl group would be formed by the exposure. With the increases of the substrate temperatures, the formation of OH components in the film was suppressed; moreover, the hydrophilic property was decreased with the substrate temperatures. On the other hand, the etching rate due to the oxygen plasma exposure was increased with the substrate temperatures. It is suggested that the etching rate is increased with substrate temperature, compared with the preservation of the OH components in the film.

**IS-TuP3 In Situ TEM Studies of Nanoparticle Growth in a Fluorozirconate (ZBLAN) Glass Matrix.** *J. Johnson*, University of Tennessee Space Institute

ZBLAN glass-ceramic materials are being developed as x-ray imaging plates. The materials are doped with europium and chlorine and can be heat treated in such a way that they form a novel nanocomposite material containing barium chloride nanocrystals, with the ability to convert x-rays into stable electron-hole pairs. The image can be read out afterwards with a scanning laser beam in a photostimulated luminescence process.

The ZBLAN glass only acts as an imaging plate upon annealing. As the annealing temperature and annealing time are increased, so a higher degree of nucleation of BaCl<sub>2</sub> crystallites inside the glass matrix is observed. As a result, more crystallites are available to incorporate Eu<sup>2+</sup> and hence increase the fluorescence intensity. However, a higher annealing temperature and a longer annealing time also lead to a larger degree of crystal growth, resulting in bigger nanoparticles. This leads to a decrease in spatial resolution of a ceramic-glass storage phosphor. The optimal annealing condition thus needs to compromise between the fluorescence intensity and the spatial resolution.

Here we present *in situ* TEM studies of ZBLAN glasses, being carried out to further understand the growth of nanoparticles inside a glass matrix under various heating conditions.

## Surface Science Division

Room: East Exhibit Hall - Session SS-TuP

### Surface Science Poster Session

**SS-TuP1 Oxidative-Coupling Reactions via Nucleophilic Attack on Gold Surface.** *B. Xu, C.M. Friend, R.J. Madix*, Harvard University

Metallic gold owes its centuries-old mystique and intrinsic value to its chemical inertness toward bulk compound formation. In the past decade, however, it has been discovered that the surface of gold is far from inert, and that gold can catalyze important chemical transformations – particularly with the assistance of molecular oxygen or other oxidizing agents. These processes are of particular significance because they may occur at remarkably low temperatures and pressures, suggesting the possibility of energy efficient and environmentally benign reaction conditions using

metallic gold catalysts. Recently, there has been a focus on selective oxidation of alcohols to aldehydes, oxidative self-coupling of alcohols to form esters and, most recently, acylation via amine-formaldehyde coupling. Our work under ultra-high vacuum (UHV) condition on the well defined model system of Au(111) surface has unequivocally proved that surface adsorbed atomic oxygen is critical in facilitating a range of nucleophilic coupling-reactions among alcohols, aldehydes and amines. A general reaction mechanism for this class of coupling-reactions is established: surface alkoxy or amide is formed via the deprotonation of the corresponding alcohol or amine by surface atomic oxygen, which can subsequently nucleophilically attack the aldehydes (formed in situ from alkoxy or introduced directly) and produce the corresponding ester or amide. The product distribution of our low-pressure experiments match remarkably well with gas phase reactions carried out in the ambient condition as well as liquid phase reactions, proves the generality of the mechanism.

**SS-TuP2 Many-Body Interactions in Quasi-Freestanding Graphene.** *D.A. Siegel, C.H. Park*, University of California, Berkeley, *C.G. Hwang*, Lawrence Berkeley National Laboratory, *J. Deslippe*, University of California, Berkeley, *A.V. Fedorov*, Lawrence Berkeley National Laboratory, *S.G. Louie, A. Lanzara*, University of California, Berkeley

Until recently it had been extremely difficult to experimentally address one of the most fundamental questions about graphene: How do the quasiparticles behave in neutral graphene, i.e. when the chemical potential coincides with the Dirac point energy? Here we address this question by investigating graphene on a particularly interesting substrate, the carbon face of SiC, with high-resolution angle-resolved photoemission spectroscopy (ARPES). We present the first direct measurements of the self-energy in graphene near the neutrality point, and show that the many-body physics in graphene differ from those of an ordinary metal. These exciting findings set a new benchmark in our understanding of many-body physics in graphene and a variety of novel materials with Dirac fermions.

**SS-TuP3 Edge Termination of Modified Graphene Oxide during Thermal Exfoliation.** *M. Acik, Y.J. Chabal*, The University of Texas at Dallas

Nanopore formation in carbon materials (e.g. exfoliated nanostacks of graphite) has been widely studied through mechanical exfoliation, intercalation, electrochemical separation, chemical or thermal exfoliation of graphite oxide (GO) via expansion with partial oxygen removal. Amongst all these methods, exfoliation of modified graphene (GO), a solution-processable precursor compound where aromatic and heterocyclic rings with embedded oxygen functionalities exist, by thermal processing still remains elusive for the following reasons: (1) poor control of GO composition (initial oxygen content), (2) poor understanding of the chemical composition, (3) unknown role of oxygen, adjoining oxygen interactions, and edge termination with oxygen. Infrared absorption spectroscopy coupled with *in-situ* thermal annealing process [1] makes it possible to examine the chemical changes taking place during thermal reduction to identify and understand interacting molecular environment and the edge functionalization. To unravel the complex mechanisms leading the removal of oxygen in GO, we have performed *in-situ* transmission infrared absorption spectroscopy (IRAS) measurements of graphene/graphite oxide (GO) thin and bulk films upon thermal annealing (60-850°C) in vacuum (10<sup>-3</sup>-10<sup>-4</sup> Torr). Control of the edge geometry of finite-sized modified graphene flakes depends very much on the control of the processing methods. This edge reconstruction further determines electronic, electric, optical and mechanical properties of the exfoliated modified graphene flakes. Therefore, we not only perform studies deriving a thermal reduction mechanism, but also examine the edge reconfiguration with oxygen. We report here the observation of a surprisingly strong IR absorption band that occurs only upon thermal reduction of GO. After annealing at 850°C in vacuum, the strong enhancement of the new IR active absorbance band is observed at ~800 cm<sup>-1</sup>[2]. The intensity of this band is 10-100 times larger than what is expected for the oxygen content of the reduced GO, namely between 5 and 8 at.%. This band is assigned to a specific oxidation state, involving oxygen located in the basal plane (forming C-O-C bonds) and at *atomically straight* edges of reduced graphene. The large enhancement in IR absorption is attributed to the direct participation of electrons, induced by the asymmetric C-O-C stretch mode displacement. These findings open new possibilities in the field of nanoelectronics for all sensor and energy storage applications. [1] M. Acik, *et al.* J. Am. Chem. Soc. (2011), *in preparation*. [2] M. Acik, *et al.* Nat. Mater. 9, 840-845 (2010).

**SS-TuP4 Electrocatalytic Surfaces: Structure, Reactivity and Nanotemplating.** X.F. Yang\*, Lehigh University, B.E. Koel, Princeton University

Electrocatalysis in energy related applications such as fuel cells and hydrogen production impacts and possibly defines the future energy technology picture. Pt-based electrocatalysts are widely used because of their exemplary performance, but these catalysts have serious drawbacks, e.g., cost, modest efficiency, and low durability, which limit fuel cell development. Our research explores non-Pt electrocatalysts or ultrathin-Pt film electrocatalysts to gain insight and discover materials that can replace Pt or greatly reduce Pt loadings while retaining or even increasing activity and/or stability. Our approach is to use model electrocatalyst surfaces with well-defined composition and structure to simplify and exert control on the system to improve our understanding of the surface phenomena that control electrocatalytic reactions. In this work, four types of model electrocatalysts were prepared in UHV: (i) Pd<sub>3</sub>Fe(111), (ii) Au/Pd<sub>3</sub>Fe(111), (iii) Pt on a faceted C/Re(11-21) nanotemplate, and (iv) Pt/HfIr<sub>3</sub> (poly). These surfaces were characterized using LEED, XPS, LEIS, and AES, and then their electrocatalytic activity for the oxygen reduction reaction (ORR), the hydrogen evolution reaction (HER), and ethanol oxidation (EO) reaction was measured.

Significant surface segregation of Pd was discovered after clean Pd<sub>3</sub>Fe(111) was annealed at high temperatures in UHV. The surface structure strongly depends on the annealing temperature, with the formation of an atomically smooth, random substitutional alloy by heating to 1000 K, and the formation of Pd monomer and dimer adatoms by heating to 1250 K. The annealed Pd<sub>3</sub>Fe(111) surfaces exhibit higher ORR reactivity than pure Pt. When a submonolayer amount of Au was deposited on Pd<sub>3</sub>Fe(111), the Au/Pd<sub>3</sub>Fe(111) surface was found to be highly active for the ORR. The activity was strongly dependent on the Au coverage, with the highest activity found at 0.6-ML Au. A Pt monolayer deposited on a nanofaceted C/Re(11-21) surface had a catalytic activity higher than Pt(111) for the HER. In addition, a Pt monolayer on a polycrystalline HfIr<sub>3</sub> substrate displayed great improvement in reactivity for electrochemical ORR and EO. In summary, we have investigated a range of non-Pt and ultrathin-Pt film model electrocatalysts that are more active than pure Pt and that point to new materials that could be used to reduce cost and improve activity by nanoengineering novel electrocatalysts.

**SS-TuP5 Characterization and Chemical Activity of Pt-Au and Ni-Au Bimetallic Clusters on TiO<sub>2</sub>(110).** S.A. Tenney†, B.A. Cagg, W. He, M.S. Levine, R.P. Galhenage, D.A. Chen, University of South Carolina

Oxide-supported bimetallic Pt-Au and Ni-Au clusters were studied as model catalysts for low temperature oxidation reactions. The growth, composition, and chemical activity of Ni-Au and Pt-Au clusters deposited at 300 K on TiO<sub>2</sub>(110) were investigated using scanning tunneling microscopy (STM), low energy ion scattering (LEIS), X-ray photoelectron spectroscopy (XPS), and temperature programmed desorption (TPD). The importance of the Au-titania interface for low temperature oxidation was illustrated by a series of TPD and STM experiments that show a direct correlation between the number of Au-titania interfacial sites and the activity on the surface. Bimetallic clusters were grown by first depositing Ni or Pt onto the surface in order to seed the more mobile Au at existing Ni or Pt clusters. The surfaces of the bimetallic clusters are significantly enriched in Au and are almost entirely pure Au for clusters with > 50% bulk Au composition. TPD of methanol and CO on bimetallic clusters that are highly enriched in Au at the surface still show significant activity characteristic of Ni or Pt at the surface, suggesting that methanol and CO are able to induce the diffusion of Ni and Pt to the surface of the clusters. Heating the bimetallic clusters above 600 K results in the selective encapsulation of Pt or Ni by a thin film of titania. Pre-annealed Pt-Au and Ni-Au bimetallic clusters show promise for enhanced activity towards the conversion of methanol to formaldehyde.

**SS-TuP6 Pattern Formation through Leveled Copper Etching after Dysfunctional Electropolishing.** A.D. Pauric, P. Kruse, McMaster University, Canada

Electropolishing is a common industrial practice whereby a metallic surface is subjected to an anodic potential in an appropriate electrolyte to produce a microscopically smooth surface. It is typically performed in concentrated acid with cell potentials ranging from between 1.3 and 2.3V. However, little research has been conducted in the parameter space outside the electropolishing regime. Previous research in our group using deviations from electropolishing conditions has characterized a wide range of fascinating surface structures including terraces, oxide nanotubes, stripes, and dimples. Our current work involves using the copper/phosphoric acid system as a model system to study deviations from electropolishing conditions and the resultant surface features.

Upon exposing copper substrates to a high applied cell potential in concentrated phosphoric acid, etched surface patterns up to over a micron in depth are observed. Characterization of the patterns includes the use of atomic force microscopy (AFM), scanning electron microscopy (SEM), and surface enhanced Raman spectroscopy (SERS). The surface patterns evolve with variation in temperature and phosphoric acid concentration. A distinguishing feature is that the patterns are etched into rather than grown upon the copper substrate, promoting mechanical stability. Additionally, the tops of the surface features are level with respect to their surroundings. Potential applications include electrodes, current collectors for lithium ion batteries, catalysts, micro-cooling, and substrates for the fabrication of other surface morphologies.

**SS-TuP7 Surface Chemistry of Atomic Layer Deposition of Manganese Thin Films.** H. Sun, X. Qin, F. Zaera, University of California, Riverside

Manganese thin films can potentially be used as Cu diffusion barriers in microelectronic devices, and may possibly be grown by atomic layer deposition (ALD), to produce highly uniform thin films with good conformality in high aspect-ratio structures. Here, the early stages of film growth of two precursors, methylcyclopentadienyl manganese tricarbonyl (CH<sub>3</sub>C<sub>5</sub>H<sub>4</sub>)Mn(CO)<sub>3</sub> and dimanganese decacarbonyl (Mn<sub>2</sub>(CO)<sub>10</sub>), were investigated by X-ray photoelectron spectroscopy (XPS) to assess their viability for ALD of manganese thin films. In most cases, only oxidized manganese could be deposited on silicon substrates covered with their native oxide layer. Only in depositions using (CH<sub>3</sub>C<sub>5</sub>H<sub>4</sub>)Mn(CO)<sub>3</sub> at relatively high temperatures (>300°C) it was possible to detect a low binding energy feature in the Mn 2p XPS that could be assigned to metallic Mn (although it is also possible to come from manganese silicate). It was also determined that that low-binding-energy manganese species appears only after the growth of a layer of oxidized manganese, and seems to form in the sub-surface. Electron-induced deposition was also studied and compared with the thermal process. The Mn<sub>2</sub>(CO)<sub>10</sub> precursor was much more reactive, and could lead to multilayer deposition by itself at temperatures as low as 200°C

**SS-TuP8 Spin Effects on Metal Surface Reactions: O<sub>2</sub> on Ferromagnetic Pt.** M.C. Escano, N.T. Quang, H. Nakanishi, Osaka University, Japan, E. Gyenge, The University of British Columbia, Canada, H. Kasai, Osaka University, Japan

We studied O<sub>2</sub> chemisorption on Pt surface in the need to promote O<sub>2</sub> activation. Activation, in this case, is defined as lowered activation barrier for O<sub>2</sub> dissociation but minimized O adatom (O<sub>ad</sub>) binding energies; or a significantly stretched O-O bond in a loosely bound molecular O<sub>2</sub>. This kind of reaction is not easy to attain since O<sub>2</sub> may present the same affinity to surface in its reaction path. However, such unique reaction is often sought in many electrochemical/chemical systems (i.e. fuel cell cathode catalyst, three-way automotive catalyst). Here, we show how the magnetic state of Pt can achieve this desired reaction. The model system involves a non-magnetic Pt layer pseudomorphically laid on top of magnetic surface (M=Fe(001), Co(001)). The *ab-initio* calculation based on spin-polarized density functional theory, suggests that the magnetic ground state of the system is a ferromagnetically coupled Pt-M layers[1]. The induced spin moment of 0.50μ<sub>B</sub> in the Pt layer is in agreement with X-ray Magnetic Circular Dichroism (XMCD) [2]. The hybridization of Pt-5d with the M-3d states give characteristic exchange splitting similar to the spin-resolved inverse photoemission spectroscopy [3]. Using the Heisenberg spin Hamiltonian to determine the exchange interaction, we note that strong inter-layer coupling of the Pt-M spins gives a transition temperature of Pt layer higher than room temperature, in agreement with [2,3].

Potential energy surfaces obtained for O<sub>2</sub> dissociative adsorption on ferromagnetic Pt layer show much lower activation barrier for dissociation and also lowered O<sub>ad</sub> binding energy. For molecular adsorption, the O<sub>2</sub> vibrational frequency is lower on ferromagnetic Pt as compared to paramagnetic Pt, despite the much lower binding energies on the former. We note that spin effects played significant role rather than charge transfer effects on the over-all structure and binding of the O<sub>2</sub> at transition state and on the surface [4]. This will be discussed in the meeting in terms of local density of states, charge transfer and spin density, and other parameters involved in the bonding and magnetic interactions.

**References**

1. M.C. Escano, T.Q. Nguyen, H. Nakanishi, H. Kasai. J. Phys.: Condens. Matter. 21 (2009) 49221.
2. J. Lyubina, I. Opahle, M. Richter, O. Gutfleisch, K. Muller and L. Schultz Appl. Phys. Lett. 89 (2006) 032505
3. R. Bertacco and F. Ciccacci, Phys. Rev. B, 57 (1998) 96.
4. M.C. Escano, H. Nakanishi and H. Kasai, J. Phys. Chem. A 113 (2009) 14302.

\* Morton S. Traum Award Finalist

**SS-TuP9 X-ray Diffraction Study on Hydrogen-Induced Pd(110) Surface Reconstruction, M. Takahashi, S. Fujikawa, W. Hu, Japan Atomic Energy Agency, H. Tajiri, Japan Synchrotron Radiation Institute**

Absorption of hydrogen into a substrate begins with dissociated adsorption of hydrogen molecules. The mechanism of the transition from adsorption to absorption is an important knowledge for improving the performance of hydrogen storage materials. The aim of the present study is to verify the hydrogen absorption model in atomic scale through quantitative determination of structures of hydrogen-adsorbed Pd(110) by synchrotron X-ray diffraction.

Experiments were performed at a synchrotron beamline 13XU at SPring-8 using a surface X-ray diffractometer integrated with a UHV chamber equipped with a cryostat. The sample was Pd(110) single crystal which was 10 mm in diameter and 3 mm in thickness. The clean Pd(110)-(1x1) surface was prepared by electrochemical etching in HCl solution and cycles of Ar-sputtering and annealing at ca. 900 K in UHV. For the hydrogen adsorption experiments, the hydrogen pressure was carefully controlled with a needle valve and a nude ion gauge.

We measured five crystal truncation rod (CTR) profiles with increasing substrate temperature to room temperature from 57 K after the substrate was exposed to  $10^{-6}$  Torr s hydrogen. Before and after hydrogen adsorption at 57 K, the CTR profiles changed only slightly. More distinctive changes were observed when the sample temperature reached 180 K. At room temperature, the CTR profiles were accounted for by a structure model with disordering of surface atoms. According to past Low-energy electron diffraction, He diffraction and thermal desorption spectroscopy studies, hydrogen adsorption below a substrate temperature of 120 K induced the (1x2) surface reconstruction with 1.5 monolayer (ML) hydrogen through the (2x1) structure at a hydrogen coverage of 1 ML. When the temperature is raised to 200 K, the (1x2) reconstruction returns to a low-coverage 2x1 phase without hydrogen desorption. A comparison with our X-ray diffraction results and these past studies shows that the change of the CTR profiles at 180 K corresponds to the transition from the (2x1) to (1x2) reconstructions and concomitant incorporation of hydrogen into subsurface. These results provide us with an atomic-scale picture that explains how adsorbed hydrogen is absorbed into the Pd bulk.

**SS-TuP10 Single Molecule Force Spectroscopy Studies on Nanoclay Surfaces, B. Ozkaya, G. Grundmeier, University of Paderborn, Germany**

Sequential adsorption of oppositely charged polyelectrolytes leads to multilayered thin films via electrostatic self-assembly. Incorporation of sheet-like inorganic nanoparticles is a promising method to improve barrier and ion transport properties, as well as mechanical properties in such films. The interface chemistry between the nanosheets and the polyelectrolyte segments plays a crucial role on design of thin coatings with tailored properties. In the present study, we have investigated the effects of pH and ionic strength on the adsorption of single polyelectrolyte molecules on natural clay (Na-Montmorillonite) platelets by means of AFM-based single molecule force spectroscopy (SMFS). SMFS is one of the few methods where in-situ experiments can be performed to obtain precise and quantitative information on interaction forces at a molecular level. In order to perform SMFS on clay platelets (lateral size: 50-300 nm), a heterogeneous model surface has been obtained via electrostatic immobilization of exfoliated clay platelets on template stripped ultra-flat Au(111) surfaces. Probe molecules (polyallylamine) were covalently attached to the gold coated AFM cantilever. Equilibrium desorption plateaus of constant force were obtained from the successive force-distance measurements. By adjusting the ion valency in the electrolyte, selective information from clay platelets could be obtained. In the presence of monovalent ions, desorption plateaus of constant force in the range of ~50 pN were obtained from pH 3 to pH 7. At pH values above the  $pK_b$  value of polyallylamine, confirmed with polarization modulation infrared reflection absorption spectroscopy (PM-IRRAS) measurements on cast polyallylamine- no detectable desorption event took place. The constant negative surface charge of clay platelets simplifies the evaluation of effects of electrical double layer and polymer line-charge density on adsorption of the polyelectrolyte molecules. Overall, the results of pH and ionic strength dependent de-adhesion measurements provide valuable information on the interplay between surface properties and polyelectrolyte adsorption giving the basis for an improved understanding of the behavior of silicate nanoparticles in polyelectrolyte films.

**SS-TuP11 Atomic Structure of Aluminum on Si(110): STM and First-principles Study of "4 × 6" Reconstruction, M. Yoshimura, D. Matsuoka, Toyota Technological Institute, Japan**

With the miniaturization of semiconductor devices, low-dimensional structures such as quantum wires and quantum dots have recently attracted much attention. The "16 × 2" on a clean Si(110) surface has been noticed as an effective and unique substrate for the fabrication of low-dimensional

nanostructures, because the one-dimensional undulated terrace structure of monatomic height and of about 2.5 nm width are formed. Because the hole mobility of Si(110) surface is about 1.5 times as large as that of Si(100) typically used as substrates of present semiconductor devices, higher speed operation is expected [1]. Thus, the interaction between Si(110) and metal is very important [2,3]. Aluminum is the typical metal forming Schottky barrier with silicon and the Al-adsorbed structures have been well examined on Si(111) or Si(001) plane [4,5]. In contrast, little is known about the structures of the Al/Si(110), particularly in real-space. In this study Al/Si(110) surfaces are investigated in real space using STM and first-principle calculation.

The experiments were carried out in an ultrahigh vacuum (base pressure:  $2.0 \times 10^{-8}$  Pa). First-principles calculation was performed using VASP program [6]. Aluminum was deposited on a clean Si(110)-"16 × 2" at 600 °C for 10 min to prepare a "4 × 6" reconstruction [7]. In the empty state, alternative arrangement of zigzag rows and straight rows is visible in empty states. In filled states, bright spots are prominent at the position of defects in the zigzag row. They are assumed to be silicon substitutional defects, as is the case for Al/Si(111) [8]. Thus we conclude Al and Si atoms formed zigzag and straight rows, respectively. In addition, the straight row of the silicon was composed of the silicon pentagon [9] as revealed by high-resolution STM. Based on the above observation, an atomic structural model is proposed and discussion will be made based on the theoretical calculation.

[1] T. Sato et al., *Phys. Rev.* **B4** (1971) 1950. [2] Y. Ohira, Master Thesis, Toyota Tech. Inst. (2007). [3] Y. Ohira et al., *Jpn. J. Appl. Phys.* **47** (2008) 6138. [4] M. Yoshimura et al., *Phys. Rev.* **B47** (1993) 13930. [5] H. Itoh et al., *Phys. Rev.* **B48** (1993) 14663. [6] G. Kresse et al., *Phys. Rev.* **B54** (1996) 11196. [7] A. V. Zotov et al., *Surf. Sci.* **277** L77 (1992). [8] R. J. Hamers, *Phys. Rev.* **B40** (1989) 1657. [9] T. An et al., *Phys. Rev.* **B61** (2000) 3006.

**SS-TuP12 Adsorption Dynamics of Ethylene on Si(001), M.A. Lipponer, N. Armbrust, University of Marburg, Germany, M. Durr, HS Esslingen, Germany, U. Hofer, University of Marburg, Germany**

The functionalization of semiconductor surfaces by means of organic molecules is of great interest due to possible applications in the field of nanoelectronics. However, only little information on the reaction dynamics of these systems is available. In this work, the adsorption dynamics of ethylene on Si(001) has been investigated. With ethylene being the most simple unsaturated organic molecule, the system serves as a model system for non-activated adsorption on semiconductor surfaces. In order to investigate its reaction dynamics, we employed a supersonic molecular beam which allows for the control of the kinetic energy of the impinging molecules. Additionally, surface temperature and the excitation of internal degrees of freedom were varied when measuring the sticking coefficients as a function of relative surface coverage by means of King and Wells techniques.

With increasing kinetic energy of the impinging molecules, we find a decrease of the initial sticking coefficient as it is typical for non-activated reaction channels; the excitation of the internal degrees of freedom is shown to have a minor impact on the reactivity. With increasing surface temperature, a decrease of the initial sticking coefficient is observed. Surprisingly, the maximum surface coverage also decreases with increasing surface temperature. The results are discussed in the context of a reaction channel via a mobile precursor with long lifetime at low temperatures.

**SS-TuP13 Surface Characterization of Polymeric Materials using TOF-SIMS and XPS, J. Lee, K.-J. Kim, Korea University, Republic of Korea, Y. Lee, Korea Institute of Science and Technology, Republic of Korea**

TOF-SIMS and XPS are very useful techniques for the analysis of solid surfaces composed of organic and polymeric species. In order to widen the application of TOF-SIMS and XPS to archeology and plasma process, we analyze the dyed fabrics and the fluorocarbon thin films. First, the fabrics dyed with natural dyes and synthetic dyes were investigated with TOF-SIMS and XPS. Dyes investigated belong to various chemical groups, which include indigo, carthamin, crocin, shikonin, curcumin, purpurin and alizarin. TOF-SIMS and XPS spectra for the dyed textiles showed specific molecular ions and fragment ions from organic dyes as well as elemental ions from metallic mordants. Several ancient fabrics were also analyzed to identify the natural dyes. Secondly, Fluorine-containing hydrophobic thin films were obtained by two different plasma methods : inductively coupled plasma (ICP) and pulsed plasma (PP). Three kinds of fluorine-containing gases such as  $C_2F_6$ ,  $C_3F_8$ , and  $c-C_4F_8$  were used to generate hydrophobic plasma polymer films. Process parameters for plasma polymerization such as gas ratio, gas pressure, pulse frequency, and processing time were investigated. Surface analytical instruments such as TOF-SIMS, XPS, and AFM were used to characterize the fluorocarbon thin films generated by

ICP and PP. In this work, TOF-SIMS was used to provide useful information about the chemical properties including surface composition and XPS was used to examine the chemical structure of dyed fabrics and fluorocarbon films.

**SS-TuP14 Links Between the Surface Atomic Arrangement and Catalytic Properties of Bimetallic Alloys: A First Principles-based Investigation**, J.A. Stephens, H.C. Ham, G.S. Hwang, University of Texas at Austin

Catalysts composed of more than one metallic element often exhibit remarkable activity and selectivity compared to their monometallic constituents. These synergistic properties often can be explained in terms of two kinds of effects: modification of catalyst electronic structure due to interactions between dissimilar metal atoms (ligand effects) and the presence of mixed-metal surface sites that, because of their size and shape, promote some chemical reactions more than others (ensemble effects). Understanding in detail how ligand and ensemble effects operate in particular cases is an important step toward realizing the longer term goal of rational catalyst design. Experimental study has provided valuable insight into this problem, but progress has been hampered by the difficulty of studying reacting systems with atomic resolution. We employ the tools of molecular simulation in a two-pronged approach to complement these efforts. First, we use density functional theory to explore how particular atomic arrangements in the surfaces of bimetallic alloys influence their catalytic function. We have found, for example, that the experimentally-observed ability of Au-Pd catalysts to promote the direct synthesis of hydrogen peroxide may depend on the presence of surface Pd monomers surrounded by Au. Our calculations indicate that on larger Pd ensembles, O-O bond scission can more readily occur, leading to the formation of water. We have similarly studied the oxygen reduction reaction and carbon monoxide oxidation on Au-Pd alloys. In the second prong of our work, we attempt to predict how the metal atoms in catalyst surfaces are actually arranged using a combination of density functional theory, the cluster expansion method, and Monte Carlo simulation. From these simulations, we have obtained the temperature- and composition-dependent ensemble size and shape distributions for the (111) and (100) surface facets of Au-Pd and Au-Pt alloys. Our results are in good agreement with available experimental observations.

**SS-TuP15 Nitrogen-Rich Heterocycles and Stimulus-Induced Switching Imaged by Liquid STM**, B.E. Hirsch, K.P. McDonald, A.H. Flood, S.L. Tait, Indiana University

Supramolecular motifs that provide controllable functionalization of surfaces on a nanometer scale offer significant advances in organic solar cells and other surface supported systems. Based on recent advances in two-dimensional organic self-assembly at the liquid/solid interface, we are developing complex surface architectures based on versatile nitrogen-rich heterocycles. This work focuses on the molecular design and subsequent adsorption of this class of compounds onto graphite (HOPG) utilizing liquid scanning tunneling microscopy to resolve the packing of the individual molecules. Current molecular design includes extended alkyl chains and other substituents including amide linkages to facilitate intermolecular ordering. Exploration of photo-activated, tip-induced, and chemically stimulated switching of these molecules is underway to enable manipulation of patterning and packing.

**SS-TuP17 Electrical, Physical, and Chemical Properties of the Metal to Amorphous Hydrogenated Boron Carbide Interface**, M.S. Driver, S. Karki, A.N. Caruso, University of Missouri - Kansas City

Boron carbide (BC), as a semiconducting material, has been under scrutiny for several decades for its use in heterostructure devices toward applications in solid-state neutron detection and thermoelectric energy conversion. The heterostructure devices are typically heterojunctions in which p-type amorphous hydrogenated boron carbide ( $a\text{-B}_5\text{C:H}_x$ ) is deposited onto n-type Si, and a Cr/Au contact is applied at the  $a\text{-B}_5\text{C:H}_x$  surface. Traditionally it has been believed that Cr forms an ohmic contact at the  $a\text{-B}_5\text{C:H}_x$  interface and that the heterostructure current-voltage rectification is a classical function of the p-n junction. However, we have found through photoemission studies of Cr overlayers on  $a\text{-B}_5\text{C:H}_x$  that a complex series of interfaces is formed, involving various oxides and borides, which are likely convoluting—and could be dominating—the observed rectification. To follow up the Cr findings, we have explored Al, Cu, Au, Ag, and Ti using the same set of studies. This talk will provide an overview of the electronic, physical, and chemical interfaces between the above metals and  $a\text{-B}_5\text{C:H}_x$  in the context of understanding the  $I(V)$  characteristics of the presumed p-n junction.

**SS-TuP22 Electron Stimulated Reactions on Graphene-Coated Ru: Relevance to Extreme Ultraviolet Lithography (EUVL)**, B.V. Yakshinskiy, R.A. Bartynski, Rutgers University

The contamination of optical surfaces in EUVL exposure tools, operating at 92 eV photon energy, results in degradation of the mirror reflectivity. We report studies of the thermal and electron-induced interaction of benzene and toluene vapors, typical background gases, with the Ru surface, as model cap layer for multilayer mirrors (MLM), using temperature programmed desorption (TPD), X-ray photoelectron spectroscopy (XPS), low energy ion scattering (LEIS), electron stimulated desorption (ESD), low electron energy diffraction (LEED), and scanning tunneling microscopy (STM). A low energy electron source (100 eV) is used to simulate radiation excitations on the surface produced by EUV photons. Heating of adsorbed hydrocarbons leads to a stepwise dehydrogenation and buildup a self-limited carbon monolayer. Electron bombardment of the bare Ru surface in the presence of gas phase hydrocarbons inevitably results in rapid accumulation of 1 ML of carbon or carbonaceous species. Subsequent contamination growth is determined by the electron-stimulated surface chemistry on the graphitized surface. Graphene monolayer and bilayer formation on Ru(0001) by hydrocarbon pyrolysis or by carbon segregation from the sample bulk is examined as a possible way to reduce the surface contamination rate. Graphene buildup has been confirmed by the presence of corresponding superstructures in LEED patterns and STM images. The binding energy of the hydrocarbon molecule is found to be smaller on a graphene layer than on disordered carbon. Electron irradiation of both bare and graphene covered Ru surface in the presence of benzene and toluene vapors leads to C-buildup. However, in a case of low irradiation density, when the electron flux is rate-limiting parameter, graphene monolayer exhibits its protective properties by slowing down carbon accumulation initially, until sufficient thick overlayer is formed. But in a case of high electron flux, when the adsorption of hydrocarbons is rate-limiting parameter, the carbon accumulation rate is invariant to the surface morphology.

The work is supported by Intel and DOE.

**SS-TuP23 Photoelectron Spectroscopy Studies of Superconducting  $\text{Mo}_2\text{B}$  and  $\text{Mo}_2\text{BC}$** , L. Huerta, Universidad Nacional Autonoma de Mexico, R. Falconi, Universidad Juárez Autónoma de Tabasco, Mexico, M. Flores, Universidad de Guadalajara, Mexico, A. Duran, R. Escamilla, Universidad Nacional Autonoma de Mexico

The effect of carbon in the structure of  $\text{Mo}_2\text{B}$  is increasing the superconducting transition temperature from 5.8 K to 7.5K. Polycrystalline samples of the  $\text{Mo}_2\text{B}$  and  $\text{Mo}_2\text{BC}$  were synthesized by the arc melting technique. The samples were characterized by x-ray diffraction (XRD), x-ray photoelectron spectroscopy (XPS) and ultraviolet photoelectron spectroscopy (UPS). XRD results shown that when carbon atoms are added to the structure of the  $\text{Mo}_2\text{B}$  compound a transition structural from body centered tetragonal to face centered orthorhombic is induced forming the  $\text{Mo}_2\text{BC}$  compound. XPS spectra revealed the presence of the Mo 3d, C 1s, and O 1s core levels associated to the chemical states  $\text{Mo}_2\text{B}$  and  $\text{Mo}_2\text{BC}$ . In order to explain the increase of transition temperature in the  $\text{Mo}_2\text{B}$  doped with carbon, we measured the valence band spectra (XPS and UPS), the results were compared with the density of states at the Fermi level  $N(E_F)$  of  $\text{Mo}_2\text{B}$  and  $\text{Mo}_2\text{BC}$ .

**SS-TuP24 Electrical and Photo-Functional Properties of Copper Oxide Thin Films Prepared by Reactive Magnetron Sputtering**, A. Shukur, H. Shukur, M. Sato, I. Takano, Kogakuin University, Japan

Copper oxide-based materials have been widely investigated due to their potential application in many technological fields. Cupric oxide ( $\text{CuO}$ ) is a monoclinic n-type semiconductor with a band gap of 1.2-1.5 eV, whereas cuprous oxide ( $\text{Cu}_2\text{O}$ ) is cubic p-type semiconductor with a band gap of 2.0 eV [1]. Copper oxides have been employed as a heterogeneous catalyst for several environmental processes, e.g. NO selective reduction, CO oxidation and  $\text{NO}_2$  decomposition and it is a very promising material for the development of photovoltaic devices like solar cells.

Copper oxide thin films were prepared by reactive magnetron sputtering. Firstly the sputtering chamber was pumped down to  $1.2 \times 10^{-5}$  Pa. The substrate was a corning glass (#1737) and mirror finishing stainless steel (304ss). The Ar gas was kept at 15sccm and the substrate temperature was kept at 300°C. The amount of oxygen flow rate was varied at 0-10sccm and also the deposition power was varied at 10-40W in order to prepare films with different structures. The structure of the deposited films was measured by X-ray diffraction method (XRD: MAC Science. Co, Ltd). The surface morphology was observed by atomic force microscopy (AFM). The resistivity, mobility and carrier concentration were measured by employing the Hall Effect measurement system. The optical properties of the films were determined by a UV-VIS spectrophotometer (Shimadzu).

In this study, the copper oxide thin films were deposited by a reactive DC magnetron sputtering method. Single Cu<sub>2</sub>O and CuO phase can be obtained by controlling the sputtering power. The p-type Cu<sub>2</sub>O thin films were prepared with 30-40W. The n-type CuO was observed at power 10-20W. Low electrical resistivity of 90.18Ωm was obtained for the thin film formed at sputtering power of 30W. The thin film was showed a band gap of 2.5eV attributed to Cu<sub>2</sub>O at sputtering power 30W whereas the band gap of 10w is 1.9eV. Our experimental investigation indicated that the sputtering power and oxygen flow rate has a significant influence on the electrical properties and optical band gap of the films.

**SS-TuP25 Influence of Crystal Structure for Electrochromism of WO<sub>3</sub> Thin Films Prepared by Reactive Magnetron Sputtering.** *H. Suzuki, H. Shukur, S. Ibrahim, I. Takano*, Kogakuin University, Japan

WO<sub>3</sub> is known as the material with an n-type semiconductor characteristic showing electrochromism (EC). The amorphous WO<sub>3</sub> thin film especially is used for a display device or a high-speed reaction sensor using electrochromism. WO<sub>3</sub> thin films for electrochromism have been fabricated by various film formation methods such as reactive sputtering and vacuum evaporation. The relationship between Ar gas and O<sub>2</sub> gas introduced during the film formation is the important condition for the structure of WO<sub>3</sub> thin film. The structure decides the electrochromic characteristic of the WO<sub>3</sub> thin film. In the reactive sputtering method Ar/O<sub>2</sub> gas flow rate especially induces the structure change of WO<sub>3</sub> thin film and the surface morphology.

In this study, WO<sub>3</sub> thin films were deposited by reactive magnetron sputtering with a W target in the condition of changing an Ar/O<sub>2</sub> gas flow rate. In the condition the WO<sub>3</sub> thin films with various crystal structures were fabricated. The relationship between the crystal structure and the electrochromic property were investigated with the great interest.

The WO<sub>3</sub> thin films were deposited by the multi process system with the helicon sputtering source on an Indium-tin oxide (ITO) coated glass and stainless steel (304SS) used as a substrate. The formation conditions of the WO<sub>3</sub> thin film were changed from 5 to 10 sccm in Ar gas flow rate and from 10 to 20 sccm in O<sub>2</sub> gas flow rate under a constant DC source power. The substrate temperature was kept at 473 K using an infrared lamp. The crystal structure and electrochromic property were investigated by X-ray diffraction (XRD) and UV-VIS spectrometer respectively. The crystal structure turned from the WO<sub>3</sub> thin film with the peak (112) to the WO<sub>3</sub> thin film with the peak (002), (112) and (022) with increasing Ar gas flow rate, while increase of O<sub>2</sub> gas flow rate gradually turned up the main peak (112). The maximum efficiency of electrochromic property was obtained at 7.5 sccm in Ar gas flow rate and 15 sccm in O<sub>2</sub> gas flow rate.

**SS-TuP26 The Friction Properties of F-Doped DLC Thin Film Prepared in a C<sub>7</sub>H<sub>8</sub> Atmosphere by the Ion-Beam Assisted Method.** *M. Kurosu, I. Takano*, Kogakuin University, Japan

DLC (Diamond-Like Carbon) is known as amorphous carbon including hydrogen and has a characteristic between graphite and diamond. DLC film has been prepared by various methods of chemical vapor deposition (CVD) or physical vapor deposition (PVD) including the sputtering method. The property of DLC shows wear resistance, high hardness and low friction coefficient. DLC is applied in various fields such as motor parts, tools and molds.

In this study, DLC films were prepared by the ion-beam assisted method that was the PVD method allowing a low-temperature formation. In this method the mixing layer which led to high adhesion was formed between the substrate and the DLC thin film. PTFE-Doped DLC (F-DLC) films were prepared by He<sup>+</sup> ion irradiation in the toluene (C<sub>7</sub>H<sub>8</sub>) gas. He<sup>+</sup> ion beam was irradiated at a current density of 5 μA/cm<sup>2</sup> with a constant accelerating voltage of 5 kV. PTFE doping was performed by using the electron-beam deposition method with PTFE evaporation rate from 0.05 to 0.2 nm/sec. The film thickness measured using QCM was kept at 200 nm. Film composition and microstructure were investigated by X-Ray photoelectron spectroscopy and Raman spectroscopy, respectively. The hardness was measured by an indentation method with a Knoop indenter. The friction coefficient was measured for an SUJ2 ball with a constant load of 0.98 N until the sliding distance reached to a length of 100 m. The friction coefficient property under the vacuum was measured in 5 x 10<sup>-4</sup> Pa.

Frictional properties changed under the vacuum and the atmosphere. Friction coefficient of the F-DLC thin film with PTFE deposition rate of 0.2 nm/sec showed 0.25 at a sliding distance of 100 m. Friction coefficient property of the F-DLC thin film under a vacuum showed 0.12 at a sliding distance of 100 m. It was found that F-DLC indicated a low friction coefficient in a vacuum. F-DLC can be expected to be used as one of space materials in the future.

**SS-TuP27 Photo-functional Properties of Cu-Added Titanium Dioxide Thin Films Prepared by Reactive Magnetron Sputtering.** *S. Arahara, H. Shukur, M. Sato, I. Takano*, Kogakuin University, Japan

TiO<sub>2</sub> has been known as one of a promising photocatalyst and is already used in various practical applications, such as the degradation of environmental pollutants and the self cleaning of glasses. Furthermore, the surface of TiO<sub>2</sub> exhibits high hydrophilicity under ultra-violet (UV) light irradiation. A crystal form of TiO<sub>2</sub> is classified according to structure as anatase, rutile and brookite. TiO<sub>2</sub> shows relatively high reactivity and chemical stability under UV light whose energy exceeds the band gap of 3.2eV in the anatase crystalline phase. The sun can provide an abundant source of photons. However, UV energy accounts for only a small fraction (~5%) of the sun's energy compared to the visible region (45%). Many techniques have been examined to improve this problem by the doping of transition metals into TiO<sub>2</sub>.

In this study, TiO<sub>2</sub> films were prepared by reactive magnetron sputtering using a Ti target in an Ar/O<sub>2</sub> gas mixture. Cu addition was performed by Cu sputtering onto those TiO<sub>2</sub> films. It was considered that the charge separation between an electron and a hole was improved by adding Cu to the TiO<sub>2</sub> surface. Composition and microstructure of these films were investigated by X-ray photoelectron spectroscopy and X-ray diffraction, respectively. Chromatic change of a methylene blue solution was applied to a photocatalytic property. Light irradiation to TiO<sub>2</sub> films in a methylene blue solution was carried out by using a commercial sterilizing lamp as ultraviolet light and an artificial sun light as visible light. Transmittance of a methylene blue solution was measured by a spectrophotometer. Furthermore, photocurrent between the TiO<sub>2</sub> film and a platinum electrode was measured by a volt-ampere characteristic using an unresisted ammeter in a KCl solution of 0.5 mol/l.

The crystal structure of TiO<sub>2</sub> turned from a rutile type into an anatase type with increase of O<sub>2</sub> gas flow rate. Photocatalytic property and photocurrent property of an anatase type of TiO<sub>2</sub> showed the high value. The effect of the Cu addition exhibited different behavior according to each crystal structure. As for the photocatalytic property, the effect of the Cu addition was observed in rutile type, while on the photocurrent property the effect of the Cu addition was observed in anatase type. It was considered that the charge separation between an electron and a hole was enhanced by adding Cu to the TiO<sub>2</sub> surface.

**SS-TuP28 Deviation from Wulff Structures for Pt Nanoparticles Supported on TiO<sub>2</sub>(110): A STM Study.** *F. Behafarid, B. Roldan Cuenya*, University of Central Florida

This study reports the shape of micellar platinum nanoparticles (NPs) supported on TiO<sub>2</sub>(110) resolved by scanning tunneling microscopy (STM). Since micellar NPs are initially spherical in shape at room temperature, the 3D faceted shapes obtained after high temperature annealing display structures typical of thermodynamic equilibrium, in contrast with kinetic shapes of physical vapor deposited NPs, which are normally 2D and dominated by the diffusion of metal atoms on the support. All of the NPs resolved show an epitaxial relationship with the support, evident by TiO<sub>2</sub>(110)[001] direction being one of the symmetry axis of the NPs. Analyzing these shapes reveals that in addition to hexagonal top (type A) and square top (type B) NPs reported for evaporated NPs, there are two additional categories of shapes observed for micellar NPs (Type C and D). Type A and B consist only of 111 and 100 facets at the interface with the support and the free top surface. However, type C and D feature also 110 facets either at the interface with the support or at the free surface. This facet orientation was not observed before in other studies due to its instability and high surface energy. The ratio of 100/111 facets obtained for these shape deviates from the Wulff structure. This deviation could be attributed to size effects, interface-induced strain, and/or possible TiOx adsorbates on exposed facets.

**SS-TuP29 Slope Selection in Au Growth Fronts by Protrusion Interactions.** *J.L. Sacedón, A. González González, J.A. Aznárez, E. Rodríguez Cañas, E. Vasco*, Consejo Superior de Investigaciones Científicas, Spain

Growth fronts of polycrystalline films composed by paraboloid-like surface protrusions (SPs) have been recently decomposed into elemental paraboloidal meridian zones, which allow a comprehensive statistical analysis of the film surface [1]. Using this analysis, local height distribution curves have been synthesized [2] and the interface width expressed as function of the statistical parameters [3]. The method evidences that the average value of the slopes obtained at the SP border remains constant during the growth [2]. The analysis of distribution curves of the terrace width (~ the inverse of the slope) at the SP borders provides three terrace-width limit values [4]: two of them in close agreement with the predicted ones within the frame of the standard slope selection theory, which is based on the balance between downhill/uphill surface currents for the A,B flanks

of preferential (111) fcc growth (an intra-SP mechanism); and the third one has been interpreted as a result of an external interaction between SPs and the borders of crystalline plates on which the SPs grew. In the selected slope theory formalism, the surface current balance is the condition to keep constant a characteristic terrace width along a straight infinite flank formed by uniform terraces. In this work, we show that is possible to obtain limit terrace-width values close to those observed experimentally for limited and curved profiles by using, at the SP border terraces, an external interaction parameter and upward “*Pav*” coefficients predicted by the theory [5]. Finally, we will propose a general self-organization formalism, which applied as an inter-SP mechanism to the over-growing and under-growing protrusions, allows to predict limit values of terrace widths for the A and B flanks, in a reliable agreement with the experimental ones.

[1] E. Rodríguez-Cañas, J. A. Aznárez, A. I. Oliva, and J. L. Sacedón, *Surf. Sci.* **600**, 3110 (2006)

[2] J. L. Sacedón, E. Rodríguez-Cañas, C. Munuera, A. I. Oliva, and J. A. Aznárez, *Phys. Rev. B* **72**, 195413 (2005)

[3] E. Rodríguez-Cañas, E. Vasco, and J. L. Sacedón, *Appl. Phys. Lett.* **90**, 013112 (2007)

[4] E. Rodríguez-Cañas, E. Vasco, J. A. Aznárez, A. Ruiz, C. Munuera, A. González-González, and J. L. Sacedón, *Surf. Sci.* **604**, 974 (2010)

[5] J. Yu, and J. G. Amar, *Phys. Rev. B* **69**, 045426 (2004)

**SS-TuP30 UV Induced Photodesorption of O<sub>2</sub> on Rutile TiO<sub>2</sub>(110): An Angular Imaging Study, D.P. Wilson, M.D. Kershis, Brookhaven National Laboratory, M.G. White, Stony Brook University and Brookhaven National Laboratory**

The binding states of oxygen on TiO<sub>2</sub>(110) are important for many reactions, including the degradation of organic compounds and photodesorption. Experimental data and theoretical calculations have shown many different configurations for O<sub>2</sub> on TiO<sub>2</sub>(110), including O<sub>2</sub><sup>-</sup>, O<sub>2</sub><sup>2-</sup>, and O<sub>4</sub><sup>-</sup>. Defect sites in titania (bridging oxygen vacancy, Ti<sup>3+</sup> interstitial), while necessary for the adsorption of oxygen, also play a role in the initial binding states. In this experiment, the angular distributions and images of oxygen photodesorption from a rutile TiO<sub>2</sub>(110) surface are studied under UHV conditions using a pump-probe Time-of-Flight (TOF) detection scheme to help determine the initial binding states of oxygen on this surface. Excitation occurs via exposure to 3.7 eV photons followed by one-photon ionization using 13.05 eV photons. The delay time between the lasers can be varied according to the maximum desorption velocity of the oxygen molecules. Ions were detected using a dual microchannel plate and a phosphor screen. A CCD camera positioned behind a phosphor screen captured the light emission of the phosphor, allowing for the imaging of the desorbing neutral O<sub>2</sub> molecules. SimION 3D was used to simulate the motion of the ions through a Time-of-Flight (TOF) mass spectrometer to generate a probability distribution for detection that was used to compare images at different delays.

Previous experiments on the oxygen velocity distribution on TiO<sub>2</sub> (110) showed 3 different “channels” for desorption, with two being “fast” and one being “slow”. The velocity distribution for the slow channel tracked with surface temperature, indicating that a trapping desorption mechanism dominated this channel. The two “fast” channels, however, did not depend on temperature and were attributed to two different oxygen binding states on TiO<sub>2</sub> (110). Many different binding states of oxygen have been predicted and it is unclear which state is responsible for which channel. Images of the fastest channel and comparisons at different coverage and photon flux are shown.

The methyl radical velocity distributions from 4 different ketones (acetaldehyde, acetone, butanone, and acetophenone) were also investigated. For ketones where methyl radical desorption is not the preferred pathway (butanone), a 2+1 REMPI scheme was used for signal enhancement. Using these model systems allows for direct comparison of different properties of each molecule.

# Wednesday Morning, November 2, 2011

## Plasma Science and Technology Division

Room: 202 - Session PS+SS-WeM

### Plasma Surface Interactions (Fundamentals & Applications) I

Moderator: C. Labelle, GLOBALFOUNDRIES

8:00am **PS+SS-WeM1 Investigation of Sidewall Passivation Mechanism in a 'CMOS-compatible' Plasma Etching Process for InP-based Photonic Devices**, *S. Bouchoule*, CNRS-LPN, France, *L. Vallier*, CNRS-LTM, France, *L. Gatilova*, *G. Patriarche*, *S. Guilet*, *L. Le Gratiet*, CNRS-LPN, France

Inductively coupled plasma (ICP) etching of II-V semiconductors is now widely used for the development of high-performance emitters, and various chlorine- or HBr- containing chemistries have been proposed for the patterning of InP-based heterostructures required to reach the NIR region. Smooth and anisotropic etching is generally a key-requirement, but only few studies exist on the understanding of the sidewall passivation mechanisms occurring during the etching of InP and related materials. We have shown for the  $\text{Cl}_2\text{-H}_2$  and HBr chemistries [JVSTB 26, 666 (2008)] that a silicon oxide layer acting as a lateral etch-inhibitor can build-up on the etched sidewalls of InP-based heterostructures, when a Si wafer is used as the sample tray. This configuration corresponds to most commercial ICP etch systems having an electrode diameter of 4-in or more, used to etch III-V samples of 2-in or less size. However, this may not be the case for future large surface processing of III-V when the III-V wafer will have the same size as the electrode or when III-V dies bonded onto a 200/300 mm wafer have to be etched, where most of the wafer surface is covered by a protecting layer that is not silicon. This may occur in III-V/Si photonic technologies. We have shown that high-aspect-ratio etching of the photonic patterns via a  $\text{SiO}_x$  sidewall passivation mechanism independent of the electrode surface can be obtained when a Si-containing gas such as  $\text{SiH}_4$ , or  $\text{SiCl}_4$  added [JVSTB 29, 020601 (2011)]. A more detailed analysis of the plasma has shown that hydrogen may promote the deposition of a Si-rich passivation layer on the sidewalls of the etched patterns.  $\text{SiOCl}$  sidewall passivation takes place during Si ICP etching using  $\text{Cl}_2\text{-HBr-O}_2$  chemistry in CMOS technology. We have therefore investigated  $\text{SiCl}_4/\text{Cl}_2/\text{HBr/O}_2/\text{Ar}$  plasma for the etching of InP dies in a 300-mm CMOS etching tool. This gas mixture provides the Si, O, and H species required for the build-up of a  $\text{SiO}_x$  passivation layer on the InP sidewalls. We show that the passivation mechanism is enhanced when the HBr concentration is increased in the feed gas. We have performed a local analysis of the passivation layer deposited on the InP sidewalls using EDX spectroscopy coupled to TEM. We show that the nature of the passivation layer can be changed from a-Si or nc-Si to  $\text{SiO}_2$  depending on the hydrogen and oxygen concentrations in the gas mixture. Finally we demonstrate smooth and anisotropic etching of ridge waveguide and vertical Bragg reflector patterns in the CMOS etching tool.

8:20am **PS+SS-WeM2 Coupling of Surface Mixed-Layer Kinetics and Monte Carlo Modeling for Profile Evolution in Patterning Complex Oxides**, *N. Marchack\**, *C.D. Pham*, *J.P. Chang*, University of California Los Angeles

As the downscaling of integrated circuit devices continues, minute variations in the feature profiles from processing techniques such as plasma etching significantly affect device performance. With the increasing introduction of novel materials into integrated circuits, the need to predict surface response during etching of these materials, such as complex oxides, becomes critical to attainable device performance. In this work, a phenomenological model<sup>1</sup> based on high-k oxide etching in chlorine based plasmas is adapted into a translated mixed layer (TML)<sup>2</sup> kinetics-based format to be used a Monte Carlo-based feature profile simulator. To accurately represent the kinetics involved, experiments are conducted in this work in an inductively coupled plasma (ICP) reactor equipped with a quadrupole mass spectrometer (QMS) for analyzing etch products and a quartz crystal microbalance (QCM) for measuring the etch rate *in situ*. This reactor is connected to a UHV transfer tube which allows the surface composition to be studied via x-ray photoelectron spectroscopy (XPS) without exposure to ambient conditions. In the TML model, surface reactions such as ion impingement, neutral adsorption, physical sputtering and chemically enhanced ion etching are accounted for, and reaction parameters are either measured directly or extracted by comparing the model to etch yield data. The MC model used ion incident angle

dependence and an elliptical energy deposition model to capture the effects of surface morphology on the profile evolution under the bombardment of energetic and directional ions. The material systems studied include HfLaO and HfSiON etched in  $\text{Cl}_2/\text{BCl}_3$  plasmas, for both blanket films and trenches patterned by e-beam lithography. Very good agreement was demonstrated between the phenomenological and TML models, as well as between simulated profiles and cross-sectional SEM images of the patterned material systems.

<sup>1</sup> Martin et al. Journal of Vacuum Science and Technology A 27(2) 2009

<sup>2</sup> Kwon et al. Journal of Vacuum Science and Technology A. 24(5) 2006

8:40am **PS+SS-WeM3 Plasma Diagnostics and Nanoscale Surface Processing - Application to  $\text{SiO}_2$ , High-k PVD and ALD**, *T. Kitajima*, National Defense Academy, Japan

INVITED

#### Introduction

Reactive plasmas are widely used for surface processings due to its controllable ion energy and radial fluxes.

Nano size feature control with plasma processing requires nonthermal chemistry with low energy ion exposure. Metastable atoms with internal energy of a few eV become important for the quality and throughput of deposition as ion energy is reduced.

Minimizing the processing target to the nanoscale also reveals the new properties of materials interacting with plasmas due to the size effect. Namely, sticking coefficients of radicals on metal significantly increase.

In the presentation, some recent results on metastable radical induced deposition including HfO<sub>2</sub> ALD are shown. The latest findings of nano particle interaction with reactive plasmas are introduced for the model case of PVD based HfSiON film growth.

#### Reactive metastables for oxide growth : $\text{SiO}_2$ and HfO<sub>2</sub>

The density of metastable O(1D) (1.9eV) in Ar-diluted O<sub>2</sub> ICP shows maximum at O<sub>2</sub> fraction of 1% and the flux shows significant increase due to the reduced quenching by O<sub>2</sub>. O(1D) density is measured by Vacuum UltraViolet Absorption Spectroscopy (VUVAS). The XPS analysis shows the stoichiometry of the grown  $\text{SiO}_2$  is comparable to the thermal oxide as well as the electrical breakdown.

The scheme is applied to the plasma enhanced atomic layer deposition (PEALD) of HfO<sub>2</sub>. The reagent is TEMAH and the oxidant is Ar-diluted O<sub>2</sub> ICP. The increased O(1D) flux enables less particle film surface with fewer carbon contamination.

#### Reactive surface nano particles interacting with plasma : HfSiON growth

Hf nanoparticles self assembled on  $\text{SiO}_2/\text{Si}(100)$ , origin of HfSiON, have sticking coefficient of N radicals close to 1 in the initial stage of N<sub>2</sub> ICP exposure. The reactivity of the nanoparticles with underlying  $\text{SiO}_2$  is enhanced by the plasma exposure, results in the formation of carbon free HfSiON film.

#### Concluding remarks

Metastables are important reactant for low temperature non-biased deposition processes

Metastable flux is controllable with the base gas chemistry

Nanoscale surface features are current concerns for plasma deposition

Nano sized surface has totally different reaction kinetics including interface with underlayer

Nano size effect of the surface is evident for radical reactivity

Self assembly (bottom up scheme) is highly important for next generation nano scale plasma processing as well as lithographic techniques (top down scheme)

#### Acknowledgement

This work was supported by MEXT Grant-in-Aid for Scientific Research on Innovative Areas (22110520) and JSPS Grant-in-Aid for Young Scientists (B) (21760033).

9:20am **PS+SS-WeM5 Nitric Oxide Reactivity Investigation via Plasma Processing**, *J.M. Blechle*, *E.R. Fisher*, Colorado State University

With increasing concern about environmental health, there is a greater need to investigate fundamental reactivity of pollutant species with and without the influence of surface effects. Here, inductively coupled plasmas are used to examine the catalyzed conversion of industrial exhaust, with an emphasis on elucidating the surface and gas-phase chemistry. Literature studies have thus far failed to explore the primary driving forces present in these catalytic plasma systems. The present work focuses on investigating the

\* Coburn & Winters Student Award Finalist



properties of nitric acid within plasmas formed from a collection of precursor gases including NO, NO<sub>2</sub>, N<sub>2</sub>O, and N<sub>2</sub>+O<sub>2</sub>. The behavior of the NO radical is determined by various methods that include catalytic surface reactivity measurements via the imaging of radicals interacting with surfaces (IRIS) technique as well as kinetic formation and destruction via time-resolved optical emission spectroscopy (TR-OES). Species density, surface scatter coefficients (*S*), along with vibrational and rotational temperatures establish inherent characteristics of NO. Results from these studies show the density of NO is strongly dependent on system pressure, which is in part attributable to formation of gas-phase dimers. In addition, *S*(NO) using non-catalytic surfaces (e.g. Si) increases with increasing plasma power. Additional results from studies of NO formation through bimolecular reactions in N<sub>2</sub>/O<sub>2</sub> plasmas will be presented. Collectively, these data allow for unparalleled insight into the properties of atmospheric species during plasma processing and the interactions they undergo in the presence of catalytic substrates.

**9:40am PS+SS-WeM6 Near-Threshold Ion-Enhanced Silicon Etching.** *H. Shin, W. Zhu, V.M. Donnelly, D.J. Economou*, University of Houston

Nearly mono-energetic ion energy distributions (IED) were obtained on the substrate electrode in a Faraday-shielded inductively couple plasma. This was accomplished by pulsing the plasma, and applying a synchronous DC bias on a “boundary” electrode, during a specified time window in the afterglow. Both the peak ion energy and the width of the IED could be controlled.[1] The ability to precisely control the IED enabled a study of ion-enhanced etching of silicon with chlorine, at near-threshold ion energy. Unlike “beam” experiments, where there is no plasma over the substrate, this work involves etching under “realistic” plasma conditions. The progress of etching in an argon-diluted chlorine plasma was monitored as a function of pressure and ion energy using optical emission spectroscopy. The silicon etch rate was measured using infrared laser interferometry. The etch rate of a p-type blanket silicon substrate was proportional to Cl-atom density, but did not depend on ion energy for sub-threshold (less than ~ 20 eV) ions. Under these conditions, however, the etch rate was much higher than that expected based on reported experiments in downstream plasmas where the surface is exposed to Cl atoms alone. Above threshold, the etch rate increased with the square root of ion energy. A comparison with n-type silicon substrate was also made. The carrier-mediated mechanisms of p-type Si etching in a plasma under very low energy ion bombardment will be proposed and discussed.

Work supported by the DoE Plasma Science Center and NSF.

[1] H. Shin et al., to appear in *Plasma Sources Science and Technology*.

**10:40am PS+SS-WeM9 Atomic Chlorine Absolute Densities and Surface Recombination Coefficients in Inductively-Coupled Plasmas in Pure Cl<sub>2</sub>.** *J.-P. Booth*, LPP-CNRS, France, *N. Sirse*, NCPST Dublin City University, Ireland, *Y. Azamoum, P. Chabert*, LPP-CNRS, France

Two-photon laser-induced fluorescence (TALIF) at 233.2nm was used to measure the density of Cl atoms in a 13.56MHz Inductively-coupled plasma in pure chlorine. Initial attempts to use the technique proposed by Ono et al [1], to calibrate the signal using photolysis of CCl<sub>4</sub> gave unphysically high values, probably due to poor knowledge of the laser spatial profile at the focal point. Therefore we developed a new technique, based on 355nm (tripled YAG) photolysis of Cl<sub>2</sub> to generate a known density of Cl atoms. The variation of the absolute Cl density at the reactor centre was measured as a function of pressure and RF power in the range 3-90 mTorr and 20-500W. We also used the TALIF technique to determine the recombination coefficient,  $\gamma_{Cl}$ , of atomic chlorine at the reactor walls from the rate of decay of the Cl density in the afterglow of a pulsed discharge. The signal to noise ratio is good enough to make measurements far into the afterglow (50 ms), when the gas has cooled to the wall temperature, making a precise measurements possible. We found that  $\gamma_{Cl}$  varies in the range 0.05-0.15, decreasing with increased pressure and RF power, and increasing with gas residence time. We show that the latter effect is due to the increased proportion of O<sub>2</sub> due to inevitable small air leaks: the presence of 0.5% O<sub>2</sub> was shown to double the value of  $\gamma_{Cl}$ . The origin of the pressure and power dependencies will be discussed.

Work partly supported by Agence Nationale de la Recherche project INCLINE (ANR-09 BLAN 0019)

[1] K. Ono, T. Oomori, M. Tuda, and K. Namba, *Journal of Vacuum Science & Technology a-Vacuum Surfaces and Films*, **10**, 1071, (1992).

**11:00am PS+SS-WeM10 Silicon Etching Characteristics by Hydrogen Halide Ions (HCl<sup>+</sup> and HBr<sup>+</sup>) and Ions of Desorbed Species (SiCl<sub>x</sub><sup>+</sup>).** *T. Ito, K. Karahashi*, Osaka University, Japan, *S.-Y. Kang*, Tokyo Electron Ltd., Japan, *S. Hamaguchi*, Osaka University, Japan

In recent reactive ion etching (RIE) processes for Si, halogen and hydrogen halide gases, such as Cl<sub>2</sub> and HBr, have been widely used to achieve high

selectivity, etching anisotropy, and high etching rates. Furthermore, in some highly selective silicon etching processes, higher gas-pressure processes have been found to be more effective. In higher-pressure systems, chemical compounds formed from the input gas and some of desorbed species containing Si may serve as additional etchants. To develop etching equipments based on such plasma chemistry, it is important to understand basic etching reactions on silicon surfaces by energetic ion species associated with silicon and/or hydrogen containing species. To clarify the roles of SiCl<sub>x</sub>, SiBr<sub>x</sub>, HCl, and HBr in silicon etching processes, we have employed a mass-analyzed ion beam system that can irradiate a sample surface with a specific ionic species under an ultra-high vacuum condition and evaluated the etching yields. The change in chemical nature of the substrate surface during the process can be observed *in situ* by X-ray photoelectron spectroscopy (XPS) installed in the reaction chamber. Time of Flight (TOF) measurement of species desorbed from the sample surface in a pulsed ion beam operation is also possible with the use of a differentially pumped quadrupole mass spectrometer (QMS). In this study, etching yields of silicon by Cl<sup>+</sup>, SiCl<sup>+</sup>, SiCl<sub>3</sub><sup>+</sup>, Br<sup>+</sup>, H<sup>+</sup>, HCl<sup>+</sup>, and HBr<sup>+</sup> ion beams were evaluated with incident energies of 100 – 1000 eV. A typical ion dose for each ion irradiation was 2–4E17/cm<sup>2</sup>. Yields by some of these ionic species have been known and our etching yield data are confirmed to be in good agreement with the earlier data. It is found that, for a given incident energy, the etching yield by SiCl<sub>3</sub><sup>+</sup> ions is higher than that by Cl<sup>+</sup> ions whereas the etching yield by SiCl<sup>+</sup> ions is lower than that of Cl<sup>+</sup> ions, which may be accounted for by the number of Cl atoms and a possible deposition effect of Si. It has been also observed that deposition occurs under SiCl<sup>+</sup> ion irradiation when the injection energy is lower than 300eV. Energy dependence of etching yields and effects of hydrogen will be discussed in detail.

**11:20am PS+SS-WeM11 Interaction of Chlorine Plasma with Si<sub>x</sub>Cl<sub>y</sub> Coated Plasma Reactor Chamber Walls.** *R. Khare\*, A. Srivastava, V.M. Donnelly*, University of Houston

The interplay between chlorine plasmas and silicon chloride (Si<sub>x</sub>Cl<sub>y</sub>) coated reactor walls has been studied by line-of-sight mass spectrometry in a radio frequency (rf) inductively coupled Cl<sub>2</sub> plasma (ICP), using the spinning wall method. A bare silicon wafer was etched in a 400 Watt Cl<sub>2</sub> ICP, with rf power applied to the stage resulting in a -110 VDC self-bias. Etch products were deposited on the plasma reactor walls and the rotating substrate surface, resulting in a thick layer of Si<sub>x</sub>Cl<sub>y</sub> that was characterized *in situ* by Auger electron spectroscopy. Some oxygen also incorporated into the film due to erosion of the fused silica discharge tube. The reactions of chlorine plasmas with this prepared surface were then studied by line-of-sight mass spectrometry. Without substrate bias, the chlorine plasma etches the Si<sub>x</sub>Cl<sub>y</sub> layer to form products that result in detection of SiCl<sub>x</sub> (x = 1-4) m/e components, as well as oxy-silicon-chloride products (m/e= 177, 247, 307, 361). In one experiment, after the deposition of dense Si<sub>x</sub>Cl<sub>y</sub> layer on reactor and substrate surfaces, substrate rotation was stopped and the film was etched from the reactor walls with the chlorine plasma, leaving only the Si<sub>x</sub>Cl<sub>y</sub> layer on 2/3<sup>rd</sup> of the substrate surface that was out of the plasma. Upon resuming rotation, and exposing the Si<sub>x</sub>Cl<sub>y</sub> loaded surface to the Cl<sub>2</sub> plasma, SiCl<sub>x</sub> products were detected, but at suppressed levels, indicating that the evolution of etch products is a complex “recycling” process in which these species deposit and desorb from the walls many times, and repeatedly fragment in the plasma. These and other experiments will be discussed. This work is supported by the National Science Foundation and Lam Research Corporation.

**11:40am PS+SS-WeM12 Numerical Simulation of Enhanced Oxygen Diffusion in Silicon as a Cause of Si Recess.** *K. Mizotani, M. Isobe*, Osaka University, Japan, *M. Fukasawa, T. Tatsumi*, Sony Corporation, Japan, *S. Hamaguchi*, Osaka University, Japan

In a gate etching process, the formation of hollowed Si profiles around the polysilicon (poly-Si) gates, which is now widely known as “Si recess,” has raised serious concern in the semiconductor processing community as such hollows on a Si surface can severely degrade the device performance and reliability. In a typical process that causes Si recess, a plasma based on HBr and oxygen gases are used to etch polysilicon gates anisotropically. A recent study [1] based on multiple-beam and plasma experiments has shown that Si recess is caused by ion assisted oxygen diffusion, i.e., oxygen diffusion enhanced by hydrogen ion injections. In this study, we have used molecular dynamics (MD) simulations to understand the mechanism of enhanced oxygen diffusion in Si under such conditions. In the simulations, energetic hydrogen ions and low-energy oxygen atoms (with kinetic energies close to room temperature) are simultaneously injected into a crystalline Si substrate initially covered with a native oxide layer. Simulation results are in good agreement with ion beam experiments

\* Coburn & Winters Student Award Finalist



performed under similar conditions given in Ref. [1]. In our simulations, O atoms are transported into the bulk Si due to momentum transfer from energetic hydrogen ions. In other words, the enhanced ion transport is not typical “diffusion” associated with thermal motion in solid. However, random walk characteristics of O atoms in Si under such conditions are interestingly similar to those of diffusion. In this study, we relate this oxygen transport to diffusion transport and present its effective diffusion coefficient as a function of hydrogen ion injection energy.

[1] T. Ito, K. Karahashi, M. Fukasawa, T. Tatsumi and S. Hamaguchi, “Si recess of Poly-Si Gate Etching: Damage Enhanced by Ion Assisted Oxygen Diffusion,” *Jpn. J. Appl. Phys.* (2011) *in press*.

## Advanced Surface Engineering Division

Room: 104 - Session SE+SS-WeM

### Surface Engineering for Thermal Management

Moderator: A.A. Voevodin, Air Force Research

Laboratory, H. Barankova, Uppsala University, Sweden

8:20am **SE+SS-WeM2 Near-Field Radiation Heat Transfer**, A. Mavrokefalos, P. Sambegoro, K. Esfarjani, G. Chen, Massachusetts Institute of Technology **INVITED**

Radiation heat transfer in nanostructures can differ significantly from that in macrostructures due to wave effects. Max Planck himself realized that the blackbody radiation law that now bears his name was limited to geometries much larger than wavelength of thermal radiation. Theory has predicted that thermal radiation heat transfer between two surfaces separated by tens of nanometers can exceed that of Planck’s blackbody radiation law by several orders of magnitude. We have designed an experiment measuring near-field radiation heat transfer between a sphere and a flat plate using bi-layer atomic force microscope cantilevers as a heat flux and a temperature sensor. We demonstrated experimentally that near-field radiation heat transfer can exceed Planck’s law prediction by four orders of magnitude, mediated by surface phonon polaritons. We will also show that existing fluctuating electrodynamics theory cannot predict experimental results in the extreme limit of small separation between two surfaces. Our experiments raise interesting question on the convergence of radiation heat transfer mechanism and interfacial heat conduction mechanism. Theoretical approaches bridging these two regimes will be discussed.

9:00am **SE+SS-WeM4 Atomic Level Temperature Measurements and Nearfield Thermal Energy Tunneling**, A.A. Voevodin, I. Altfeder, J. Hu, V. Varshney, A. Roy, Air Force Research Laboratory

An atomic level thermometer was developed to study interfacial thermal conductivity using a scanning tunneling microscope with inelastic electron tunneling spectroscopy (STM-IETS), where inelastic peak broadening was used to measure temperature of the CO molecular group at the platinum probe apex, while Au substrate with (111) surface was cryogenically cooled. The experiments led to a discovery of vacuum phonon tunneling across nanometer contact gaps. This discovery showed that contact thermal transport can exceed by 10 orders of magnitude Planck’s radiation Law for heat transfer in vacuum [1]. This indicated that there should be an alternative mechanism for thermal energy transfer, where near field effects support energy tunneling across such small vacuum gaps. A hypothesis about mirror charge coupling at the interfaces was formulated and tested in the experiments with varied tip-sample temperature gradients. Based on these developments, the STM-IETS experimental approach was further extended to study interfaces made of the surfaces with different Debye temperatures. The second derivative of the tunneling current was used to obtain information on the interfacial thermal coupling and energy transfer. This paper reports on the experimental set-up for atomic scale thermometry, corresponding first principle calculation approaches for small gap interfacial thermal coupling, and discusses experimental and modeling results for different tip-surface combinations toward understanding near-field effects for thermal energy transfer.

1. “Vacuum phonon tunneling”, I. Altfeder, A. A. Voevodin, A. K. Roy, *Physical Review Letters*, 105, 166101 (2010).

9:20am **SE+SS-WeM5 Two-Color Time-Domain Thermoreflectance with an Optical Parametric Oscillator**, J. Gengler, Spectral Energies, LLC, C. Muratore, Air Force Research Laboratory, S. Roy, Spectral Energies, LLC, J.R. Gord, Air Force Research Laboratory

Conventional single-color laser pump-probe methods for measuring thermal properties are limited by sample requirements that arise from considerations of surface roughness and compatible thermoreflectance transducers. Here we describe a new experimental arrangement for performing two-color

time-domain thermoreflectance (TDTR). The technique is a variation of traditional pump-probe spectroscopy that is based on a femtosecond Ti:sapphire oscillator of fixed wavelength and an optical parametric oscillator (OPO), with the goal being to create an independently tunable probe wavelength. This method offers two advantages: 1) spectral filtering of diffusely scattered pump light (to prevent it from reaching the detector), and 2) generation of thermoreflectance signal from different metal thin films. The wavelength tunability of the system allows enhancement of TDTR signal generation for multiple thermoreflectance transducer materials. This wavelength-adjustable feature, in turn, facilitates direct measurement of the thermal transport properties of various thin films and substrates, which would be difficult with single-color femtosecond pump-probe systems. Demonstrated results include optimization of the probe wavelength for different metals, measurement of metal-graphite interfacial conductances on relatively rough samples, and two orders-of-magnitude calibration of thermal conductivity measurements using copper as a thermoreflectance transducer.

9:40am **SE+SS-WeM6 Low-Friction V-alloyed ZrO<sub>2</sub> Thin Films with Temperature Homogenization Functions for High Temperature Sliding Interfaces**, O. Jantschner, C. Walter, C. Mitterer, University of Leoben, Austria, C. Muratore, A.A. Voevodin, Air Force Research Laboratory

The effect of vanadium on reactively magnetron-sputtered zirconia coatings was investigated with respect to its structural and mechanical properties as well as its thermal management abilities for high temperature sliding interfaces. ZrO<sub>2</sub> coatings with different V-content (0, 2.2, 5.8 and 17.4 at%) were co-sputtered from Zr and V targets using an Ar/O<sub>2</sub> discharge. The X-ray diffraction pattern of the as-deposited coatings show a change in crystal structure from monoclinic (0-2.2 at% V) to cubic/tetragonal (5.8 at% V) and finally X-ray amorphous structure at even higher V content (17.4 at% V). Hardness and Young’s modulus were evaluated by nanoindentation showing a decrease beyond 2.2 at% V from 17.4 to 7.5 GPa and from 230 to 150 GPa, respectively. The tribological investigations by ball-on-disc tests against alumina balls were carried out at three different temperature levels (25, 600 and 800°C). Additional in-situ Raman analyses have been done to study the formation of tribolayers in the sliding contact. At 25°C, the coefficient of friction (COF) is about 0.2 for low V contents ( $\leq 2.2$  at%). For higher V contents, the COF increases up to 0.5 and higher. At 600°C, the COF measured was between 0.4 and 0.8. At the even higher temperature of 800°C, the COF decreased to below 0.2 for V contents of 17.4 at%, where a self-lubricating film was formed in the sliding contact. Differential scanning calorimetry (DSC) measurements of virgin powder samples showed a characteristic exothermic peak at  $\sim 600^\circ\text{C}$  which is due to the formation of a stoichiometric ZrV<sub>2</sub>O<sub>7</sub> phase. This phase was found to decompose at  $\sim 800^\circ\text{C}$  by an endothermic reaction in ZrO<sub>2</sub> and V<sub>2</sub>O<sub>5</sub>. The re-runs of the DSC measurements indicated melting of V<sub>2</sub>O<sub>5</sub> at 670°C.

In summary, alloying of V to ZrO<sub>2</sub> coatings has on the one hand been proven to result in self-lubricious properties at temperatures above 700°C. On the other hand, the endothermic reactions needed for formation of the self-lubricious phase have the potential to reduce high local temperatures in the sliding contact, enabling thermal management abilities of these coatings.

10:40am **SE+SS-WeM9 Thermal Characterization of Metal/Carbon Interfaces: Comparison of Metallized Nanotubes and Graphite**, C. Muratore, S. Shenogin, A. Waite, A. Reed, J. Gengler, T. Smith, J. Hu, J. Bultman, A.A. Voevodin, Air Force Research Laboratory

Most applications of carbon nanotubes require contact with more ordinary materials, such as metals or polymers. Unfortunately, the extraordinary thermo-electro-mechanical properties of nanotubes are often negated at the interface between the nanotubes and whatever they touch, resulting in a major shortfall between the measured and predicted performance of nanotube-based materials. One of the most troubling discrepancies in projected versus measured properties is found in thermal conductivity measurements of nanotube-containing composite materials. For example, a continuous network of thermally conductive nanotubes (or about 1 percent, by volume) within an organic matrix ( $k = 0.3 \text{ W m}^{-1} \text{ K}^{-1}$ ) should yield a 30-fold increase in thermal conductivity over the pure matrix phase alone, based on simple effective medium theory. Despite this potential increase, experimental results typically show an increase of only a factor of 2 at best in composites with nanotube additives. To better understand the nature of interfacial resistance in carbon nanotubes, modeling and experimental studies investigating engineered interfaces on highly oriented pyrolytic graphite (HOPG) samples were conducted. This substrate was selected as a practical 2-dimensional analog for nanotube sidewalls to facilitate modeling and experimentation. Molecular dynamics simulations of heat transfer through metal carbon interfaces were conducted, and measurements of thermal conductance at these interfaces were made by analysis of the two-color time domain thermoreflectance (TDTR) data from the samples. The TDTR analysis of the different metals on HOPG was made possible by having an optical parametric oscillator on the probe beam which allows for

tuning the wavelength to match absorption bands for each metal studied. Comparison of simulation and experimental results between graphite and nanotubes is highlighted. Metal films were selected to identify effects of atomic mass, chemical interactions and mechanical properties. For example, metals known to exhibit in situ formation of an interfacial carbide layer when in contact with a carbon source and heated, such as titanium and boron, were investigated, and the effect of this carbide layer formation on interfacial conductance was examined. Graded and sharp interfaces were also considered with computational and experimental efforts.

11:00am **SE+SS-WeM10 The Experiment of Surface Tension Driven Flow with Various Parameters on JEM/ISS**, *S. Yoda*, Japanese Aerospace Exploration Agency, *S. Matsumoto*, JAXA, Japan, *A. Komiya*, Tohoku University, Japan

The surface tension driven flow (Marangoni) experiments were carried out by using 50mm diam. with liquid bridge of Silicones oil under microgravity condition on Japanese Experiment Module on International Space Station. The parameters in these experiments were liquid bridge length being corresponded to aspect ratio which is defined as liquid length/liquid diam., and temperature difference between hot and cold disks which sustains the liquid bridge. The particles coated by gold to fit with the density of the liquid silicones were inserted into the liquid bridge. Observing the movement of the particles by three CCD camera, we can determine the flow behavior of Marangoni with different temperature as 3 dimension observation of the flow. Moreover, two ultrasonic transducers were attached in the cold disk to measure the particles velocity. The number of experiments done on JEM were more than 40 times with around 6 hr for all each experiment. The Marangoni number was changed with aspect ratio. The smaller aspect ratio around showed smaller critical Marangoni numbers, whereas the larger those were larger the numbers.

11:20am **SE+SS-WeM11 Enhanced Thermal Transport at Covalently Functionalized Carbon Nanotube Interfaces**, *S. Kaur*, Lawrence Berkeley National Lab, *N. Ravivakar*, Intel Corporation, *D.F. Ogletree*, Lawrence Berkeley National Lab

Thermal transport is restricted in systems including carbon nanotubes (CNT) due to high thermal interface resistance. We have substantially improved thermal transport at CNT-metal interfaces by functionalizing the contacting surfaces with amino-propyl silane to form covalent chemical bonds bridging the CNT-metal gap. This strategy was suggested by molecular dynamics calculations of Hu *et al.* (1)

We have characterized the resulting interface using multi-frequency and multi-wavelength time-domain thermo-reflectance (TDTR) measurements, which are able to independently determine interface and bulk CNT contributions to thermal transport. TDTR analysis showed that thermal contacts were made between a functionalized Al surface and 4-5% of the CNTs in an array grown on silicon. The intrinsic CNT interface conductivity exceeded 300 MW/m<sup>2</sup>-K, resulting in an effective thermal interface resistance of less than 0.8 mm<sup>2</sup>-K/W. Successful interface functionalization was independently verified by mechanical adhesion testing, which showed a correlation between interface strength and thermal transport, as discussed by Prashar. (2).

(1) Ming Hu, Pawel Koblinski, Jian-Sheng Wang, Nachiket Ravivakar, J. Appl. Phys. 104 083503 (2008).

(2) Ravi Prashar, Appl. Phys. Lett. 94 041905 (2009).

## Surface Science Division

**Room: 107 - Session SS1-WeM**

### Atomistic Control of Structure & Evolution

**Moderator:** T.S. Rahman, University of Central Florida

8:40am **SS1-WeM3 Destabilization of Ag Nanoislands on Ag(100) by Adsorbed Sulfur**, *M. Shen*, *S.M. Russell*, Iowa State University, *D.-J. Liu*, Ames Laboratory - US DOE, *P.A. Thiel*, Iowa State University & Ames Laboratory - US DOE

Studies of chalcogen (O, S) interactions with coinage metal surfaces elucidate how those interactions affect mass transport on the surface and whether a general mechanism exists for these systems. Sulfur accelerates coarsening of Ag nanoislands on Ag(100) at 300 K, and this effect increases with sulfur coverage over a range spanning a few hundredths of a monolayer, to nearly 0.25 monolayers. We propose that acceleration in this system is strongly tied to the formation of Ag<sub>2</sub>S complexes at step edges. These complexes can transport Ag more efficiently than Ag adatoms (due to a lower diffusion barrier and comparable formation energy), hence leading to enhanced coarsening. The mobility of isolated sulfur on Ag(100) is very

low, so that complex formation is kinetically-limited at low sulfur coverages, and thus enhancement is minimal. However, higher sulfur coverages force the population of sites adjacent to step edges, so that formation of the complex is no longer limited by diffusion of sulfur.

9:00am **SS1-WeM4 Pt Terminated Mono- and Multilayer CuPt Alloys Supported on Ru(0001) Single Crystals as Model System for Core Shell Particles**, *A.K. Engstfeld*, *R.J. Behm*, Ulm University, Germany

A popular concept to improve the catalytic activity of metal particles is the utilization of core shell particles. This means that a metal/alloy core is encapsulated by an additional metal in the shell of the particle. An interesting example has recently been published by R. Srivastava *et al.* [1], who found that Pt enclosed alloy particles containing Cu, Co and Pt, have a much better activity towards oxygen reduction than pure Pt. Whereas the principle concept is thus proven to work, the "optimum catalyst" for oxygen reduction has not yet been found.

For a better understanding of the structure and the formation of such core shell particles we prepare nanostructured planar model surfaces under well defined conditions, such as in ultra high vacuum (UHV). The surfaces consist of mono- and multilayer CuPt alloys on a Ru(0001) single crystal. They can be prepared by subsequent evaporation of the single metals and annealing at elevated temperatures. By this means the composition of the core can be well defined. The shell can be achieved by terminating the alloy by an additional Pt layer.

In this work we focus on the preparation of mono and bimetallic CuPt layers. They are characterized via STM to elucidate the morphology as well as the atom distribution. From the atom distribution within the alloy we will discuss the dominant factor for alloy formation, in view of the different size of the atoms and difference in their intermetallic bonding. Furthermore we will elucidate the surface segregation behavior of Pt in the bilayer alloy during the alloying process.

[1] Srivastava, R., P. Mani, N. Hahn, and P. Strasser, 'Efficient Oxygen Reduction Fuel Cell Electrocatalysis on Voltammetrically Dealloyed Pt-Co Nanoparticles', *Angewandte Chemie*, 8988 (2007).

9:20am **SS1-WeM5 Carbon-induced Nano-Faceting of Re(11-21): Synthesis and Performance of a Pt ML-C/Re(11-21) Electrocatalyst**, *X.F. Yang*, Lehigh University, *H. Wang*, Columbia University, *W. Chen*, *R.A. Bartynski*, Rutgers University, *B.E. Koel*, Princeton University

Faceted surfaces can provide unique opportunities to explore how catalytic reactions respond to changes in the catalyst surface structure. In this study, using LEED, XPS, AES, and STM, we report on how the presence of surface carbon significantly modifies the surface structure of a Re(11-21) single crystal and causes faceting, *i.e.*, an initially planar Re(11-21) surface becomes "nano-textured" to expose new crystal faces and form "pyramids" on the nanometer scale. In addition to describing these nanostructures, we identify different states of surface carbon and describe their dependence on the coverage of carbon. We also utilized the faceted Re(11-21) surface containing these nanoscale pyramids to explore for unusual catalytic properties. Here, we describe the synthesis of a model electrocatalyst by deposition of one monolayer of Pt on the faceted C/Re(11-21) surface and investigation of its performance for the hydrogen evolution reaction (HER). This Pt ML-C/Re(11-21) surface displayed higher activity for the HER than pure Pt. This is particularly promising since Re is only one-fifth the price of Pt. This study is the first application of using a nanoscale faceted surface as a template for electrocatalyst synthesis, and illustrates the potential for other such investigations. It is also of interest to further explore the catalytic activity of such faceted surfaces for heterogeneous catalytic reactions, *e.g.*, selective reduction of NO<sub>x</sub> with NH<sub>3</sub> and selective oxidation of methanol, in order to understand the various effects of facet size, orientation, and low-coordination sites that are available for reaction.

W.C. and R.A.B. acknowledge support under DOE Contract No. DE-FG02-93ER14331. B.E.K. acknowledges support by NSF Grant No. CHE-1129417.

9:40am **SS1-WeM6 Nucleation and Growth of Ag Islands on the (√3x√3)R30° Phase of Ag on Si(111)**, *A. Belianinov*, Iowa State University & Ames Laboratory - US DOE

Using STM, we measure densities and characteristics of Ag islands that form on the (√3x√3)R30o-Ag phase on Si(111), as a function of deposition temperature between 50 and 300 K. Assuming that Ag diffusion occurs via thermally-activated motion of single atoms between adjacent sites, the data can be explained as follows. At 50-125 K, islands are relatively small, and island density decreases only slightly with increasing temperature; the island density does not follow conventional Arrhenius scaling, probably due to limited mobility and lack of steady-state between deposition and consumption of Ag atoms. At higher temperatures there is a transition to conventional Arrhenius scaling, from which a diffusion barrier of 0.20-0.23

eV can be derived. At 300 K Ag atoms can travel for distances on the order of 1  $\mu\text{m}$ , and they nucleate preferentially at step bunches. We have used this information to nanopattern the surface with Ag. We have done this by creating artificial defects in the  $\sqrt{3}$ -Ag structure with the STM tip, and then subsequently depositing Ag at 300 K. This leads to strong preferential aggregation at these sites.

10:40am **SS1-WeM9 Surface Diffusion of In and Sn on Si(001) at Room Temperature**, *N. To, S. Dobrin, J. Nogami*, University of Toronto, Canada

A self-aligning nanostencil mask was used to pattern circular features of tin and indium on an atomically clean Si(001) substrate. The shadow mask limited material deposition to below where the membrane was open, leaving adjacent areas of clean surface for material to diffuse. STM was used to study the room temperature surface diffusion of these metals in UHV and DFT was used to calculate relevant activation barriers. The comparison of these two metals is significant since they have the same atomic structure in the first atomic layer when grown on Si(001). The diffusion of tin is limited in comparison with indium, and remains so even at increasing metal coverage. Indium forms unstable 3D islands that dissolve over time and contribute to the spreading of a single atomic layer thick film on the surrounding clean surface. The difference in behavior between the two metals can be attributed to the energy balance between 3D islands and the 2D wetting layers, as well as differences in activation energy for diffusion of atoms on top of the first atomic layer of metal. These results also show the potential for stencil patterning to provide insight into aspects of thin film growth.

11:20am **SS1-WeM11 The Effect of Surface Fluoride on the Crystallization and Photocatalytic Activity of Titania**, *J.I. Brauer, G.J. Szulcowski*, University of Alabama

A two-step strategy to improve the photocatalytic activity of titania is reported. First, nitrogen doped titanium dioxide, denoted N-TiO<sub>2</sub>, has been synthesized by sol-gel methods to increase the absorption of visible radiation. Second, surface hydroxyl groups of the as-synthesized powders are replaced with fluoride ions. The two-step strategy gives independent control of “bulk” doping and surface modification. The as-synthesized and annealed powders were characterized by x-ray photoelectron spectroscopy, x-ray diffraction, diffuse reflection UV/Vis spectroscopy, IR spectroscopy, and scanning electron microscopy. Surface fluorination has two important consequences: it lowers the temperature to crystallize the as-synthesized powders into the photoactive anatase phase and improves the retention of nitrogen-dopants upon annealing. The photoactivity of the titania powders were characterized by assessing the ability to degrade aqueous solutions of methylene blue, a common dye molecule, with visible radiation greater than 420 nm. The photodegradation experiments show that the rate of methylene blue decomposition follows the trend: F, N-doped TiO<sub>2</sub> > N-TiO<sub>2</sub> > undoped TiO<sub>2</sub>. A mechanism to explain the observed effects will be presented.

11:40am **SS1-WeM12 Microscale Corrosion of an Aerospace Al 2024 Alloy with Low Mg and the Effect of Chromate and Cerium Based Conversion Coatings**, *J.A. DeRose, T. Suter*, EMPA, Switzerland, *A. Balkowiec, J. Michalski, K.J. Kurzydowski*, Warsaw University of Technology, Poland, *I. De Graeve, H. Terryn*, Vrije Universiteit Brussel, Belgium, *P. Schmutz*, EMPA, Switzerland

An aluminum alloy, AA2024-T351 (Al 2024), with a composition having a higher proportion of Cu to Mg (Cu/Mg = 3.7), which is used in the aerospace industry, has been studied for corrosion simulation development. Results show that the Al 2024 alloy's microstructure and corrosion behavior is quite different from that reported for Al 2024 alloy with higher Mg, a more common composition (normally Cu/Mg = 2.9) [1]. Characterization of the Al 2024 indicates a dominant presence of 2nd phase (AlCuFeMnSi) intermetallic particles (>70%), but that the S phase (Al<sub>2</sub>CuMg) and  $\theta$  phase (Al<sub>2</sub>Cu) precipitate particles are much smaller in population (<30%). Microscale corrosion studies show that open circuit (OCP) and pitting potential (PP) values extracted from micropolarization curves [2] measured for Al 2024 (Cu/Mg = 3.7) 2nd, S, or matrix phase have a large variation within a similar range of values. These results are in contrast to those already reported for Al 2024 with a more common composition (Cu/Mg = 2.9) where the electrochemical potential values separate with respect to the alloy phase and the microstructure shows S phase particles to be in the majority (>60%) [2]. Nanoscale dispersoid particles and, to a much lesser degree, nanoscale 2nd phase particles were also found present throughout the matrix of the Al 2024 studied. The impact of chromate and cerium based conversion coatings, which inhibit corrosion, on the microscale corrosion properties of the Al 2024 alloy has been studied. Electrochemical current density data extracted from micropolarization curves measured for Al 2024 2nd, S, and matrix phase exposed to electrolytic solutions containing chromate (Na<sub>2</sub>Cr<sub>2</sub>O<sub>7</sub>) or cerium based (Ce(NO<sub>3</sub>)<sub>3</sub>) molecules

show the chromate coating to be more efficient as an corrosion inhibitor. However, other cerium based molecules, such as cerium dibutylphosphate (Ce(dbp)<sub>3</sub>) and cerium chloride (CeCl<sub>3</sub>), which have shown more promising results [3], deserve further investigation. [1] R.G. Buchheit, R.P. Grant, P.F. Hlava, B. Mckenzie, G.L. Zender, J. Electrochem. Soc. 144 (1997) 2621. [2] T. Suter, R.C. Alkire, J. Electrochem. Soc. 148 (2001) B36. [3] S.J. Garciaa, T.H. Muster, Ö. Özkanata, N. Sherman, A.E. Hughes, H. Terryn, J.H.W. de Wita, J.M.C. Mol, Electrochim. Acta 55 (2010) 2457.

## Surface Science Division

Room: 109 - Session SS2-WeM

### Chemisorption on Metal & Oxide Nanoparticles

Moderator: B. Roldan Cuenya, University of Central Florida

8:00am **SS2-WeM1 Temperature Program Desorption and X-ray Photoelectron Spectroscopy Study of Cu<sub>x</sub> on CeO<sub>2</sub>/YSZ (111)**, *J.C. Lofaro, Jr.*, Stony Brook University, *M.G. White*, Stony Brook University and Brookhaven National Laboratory

Energy research has increased in importance in the past decade due to our growing understanding of climate science and rising oil prices. Many catalysts center around expensive and rare transition metals, such as Pt and Pd, supported on oxide substrates. However, copper, a relatively cheap and abundant metal, supported on metal oxides has been used as a heterogeneous catalyst in industrial settings for various chemical processes.<sup>1,2</sup> Recent works have shown that copper nanoparticles supported on metal oxides (ZnO, CeO<sub>2</sub>, TiO<sub>2</sub>) have higher activity for the water gas shift reaction (WGSR) as well as other important chemical reactions when compared to their individual components.<sup>3,4</sup> Understanding how these complex catalysts work on a fundamental level will allow for the design and implementation of more efficient and selective systems in the future. Here, using a homemade thermal evaporator, a model system of copper nanoparticles deposited on CeO<sub>2</sub> films (200 nm thick) grown on YSZ (111) single crystals is used. X-ray photoelectron spectroscopy (XPS) is used to characterize the oxidation state of supported copper nanoparticles and temperature programmed desorption (TPD) is used to probe their reactivity and thermal stability. Copper coverages ranging from 0.25ML to 1ML are investigated. Carbon monoxide and water are used as probe molecules since they are the reactants involved in the WGSR. We have found that copper's stability is highly temperature dependent and have found evidence of its encapsulation by the support.

1. K. Klier, Adv. Catal., 1982, 31, 243.

2. J. C. Bart and R. P. A. Sneedon, Catal. Today, 1987, 2, 124.

3. J. A. Rodriguez, P. Liu, J. Hrbek, J. Evans, M. Pérez, Angew. Chem. Int. Ed., 2007, 46, 1351.

4. X. Zhao, J. A. Rodriguez, J. Hrbek, M. Pérez, Surface Science, 2005, 600, 229.

8:20am **SS2-WeM2 X-ray Photoelectron Spectroscopy and Scanning Tunneling Microscopy Characterization of the Active Edge Sites of MoS<sub>2</sub> Nanoclusters**, *A. Tuxen, S. Porsgaard, H. Goebel, F. Besenbacher, J.V. Lauritsen*, Aarhus University, Denmark

The atomic and electronic structure of MoS<sub>2</sub> nanoclusters is of considerable interest due to the catalytic application of MoS<sub>2</sub> in e.g. hydrotreating catalysis of crude oil and in photocatalysts and hydrogen evolution reactions. Previous atom-resolved STM results have shown in great detail that both the overall morphology and in particular the edge structure of MoS<sub>2</sub> nanoclusters, which are known to contain the most catalytically active sites for hydrotreating and H<sub>2</sub> dissociation, adopt a structure which is very dependent on the conditions under which the cluster are kept. Under sulfiding conditions, atom-resolved STM images show that the MoS<sub>2</sub> nanoclusters expose fully sulfide edges, whereas activation by H<sub>2</sub> or mixed H<sub>2</sub>/H<sub>2</sub>S exposures show that sulfur vacancies and S-H form on the cluster edges reflecting the MoS<sub>2</sub> catalyst in its active state. To dynamically follow such structural changes at the MoS<sub>2</sub> edges induced e.g. by hydrotreating reaction conditions we have here combined high-resolution x-ray photoelectron spectroscopy (XPS) and scanning tunneling microscopy (STM) studies of single-layer MoS<sub>2</sub> nanoclusters with a well known structure. The XPS studies done on well-characterized samples reveal a set of edge specific core level shifts in the Mo3d photoemission peak that can be uniquely associated with the fully sulfide edges, edge with S vacancies or fully reduced edges. The XPS fingerprint thus allows us to dynamically follow changes between the catalytically active states of MoS<sub>2</sub> when exposed to sulfiding of sulforeductive conditions. Preliminary *in-situ* XPS results on the same MoS<sub>2</sub> samples obtained under a 10<sup>-2</sup> torr H<sub>2</sub> atmosphere

on the Ambient Pressure X-ray Photoelectron Spectroscopy on beamline 11.0.2 of the Advanced Light Source Berkeley show a characteristic sequence of sulfur reduction steps on the catalytically interesting edges followed by decomposition of MoS<sub>2</sub> at higher temperatures. The present studies thus successfully shows that XPS in combination with STM can be successfully used as a tool to characterize the chemistry of highly dispersed active sites of well-defined nanoclusters, such as the active edges on MoS<sub>2</sub>.

**8:40am SS2-WeM3 Charge-Mediated Chemisorption on Supported Clusters, M. Sterrer, Fritz-Haber-Institute of the Max-Planck-Society, Germany** **INVITED**

Among the many factors that influence catalytic activity of supported metal clusters, the effects of size and charge state of the clusters are most frequently discussed, e.g., in CO oxidation over supported gold. In this contribution, I will present results of our recent experimental efforts to characterize metal clusters supported on single-crystalline model oxide surfaces, using Au on MgO thin films as example. Using a combination of various surface science techniques including low-temperature scanning tunneling microscopy, infrared spectroscopy, X-ray photoelectron spectroscopy, and electron paramagnetic resonance, the properties of supported Au atoms and clusters were addressed in detail. Starting with the unusual CO chemisorption behavior of single Au atoms on the perfect MgO(001) surface, I will move on and show how the charge state of Au particles on the MgO surface, which in most cases is inferred from distinct CO chemisorption features, may be influenced by modification of the oxide surface, e.g. by their interaction with defects or hydroxyl groups, or by the MgO film thickness.

**9:20am SS2-WeM5 The Structure and Chemical Activity of Two-dimensional Gold Islands on Single-layer Graphene/Ru(0001), L. Liu, Texas A&M University, Y. Xu, Oak Ridge National Laboratory, Z. Zhou, Texas A&M University, Q. Guo, Chinese Academy of Sciences, China, Z. Yan, Y. Yao, Texas A&M University, L. Semidey-Flecha, Oak Ridge National Laboratory, D.W. Goodman, Texas A&M University**

Single-layer graphene supported on transition metals provides a unique substrate for synthesizing metal nanostructures due to the high crystallographic quality, thermal stability, and chemical inertness of the graphene. Contrary to its formation of three-dimensional (3-D) nanoclusters on graphene supported on a SiO<sub>2</sub> substrate, Au forms two-dimensional (2-D) islands on graphene moiré/Ru(0001). These Au islands maintain their 2-D structures up to 1 monolayer (ML) equivalent of Au dosage and are stable at room temperature. Our scanning tunneling microscopic study further shows that the 2-D Au islands are most likely two layers high, and conform to the graphene moiré in the lateral direction. Spin- and angle-resolved photoemission studies indicate even though these Au islands are largely electronically isolated, a weak through-graphene coupling exists between the Au islands and the Ru(0001) substrate. The structure for these 2-D Au islands and the corresponding electronic band structures are proposed based on DFT calculations.

Parallel studies using polarization modulation infrared reflection absorption spectroscopic (PM-IRAS) and high resolution electron energy loss spectroscopic (HREELS) indicate that CO adsorbs on these 2-D gold islands at 85 K with a characteristic CO stretching feature at 2095 cm<sup>-1</sup> for a saturation coverage. Preliminary data obtained by dosing molecular oxygen onto this CO pre-covered surface suggest that the 2-D gold islands catalyze the oxidation of CO. These electron-rich, weakly coupled 2-D Au islands provide a unique platform to study the intrinsic catalytic activity of low-dimensional Au nanostructures.

**9:40am SS2-WeM6 Spatially Resolved Measurements of Catalytic Activity on Variable-Composition Pd-Cu and Pd-Cu-Au Thin Films using a Microfluidic Reactor Array, P. Kondratyuk, G. Gumuslu, Carnegie Mellon University, B.D. Morreale, National Energy Technology Laboratory, J.B. Miller, A.J. Gellman, Carnegie Mellon University**

A new experimental approach to mapping the relationship between composition and catalytic activity in metal alloy catalysts is presented. We apply this methodology to study H<sub>2</sub>-D<sub>2</sub> exchange reaction on Pd-Cu and Pd-Cu-Au alloys. The activity measurements were performed on thin alloy films deposited in such a way that the elemental composition varied continuously across the film. We refer to these films as composition spread alloy films (CSAFs). CSAFs were prepared by co-deposition of Pd, Cu and Au onto a molybdenum substrate under UHV conditions. The top-layer and near-surface composition of the CSAFs were determined by low-energy ion scattering (LEIS) and X-ray photoemission spectroscopy (XPS) respectively. The activity of the alloy films in the H<sub>2</sub>-D<sub>2</sub> exchange reaction was analyzed at atmospheric pressure using a 100-channel glass microfluidic device. During the spatially-resolved activity measurements, the microfluidic device delivers reactant gases to a 10x10 array of measurement points on the CSAF surface covering an area of 1 cm<sup>2</sup>, each

measurement point corresponding to a different catalyst composition. After coming in contact with the catalyst, the gases are withdrawn for mass-spectrometric analysis through a separate set of channels. The activity-composition relationship can then be established by correlating the XPS (or LEIS) data with the product concentration in each channel of the microfluidic device.

**10:40am SS2-WeM9 Surface Structure Dependence by Monofaceted CeO<sub>2</sub> Nanoparticles: Catalytic Oxidation Reactions, M. Li, Z. Wu, F.C. Calaza, D.R. Mullins, S.H. Overbury, Oak Ridge National Laboratory**

Reducibility of pure and doped CeO<sub>2</sub> is of interest in emission control catalysts because of the ability of the CeO<sub>2</sub> to store and supply oxygen during oxidation catalysis. But, it is not known how the structure or crystallographic termination of the CeO<sub>2</sub> affects the catalytic reaction rates and selectivity. Using CeO<sub>2</sub> nanoparticles with controlled shapes including cubes, octahedra and rods that are terminated on (100), (111) and (110) surfaces respectively, we have investigated this structure dependence. Temperature programmed desorption, temperature programmed reaction, flow reactor rates, and in situ DRIFTS were used to probe adsorption states, desorption, reaction, oxidation rates and product selectivity for CO and ethanol oxidation. Results show pronounced differences between the three different morphologies. All morphologies show evidence of surface ethoxide species at room T, but during subsequent TPD, the DRIFTS exhibits variation in surface species between the different surfaces with evidence for formation of adsorbed acetaldehyde and acetate. Temperature induced changes in the C-H stretching regions, different also for each polymorph, suggest competing dehydrogenation and dehydration of surface species. Desorption temperatures and product distributions also vary. The ratio of H<sub>2</sub>/H<sub>2</sub>O, and the H<sub>2</sub> peak desorption temperature is highest for the octahedra, consistent with its highest vacancy formation energy and therefore least available oxygen. This ratio is lowest for high surface area multi-faceted nanoparticles, and its variability has important implications for tailoring and understanding CeO<sub>2</sub> catalysts or supports for production of H<sub>2</sub> in ethanol fuel cells. Product profiles during TPR of ethanol in O<sub>2</sub> were also dependent upon the surface structure. Octahedra show the highest selectivity to acetaldehyde and an onset of H<sub>2</sub> evolution above 400 °C while the cubes and rods showed lower temperatures for the onset of H<sub>2</sub>, indicating that the hydrogen is evolved by two different pathways on different shaped ceria. Similarly, in a steady state flow reactor, the ratio of selective oxidation product (acetaldehyde) to the total oxidation product (CO<sub>2</sub>) followed the order (111) > (100) > (110). Such results provide a basis for fundamental understanding of how surface coordination, bonding, decomposition and reaction are affected by the atomic structure of an oxide surface, especially important for reducible oxides.

Research sponsored by the Division of Chemical Sciences, Geosciences, and Biosciences, Office of Basic Energy Sciences, US DOE.

**11:00am SS2-WeM10 Tuning the Adsorption Properties of an Oxide Material Via Doping: Au Clusters onto Cr-doped MgO(001) Films, F. Stavale, N. Nilius, H.-J. Freund, Fritz-Haber-Institute of the Max-Planck-Society, Germany**

The doping of metal oxides has been explored in several investigations with the aim to prepare better materials for catalysis, optics and electronic applications. Doping of wide-gap oxide materials can be realized by the controlled introduction of various types of lattice defects, including point defects such as oxygen vacancies, line defects (e.g. grain boundaries and dislocations) and impurity atoms. In this study, we have exploited photon-scanning tunneling microscopy used in imaging as well as in cathode-luminescence mode to investigate Au clusters supported on thin, single crystalline MgO(001) and Cr-doped MgO(001) films grown on Mo(001). First of all, we have prepared Cr-doped MgO films on a Mo(001) support as a model system for a transition-metal doped wide-gap insulator with interesting applications in catalysis. To elucidate the role of the Cr in the MgO matrix, the morphological and optical properties of the system were analyzed as a function of the Cr load, using the STM. The Cr was incorporated into the film either by Cr-Mg co-deposition in oxygen or post-evaporation followed by an annealing step. From the distinct light emission properties of the doped oxide, a detailed picture has been developed on the Cr<sup>3+</sup> position inside the MgO lattice and the associated modifications in the electronic structure. The role of the Cr dopants on the adsorption behaviour of the oxide film was investigated by depositing small amounts of Au. While on pristine MgO films, Au nucleates into 3D particles, mainly 2D aggregates form on the doped oxide support. We assign this change in the Au growth mode to charge transfer processes from the Cr centres into the Au clusters and will discuss possible consequences on the chemical activity of the doped metal-oxide system.

11:20am **SS2-WeM11 Hydrogen Adatom Manipulation on the Rutile TiO<sub>2</sub>(110) Surface using LT-STM**, *P. Sutter, D. Acharya, N. Camillone III*, Brookhaven National Laboratory

Characterization and control of the structure of TiO<sub>2</sub> surfaces at the single-atom level are vital to the development of a fundamental understanding of the chemistry and physics of this technologically important oxide. In this work we investigate the use of a low-temperature scanning tunneling microscope (LT-STM) tip to manipulate individual hydrogen adatoms on the rutile TiO<sub>2</sub>(110) surface at 77 K. We show that applied voltage pulses are effective for transferring hydrogen atoms from the surface to the STM tip with single-atom control. This tip-induced ‘desorption’ is useful for unambiguously distinguishing between surface hydroxyls (OH<sub>br</sub>) and bridging oxygen (O<sub>br</sub>) vacancies—two common surface defects whose appearance in STM images is quite similar. In addition we show that individual atoms can be redeposited on the surface precisely at selected O<sub>br</sub> sites, allowing for the controlled preparation of arbitrary hydrogen adatom assemblies. Such control is a prerequisite for the investigation of the structural dependence of surface photo- and thermal reactivity at the single-molecule level.

11:40am **SS2-WeM12 Reaction of Water with Terminal Hydroxyls on TiO<sub>2</sub>(110) Surface**, *I. Lyubinetsky, Y.G. Du*, Pacific Northwest National Laboratory, *N.A. Deskins*, Worcester Polytechnic Institute, *Z. Zhang*, Baylor University, *Z. Dohnalek, M. Dupuis*, Pacific Northwest National Laboratory

We report a combined experimental and theoretical investigation of the reaction of molecular water with terminal hydroxyls (OH<sub>t</sub>'s) on reduced TiO<sub>2</sub>(110)-(1x1) surface at 300 K. We show that OH<sub>t</sub>'s have a significant effect on the water reactivity and extract molecular-level details about the underlying reaction mechanisms. By tracking the same surface area with high-resolution scanning tunneling microscopy before and after water exposure, we demonstrate that there are two distinctive reaction pathways involving multiple proton transfers [1]. For water interaction with OH<sub>t</sub> on an adjacent Ti row, the proton can be transferred through bridging oxygen to OH<sub>br</sub>, which leads to the formation of a new water molecule and apparent across-row motion of OH<sub>t</sub> due to O scrambling. This process further manifests the existence of the equilibrium between molecular and dissociated states of water on TiO<sub>2</sub>(110) [2]. If H<sub>2</sub>O interacts with OH<sub>t</sub> along the same Ti row, fast multi-step OH<sub>t</sub> motion along the Ti row is observed. Our density functional theory results show that this process is caused by the fast diffusion of (OH<sub>t</sub> + H<sub>2</sub>O) pairs, whereby the underlying mechanism involves proton transfer and H<sub>2</sub>O hopping over OH<sub>t</sub>.

[1] Y. Du, N. A. Deskins, Z. Zhang, Z. Dohnálek, M. Dupuis, and I. Lyubinetsky, *Phys. Chem. Chem. Phys.* 12 (2010) 6337.

[2] Y. Du, N. A. Deskins, Z. Zhang, Z. Dohnálek, M. Dupuis, and I. Lyubinetsky, *Phys. Rev. Lett.* 102 (2009) 096102.

This work was supported by the U.S. Department of Energy (DOE) Office of Basic Energy Sciences, Division of Chemical Sciences, and performed at EMSL, a national scientific user facility sponsored by the DOE's Office of Biological and Environmental Research and located at PNNL.

# Wednesday Afternoon, November 2, 2011

## Biomaterial Interfaces Division

Room: 108 - Session BI+AS+NS+SS-WeA

### Functionalization and Characterization of Nanostructures

Moderator: A. Belu, Medtronic, Inc.

#### 2:00pm BI+AS+NS+SS-WeA1 Characterization of Nano-objects by Cluster-SIMS, E.A. Schweikert, Texas A&M University INVITED

Secondary ion mass spectrometry, SIMS is a method of choice for the chemical analysis of nanodomains embedded in solids. We examine here a case which has received little attention, the analysis of individual, free-standing nano-objects. Our approach uses a variant of SIMS. The nano-objects are bombarded with a sequence of individual projectiles resolved in time and space, in the present case  $\text{Au}_{400}^{4+}$  of up to 520 keV impact energy. The successive projectiles impact stochastically the nano-objects dispersed on a solid support. Typically tens of secondary ions are ejected from each impact. They are identified with time-of-flight mass spectrometry and recorded individually. This approach reveals molecules co-located within the 10-20 nm diameter area of emission from one  $\text{Au}_{400}^{4+}$  impact. We demonstrate that the event-by-event bombardment-detection mode is sensitive to the chemical and/or physical nano-scale separation of molecular species. The performance is illustrated with the determination of the relative abundance of the oxide layer in the near surface of 50-100 nm nanoparticles; the nature and abundance of different nano-objects (5-20 nm in diameter) in mixtures of nano-sized solids; the composition of bio-objects such as a bacteriophage including the amino acids of the proteins surrounding the phage and the bases from the encapsulated DNA. The distinct feature of the nanoprobe technique presented here is in the detection of co-emitted ejecta from individual projectile impacts which allows to test chemical composition, in a nonimaging mode, yet at an exquisite level of spatial resolution. Moreover the co-emission of fragment and parent ions enhances the accuracy of molecular identification.

Work supported by NSF grant CHE-0750377

#### 2:40pm BI+AS+NS+SS-WeA3 Strategies for Studying the Surface Chemistry of Engineered Nanoparticles with SIMS, C. Szakal, J. McCarthy, National Institute of Standards and Technology, K. Louis, R.J. Hamers, University of Wisconsin-Madison, R.D. Holbrook, National Institute of Standards and Technology

The environmental toxicity of engineered nanoparticles (ENPs) is of increasing importance as these materials become more widely used in manufacturing processes and consumer products. Nanoparticles have extremely high surface-to-volume ratios, which makes the surfaces more critical than their corresponding bulk materials in terms of reactivity, aggregation, and toxicity to various life forms. Therefore, it is critical that we develop methods to distinguish small chemical changes on nanoparticle surfaces in order to understand how these materials will interact outside of controlled laboratories. Conventional approaches of nanoparticle characterization have focused on high resolution morphological imaging (TEM, SEM) and physical property measurements such as surface charge. However, chemical information is generally only inferred from these materials with most current methods. If it is possible to obtain both elemental and molecular information from ENP surfaces, we may be able to determine the eventual fate of ENPs in the environment.

We have developed a comprehensive approach for studying the surface chemistry of ENPs, including 1) preparation of ENPs to controllably study desired variables, 2) development of methods such as time-of-flight secondary ion mass spectrometry (ToF-SIMS) and environmental scanning electron microscopy (ESEM) to probe small changes in ENP surface chemistry and/or aggregation, and 3) development of methods to improve the speed and reproducibility of ENP aggregation for batch studies. These approaches will be utilized as the basis of future toxicity studies of selected ecosystems.

#### 3:00pm BI+AS+NS+SS-WeA4 Unusual Hydrogenation Isotherms for Pd Nanoring Model Systems Observed Via Nanoplasmonic Sensing, C.B. Langhammer, E.M.K. Larsson, I.L. Zoric, Chalmers University of Technology, Sweden, V.P. Zhdanov, Boreskov Institute of Catalysis, Russian Federation

Nanostructured materials have been proposed as a solution for the development of efficient hydrogen storage systems. As the size of the system gets reduced in the nanometer range enthalpies and entropies of hydrogen dissolution in the metal ( $\alpha$ -phase) and hydride formation ( $\beta$ -

phase) as well as activation barriers for diffusion and desorption of hydrogen become size dependent thus influencing both thermodynamics (pressure-composition isotherms) and kinetics (loading/unloading kinetics). The pressure-composition isotherms for a H<sub>2</sub>/M system show a well-known behavior typical for an  $\alpha$ -phase in the low pressure-composition range followed by a plateau signaling the onset of a hydride formation ( $\beta$ -phase) via a first order phase transition and a coexistence of the two over a wide composition range. At higher pressure a pure  $\beta$ -phase exists characterized by a pressure-composition curve with a steep slope. The plateau pressure of the H<sub>2</sub>/M system is determined by the requirement of equilibrium between the three phases in coexistence, thus primarily by the enthalpy and entropy of hydride formation. In case of more than one hydride type a coexistence region exhibits multiple plateaux determined by appropriate energetics as described above. In all known cases the same multiple plateaux features were observed both during the charging and discharging process, i.e. when hydrogen pressure was increased/decreased, accompanied of course by a perennial hysteresis.

In this work we report unusual pressure-composition isotherms for H<sub>2</sub>/Pd nanosized rings where a double plateau isotherms are observed during the charging process and a single plateau one during the hydrogen discharging. The Pd nanorings were fabricated using colloidal lithography. Hydrogen isotherms were followed by monitoring the shift in the ring Localized Surface Plasmon Resonance, LSPR, upon exposing the system to increasing/decreasing hydrogen pressure steps (and equilibrating the sample at each pressure step). The shift of the LSPR resonance was calibrated by preparing the same ring structure on a quartz crystal microbalance and "weighing" directly absorbed hydrogen. A linear relation between the LSPR shift and QCM frequency shift (proportional to hydrogen concentration) was observed.

We present a simple model, based on the observed heterogeneity of the nanorings (as seen in TEM) and by taking into account the defect induced lattice strain, that accounts for the unusual behavior of the observed isotherms.

#### 4:00pm BI+AS+NS+SS-WeA7 Surface Functionalization and Analysis of Functional "Soft" Nanostructures: From 2 to 3 Dimensions, H. Schönherr, University of Siegen, Germany INVITED

The local properties of soft matter, e.g. for the fabrication of functional biointerfaces or nanostructures, are of tremendous importance for ultimate functionality. In this presentation, the closely interrelated areas of surface chemical functionalization / engineering and analysis of properties will be discussed based on three key examples. These examples include: (i) synthesis and modification of polymer brushes with particular focus on the nanomechanical properties, (ii) ultra small diameter nanotubes obtained by the layer-by-layer assembly of polyelectrolytes inside a sacrificial porous template and (iii) block copolymer nanocapsules that are developed for advanced wound management. In all examples, confinement effects are expected to play a significant role in determining e.g. the mechanical properties, as assessed by atomic force microscopy (AFM) nanoindentation.

For thin polymer films (2D) the dependence of the mechanical properties on the film architecture was unraveled. Compared to spin-coated films, brushes synthesized on gold surface by surface initiated polymerization showed higher elastic moduli, which is attributed to entropy effects. Upon chemical crosslinking tunable elastic properties are obtained, which provides interesting pathways for the fabrication of defined cell - surface contacts.

Similarly important are defined nanoscale objects that can be obtained via the replication of small templates by the so-called layer by layer (LbL) deposition of polyelectrolytes (G. Decher Science 1997, 277, 1232). LbL deposition in porous Anodic Aluminum Oxide (AAO) was only very recently expanded to the 100 nm length scale due to an alleged entropic barrier caused by adsorbed polyelectrolytes close to the pore orifice [Y. Cho et al. Small 2010, 6, 23, 2683]. However, in contrast to this report, we show that the adsorption of polyelectrolytes on the top plane of the AAO and polymer sedimentation have been identified as main bottlenecks. Suppressing these processes enabled us to produce free standing polymer nanotubes with external diameters of < 55 nm.

Finally, first steps in the development of active nanocapsules filled with a reporter dye or an antimicrobial agent for applications in burn wound management will be presented. In particular the case of burn wounds and the devised biomimetic strategy of BacterioSafe will be introduced. Subsequently, the fabrication and characterization of a polystyrene-block-poly(acrylic acid) amphiphile-based model vesicle system, in particular the loading and release behavior and mechanical properties will be discussed.

4:40pm **BI+AS+NS+SS-WeA9 Large Area Fabrication of Biological Nanostructures**, *G. Tizazu, O. El-Zubir*, University of Sheffield, UK, *S. Brueck*, University of New Mexico, *D. Lidzey, G. Leggett*, University of Sheffield, UK, *G.P. Lopez*, Duke University

There has been enormous interest in the control of biological interactions at interfaces with nanometer spatial resolution, but important challenges still remain to be addressed. Of the established fabrication techniques, electron beam lithography is expensive, and requires exposure under vacuum, while scanning probe methods are slow and (with few exceptions) do not permit fabrication over large areas. In contrast, interferometric lithography (IL) is a simple approach that uses inexpensive apparatus to fabricate sub-wavelength structures over macroscopic areas. When two coherent laser beams interfere, they yield a sinusoidal pattern of intensity that may be used to modify photosensitive materials. Previously IL has been used extensively for semiconductor nanofabrication, but our recent data show that combined with self-assembled monolayer resists it provides a fast, simple method to create molecular nanostructures over macroscopic areas. Illustrations will be provided of bionanofabrication using interferometric modification of protein-resistant (oligo ethylene glycol) functionalised surfaces, where feature sizes as small as 30 nm ( $\lambda/8$ ) have been achieved over square cm areas, and the controlled growth of protein-resistant brush structures from patterns of initiators for atom-transfer radical polymerisation. The fabrication of metallic nanostructures over macroscopic regions, including Ti structures as small as 35 nm, and gold nanostructures of controlled size and periodicity will also be demonstrated.

5:00pm **BI+AS+NS+SS-WeA10 Functionalization of Mesoporous Silicon Biosensors to Achieve Tunable DNA Bioreceptor Density**, *J. Lawrie, R.R. Harl, B.R. Rogers, P. Laibinis, S.M. Weiss*, Vanderbilt University

Porous silicon has become a widely studied material for sensing over the last decade based on its large surface to volume ratio and easily tunable morphology. With growing interest in the detection and analysis of genetic material, DNA oligos have become an increasingly important biorecognition element in porous silicon and many other sensor platforms. As aptamers, nucleic acids serve as high affinity bioreceptors to a wide range of small molecules and biological materials, opening up a number of potential applications in environmental science, chemical and biological defense, and medical diagnostics. In this work, tuning of the porous silicon surface chemistry is described. Controlling surface silanization, bioreceptor density, and bioreceptor charge and secondary structure enables the fabrication of reusable, label-free optical sensors toward specific nucleic acid targets. Detection limits in the nanomolar range have been demonstrated.

We have previously shown that in situ DNA synthesis via the phosphoramidite method in porous silicon produces high bioreceptor coverage for label-free optical biosensing applications. Low hybridization efficiency, despite high sensitivity, for such sensors indicated that tuning the receptor surface density could further improve detection limits. To modify surface receptor density, two-component trichlorosilane monolayers were deposited from solution onto porous silicon. One monolayer component remained active to phosphoramidite chemistry while the second component was inert. This method enabled a range of surface probe densities to be achieved and controlled via silanization conditions. Monolayer composition and DNA receptor density were verified using XPS, contact angle, and UV-Vis spectrophotometry. For a 16mer DNA oligo bound within a porous silicon waveguide, detection of the complementary target nucleic acid was maximized when 25% of the internal pore surface area was active toward DNA synthesis. Tuning surface DNA density increases sensitivity by a factor of 2-3. Label-free, target-specific detection of oligos was observed at concentrations of 25nM.

We will present results from hybridization efficiency studies in which DNA bioreceptor surface density, length, and secondary structure are varied. These parameters are vital to nucleic acid aptamer sensing strategies in label-free optical biosensors. Predicting appropriate receptor surface density for aptamer sensors based upon oligo sequences will provide advantages in achieving fast and sensitive waveguide sensors for detection in complex media.

Acknowledgements: This work is supported in part by the Army Research Office (W911NF-08-1-0200).

5:20pm **BI+AS+NS+SS-WeA11 Composite Fluorocarbon Membranes by Surface-Initiated Polymerization**, *C.A. Escobar, A.R. Zulkifli, G.K. Jennings*, Vanderbilt University

This presentation describes the fabrication and characterization of a novel composite membrane that consists of two types of nanoporous materials, namely, nanoporous gold leaf (NPGL) and nanoporous alumina, and a selective poly(perfluorohexyl norbornene) (pNBF6) polymer. Integration of the three materials is achieved by means of silane and thiol chemistry, and

the use of surface-initiated ring-opening metathesis polymerization (SI-ROMP). The former two provide functionalization of the nanoporous substrates, and the latter promotes the generation of the polymer film within and atop of the alumina-NPGL membrane. The synthetic process is versatile in that simultaneous or selective growth of the polymer film in each nanoporous layer is straightforward. The use of SI-ROMP allows tailoring of the extent of polymerization of pNBF6 throughout the structure by varying polymerization time. Advancing contact angle measurements show that the surface of these composite membranes exhibits both hydrophobic and oleophobic behavior. Scanning electron microscopy (SEM) images indicate that the thin polymer films cover the porous substrates entirely. Results from electrochemical impedance spectroscopy (EIS) confirm that the membranes provide effective barriers to aqueous ions and that sulfonation of the polymer backbone substantially enhances ion transport through the composite membrane. Ion transport and selectivity of the membrane change by regulating the polymerization time. The fluorinated nature of the polymer thin film renders the membrane selective towards molecules with similar chemical characteristics.

## Surface Science Division

Room: 107 - Session SS-WeA

### Adsorption & Reactions on Oxide Surfaces

Moderator: S.L. Scott, University of California, Santa Barbara

2:00pm **SS-WeA1 Direct Observation of O<sub>2</sub> Molecular Chemisorption at Two Distinctive Sites of TiO<sub>2</sub>(110)**, *Z.T. Wang, Y.G. Du, Z. Dohnálek, I. Lyubinetzky*, Pacific Northwest National Laboratory

The chemistry of oxygen on TiO<sub>2</sub> surfaces is an important component in many catalytic and photocatalytic processes, such as water splitting and waste remediation, and has been extensively studied. So far, the majority of fundamental research has been carried out on the model transition-metal oxide surface of the rutile TiO<sub>2</sub>(110). The investigation of molecular adsorption of O<sub>2</sub> can be considered as a natural first step providing information about possible O<sub>2</sub> surface chemistry on TiO<sub>2</sub>(110). Both experiment and theory have demonstrated that O<sub>2</sub> dissociatively adsorbs at bridging oxygen vacancies (V<sub>O</sub>) sites and five-fold coordinated terminal titanium atoms (Ti<sub>5c</sub>) at elevated temperatures. At sufficiently low temperatures, the majority of the ensemble-averaging technique studies suggested that O<sub>2</sub> molecularly chemisorbs at V<sub>O</sub> sites on reduced surfaces (at  $T < 150$  K). However, recent STM studies reported a contradict result that the O<sub>2</sub> dissociation at V<sub>O</sub> sites has been observed at temperatures as low as  $\sim 110$  K.

In this work, we investigated the initial stages of oxygen adsorption on reduced TiO<sub>2</sub>(110) with high-resolution scanning tunneling microscopy (STM) at 50 K. Molecularly chemisorbed O<sub>2</sub> species, not directly observed until now on TiO<sub>2</sub>(110), have been imaged at two distinctive adsorption sites (V<sub>O</sub> and Ti<sub>5c</sub>) using "extremely mild" tunneling conditions. While O<sub>2</sub> species at Ti<sub>5c</sub> site appears as a single protrusion centered on the Ti<sub>5c</sub> row, the O<sub>2</sub> at V<sub>O</sub> manifests itself by a disappearance of the V<sub>O</sub> feature. The dissociation of chemisorbed O<sub>2</sub> can be readily induced by tunneling conditions that are normally used for TiO<sub>2</sub>(110) imaging, and the dissociation details strongly depend on the scanning parameters and the type of the O<sub>2</sub> adsorption site. The O<sub>2</sub> molecules chemisorbed at low temperatures at these two distinct sites are the most likely precursors for the two O<sub>2</sub> dissociation channels, observed at temperatures above 150 and 230 K at the V<sub>O</sub> and Ti<sub>5c</sub> sites, respectively. In general, our results provide a molecular level insight into the thermal chemistry of O<sub>2</sub> on reduced TiO<sub>2</sub>, and assist in understanding of the surface reactivity of transition-metal oxides.

2:20pm **SS-WeA2 The Interaction of Carboxylic Acids with Rutile TiO<sub>2</sub> (110) Single Crystal Surfaces: Results from IR-Spectroscopy**, *M. Buchholz*, Karlsruhe Institute of Technology (KIT), Germany, *M.C. Xu, Y.M. Wang*, Ruhr-University Bochum, Germany, *A. Nefedov, C. Wöll*, Karlsruhe Institute of Technology (KIT), Germany

The role of oxides is central in many technological areas such as gas sensing, catalysis and thin film growth. Zinc oxide and titanium oxide are also important for photocatalysis and photooxidation, e.g. of CO to CO<sub>2</sub><sup>[1]</sup>. In the Graetzel-cell, organic molecules bound to TiO<sub>2</sub>-substrates via carboxylate bonds effectively convert photons into electric energy. In last decades numerous IR investigations of oxide powders, including the different modifications of TiO<sub>2</sub>, have been reported. An unambiguous assignment of the features in the complex IR spectra recorded for molecules bound to the oxide powder particle surfaces, however, is only possible on the basis of data recorded for well-defined reference systems, e.g. surfaces



of single crystals. Unfortunately, studies on oxide single crystals are extremely scarce due to the fact that the sensitivity of reflection IR-spectroscopy for molecular adsorbates is two orders of magnitude lower for oxides than for metal single crystals. Only recently was it possible to overcome these technical problems by employing a novel, optimized spectrometer.<sup>[2]</sup> Here, we will demonstrate the performance of this highly sensitive IRRAS-setup by presenting high-quality IR-spectra obtained for two molecules, benzoic acid and terephthalic acid, adsorbed on rutile TiO<sub>2</sub> (110). Owing to the fact that many Dye Sensitized Solar Cells (DSSCs) consist of dyes grafted to the oxide support via carboxylate groups determining and controlling the adsorption of carboxylic acids on oxidic substrates is fundamental to understanding the energy transfer from the molecule to the substrate. For the present experiments, monolayers of terephthalic acid (TPA) and benzoic acid (BA) were first deposited under UHV-conditions on a rutile TiO<sub>2</sub> (110) surface at room temperature. Subsequently the sample was transferred in the main chamber and subjected to an analysis in a highly sensitive UHV IRRAS system. While for BA the expected bidentate carboxylate bonding is observed, for TPA the presence of two carboxylic acid groups leads to interesting complications. The IR-spectra allow, in particular, answering the question whether for the flat-lying TPA species observed in scanning probe techniques<sup>[3]</sup> the carboxylic acid group is still protonated, a question which could not be answered by the results from x-ray absorption spectroscopy<sup>[3]</sup>.

[1] M. C. Xu, Y. K. Gao, E. M. Moreno, M. Kunst, M. Muhler, Y. M. Wang, H. Idriss, C. Wöll, *Phys. Rev. Lett.* **2011**, *106*, 138302.

[2] Y. M. Wang, A. Glenz, M. Muhler, C. Wöll, *Rev. Sci. Instrum.* **2009**, *80*, 113108.

[3] P. Rahe, M. Nimmrich, A. Nefedov, M. Naboka, C. Wöll, A. Kühnle, *Journal of Physical Chemistry C* **2009**, *113*, 17471.

**2:40pm SS-WeA3 The Adsorption Dynamics and Interfacial Charge Trapping Behavior for Acetic Acid on Rutile TiO<sub>2</sub> Surfaces, J. Tao, T. Luttrell, M. Batzill, University of South Florida**

Using temperature programmed desorption (TPD), scanning tunneling microscopy (STM) and ultraviolet photoemission spectroscopy (UPS), we have observed very different adsorption dynamics for acetic acid on rutile TiO<sub>2</sub>(110) and (011)-2×1 surfaces at room temperature. While the bidentate adsorption of carboxylic acids on the (110) surface is well-established, we find a monodentate adsorption on the (011)-2×1 surface as the most likely adsorption geometry. On the (011)-2×1 surface, the initial sticking of adsorbed acetic acid is low. It appears that initial adsorption occurs at defects. These adsorbed acetates then act as nucleation sites for further adsorption. This adsorption mechanism results in the formation of quasi-1D acetate clusters running along direction. The role of acetate adsorption in the formation or annihilation of excess charges in TiO<sub>2</sub> is also found to be different on these two surfaces. We find that bidentate adsorption of acetate on the (110) surface results in extraction of excess charges from the substrate, while mono-dentate adsorption on the (011)-2×1 surface causes net-charge donation to the substrate. More interestingly, a difference in the binding energy of excess charges, or Ti-3d band gap states, has been observed. On the TiO<sub>2</sub>(011)-2×1 surface the binding energy is ~0.3 eV higher than on the (110) surface. This difference is explained by the different crystal fields on the reconstructed (011) surface compared to the bulk-truncated (110) surface. At the rutile TiO<sub>2</sub>(011)-2×1 surface, Ti-ions are located in a distorted square pyramidal coordination environment, which we propose causes the shift in binding energy of excess electrons at the Ti-site. The differences in binding energy of electrons trapped at the surface for the two surfaces may contribute to the face dependent photocatalytic activity of rutile TiO<sub>2</sub>.

References:

1. J. Tao, T. Luttrell, J. Bylisma, and M. Batzill, *J. Phys. Chem. C* **2011**, *115*, 3434

2. J. Tao and M. Batzill, *J. Phys. Chem. Lett.* **2010**, *1*, 3200.

**3:00pm SS-WeA4 Effect of the Adsorption Geometry of Zinc-Tetraphenylporphyrin Derivatives on ZnO and TiO<sub>2</sub>, on the Exciton Delocalization Pathways, S. Rangan, S. Coh, R.A. Bartynski, K. Chitre, J. Rochford, E. Galoppini, Rutgers University, C. Jaye, D.A. Fischer, National Synchrotron Light Source**

ZnTPP derivatives are attractive candidates for photoinduced electron-transfer mediators in dye sensitized solar cells (DSSCs). Many fundamental properties of the dye/metal oxide interface are not known and need careful consideration. In particular, the influence on solar cells efficiency, of the energy alignment and of the molecular packing at the surface, remains unclear. In this work, using x-ray, UV and inverse photoemission spectroscopies in conjunction with density functional theory (DFT) calculations, we have determined the energy alignment of molecular levels with respect to the substrate band edges for several ZnTPP derivatives

adsorbed on ZnO(11-20) and TiO<sub>2</sub>(110) surfaces. The ZnTPP derivatives were functionalized with COOH anchoring groups, to allow a priori either upright or flat adsorption on the surfaces. While the energy alignment, a critical parameter to allow charge separation at the dye/semiconductor interface, is found similar for all of these systems, large differences in solar cells efficiencies are observed. We have thus explored the adsorption geometry of the same ZnTPPs at the surface of ZnO and TiO<sub>2</sub> using UV-visible absorption and NEXAFS spectroscopies and scanning tunnel microscopy. It is found that that dye/dye interactions is an important factor, for electron transfer to the substrate. For ZnTPPs, upright adsorption opens deleterious exciton delocalization pathways, due to dipole/dipole interactions competing with electron transfer to the substrate. Choosing the adsorption geometry is thus critical for the electronic pathway control.

**4:00pm SS-WeA7 Adsorption of Trimethylacetic Acid on Stoichiometric and Reduced CeO<sub>2</sub>(111) Surfaces, S.P. Sanghavi, A.S. Karakoti, M.I. Nandasiri, W. Wang, P. Nachimuthu, P. Yang, S.V.N.T. Kuchibhatla, S. Thevuthasan, Pacific Northwest National Laboratory**

The use of nanoparticles in energy, environmental and medical applications has been growing significantly in recent years. In most of these applications, the nanoparticles are being used in as-synthesized form and/or functionalized through ligand conjugation. When particle size decreases to nanometer scale, a large percentage of the atoms are at or near the surface which makes the surface highly dynamic and reactive in nature. Consequently, these particles exhibit unique properties that make their characterization more difficult by conventional spectroscopic methods. Furthermore, knowledge on how the ligand molecules bind to the surface of nanoparticles is very limited. To better understand the interactions between ligand molecules and the surface of nanoparticles, we used a model system approach to study the interaction between the carboxylate anchoring group from trimethylacetic acid (TMAA) and CeO<sub>2</sub>(111) surfaces as a function of oxygen stoichiometry. The epitaxial CeO<sub>2</sub>(111) thin films 50nm in thickness were grown on YSZ(111) by oxygen plasma-assisted molecular beam epitaxy at 650°C under 2.5x10<sup>-5</sup> Torr of oxygen plasma. The sample films from MBE system were transferred to X-ray photoelectron spectroscopy (XPS) system and sputter cleaned to remove any surface contamination during the transfer. Following sputtering, stoichiometric CeO<sub>2</sub>(111) surface was obtained by annealing the thin film under 2.0x10<sup>-5</sup> Torr of oxygen at ~550°C for 30 min. In order to reduce the CeO<sub>2</sub>(111) surface, the thin film was annealed in ~5.0x10<sup>-10</sup> Torr vacuum at 550°C, 650°C, 750°C and 850°C for 30 min to progressively increase the oxygen defect concentration on the surface. XPS was used to characterize these surfaces prior to and following dissociative adsorption of TMAA on these surfaces using a molecular doser. The saturated TMAA coverage and the oxygen defect concentration were determined from XPS elemental composition. The saturated TMAA coverage on CeO<sub>2</sub>(111) surface is found to increase with increasing oxygen defect concentration. This is attributed to increase in under coordinated cerium sites on the surface with increase in the oxygen defect concentrations. In parallel, we studied the interactions of TMAA adsorbed at various sites on the stoichiometric CeO<sub>2</sub>(111) surface using periodic density functional theory (DFT) calculations. Both energetics and electronic properties of the surface and TMAA will be presented and correlated with experimental observations.

**4:20pm SS-WeA8 Reactivity Differences between CeO<sub>2</sub>(100) and CeO<sub>2</sub>(111) Thin Films, D.R. Mullins, F.C. Calaza, S.H. Overbury, M.D. Biegalski, H.M. Christen, Oak Ridge National Laboratory**

Cerium oxide is a principal component in many heterogeneous catalytic processes. One of its key characteristics is the ability to provide or remove oxygen in chemical reactions. The different crystallographic faces of ceria present significantly different surface structures and compositions that may alter the catalytic reactivity. The structure and composition determine the availability of adsorption sites, the spacing between adsorption sites and the ability to remove O from the surface.

To investigate the role of surface orientation on reactivity, CeO<sub>2</sub> films were grown with two different orientations. CeO<sub>2</sub>(100) films were grown *ex situ* by pulsed laser deposition on Nd-doped SrTiO<sub>3</sub>(100). The structure was characterized by RHEED, XRD and reflectometry. CeO<sub>2</sub>(111) films were grown *in situ* by thermal deposition of Ce metal onto Ru(0001) in an oxygen atmosphere. The structure of these films has been studied by LEED and STM. Attempts to grow CeO<sub>2</sub>(100) *in situ* by physical vapor deposition on Pt(100) and Pd(100) failed due to preferential growth of CeO<sub>2</sub>(111) on these supports.

The chemical reactivity was characterized by the adsorption and decomposition of various molecules such as methanol, water and acetaldehyde. Reaction products were monitored by TPD and surface intermediates were determined by soft x-ray photoelectron spectroscopy. In



general the CeO<sub>2</sub>(100) surface was found to be more active, i.e. molecules adsorbed more readily and reacted to form new products, especially on a fully oxidized substrate. However the CeO<sub>2</sub>(100) surface was less selective with a greater propensity to produce CO, CO<sub>2</sub> and water as products. The differences in chemical reactivity are discussed in light of possible structural terminations of the two surfaces.

Research sponsored by the Division of Chemical Sciences, Geosciences, and Biosciences, Office of Basic Energy Sciences, U.S. Department of Energy. Portions of this work were conducted at the National Synchrotron Light Source, Brookhaven National Laboratory, and Oak Ridge National Laboratory's Center for Nanophase Materials Sciences, which are sponsored by the Office of Basic Energy Sciences, U.S. Department of Energy.

4:40pm **SS-WeA9 Adsorption and Photo-Reactivity of CO on TiO<sub>2</sub>(110)**, *N.G. Petrik, G.A. Kimmel*, Pacific Northwest National Laboratory

We have studied the low-temperature adsorption and reactions of CO on reduced, oxidized, hydroxylated, and electron-irradiated TiO<sub>2</sub>(110) using temperature programmed desorption, photon-stimulated desorption (PSD) and reflection-absorption infrared spectroscopy (RAIRS). Changing the condition of the crystal surface and the adsorbate coverage provides insight into the interactions of adsorbed CO with 5-fold coordinated Ti sites, (Ti<sub>5c</sub>), bridge-bonded oxygen (BBO) sites, and defect sites (oxygen vacancies, bridging hydroxyls and radiation-induced surface defects). Infrared spectra were obtained for light with the plane of incidence parallel and perpendicular to the [001] azimuths of TiO<sub>2</sub>(110). For adsorption on Ti<sub>5c</sub> sites, the RAIRS spectra are consistent with CO adsorbed nearly perpendicular to the surface. For adsorption on BBO sites, the molecules adsorb parallel to the surface and perpendicular to the rows of BBO atoms. The reactivity of various molecular adsorption forms of CO is probed using PSD. In CO photo-oxidation, the PSD yields of CO and CO<sub>2</sub> change dramatically with initial CO coverage, indicating the importance of the relative position and orientation of O<sub>2</sub> and CO molecules for the photochemical reaction.

5:00pm **SS-WeA10 Adsorption of Carbon Dioxide on Rutile TiO<sub>2</sub>(110): A Scanning Tunneling Microscopy Study**, *X. Lin, B.D. Kay, Z.T. Wang, I. Lyubnitsky, Z. Dohnalek*, Pacific Northwest National Laboratory

Understanding the fundamental aspects of CO<sub>2</sub> adsorption and reaction on well-characterized oxide surfaces is critical in providing fundamental understanding on how to control catalytic carbon sequestration and CO<sub>2</sub> conversion to fuels. A model oxide surface, rutile TiO<sub>2</sub>(110) is used to investigate the adsorption properties of CO<sub>2</sub> using scanning tunneling microscopy (STM). STM images obtained before and after *in-situ* doses of CO<sub>2</sub> at 50 K reveal that the CO<sub>2</sub> molecules preferentially bind in bridge-bonded oxygen vacancy (V<sub>O</sub>) defect sites. We show that electron injection from the STM tip can induce CO<sub>2</sub> reduction to CO and V<sub>O</sub> annihilation. After the saturation of V<sub>O</sub>'s, CO<sub>2</sub> molecules preferentially adsorb on five-fold coordinated Ti sites, where they remain mobile even at 50 K. The mobile CO<sub>2</sub> molecules may be corralled by other immobile species such as CO. The contrast observed in the STM images suggests that the distribution of mobile CO<sub>2</sub> molecules tracks the distribution of the subsurface charge as demonstrated by the CO<sub>2</sub> induced standing wave patterns along the Ti rows. The adsorption behavior of CO<sub>2</sub> on hydroxylated TiO<sub>2</sub> surfaces will also be presented.

5:20pm **SS-WeA11 Interaction of ZnO-supported Cu Oxides with CO and CO<sub>2</sub>**, *Z. Zhang, F. Wang, M. Le, M. Ren, J. Flake, P. Sprunger, R. Kurtz*, Louisiana State University

Cu and Cu-oxide nanoclusters supported on ZnO are prototypical catalysts for the electrochemical reduction of CO and CO<sub>2</sub> to methanol. In this report we describe the interaction of CO and CO<sub>2</sub> with Cu oxide nanoclusters on ZnO(10 $\bar{1}$ 0) with a combination of surface sensitive tools including STM for structural information, EELS for electronic and vibrational studies as well as synchrotron-based photoemission for electronic properties. Cu is deposited onto ZnO and oxidized with a combination of O-exposure and annealing procedures to result in two distinct Cu-oxide (CuI and CuII) clusters, which preferentially nucleate and grow at step edges. Photoemission shows a large charge transfer between the oxide cluster and the substrate surface as well as significant band bending. It is believed that the CO<sub>2</sub> adsorption, forming a carbonate species, and consequent reduction, is coupled to the induced defects and electronic perturbation of the Cu<sub>x</sub>/ZnO nanoclusters, absent in the case of Cu/ZnO nanoclusters. In addition to vibrational EELS and TDS to characterize the adsorption of the CO and CO<sub>2</sub> adsorption species, similar results from Au on ZnO(10 $\bar{1}$ 0), which shows a lack of cluster formation growth, will be compared and contrasted.

*This material is based upon work supported as part of the Center for Atomic Level Catalyst Design, an Energy Frontier Research Center funded by the U.S. Department of Energy, Office of Science, Office of Basic Energy Sciences under Award Number DE-SC0001058*

5:40pm **SS-WeA12 Microfabricated Nitrogen-Phosphorus Detectors: Surface Work Function and Thermionic Emission**, *M.T. Brumbach, R.F. Hess, R.J. Simonson, M.W. Moorman, T.J. Boyle*, Sandia National Laboratories

Chemically selective sensors are required for detection of chemical warfare agents with ever increasing demands on the selectivity, sensitivity, lifetime, speed, and reduced power consumption of these devices. Strategies for reducing the scale of these sensors have been explored to produce microfabricated Nitrogen-Phosphorus Detectors (NPDs) to accommodate these many requirements. The device incorporates sol-gel derived alkali metal silicate thin films on low thermal mass silicon substrates for field portable gas chromatography applications. In spite of the long history of NPDs, the details of the chemically-mediated emission related to their selectivity are not well understood. The NPD signal current ultimately depends on the transfer of electrons across the surface potential barrier of the thermionic cathode emitter. Two classes of competing mechanisms have been described in the literature to account for the chemically-selective ionization observed in NPDs: (a) gas-phase ionization models and (b) surface mediated electron emission. The latter mechanism has been the focus of our measurements of the surface work function of candidate emitter materials as a function of composition, structure, temperature, and ambient atmosphere. Specifically, both the local work function variations by scanning probe measurements and effective average work function by measuring total emission will be discussed.

# Thursday Morning, November 3, 2011

## Actinides and Rare Earths Focus Topic

Room: 207 - Session AC+SS-ThM

### The Surface Science of Actinides and Rare Earths

Moderator: R. Schulze, Los Alamos National Laboratory

8:00am AC+SS-ThM1 **The XPS of Heavy Metal Oxides: New Insights Into Chemistry**, P.S. Bagus, University of North Texas, E.S. Iltis, Pacific Northwest National Laboratory, C.J. Nelin, Consultant **INVITED**

The XPS of Rare Earth and Actinide oxides are commonly used to obtain information about the oxidation state of the metal by taking various features of the spectra as fingerprints of the metal oxidation state. However, it is possible to obtain detailed information about the nature of the chemical interactions from these features by using the predictions of rigorous theoretical analyses. One of our important concerns is to make direct assessments of the covalent character of the metal-ligand interaction; i.e., the mixing of O(2p) with partly occupied, or unoccupied, metal levels to form bonding and anti-bonding orbitals. We relate this covalent character to the XPS features. In particular, we investigate the connection between the covalent character of the interaction and the satellite intensity. We also investigate the characterization of the satellites and discuss their assignment as shake satellites, an assignment that is naturally connected with the extent of the covalent mixing of the metal and oxygen levels. Furthermore, we examine how vibrational excitations can lead to broadening of the XPS features and suggest that the observed broadening of XPS peaks may contain, hitherto not utilized, information about the chemical interactions in an oxide. Our focus will be on the XPS of two Rare Earth oxides, CeO<sub>2</sub> and LaAlO<sub>3</sub>, and two actinide oxides, UO<sub>2</sub> and UO<sub>3</sub>; these systems have different electronic character that permit the mechanisms discussed above to be explored and compared. Our theoretical analyses are based on relativistic molecular orbital wavefunctions, WF's, for both initial states, before ionization, and final states, after ionization. The WF's are for materials models that contain explicit cations and anions embedded in a point charge field. With the variationally optimized orbitals for these WF, covalent mixing is naturally taken into account. The cluster WF's include one-body and many-body effects and do not use parameters that are adjusted to make calculated relative energies and intensities fit to experiment.

8:40am AC+SS-ThM3 **New Insights into the Oxidation/Corrosion of Plutonium**, D.L. Pugmire, H.G. Garcia Flores, D.P. Moore, A.L. Broach, Los Alamos National Laboratory, P. Roussel, Atomic Weapons Establishment, UK **INVITED**

An understanding of the oxidation and corrosion processes of plutonium metal at room temperature is important to the safe, effective use and storage of this reactive metal. The oxidation rate for the  $\delta$ -phase stabilized, plutonium/gallium alloy (a commonly employed alloy) can be significantly affected by a number of parameters including the gallium content and the composition of the oxidizing atmosphere (O<sub>2</sub>, O<sub>2</sub>/H<sub>2</sub>O, H<sub>2</sub>O). The nature of plutonium oxidation has typically been thought of as the growth of a dioxide (PuO<sub>2</sub>) overlayer on the metal to a thickness at which the film begins to spallate ( $\mu$ 's). Based on thermodynamic arguments, it has been pointed out that a relatively thin layer of the sesquioxide (Pu<sub>2</sub>O<sub>3</sub>) should exist at the dioxide/metal interface for thick oxide films.

Historically, the oxidation/corrosion of plutonium has been studied by oxygen uptake of samples at elevated temperatures inferred from mass gain measurements. Accuracy of these experimental setups likely limited measurements to oxide films thicker than ~0.05 to 0.1  $\mu$  (50 - 100 nm). This is at the upper-limit of the thicknesses typically observed for plutonium oxide films. Little work has been published for studies of plutonium oxide thin-films (< 50 nm) on metal substrates. Additionally, very little is known about the role that gallium plays during the oxidation of the alloy other than it can significantly slow the rate.

We report here our studies of the initial stages of plutonium oxidation with O<sub>2</sub> in the thin-film regime with x-ray photoelectron spectroscopy (XPS) and Auger electron spectroscopy (AES). The results indicate that not only does a Pu<sub>2</sub>O<sub>3</sub> layer exist in thin plutonium oxide films, but that the sesquioxide exists as a substoichiometric species on a metal substrate, and is probably best described as Pu<sub>2</sub>O<sub>3-y</sub>. It also appears that the oxide thin-film is comprised mainly of the sesquioxide species, with PuO<sub>2</sub> accounting only for a relatively thin portion of the overall oxide film thickness. While the surface sensitive techniques employed here suffer from relatively high limits of detection, we have also been able to qualitatively, and in some cases quantitatively, study the behavior of gallium during the oxidation of the  $\delta$ -plutonium alloy. The gallium content relative to plutonium is observed to decrease within the oxide film during oxidation, with the

displaced gallium moving to the oxide/metal interface to form a thin gallium rich region. These new results will be compared and contrasted with existing literature. Additionally, how these results have altered our understanding of the Pu/O thin-film system and the oxidation/corrosion of plutonium will be discussed.

9:20am AC+SS-ThM5 **The Oxidation of Uranium Dioxide at High Pressures in Pure Oxygen**, J.C. Crowhurst, Z. Dai, J.M. Zaig, K.B. Knight, A.J. Nelson, W.J. Siekhaus, I.D. Hutcheon, Lawrence Livermore National Laboratory

The oxidation of uranium dioxide has received much experimental and theoretical attention over the last several decades in large part because of its relevance to the operation and storage of uranium-based nuclear fuel. The oxidation process is inherently complicated, involving the formation of multiple different phases via distinct mechanisms even at relatively low temperatures. In the range of a few hundred degrees centigrade oxidation is generally assumed to be a two step process[1]: UO<sub>2</sub> → U<sub>3</sub>O<sub>7</sub>/U<sub>4</sub>O<sub>9</sub> → U<sub>3</sub>O<sub>8</sub>. At low pressures the intermediate phases adopt crystal structures that are modifications of the UO<sub>2</sub> fluorite structure and are slightly denser. By contrast, U<sub>3</sub>O<sub>8</sub> forms a considerably less dense orthorhombic structure (by some 23%). The large volume expansion resulting from the oxidation of UO<sub>2</sub> to U<sub>3</sub>O<sub>8</sub> is a potentially serious concern in the event of oxidation of a fuel element, with consequent splitting of protective sheaths and the spalling of powder.

While attention has been focused on the oxidation of UO<sub>2</sub> at elevated temperatures, the associated experiments have all been performed at low partial pressures of oxygen. It is unclear how pressure affects the oxidation process – particularly in the context of the formation of U<sub>3</sub>O<sub>8</sub>, with its large volume change with respect to UO<sub>2</sub>. We have examined the oxidation of a nominal single crystal of UO<sub>2</sub> in pure oxygen at elevated pressures up to approximately 0.9 GPa (9000 atm) and temperatures of up to 450 °C. In-situ Raman scattering measurements were made as a function of temperature in order to monitor the oxidation. Recovered material was examined using electron based techniques including SEM, TEM, and electron diffraction and also using x-ray photoelectron spectroscopy.

Material synthesized under high pressure has a Raman spectrum that is different from both the UO<sub>2</sub> starting material and the common form of U<sub>3</sub>O<sub>8</sub>. Also, compared with common U<sub>3</sub>O<sub>8</sub>, we find that it has fewer crystalline defects and mostly adopts a hexagonal rather than orthorhombic form. Figure 1 of the supplemental document compares Raman spectra of UO<sub>2</sub> in oxygen with synthesized material. Fig. 2 compares electron diffraction obtained from recovered material with U<sub>3</sub>O<sub>8</sub> synthesized at ambient pressure.

Lawrence Livermore National Laboratory is operated by Lawrence Livermore National Security, LLC, for the U.S. Department of Energy, National Nuclear Security Administration under Contract DE-AC52-07NA27344. This work is funded by Laboratory Directed Research and Development (LDRD) Program (10-SI-016) of Lawrence Livermore National Laboratory.

[1] R. J. McEachern and P. Taylor, *JNM*, **254**, 87, (1998).

9:40am AC+SS-ThM6 **Radiation Effects on Hydrogen Reactivity in Narrow Uranium-Uranium and Uranium-LiD (or Air) Gaps using MCNPX Code**, M.A. Schildbach, W.J. Siekhaus, Lawrence Livermore National Laboratory

Preferential uranium hydriding occurs frequently in narrow gaps. There are different hypotheses about its causes, one of which could be radiation-induced chemistry in gaps. Both <sup>238</sup>U and <sup>235</sup>U generate ionizing  $\alpha$ ,  $\beta$ , and  $\gamma$  radiation capable of vibrationally or translationally exciting, ionizing, or dissociating H<sub>2</sub>, all of which increase the reactivity of H<sub>2</sub> with uranium. Dissociation of H<sub>2</sub> is necessary to initiate hydriding, and it has been shown that the sticking coefficient of H atom is about 1200 times higher than H<sub>2</sub>'s[1]. Here we use the MCNPX radiation transport code to calculate the energy dependent electron flux generated from the <sup>234m</sup>Pa  $\beta$  decay and from photoelectrons generated by brems-strahlung. We apply the code to gaps occurring in two <sup>238</sup>U cylindrical pieces welded together and filled on the inside with LiD with a 100 $\mu$ m gap between <sup>238</sup>U and LiD, and having a 100 $\mu$ m gap in <sup>238</sup>U itself, typical for step-joint-welded uranium shells.

The MCNPX Monte Carlo Code - as configured now - tracks the life cycle of electrons throughout the material and calculates the electron flux as a function of energy, putting results into "energy bins" 1 keV wide. We find that at 2 keV ( $\pm 5$  keV, the last energy bin) the calculated electron flux in the U-U gap is approximately 19 times larger than in the U-LiD gap, and fifty two times larger than in the U-air gap on the outside of the cylindrical

shells. Cross-sections for electron-hydrogen collisions peak, however, below 1 keV energy. We establish the upper limit of the effect of electron-hydrogen collisions by extrapolating the MCNPX electron flux results from the last bin to energies as low as 1 eV by fitting a function to the flux between 2 and 20 keV. To calculate the fraction of H<sub>2</sub> vibrationally or translationally excited, ionized, or dissociated per cm<sup>2</sup>/s, we integrate the product of the energy dependent cross sections (listed in reference [2]) and the energy dependent electron flux over the relevant energy range. The fraction of H<sub>2</sub> molecules calculated to be dissociated is small, but significant during long-time exposure. Future work will extend the MCNPX code below 1keV (as is done for biological radiation damage), to avoid energy extrapolation.

This work performed under the auspices of the U.S. Department of Energy by Lawrence Livermore National Laboratory under Contract DE-AC52-07NA27344.

#### References

1. Balooch M, Hamza AV. "Hydrogen and water vapor adsorption on and reaction with uranium." *Journal of Nuclear Materials*, **230**, 3, 259-270, 1996.
2. Yoon JS et al., "Cross sections for electron collisions with hydrogen molecules." *Journal of Physical and Chemical Reference Data*, **37**, 2, 913-931, 2008.

10:40am **AC+SS-ThM9 Study of the Gd<sub>5</sub>Ge<sub>4</sub> (010) Surface**, C. Yuen, G. Miller, P.A. Thiel, Ames Laboratory - US DOE

Certain intermetallics of Gd, Ge, and Si exhibit giant magnetocaloric effects, yet very little is known about their surfaces. We have investigated one such system, Gd<sub>5</sub>Ge<sub>4</sub>, with the goal of elucidating its clean and oxidized surface structure, using STM and XPS. The clean Gd<sub>5</sub>Ge<sub>4</sub> (010) surface exhibits a step-terrace morphology after repetitive sputtering and annealing at 900 K. Step heights are equal to half the bulk unit cell length in the <010> direction, consistent with the existence of an equivalent plane in the middle of the unit cell. Surface compositions of Gd and Ge are close to the bulk composition. However, at higher temperatures—between 900 K and 1200 K—the surface becomes Gd poor by 10 at.%. In STM, at these temperatures, the fine structure on the terraces changes, and a different type of terrace with a different step height emerges. We propose that the preferred surface termination is rich in Gd (which has lower surface energy than Ge), and that this termination is exposed after annealing at 900 K. At higher temperature, we propose that Gd (which has higher vapor pressure than Ge) evaporates preferentially, leading to the changes described above and exposing a Ge-rich surface termination. Finally, we find that Gd oxidizes preferentially.

11:00am **AC+SS-ThM10 Using Spatially Controlled Thin-Films Coatings Around Rare-Earth doped Nanophosphors for High Efficiency Energy Applications**, J.A. Dorman, A. Joshi, G. Kuzmanich, J.H. Choi, J.P. Chang, University of California Los Angeles

The development of rare-earth (RE) doped phosphors allows for the conversion of photons to energies that are more usable for the desired application. Additionally, these RE phosphors have long lifetimes, on the order of ms, which offer potential in many energy conversion and energy transfer devices. Currently, RE phosphors are used in fiber optics amplifiers, broad absorption solar cells and various other lighting applications. Energy transfer mechanisms of the excited RE states, such as defect quenching and sensitizer/emitter interactions, must be understood in order to achieve high efficiency energy conversion and propagation.

In order to increase the efficiency of solar cells, high efficiency phosphors need to synthesize in order to convert photons at the edge of the absorption band into higher energy photons while avoiding undesired quenching effects. In effort to produce these high efficiency phosphors, spatially controlled RE doped thin films are deposited around nanoparticles (NP) to produce a core-shell nanophosphor. Reduction in luminescent quenching can be achieved by increasing the distance between the surface quenching site and active ions through the deposition of a precisely controlled thin film around the NP. Secondly, the luminescent fingerprint can be further controlled through doping of the shell structure by increasing the absorption spectrum or the introduction of emission peaks. Deposition of a thin film around an Y<sub>2</sub>O<sub>3</sub>:Er<sup>3+</sup> core NP is achieved via atomic layer deposition or sol-gel synthesis to compare the effect of a spatially controlled vs. a random dopant distribution. Primarily, this work focuses on the emission of visible photons through upconversion, making them ideal components in broad absorption solar cells. By spatially controlling the position and concentration of the RE ions within the nanostructure, increased luminescence is observed due to energy transfer between the dopant ions within a critical interatomic distance. Passivation of surface sites with increasing film thickness was shown to increase luminescent lifetimes up to 53%, with a critical shell thickness of 8 nm, while lowering the theoretical lifetimes extracted from Judd-Ofelt parameters. The effect of the spatially

controlled Yb ions was probed through the extraction of the upconversion photon requirement, showing a statistical decrease in photons from 2.16 to 1.43, or ~30 %. Finally, the effective energy transfer distance and energy transfer coefficients were studied as a spacer layer is added to the system, showing energy transfer up to ~3 nm, confirming the Förster-Dexter theory.

11:20am **AC+SS-ThM11 Growth and Characterization of Scandia Stabilized Zirconia and Samaria Doped Ceria Multi-Layer Thin Films**, S. Thevuthasan, Pacific Northwest National Laboratory, M.I. Nandasiri, Western Michigan University, T. Varga, V. Shuthanandan, S.P. Sanghavi, S.V.N.T. Kuchibhatla, Pacific Northwest National Laboratory, A. Kayani, Western Michigan University

Recent studies showed a colossal enhancement in the ionic conductivity of multi-layer oxygen-ion conducting thin films compared to most commonly used solid oxide fuel cell (SOFC) electrolytes. It has been observed that, the oxygen ionic conductivity of nano-scale hetero-structures increases with the increase in number of layers. However, some of these findings were questioned due to the inability to distinguish electronic and ionic conductivity. Thus, here we investigated the scandia stabilized zirconia and samaria doped ceria (SDC/ScSZ) multi-layer system to understand the oxygen-ion conductance in multi-layer hetero-structures.

In this study, the growth of SDC and ScSZ multi-layer thin films was carried out using the optimized growth conditions, dopant concentrations and film properties established for single-layer SDC and ScSZ epitaxial thin films. The epitaxial SDC and ScSZ multi-layer thin films were grown on Al<sub>2</sub>O<sub>3</sub>(0001) substrates by oxygen plasma-assisted molecular beam epitaxy (OPA-MBE) at 650°C. The number of layers in the multi-layer hetero-structures was varied from 2 to 20 by keeping the total film thickness constant at 140 nm. Following the growth, thin films were characterized by various in-situ and ex-situ characterization techniques including reflection high energy electron diffraction (RHEED), x-ray diffraction (XRD), Rutherford backscattering spectrometry (RBS), and x-ray photoelectron spectroscopy (XPS). The initial streaky RHEED pattern indicates the epitaxial growth of SDC/ScSZ multi-layer thin films. Furthermore, RHEED patterns indicate the transition of the initial smooth surface to a rough surface with the increase in number of layers. The individual layer thickness was found to be approximately 7 nm for the twenty-layer film as confirmed by x-ray reflectivity data. RBS was also used to find the composition and thickness of the films. HRXRD patterns of ScSZ/SDC thin films exhibit only CeO<sub>2</sub>(111) and ZrO<sub>2</sub>(111) reflections, indicating the growth of epitaxial SDC(111) and ScSZ(111) multi-layers. XPS depth profile confirmed the uniform dopant concentration in both SDC and ScSZ layers, which was found to be 7 and 6 atom % for Sc and Sm, respectively. In the near future, the ionic conductivity of SDC and ScSZ multi-layer thin films will be measured by four probe conductivity method.

**Graphene and Related Materials Focus Topic**  
**Room: 208 - Session GR+NS+PS+SS-ThM**

**Graphene: Surface Chemistry, Functionalization, Plasma Processing and Sensor Applications**

**Moderator: G.G. Jernigan, U.S. Naval Research Laboratory**

8:00am **GR+NS+PS+SS-ThM1 Tailoring Graphene's Properties through Chemistry**, J.T. Robinson, Naval Research Laboratory **INVITED**

Graphene's unique electron transport properties have motivated intensive research and development to mold it into the electronic material of the future. However, graphene can be much more than an electrical switch. Its high structural integrity and chemical flexibility enable extensive control of its optical, mechanical, and electronic properties. The most scalable and inexpensive route to modify these properties is chemical functionalization. Consequently, chemically modified graphenes (CMGs) have emerged as a system of materials whose many attractive properties complement and extend those of unmodified graphene.

In this talk I will describe efforts at NRL to synthesize and characterize new CMGs as well as first steps towards applications such as sensors and nanomechanical resonators. To begin, I will discuss the interaction of small molecules (CCl<sub>4</sub>, CS<sub>2</sub>, H<sub>2</sub>O and acetone) with single-layer graphene under steady-state conditions using infrared multiple-internal-reflection. Adsorption-induced changes in the IR spectra suggest the formation of in-plane strain, where we observe important differences arising between species that form liquid-like layers under steady-state conditions and those that do not. Second, I will discuss graphene oxide, a well known derivative of graphene that has a rich ensemble of oxygen-based functional groups and related defects. These defects are readily tunable through chemical or thermal treatments and facilitate the formation of vapor and bio-sensors

with parts-per-billion and nanomolar sensitivities, respectively. Third, I will discuss the stoichiometric addition of fluorine atoms to graphene and describe their resulting properties. Experiments indicate fluorinated graphene derivatives become highly resistive and optically transparent, while DFT calculations show band gaps open depending on the fluorine coverage and ordering. Finally, through combining these two material systems, I will discuss the fabrication and performance of CMG-based nanomechanical resonators. Through chemical modification, the frequency of CMG-based resonators is tunable over 500% and their quality factors can exceed 20,000 at room temperature.

**8:40am GR+NS+PS+SS-ThM3 Water Splits Epitaxial Graphene on Ru(0001) from Domain Boundaries, X. Feng, S. Maier, M. Salmeron,** Lawrence Berkeley National Laboratory

Epitaxial growth of graphene on metal substrates has recently been demonstrated as a rational synthesis route for producing macroscopic graphene domains and may hold the key to realizing the potential of large-scale applications. However, the epitaxial graphene is generally polycrystalline, with domain boundaries that may severely affect its structure and properties. Here we report that water adsorption splits epitaxial graphene on Ru(0001) and results in nanoscale graphene flakes at temperatures as low as 90K. Scanning tunneling microscopy studies indicated that the splitting starts primarily from domain boundaries followed by water intercalation underneath graphene. The mechanism proposed is that Ru-induced water dissociation provides hydroxyl species that break the graphene starting at the dangling and stretched bonds at the boundaries.

**9:00am GR+NS+PS+SS-ThM4 Novel Strategies for the Chemical Functionalization of Graphene: Towards Graphene/Molecular Nanosheet Heterostructures, A. Turchanin, C.T. Nottbohm, Z. Zheng, M. Schnietz, A. Beyer,** University of Bielefeld, Germany, *M. Heilemann, M. Sauer,* Julius-Maximilians-University Würzburg, Germany, *A. Götzhäuser,* University of Bielefeld, Germany

Chemical functionalization of graphene is essential for implementations of the 2D carbon sheets in various functional devices (e.g. chemical and biochemical sensors, nanoelectromechanical components, etc.) and for tuning their electrical properties. However, the functionalization is difficult to achieve due to the chemical inertness of graphene sheets with high structural quality. On the other hand, ultrathin (~1 nm) molecular nanosheets made from self-assembled monolayers (SAMs) possess well-defined chemical groups intrinsically. Moreover, due to the directionality of the constituting molecules both faces of the free-standing nanosheets -*Janus nanomembranes*- can be independently and specifically functionalized. Simple mechanical stacking of the nanosheets allows fabricating ultrathin layered structures with tunable physical and chemical properties. Upon annealing these stacks are converted into graphene sheets with adjusted thickness. The engineering of graphene/nanosheet heterostructures opens up novel routes towards chemically functionalized graphene sheets for functional applications. A potential of this approach will be discussed.

Z. Zheng, C.T. Nottbohm, A. Turchanin, H. Muzik, A. Beyer, M. Heilemann, M. Sauer, A. Götzhäuser, "Janus nanomembranes: A generic platform for chemistry in two dimensions", *Angew. Chem. Int. Ed.* 49 (2010) 8493-8497

C.T. Nottbohm, A. Turchanin, A. Beyer, R. Stosch, A. Götzhäuser, "Mechanically stacked 1 nm thick carbon nanosheets: 2D layered materials with tunable optical, chemical, structural and electrical properties", *Small* 7 (2011) 874-883

A. Turchanin, D. Weber, M. Bünenfeld, C. Kisielowski, M. Fistul, K. Efetov, R. Stosch, T. Weimann, J. Mayer, A. Götzhäuser, "Conversion of self-assembled monolayers into nanocrystalline graphene: structure and electric transport", *ACS Nano* 5 (2011) DOI: 10.1021/nn200297n

**9:20am GR+NS+PS+SS-ThM5 Biosensors Based on Chemically Modified Graphene, R. Sîine, J.T. Robinson, P.E. Sheehan, C.R. Tamanaha,** U.S. Naval Research Laboratory

The sensitive and specific detection of biomolecules without using a label is a long-standing goal of the biosensors community. Several promising advances of the past several years formed biological field effect transistors (bioFETs) that have as the gate nanoscale materials such as nanowires and carbon nanotubes. The nanoscale dimensions of these materials allow the small charges associated with biomolecules to significantly change conduction through the gate. These conduction changes can be correlated with solution concentration to give precise readouts. While bioFETs are a promising way forward, there are many processing difficulties associated with these 1-D materials that inhibit large scale, reproducible fabrication of devices. Here, we will discuss our efforts to develop biosensors based on 2-D chemically modified graphene. These devices impart the sensitivity gains seen from other nanoscale materials, but offer a configuration that is

amenable to processing techniques that are common in the semiconductor industry. We will focus primarily on chemically modifying graphene for attachment of biomolecular probes. Devices utilizing both graphene and graphene oxide will be covered, and surface spectroscopic studies of the material modification will be discussed. Successful results for the detection of specific DNA hybridization will also be presented, with detection limits that compare favorably with the best results reported from nanowire bioFETs.

Acknowledgements: R.S. is an employee of Nova Research Inc., Alexandria, VA, USA. This project received support from the Defense Threat Reduction Agency-Joint Science and Technology Office for Chemical and Biological Defense.

**9:40am GR+NS+PS+SS-ThM6 Controllable Defect Healing and N-doping of Graphene by CO and NO Molecules, B. Wang,** Vanderbilt University, *S.T. Pantelides,* Vanderbilt University and ORNL

Point defects alter strongly the physical and chemical properties of graphene, e.g. they degrade electrical transport and enhance chemical reactivity. Defects could also be used to achieve graphene functionalization, e.g. N atoms, as n-type dopant, can be introduced to obtain n-type graphene. Thus, controllable defect healing and N-doping in graphene would be very valuable for potential device applications. Here we report first-principles molecular dynamic simulations that suggest a procedure for defect healing and N-doping with fast dynamics and low thermal budget. Vacancies in graphene can be healed by sequential exposure to CO and NO molecules. A CO molecule gets adsorbed at a vacancy site and a NO molecule subsequently removes the extra O by forming NO<sub>2</sub>, which desorbs quickly resulting in a defect-free graphene sheet. Controllable N-doping can be achieved by sequential vacancy creation (e.g. by electron or ion beam) and subsequent exposure to NO molecules at room temperature. NO molecules are trapped at vacancies and other NO molecules remove the extra O atoms simultaneously, leaving N atoms incorporated in graphene. Both reactions (healing and doping) are exothermic. We suggest that a combination of CO and NO molecules can potentially provide simultaneous healing and doping. Adjusting the ratio could fine-tune the N-doping level. The proposed strategy introduces no extra defects and is promising for graphene-based electronic materials in radiation environments. Finally, we propose that NH<sub>3</sub>, which is normally used in experiments to introduce N atoms, may not be a good choice for N-doping since the dissociated H atoms can be trapped at vacancies and act as impurities that increase the resistivity of graphene.

This work was supported by DTRA Grant No. HDTRA1-10-1-0016 and the William A. and Nancy F. McMinn Endowment at Vanderbilt University. The calculations were performed at ORNL's Center for Computational Sciences.

**10:40am GR+NS+PS+SS-ThM9 Aptamer Modified Graphene Bio Sensor, K. Maehashi, Y. Ohno, K. Matsumoto,** Osaka University, Japan

Since graphene has high mobility and a large surface area, it is suitable for the application of the high sensitive sensor. In the present paper, we have first succeeded in the selective detection of the bio molecule such as IgE using the aptamer modified graphene FET.

The graphene was formed using the conventional mechanical exfoliation method on the SiO<sub>2</sub>/Si substrate. The source and drain electrode were formed by the electron beam lithography and Ti/Au evaporation. The silicon rubber pool was formed on the fabricated graphene FET, and phosphoric buffer solution was poured into the silicon rubber pool. The Ag/AgCl reference electrode was introduced into the phosphoric buffer solution, which works as a top gate electrode for the graphene FET.

As a first step of the biosensor, three bio molecule such as Immunoglobulin E(IgE), Streptavidin(SA), and Bovine serum albumin(BSA) were introduced into the phosphoric buffer solution of pH of 6.8, and the change of the drain current of the graphene FET was detected. In this case, the IgE and SA shows the decrease of the drain current, while the BSA the increase of the drain current. Because, in the phosphoric buffer solution of pH of 6.8, IgE and SA are positively charged, while BSA negatively charged. Therefore, the hole current of the graphene FET change the drain current following the charge of the bio molecule. As a result, bare graphene FET can detect the bio molecule following the charge of the molecule, but it does not have the selectivity

As a second step, in order to get the selective sensing of the bio molecule, the surface of the graphene was modified by the IgE aptamer, which was connected to graphene using the linker(1-pyrenebutanoic acid succinimidyl ester). IgE aptamer was known to selectively couple to IgE. When the BSA and SA were introduced into the phosphoric buffer solution on the aptamer modified graphene FET, there occurred no change in the drain current, while the IgE was introduced in the solution, the drastic decrease of the drain current was observed. This means the BSA and SA do not couple to

IgE aptamer, and only IgE couple to the IgE aptamer on the graphene FET. Therefore, the selective sensing of the IgE was successfully carried out.

We have first succeeded in the selective sensing of IgE using the modified graphene FET.

11:00am **GR+NS+PS+SS-ThM10 A Molecular Dynamics Study of Chemical Modification of Graphene Oxide Sheets**, *T. Liang, B. Devine, S.R. Phillpot, S.B. Sinnott*, University of Florida

Graphene, the single-layered graphite, has attracted tremendous attention owing to its fascinating physical properties. One of the main obstacles in this field is to find an efficient and consistent approach to produce graphene sheets in large quantities. In addition to the mechanical exfoliation method, many chemical approaches have been developed to synthesize graphene on a large scale. The key intermediate product in these chemical approaches is the graphene oxide sheets, which are often heavily oxygenated with hydroxyl or epoxide functional groups on the surface and carbonyl or carboxyl groups at the edge. However the energetic and kinetics associated with graphene oxide sheets have not been elucidated in detail due to the inherent chemical complexity of the system. Here, a new dynamic charge empirical potential is presented that is used in classical molecular dynamics simulations to elucidate the dynamics of graphene oxidation and the resulting influence on their mechanical and structural properties. In addition, the oxygenating and hydrogenating processes of defective graphene sheets at room temperature in addition to elevated temperatures are presented. The findings are compared to the results of first principles density functional theory findings and to experimental data.

11:20am **GR+NS+PS+SS-ThM11 Enhancing and Controlling the Chemical Reactivity of Epitaxial Graphene via Growth Induced Strain**, *J.E. Johns*, Northwestern University, *M.Z. Hossain*, Gunma University, Japan, *M.C. Hersam*, Northwestern University

The high electrical and thermal conductivity of graphene, as well as its two dimensional nature, has led to its rapid incorporation into any practical applications including high frequency analog transistors and transparent conductors. However, many other potential applications, such as excitonic switches, pseudospin devices, or digital logic circuits, require covalent chemical modification of graphene. Due to the chemical inertness of its pi bonded network, previous methods for covalently modifying graphene have required extreme, irreversible conditions including acidic treatments, high energy radical polymerization, and ion beam implantation. Here we present an alternative method for increasing the chemical reactivity of graphene by systematically altering the compressive strain of epitaxial graphene (EG) on SiC(0001). Depending on its annealing history, EG has been shown to have a compressive strain of 0% to 1% due to a mismatch of thermal expansion coefficients with the underlying buffer layer and silicon carbide substrate. Using differing thermal treatments, we show that the amount of strain in EG can be tailored, as verified by characteristic peak shifts of the 2D Raman band. The resulting chemical reactivity of the strained EG is studied at the atomic-scale using ultra-high vacuum scanning tunneling microscopy following reversible gas phase reactions of EG with oxygen and fluorine. These results suggest a new method for controlling the electronic properties of graphene, and provide fundamental insight into the nature of chemical bonding on EG.

11:40am **GR+NS+PS+SS-ThM12 Plasma-based Functionalization of Graphene with Primary Amines for Biomaterials Applications**, *S.G. Walton, M. Baraket, S.C. Hernandez, R. Stine, W.K. Lee, C.R. Tamanaha, P.E. Sheehan, J.T. Robinson, C.E. Junkermeier, T.L. Reinecke*, Naval Research Laboratory (NRL)

Graphene, a sp<sup>2</sup>-structured monolayer of carbon atoms, has attracted much interest for its fundamental science and its potential in many device applications. By tailoring its surface chemistry, material properties can be regulated and thus broaden the number of potential applications. In this work, we demonstrate that by chemically functionalizing graphene the electrical properties and its interaction with adsorbates may be controlled. Electron beam generated plasmas produced in ammonia-containing gas, is used to controllably introduce nitrogen and primary amines. A study of the chemical, electrical and structural properties of the chemically-modified graphene at different functional group concentrations is discussed. In addition, the use of amine-functionalized graphene as a bio-sensing platform for DNA detection using a field-effect-transistor-based sensor is demonstrated. This work is supported by the Office of the Naval Research.

**Surface Science Division**  
**Room: 107 - Session SS-ThM**

### Oxide Surface Structure & Reactivity

**Moderator:** G.A. Kimmel, Pacific Northwest National Laboratory

8:00am **SS-ThM1 Bond Activation of Alkanes on CaO(100)**, *A. Chakradhar, U. Burghaus*, North Dakota State University

The molecular and dissociative adsorption kinetics, respectively, of ethane, butane, pentane, and hexane are studied on CaO(100) using thermal desorption spectroscopy (TDS) and Auger electron spectroscopy (AES). After adsorption/desorption cycles, AES scans show no carbon residuals on the surface. Molecular adsorption as well as bond breaking is observed for all alkanes studied, except for ethane. Molecular desorption of these alkanes is characterized by two TDS peaks while recording the parent mass. These two features are assigned to different adsorption sites/configurations of the alkanes. In addition, the binding energies of the bound alkanes, based on their desorption temperatures, are calculated by using Redhead equation. The bond activation is evident from desorption of hydrogen and mostly methane and ethylene fragments in multi-mass TDS experiments. Bond activation of hydrocarbons is pertinent for the petroleum industry, providing transportation fuels and other petrochemical products.

8:20am **SS-ThM2 Reaction Chemistry of Methyl and Methylene Species on Cr<sub>2</sub>O<sub>3</sub>(0001)**, *Y. Dong, D.F. Cox*, Virginia Tech

The reactions of methyl (CH<sub>3</sub>) and methylene (CH<sub>2</sub>) surface species formed from the dissociation of halogenated methanes have been studied with temperature programmed desorption over Cr<sub>2</sub>O<sub>3</sub>(0001). Methyl fragments undergo a rate-limiting dehydrogenation to methylene and produce methane (CH<sub>4</sub>) and ethylene (CH<sub>2</sub>=CH<sub>2</sub>) as the primary products. Comparison to earlier results for the Cr<sub>2</sub>O<sub>3</sub>(1012) surface show that methyl dehydrogenation is a structure-insensitive reaction, with the barrier to dehydrogenation being insensitive to the surface cation coordination number and/or local Cr-O site pair geometry. The ethylene formed from the dehydrogenation of CH<sub>3</sub> is associated with the surface diffusion of methylene species and subsequent coupling (C-C bond formation) reactions.

Separate studies of the reaction of methylene show that surface diffusion and coupling to ethylene can occur at lower temperatures than required for CH<sub>3</sub> dehydrogenation. The diffusion-limited coupling of CH<sub>2</sub> appears to be a structure-sensitive reaction, with the barrier to surface diffusion about 25 kJ/mol higher on Cr<sub>2</sub>O<sub>3</sub>(0001) than the (1012) surface.

8:40am **SS-ThM3 Organometallics as Probes of Functional Group Distribution on Oxide Surfaces**, *S.L. Scott*, University of California, Santa Barbara

**INVITED**

The reactivity of the hydroxyl-terminated surface of silica is important for constructing tailored interfaces in many applications, including catalysis, separations, and microelectronics. Amorphous silicas are particularly interesting because of their high surface areas. The hydroxyl content of their surfaces can be reduced thermally, but it decreases slowly because the hydroxyls have very low mobility. Their mutual condensation requires proximity, and, frequently, the formation of strained siloxane rings. Since these silicas have no long-range order, it is often postulated that the hydroxyl groups are distributed randomly, and that when the nominal hydroxyl density is low (e.g., after thermal treatment at temperatures exceeding 500 °C), these hydroxyls can be considered essentially isolated. Curiously, the Ga K-edge EXAFS shows that the reaction of Ga(CH<sub>3</sub>)<sub>3</sub> with such a silica pretreated at 800 °C generates only digallium sites, requiring that the hydroxyls be organized pair-wise, likely as vicinal silanols linked by a single siloxane bond. The origin of the preferred vicinal disposition may be hydrolysis of a strained siloxane bond. Where isolated hydroxyls do exist, they appear to be located on reactive 2-rings whose reactivity resembles that of a masked silanol. Consequently, it is unwise to assume that site isolation results from grafting onto these silicas, although the vicinal disposition of silanols provides an opportunity to create tailored bifunctional surfaces.

9:20am **SS-ThM5 Are MgO Thin Films More Reactive Than Bulk MgO Surfaces?**, *G. Cabailh, R. Lazzari, H. Cruguel, J. Jupille*, UPMC and CNRS, France, *L. Savio*, IMEM-CNR, France, *M. Smerieri, A. Orzelli, L. Vattuone, M. Rocca*, Università di Genova, Italy and IMEM-CNR, France

The ubiquity of the interface between water and oxide materials has prompted a tremendous activity to determine the adsorption mechanisms at the microscopic scale on crystalline surfaces of simple oxides. Among these, magnesium oxide MgO offers the advantage of having various morphologies of good crystalline quality, involving cleaved crystal

surfaces, high surface area samples and supported films, all of these dominated by the low index (100) orientation. On bulk MgO, the fivefold coordinated atoms of the basal (100) surface do not dissociate isolated H<sub>2</sub>O molecules. Conversely, H<sub>2</sub>O is easily dissociated at low-coordinated sites such as steps and kinks. A puzzling case is the adsorption of H<sub>2</sub>O on metal-supported MgO films in the submonolayer range of which coverage by OH groups has been estimated to 60 to 70% of a monolayer [1,2]. Similar OH coverages were obtained by aging freshly prepared films in the residual atmosphere of the vacuum chamber [1], although the observation was contradicted by the finding of a more modest effect that cast doubt on OH being the cause of aging [2]. The extraordinary uptake of OH groups was attributed to the peculiarities of the electronic properties of the thin supported MgO films [3]. However, density functional theory hardly supports this view. Little changes in both the electronic structure and the capacity to dissociate H<sub>2</sub>O are predicted for monolayer-thick MgO(100) islands that, at variance with experiment, are only expected to dissociate H<sub>2</sub>O molecules along their borders [4].

In an attempt to solve the discrepancies between experiments and between experiment and simulation, MgO films of different stoichiometry were grown on Ag(100) by reactive deposition of Mg in an O<sub>2</sub> partial pressure, prior to being exposed to H<sub>2</sub>O vapor and/or aged in vacuum [5]. Films were observed by scanning tunneling microscopy (STM) and water uptake was analyzed by x-ray photoemission spectroscopy (XPS). The stoichiometry and, consequently, the chemical activity towards hydroxylation of the MgO(100) films, was shown to strongly depend on the O<sub>2</sub> pressure during the film growth. Oxygen-deficient films undergo dramatic oxygen uptake either by exposure to H<sub>2</sub>O or by aging in vacuum. Conversely, on stoichiometric MgO islands, XPS analysis and STM images are consistent with the prediction that H<sub>2</sub>O only dissociates at the island edges.

- [1] S. Altieri et al., *Phys. Rev. B*, 76 (2007) 205413.
- [2] L. Savio et al., *J. Phys. Chem. B* 108 (2004) 7771.
- [3] S. Altieri et al., *Thin Solid Films* 400 (2001) 9.
- [4] A. M. Ferrari et al., *Phys. Chem. Chem. Phys.* 9 (2007) 2350.
- [5] G. Cabailh et al., *J. Phys. Chem. C*, in press (2011).

9:40am **SS-ThM6 The Adsorption of Silver on Fe<sub>3</sub>O<sub>4</sub>(111) Studied by Adsorption Microcalorimetry, LEIS, and AES, J.C. Sharp, Y.X. Yao, C.T. Campbell, University of Washington**

Noble metals supported on oxide surfaces are of interest due to their catalytic activity and their sintering resistance is a subject of concern in terms of their long-term stability under reaction conditions. The heat of adsorption of silver on Fe<sub>3</sub>O<sub>4</sub>(111) grown on Pt(111) was measured using adsorption microcalorimetry, and its growth morphology was measured with low-energy ion scattering spectroscopy (LEIS) and Auger electron spectroscopy (AES). The initial sticking was 0.96 rising to 0.99 after 1 monolayer of Ag deposited. The LEIS and AES data were fitted to a hemispherical cap model for the Ag nanoparticles, which were found to grow with a particle density of  $4 \times 10^{12}$  particles per cm<sup>2</sup>. The initial heat of adsorption was found to be 220 kJ/mol, rising to 285 kJ/mol after 1 monolayer of deposited Ag. From these data, we extracted the energy of metal atoms versus the Ag particle size to which they attach on Fe<sub>3</sub>O<sub>4</sub>(111), and compare it to results on other single crystalline oxide surfaces.

10:40am **SS-ThM9 Properties of TiO<sub>2</sub> Nanoparticle Arrays Functionalized with Pt Photodeposition, Y. Liu, J. Taing, M. Cheng, University of California, Irvine, H. Bluhm, Lawrence Berkeley National Laboratory, J.C. Hemminger, University of California, Irvine**

Titanium(IV) oxide (TiO<sub>2</sub>), acting as a stable support for photocatalysts and sensitizers, has applications in catalysis and energy science. Metal nanoparticles supported on TiO<sub>2</sub> have been shown to have unusual reactivity. The deposition of metal nanoparticles can alter the electronic properties of the TiO<sub>2</sub> nanoparticles. To understand the influence of metal deposition, we photodeposit platinum (Pt) onto ordered linear arrays of TiO<sub>2</sub> nanoparticles grown at the step edges of highly oriented pyrolytic graphite. X-ray photoelectron and absorption spectroscopies were used to explore the electronic structure of the TiO<sub>2</sub> nanoparticle arrays with and without photodeposited Pt. The titanium L-edge spectra, supported by multiplet calculations, provide crucial information about crystal field effects, atomic multiplet interactions, and the phase of the TiO<sub>2</sub> particles. Valence photoemission results and band structure calculations using density-functional theory indicate a narrowing of the TiO<sub>2</sub> band gap when Pt is loaded onto the TiO<sub>2</sub> nanoparticle surface. This suggests that Pt photodeposition onto linear TiO<sub>2</sub> nanoparticle arrays may enhance the solar absorption of TiO<sub>2</sub> due to narrowing of the TiO<sub>2</sub> bandgap.

11:00am **SS-ThM10 Atomic-scale Structure of the Polar Spinel MgAl<sub>2</sub>O<sub>4</sub>(100) Surface, M.K. Rasmussen, K. Meinander, Aarhus U., Denmark, A.S. Foster, Tampere Univ. of Tech., Finland, B. Hinemann, Haldor Topsøe A/S, Denmark, F.F. Canova, Tampere Univ. of Tech., Finland, S. Helveg, Haldor Topsøe A/S, Denmark, N.M. Martin, J. Knudsen, Lund U., Sweden, A. Vlad, Max-Planck-Institut für Metallforschung, Germany, E. Lundgren, Lund U., Sweden, A. Sterle, Max-Planck-Institut für Metallforschung, Germany, F. Besenbacher, J.V. Lauritsen, Aarhus U., Denmark**

Metal oxide spinels are an important class of materials in both ceramics technology and materials science. Although the prototypical ternary metal oxide spinel, magnesium aluminate spinel (MgAl<sub>2</sub>O<sub>4</sub>), is widely used, for instance, as a membrane in solid oxide fuel cells and in heterogeneous catalysis, either as a support for active metal nanoclusters or as a catalyst in its own right [1], many of the intricate details of its surface structure still remain unresolved. The atomic-scale surface characterization of similar spinel-type metal oxides has generally been challenging, due to the insulating nature of these materials, a property which limits the use of many standard surface science techniques.

Using a combination of non-contact atomic force microscopy (NC-AFM) and surface X-ray diffraction (SXRD), coupled together with density functional theory (DFT) structure calculations and NC-AFM simulations based on DFT, we have unraveled the complex structure of the polar MgAl<sub>2</sub>O<sub>4</sub> (100) surface. Surprisingly, we find that the surface is terminated by an Al and O-rich structure, with a thermodynamically favored amount of Al atoms interchanged with Mg. These cation antisites, which are low-density defects in the bulk, may be a key element in determining the substrate properties of MgAl<sub>2</sub>O<sub>4</sub>, among others its basicity and the likelihood for formation of OH-groups, which are believed to be anchoring sites for metallic nanoclusters, such as Ni, commonly used in steam reforming catalysts.

- [1] J. R. Rostrup-Nielsen, J. Sehested, and J. K. Nørskov, *Adv. Catal.* 47, 65 (2002).

11:20am **SS-ThM11 Growth and Characterization of Cu/ZnO on Au(111) as a Model Catalyst System, X. Deng, J. Lee, C. Matranga, National Energy Technology Laboratory**

Model Cu/ZnO catalysts have been grown on a single crystal Au(111) substrate and characterized with X-ray photoelectron spectroscopy (XPS) and scanning tunneling microscopy (STM). Growth of ZnO on Au(111) is achieved by oxidation of Zn that has been deposited onto the substrate or by reactive evaporation of Zn in the presence of an oxidizer. XPS confirms that Zn has been oxidized and STM reveals that ZnO forms a uniform overlayer on Au(111) with an apparent height of ~6 Å. STM also reveals that the ZnO overlayer on Au(111) forms an ordered hexagonal Moiré pattern with a periodicity of 25 Å, possibly due to the lattice mismatch between the oxide and growth substrate. The atomic structure of the ZnO overlayer is also resolved with STM, showing a hexagonal unit cell with a lattice constant of 3.2 Å. Cu is then deposited onto the ZnO overlayer by evaporation, and STM is used to characterize the structure and morphology of the Cu/ZnO system. The model Cu/ZnO on Au(111) system will be compared to "real world" Cu/ZnO catalysts used for CO<sub>2</sub> hydrogenation and low temperature water gas shift reactions.

11:40am **SS-ThM12 Iron Oxide Growth on YSZ(001) and YSZ(111), I. Ermanoski, G.L. Kellogg, Sandia National Laboratories**

We have used low energy electron microscopy (LEEM) to study in real time the growth of iron oxides on the fully oxidized and partially reduced (001) and (111) surfaces of yttria-stabilized zirconia (YSZ). The FeO<sub>x</sub>-YSZ system is currently used as a working material for solar thermochemical splitting of H<sub>2</sub>O and CO<sub>2</sub> [1], but little fundamental information is available concerning the structure and composition of the mixed oxides and their surfaces. Upon Fe deposition in ~10<sup>-6</sup> Torr of O<sub>2</sub> background pressure, iron oxides grow on the surface. Low energy electron diffraction (LEED) patterns, dark field LEEM imaging, and LEEM I-V measurements show that the composition and morphology of the surface oxide is very diverse, and depends on the substrate stoichiometry, crystallographic orientation, as well as on the deposition conditions and film thickness.

This work was supported by the LDRD program at Sandia National Laboratories, in the form of a Grand Challenge project entitled Reimagining Liquid Transportation Fuels: Sunshine to Petrol. Sandia is a multi-program laboratory operated by Sandia Corporation, a wholly owned subsidiary of Lockheed Martin Company, for the U.S. Department of Energy's NNSA under contract DE-AC0494AL85000.

- [1] Diver, R.B., Miller, J.E., Allendorf, M.D., Siegel, N.P., Hogan, R.E., "Solar thermochemical water-splitting ferrite-cycle heat engines", *Journal of Solar Energy Engineering*, 130 (2008) 041001

## Tribology Focus Topic

Room: 111 - Session TR+AS+SS-ThM

### Atomic-scale Characterization of Tribological Interfaces

Moderator: S. Perry, University of Florida

8:00am **TR+AS+SS-ThM1 Electrochemical Control of Atomic Friction**, *F. Hausen*, INM - Leibniz Institute for New Materials, Germany, *A. Labuda*, McGill University, Canada, *N.N. Gosvami*, *R. Bennewitz*, INM - Leibniz Institute for New Materials, Germany

Electrochemical methods allow for fast and reversible modification of metal surfaces through deposition and dissolution of metal films, adsorption and desorption of anions, as well as oxidation and reduction. The surface composition and structure undergo dramatic changes in these processes, which should cause significant changes in the friction on the surface.

We present friction force measurements at the nanometer scale on Au(111) and Au(100) single crystal electrodes performed by means of friction force microscopy in various electrolytes. The resolution of atomic stick-slip events in an electrochemical cell is improved by the development of a dedicated instrument [1]. A significant difference in friction is found for the bare electrodes compared to the modified surfaces. Friction is extremely weak and exhibits almost no load dependence on clean Au(111) surfaces. Upon electrochemical oxidation of the surface, significant friction with linear load dependence is observed. This process is reversible and allows switching repeatedly between high and low friction [2]. In the regime of anion adsorption our results indicate a frictional response with threshold behaviour. The threshold depends on both applied normal load and the electrochemical potential [3].

After deposition of copper on gold by underpotential deposition in perchloric acid, the atomic stick-slip changes into a periodicity which indicates frictional response of CuCl with a linear load dependence. In chloride-free sulphuric acid a different behaviour is found, indicating competing effects of ion adsorption on friction forces at small scales.

[1] A. Labuda et al., Rev. Sci. Instruments 81, 083701 (2010)

[2] A. Labuda et al., Langmuir (2011, available online)

[3] F. Hausen et al., Electrochimica Acta (2011, in print)

8:20am **TR+AS+SS-ThM2 Surface Alterations Effects on Ice Adhesion Strength**, *C. Ellis-Terrell*, *M. Miller*, Southwest Research Institute, *M. Zou*, University of Arkansas at Fayetteville, *R. Wei*, Southwest Research Institute, *S. Beckford*, University of Arkansas at Fayetteville, *G. Hatton*, Shell Global Solutions, Inc.

Ice adhesion is a serious problem in areas such as the oil, gas, and automotive industry, telecommunications and power line transmission. There is a significant amount of research directed towards designing a coating to reduce ice accumulation. This study focuses on measuring the effects of surface roughness and surface energy on ice adhesion strength. Surface texturing ranged from high to low surface roughness. A sandblasting technique was applied to the aluminum surface creating a high surface roughness. Surface energy changes were created by depositing a silicon doped hydrocarbon film, using plasma enhanced vapor deposition. A custom built apparatus was employed to specifically measure the adhesion force of an ice droplet. The results illustrate that the smoother as-received surfaces have lower ice adhesion strength than the rougher sandblasted surfaces.

8:40am **TR+AS+SS-ThM3 Atomistic Simulations of Nanoindentation and Nanoscratching of SiO<sub>2</sub>/Si and HfO<sub>2</sub>/Si Systems using COMB Potentials**, *T.-R. Shan*, *X. Sun*, *S.R. Phillpot*, *S.B. Sinnott*, University of Florida

Oxides such as SiO<sub>2</sub>, Al<sub>2</sub>O<sub>3</sub> and HfO<sub>2</sub>, are typically used together with Si in many high-performance electronic devices, including metal-oxide-semiconductor (MOS) devices/junctions and micro- and nano-electromechanical systems (MEMS/NEMS). The lack of precise control over mechanical properties can lead to the degradation of these materials. It is therefore critical to understand the nanometer-scale mechanical properties of materials or complex systems being considered for use in electronic devices. Nanoindentation and nanoscratching are important methods for investigating the mechanical behavior of small volumes of materials, such as thin film systems. Here, classical molecular dynamics simulations are used to examine the responses to nanoindentation and nanoscratching of thin films of SiO<sub>2</sub> and HfO<sub>2</sub> on silicon substrates. The goal is to determine

the influence of thin film types and the structure of thin film and substrate interface on the responses. Because these systems consist of heterogeneous interface with significant changes in bonding as one crosses from one side of the interface to the other, the empirical charge optimized many-body (COMB) potential as implemented in large-scale atomic/molecular massively parallel simulator (LAMMPS) program is used to model the structural evolution, mechanical response and charge transfer in these systems in response to a nanometer-scale spherical indenter. Aspects of the SiO<sub>2</sub>/Si and HfO<sub>2</sub>/Si interfaces during nanoindentation and nanoscratching, including the mechanisms by which fracture and plasticity occurs, will also be addressed. We gratefully acknowledge the support of the National Science Foundation through grant numbers DMR-0426870 and DMR-1005779).

9:00am **TR+AS+SS-ThM4 Accelerated Molecular Dynamics Simulations of Nanoscale Friction**, *W.K. Kim*, University of Minnesota, *M.L. Falk*, Johns Hopkins University **INVITED**

Accelerated molecular dynamics simulations are implemented to model the sliding process of atomic force microscope experiments and to lower the sliding speeds below those in a conventional MD simulation. In this study the hyperdynamics method, originally devised to extend MD time scales for non-driven systems, is applied to the frictional sliding system. This technique is combined with a parallel algorithm that simultaneously simulates the system over a range of slider positions so that the overall acceleration rate is approximately the number of processors multiplied by the boost factor from the hyperdynamics method. The new methodologies are tested using two-dimensional and three-dimensional Lennard-Jones AFM models. The methodology is then applied to simulated sliding between an oxidized silicon tip and surface achieving a range of six decades of velocity and reproducing the experimentally observed velocity dependence of the friction force. In doing so we learn something new about this system and about friction between amorphous surfaces in general. Unlike in the crystalline case, as increasing force is applied to the amorphous tip intermediate states arise. These intermediate states serve as critical transition pathways. The emergence of such states leads to the emergence of a plateau in sliding velocity at lower sliding speeds and higher temperatures. A simple theory based on these observations successfully describes both the experimental and the simulated data.

9:40am **TR+AS+SS-ThM6 Molecular Dynamics Simulations of Contact between Carbon-Based Materials: Isolating the Effects of Experimental Variables**, *J.A. Harrison*, *K.E. Ryan*, *P.L. Keating*, US Naval Academy, *D.S. Grierson*, *J. Liu*, *K.T. Turner*, University of Wisconsin Madison, *R.W. Carpick*, University of Pennsylvania

The behavior of nanoscale contacts is complex and often cannot be understood through continuum mechanics alone. Here, parallel molecular dynamics (MD) simulations using the AIREBO potential for hydrocarbons to model indentation and friction, are used to investigate nanoscale contacts of carbon-based materials, such as diamond, DLC, and ultrananocrystalline diamond (UNCD). Specifically, the contact of carbon-based AFM probes is simulated to understand the effects of experimental parameters, including tip geometry and material selection, on the adhesion between the tip and sample. Results from the MD simulations will be compared to and discussed within the context of the complementary atomic force microscope experiments and finite element simulations. The tribological response of carbon-based materials is very sensitive to environmental conditions. For example, the presence of water has been shown to negatively impact the friction performance of hydrogenated DLCs but to improve the performance of nanocrystalline and ultrananocrystalline diamond. We have been working to develop a potential energy function that is capable of modeling carbon-based materials in the presence of water. This talk will also outline our current efforts at potential development.

10:40am **TR+AS+SS-ThM9 Modeling the Pressure Dependence of Shear Strength in Sliding, Boundary-Layer Friction**, *M. Garvey*, *M. Weinert*, *W.T. Tysoe*, University of Wisconsin-Milwaukee

The pressure dependence of the shear strength of model alkali halide lubricant systems has been investigated at the density functional theory level. This is compared to the experimental dependence given by  $S = S_0 + \alpha P$ , where  $P$  is the contact pressure,  $S_0$  is the zero-pressure shear-strength and  $\alpha$  is the coefficient of pressure dependence. Sliding potentials were calculated and shear is found to occur between the film and the sliding interface. The heights of the potentials were calculated as a function of compression, allowing the lateral force to be calculated as a function of pressure. The calculated values of  $S_0$  and  $\alpha$  are in good agreement with experimental data.

11:00am **TR+AS+SS-ThM10 Lubrication Mechanisms of MoS<sub>2</sub> Fullerene-Like Nanoparticles: Coupling Computer and Experimental Works**, *E.W. Bucholz*, University of Florida, *I. Lahouij*, *F. Dassenoy*, Ecole Centrale de Lyon, France, *S.B. Sinnott*, University of Florida, *J.M. Martin*, Ecole Centrale de Lyon, France

Inorganic fullerene (IF)-like MoS<sub>2</sub> nanoparticles have been shown to be good lubricating and anti-wear additives when dispersed in a base oil. This improved tribological performance appears to be a result of the size and structure of the nanoparticles along with the test conditions. Possible lubrication mechanisms include pure rolling to sliding to the exfoliation of lamellar MoS<sub>2</sub> sheets inside the contact. *In situ* transmission electron microscopy (TEM) experiments have been used to manipulate individual MoS<sub>2</sub> nanoparticles and investigate their responses to compression and friction under different conditions. However, the very small scale of the MoS<sub>2</sub> nanoparticles makes distinguishing the properties which affect the lubrication mechanism exceedingly difficult; thus, a computational approach is used to more fully understand the most important mechanisms. Therefore, classical molecular dynamics (MD) simulations of individual nested MoS<sub>2</sub> nanoparticles are performed where they are subjected to compression and shear forces between sulfur-terminated molybdenum surfaces. Two specific nanoparticle configurations are considered, with both structures containing three layers. The first configuration is a curved, ellipsoidal MoS<sub>2</sub> nanoparticle structure with a major and minor diameter of approximately 8.9 and 6.6nm, respectively. The second nanoparticle configuration is an octahedron with grain boundaries that are approximately 6.2 nm in length. MD simulations of these structures indicate the role of curved and faceted morphologies as well as grain boundaries on the rolling/sliding behavior and nanosheet exfoliation of the particles. The results are used to interpret the experimental TEM findings and predict the dominant mechanisms associated with enhanced lubrication through the addition of these particles to base oils. This work is supported by the Office of Naval Research .

11:20am **TR+AS+SS-ThM11 Shape-Independent Lateral Force Calibration**, *E.V. Anderson*, *N.A. Burnham*, Worcester Polytechnic Institute

The primary problem with lateral force microscopy (LFM) has been the difficulty in calibrating the cantilever and tip in order to obtain quantitative friction data. Two recent review articles and several research articles have expressed this difficulty and the need for a simple, universally-accepted method [1,2]. The available procedures have numerous limitations. Some require specialized samples or setups. Others are difficult to perform. A number are indirect, or only suitable for certain cantilevers. Several risk damage to the tip or sample, or both, and might require the geometry of the cantilever, which can be hard to measure. We present a procedure that alleviates these problems [3]. The linear relationship between the detected voltage and lateral force is exploited to obtain the slope (calibration factor) and intercept that convert voltage to lateral force. The method is independent of sample shape, probe shape, and scan parameters (load force, gain, and scan rate). The accuracy was investigated on an order-of-magnitude level and was within 50% of torsional spring constants obtained from geometry, and the precision was under 10%. Small scan areas were also found to produce accurate calibration factors and could help to limit tip-sample wear. Quantification of nano-Newton friction forces might now become routine.

1. M. L. B. Palacio, B. Bhushan, *Crit. Rev. Solid State Mater. Sci.* **2010**, *35*, 73-104.

2. M. Munz, *J. Phys. D: Appl. Phys.* **2010**, *43*, 063001.

3. E.V. Anderson, S. Chakraborty, T. Esformes, D. Eggiman, C. DeGraf, K. M. Stevens, D. Liu, and N.A. Burnham, "Shape-Independent Lateral Force Calibration," submitted April 2011.

11:40am **TR+AS+SS-ThM12 Atomic Stick-Slip Friction Studied by Optimally-Matched Accelerated MD Simulations and AFM Experiments**, *Y. Dong*, Purdue University, *Q. Li*, *R.W. Carpick*, University of Pennsylvania, *A. Martini*, Purdue University

Atomic-scale stick-slip friction of platinum on gold (111) surface is quantitatively studied both experimentally and through optimally-matched accelerated molecular dynamics (MD). In order to make a direct comparison between simulation and experiment, many other factors are matched as closely as possible, such as misalignment, size effect of the tip, cantilever compliance, normal load and so on. The Parallel Replica Dynamic Method (ParRep) is used to accelerate the simulation so scan velocities can be decreased to scales approaching those used in atomic force microscope experiments. A logarithm dependence of friction on scanning velocity is observed both in Atomic Force Microscope (AFM) and MD reveals that at low speed the atomic friction lies in thermal activation regime. A further comparison shows that AFM and MD provide consistent energetics, which supports that MD can be used to interpret AFM results;

but attempt frequencies differ by orders of magnitude, which is attributed to the inertia discrepancy.



# Thursday Afternoon, November 3, 2011

Surface Science Division  
Room: 107 - Session SS-ThA

**Semiconducting & Ferroelectric Surface**  
Moderator: J. Millunchik, University of Michigan

2:00pm **SS-ThA1 Polarization Dependence of the Surface and Interfacial Chemistry of Ferroelectric Oxides.** *E.I. Altman*, Yale University **INVITED**

In analogy to ferromagnets, ferroelectric materials develop remnant macroscopic electric fields that can be switched by applying an external field. The bulk electronic polarization is stabilized by compensating charges at the surface that can be supplied by adsorption or electronic and structural reconstructions. Because opposite compensating charges are required on oppositely poled surfaces, ferroelectric materials offer unique opportunities to create surfaces with switchable chemical properties. Further, thin ferroelectric films would be expected to switch their polarization in the presence of molecules that preferentially adsorb on one of the polar surfaces, suggesting a new avenue for chemical sensing. It will be shown that the adsorption of polar molecules such as alcohols and carboxylic acids depends on the ferroelectric polarization direction, with stronger adsorption on positively poled  $\text{LiNbO}_3$ . The differences in adsorption strengths are comparable to the energy required to switch 20 nm thick ferroelectric films, thus ferroelectric chemical sensing is feasible. This possibility is further explored through *in situ* measurements of changes in polarization of thin epitaxial titanate ferroelectric films in response to oxidizing and reducing environments. A limitation to switchable chemistry, however, is the low reactivity of typical ferroelectric oxides. Efforts to increase the reactivity through deposition of catalytic metals fail because the metals form three-dimensional clusters whose surfaces are too far from the ferroelectric substrate to be affected. Results of a combined experimental/theoretical approach to identifying catalytic oxides that form stable, atomically thin layers whose reactivity is influenced by the polarization direction of the ferroelectric will be presented. Specific examples include  $\text{Cr}_2\text{O}_3/\text{LiNbO}_3$  and perovskite layers on ferroelectric titanates.

2:40pm **SS-ThA3 Surface Reconstructions of  $\text{BaTiO}_3(001)$ : STM Study.** *E.H. Morales, D.A. Bonnell*, University of Pennsylvania

$\text{BaTiO}_3$  is currently used in Random Access Memories and is a versatile material with many potential applications. Ferroelectricity at a surface provides unique possibilities to examine mechanisms of molecular adsorption. Experimentally, the polarization can be manipulated *in situ* by negatively and positively poling the surface. In this manner, the interaction with foreign gaseous species can be controlled. It is necessary to develop fundamental understanding of  $\text{BaTiO}_3$  surfaces in order to control the ferroelectric polarization and consequent interactions with adsorbates and in devices. Recent advances have indeed shown that polarization affects molecular adsorption of a variety of molecules; however, the mechanistic processes are not yet understood. Here we present STM of atomically resolved reconstructions,  $(\sqrt{5} \times \sqrt{5}) R26.6^\circ$  and  $(3 \times 1)$  and relate water adsorption to local polarization. Structural variations and adsorption sites will be discussed in terms of Density Functional Theory predictions. Preliminary results of the interaction of  $\text{BaTiO}_3(001)$ 's surface and  $\text{CO}_2$  will be presented as well.

3:00pm **SS-ThA4 Polarization Dependent Interactions at Ferroelectric Surfaces.** *J. Garra, M. Zhao, J.M. Vohs, E.H. Morales, D.A. Bonnell*, University of Pennsylvania

Ferroelectric polarization at surfaces has been exploited over the last several years to mediate reactions in aqueous solutions. More recently studies have shown that ferroelectric polarization at surfaces affects molecular adsorption. The study presented here uses a variety of surface techniques (scanning tunneling microscopy and spectroscopy, low energy electron diffraction, temperature programmed desorption) to examine molecular adsorption on ferroelectric surfaces. Various molecules and various substrates are chosen to determine the effect of polarization orientation and magnitude on physisorption, disassociative chemisorption, defect mediated adsorption and chemical reactions. Specifically, results of interactions of small molecules on  $\text{LiNbO}_3$ , and  $\text{BaTiO}_3$  surfaces will be compared. We show that ferroelectric polarization can affect both physisorption and chemisorption bond energies as well as the sticking coefficients.

3:40pm **SS-ThA6 An Atomic View of ALD of Dielectrics on Semiconductors Using STM.** *A.C. Kummel, W. Melitz, J.B. Clemens, J.S. Lee, T. Kaufman-Osborn, T. Kent, E.A. Chagarov, J. Shen*, University of California, San Diego, *R. Droopad*, Texas State University-San Marcos **INVITED**

Scaling of gate oxides on MOSFETs requires nucleating oxide ALD in every unit cell of the semiconductor channel surface without disrupting the semiconductor surface (high mobility) while eliminating dangle bond states (low  $D_{it}$ ). The reaction of TMA on the group III rich  $(4 \times 2)$  reconstructions of the  $\text{InAs}(001)$  and  $\text{InGaAs}(001)$  surfaces were been studied using *in situ* STM, scanning tunneling spectroscopy (STS), *in situ* XPS, and density functional theory (DFT). When an  $\text{As}_2$  capped III-V sample is decapped in UHV and the substrate is dosed with TMA at 300K at annealed at 200C, the TMA reaction products (dimethyl aluminum, DMA) spontaneously forms monolayer islands insuring ALD nucleation in each unit cell. For integration of III-V MOSFETs on 300 mm silicon wafers, it is possible that a gate last process may be required for which As-decapping is not suitable. A combination of atomic hydrogen dosing, annealing, and TMA dosing is observed to produce an ordered unpinned passivation layer on air exposed  $\text{InGaAs}(001)-(4 \times 2)$  surface with only monatomic steps. This TMA passivation layer on H cleaned air exposed III-V has the same horizontal rows of dimethyl aluminum (STM) and the same unpinned interface (STS) observed with the TMA/decapped  $\text{InGaAs}(100)$ . While TMA directly reacts to create a high density of sites to nucleate gate oxide ALD on III-V surface, for  $\text{Ge}(100)$  surface functionalization is required. The direct reaction of TMA on a  $\text{Ge}(100)$  surface and the effect of monolayer  $\text{H}_2\text{O}$  pre-dosing were investigated. At 300K, a saturation TMA dose produced 0.8 monolayer (ML) of semi-ordered species on a  $\text{Ge}(100)$  surface due to the dissociative chemisorption of TMA. XPS analysis of the 200°C annealed TMA/ $\text{Ge}(100)$  surface showed that only carbon content was reduced during annealing, while the Al coverage was maintained at 0.15 ML, consistent with the low density of nucleation sites due to site blocks by reaction products. Conversely, saturation TMA dosing at RT on the monolayer  $\text{H}_2\text{O}$  pre-dosed  $\text{Ge}(100)$  surface followed by annealing at 200°C formed a saturation layer of Al-O bonds with an Al coverage a factor of two greater than the TMA only dosed  $\text{Ge}(100)$ . The Ge-OH sites catalyze the dissociative chemisorption of TMA even at 300K to create a semiordered surface of Ge-O-Al bonds with an Al coverage double the coverage from a TMA surface without the  $\text{H}_2\text{O}$  pre-dose.

4:20pm **SS-ThA8 Electrostatic Coupling of Surface Charge to Bulk Defect Behavior in Metal Oxides.** *P. Gorai, K. Pangan-Okimoto, A. Hollister, E.G. Seebauer*, University of Illinois at Urbana-Champaign

The technologically useful properties of semiconductor oxides such as titania and zinc oxide often depend on the concentration and diffusion of point defects. Near-surface effects are particularly important in nanoscale devices because most of the bulk is located in the vicinity of the surface. Past work in our laboratory with silicon and titania has shown that semiconductor surfaces serve as efficient pathways for generation and annihilation of point defects in the underlying bulk. Surfaces can, in addition, support electrically charged defects which create near-surface strong electric fields that can influence the local motion of charged defects resulting in the formation of space-charge layers. The electric field-driven accumulation or depletion of charged oxygen defects in such space-charge regions in metal oxides have direct implications on the performance of nanoscale devices such as gas sensors and memory resistors. Oxygen diffusion behavior was studied by exposing natural-abundance single-crystal rutile to isotopically labeled oxygen gas. The resulting profiles were measured by secondary ion mass spectrometry and subsequently modeled with continuum equations for the reaction, Fickian diffusion and electric field-driven diffusion of the key point defects. The degree of charge build-up at the surface can be quantified by an electric potential ( $V_i$ ). The profiles calculated show a characteristic steep concentration gradient near the surface followed by a normal bulk diffusion profile. By identifying the charge-mediated field-driven diffusion mechanism as the controlling factor for the near-surface pile-up of oxygen, we demonstrate that this method allows the spatially resolved characterization of space charge regions near the surfaces of crystalline semiconductor metal oxides. The capability to predict oxygen pile-up in nanoscale metal oxide devices may be beneficial in device improvement via defect engineering of surfaces.

4:40pm **SS-ThA9 Surface Photovoltage Behavior of n-type GaN as a Function of Orientation.** *M. Foussekis, A.A. Baski, M.A. Reshchikov*, Virginia Commonwealth University

GaN is a wide-bandgap semiconductor (3.4 eV) which has approximately 1 eV of upward surface band bending for n-type material, thereby producing a

depletion region that can be detrimental to device performance. This band bending can be indirectly measured using the surface photovoltage (SPV) effect. By illuminating the surface with above-bandgap light, electron-hole pairs are created in the depletion region and holes are swept to the surface to reduce the negative charge and band bending. This change in surface charge is measured by a Kelvin probe in an optical cryostat. When the samples are illuminated with a HeCd laser, the SPV signal immediately rises to approximately 0.6, 0.3 and 0.4 eV for the Ga-polar (c-plane), N-polar, and m-plane sample orientations, respectively. The noticeably smaller SPV value for N-polar GaN indicates that this particular orientation has a smaller value of band bending. After this immediate rise, the SPV signal then begins to slowly change due to photo-induced surface processes. In an oxygen environment, the Ga-polar and m-plane orientations demonstrate a slow decrease in SPV of about 0.1 to 0.2 eV, which is attributed to the photo-induced adsorption of oxygen species [1]. There is no observable change for N-polar GaN, indicating that N-polar GaN is less reactive under UV illumination. In vacuum, all three orientations show a slow increase in the SPV signal of 0.1 to 0.2 eV over 1 h, which is due to the photo-induced desorption of charged surface species. When illumination is ceased after 1 h and the surface is restored in vacuum, subsequent illumination results in a constant, steady-state SPV signal, confirming that the photo-induced removal of any surface contamination layers is complete after approximately 1 h. The restoration behavior of the SPV can be fit for all three orientations using a thermionic model with logarithmic time decay [2]. The N-polar GaN is significantly faster, however, and fully restores in only minutes, as opposed to hours or days for the other orientations. It therefore appears that N-polar GaN has the most distinctive SPV behavior among these orientations, with the lowest SPV value, least amount of photo-induced surface reactivity, and fastest restoration behavior.

[1] M. Foussekis, A. A. Baski, and M. A. Reshchikov, *Appl. Phys. Lett.* **94**, 162116 (2009).

[2] M. A. Reshchikov, M. Foussekis, and A. A. Baski, *J. Appl. Phys.* **107**, 113434 (2010).

5:00pm **SS-ThA10 The Surface States of Lithium Tetraborate**, *L. Wang, W.-N. Mei*, University of Nebraska at Omaha, *D. Wooten, J. McClory, J. Petrosky*, Air Force Institute of Technology, *V. Adamiv, Ya. Burak*, Institute of Physical Optics, Ukraine, *I. Ketsman*, University of Nebraska - Lincoln, *Ya. Losovyj*, The J. Bennett Johnston Sr. Center for Advanced Microstructures and Devices, *P.A. Dowben*, University of Nebraska - Lincoln

The different low index surface terminations of lithium tetraborate,  $\text{Li}_2\text{B}_4\text{O}_7$ , are dominated by electronic states that fall within the projected band gap of the bulk states. As a pyroelectric material,  $\text{Li}_2\text{B}_4\text{O}_7$  is a wide band gap dielectric, yet the (110) surface has a much smaller band gap because of occupied surface states that fall at binding energies between the valence band maximum and the Fermi level. The (100) surface is dominated, however, by unoccupied surface states that also fall in the gap between the conduction band minimum and valence band maximum, but at binding energies just below the conduction band minimum. These states have been identified in photoemission studies of  $\text{Li}_2\text{B}_4\text{O}_7(110)$  and inverse photoemission studies of  $\text{Li}_2\text{B}_4\text{O}_7(100)$  [1]. There is good qualitative agreement between these experiments and the electronic band structure calculations showing that the different surface terminations of lithium tetraborate yield very different surface electronic states.

[1] D. Wooten, I. Ketsman, J. Xiao, Ya.B. Losovyj, J. Petrosky, J. McClory, Ya. V. Burak, V.T. Adamiv, J.M. Brown and P.A. Dowben, *European Physical Journal: Applied Physics* **52** (2010) 31601

## Thin Film Division

**Room: 110 - Session TF+EM+SS-ThA**

### Applications of Self Assembled Monolayers

**Moderator:** M.R. Linford, Brigham Young University

2:00pm **TF+EM+SS-ThA1 Organic Monolayers on Silicon-rich Substrates: Methods and Mechanisms**, *H. Zuilhof*, Wageningen University, Netherlands **INVITED**

SAMs on silicon-containing substrates including silicon, silicon nitride and glass widely expand the applicability of such materials. The presentation will focus on 3 recent developments:

1) The surface modification of H-terminated Si has functioned as a stepping-stone for the construction of a wide-range of hybrid materials. Recent synthetic improvements and detailed mechanistic studies have shown how to optimally construct such modified substrates. These results will be presented in the light of further developments.

2) Silicon nitride can be modified by covalent SAM attachment to achieve chemically highly robust systems. Biofunctionalization thereof with oligosaccharides and antibodies provides novel diagnostic applications in terms of specific bacterial capture in combination with generally antifouling substrates when combined with lithographic structuring of the material. Proof-of-principle and remaining challenges will be demonstrated based on recent experimental progress.

3) A photochemical method we recently developed to modify glass ( $\text{SiO}_2$ ), and the application thereof within the field of modified glass microchannels will be shown, e.g. via the on-chip embedding of enzymatic cascade reactions using a combination of local SAM attachment and DNA-enzyme hybrids. Finally, generalizations to the modification of other oxidic surfaces will be provided.

Key references:

H. Zuilhof and co-workers, *J. Am. Chem. Soc.* **2011**, *133*, 4998–5008.

H. Zuilhof, J. C. M. Van Hest and co-workers *Chemical Science* **2011**, *2*, in press (DOI: 10.1039/C1SC00146A).

H. Zuilhof and co-workers, *Angew Chem.* **2011**, *50*, in press (DOI: 10.1002/anie.201100835).

2:40pm **TF+EM+SS-ThA3 Molecularly Modulated Electrical Transport at Chemically Passivated Silicon Surfaces**, *G. Dubey*, NRC-SIMS, Canada, *F. Rosei*, INRS-EMT, Canada, *G.P. Lopinski*, NRC-SIMS, Canada

Adsorption of charged or polar species on semiconductor surfaces can modulate the electrical properties through long-range field effects. Hydrogen-terminated silicon-on-insulator (SOI-H) is an interesting model system for investigating this sensitivity to surface processes [1,2]. Accumulation mode SOI-H pseudo-MOSFETs [3] have been used to probe molecular adsorption and reaction events. Current-voltage characteristics of such *n*-channel devices are found to be sensitive to the environment, with the accumulation threshold voltage, or flat-band voltage ( $V_{FB}$ ), exhibiting large reversible changes upon cycling between ambient atmosphere, high vacuum ( $<10^{-5}$  Torr) and exposure to water and pyridine vapour at pressures in the torr range. Both these adsorbates act as effective electron donors, shifting the flat band potential to more negative values. The field-effect mobility is found to be comparatively less affected through these transitions. Adsorption of the well known electron acceptor tetracyanoethylene (TCNE), is shown to cause depletion, with ppm levels of TCNE vapour in ambient atmosphere found to rapidly decrease the saturation current by over two orders of magnitude. The effect is only partially reversible on the hydrogen terminated surface, due to the accumulation of strongly bound TCNE molecules on the surface. In addition, oxidation of the H-terminated surface is seen to result in irreversible shifts in both the flat-band voltage and field-effect mobility. In order to passivate the surface from these irreversible processes, a photochemical gas phase reaction [4] with decene was used to form a decyl monolayer on the SOI(100)-H surface. Formation of this monolayer is found to result in a relatively small shift of threshold voltage and only a slight degradation of the field effect mobility. Decyl passivation only slightly decreases the response of the FET to TCNE adsorption while significantly improving the reversibility of the response. These results suggest that alkyl monolayer dielectrics formed by the gas phase photochemical method can function as good passivating dielectrics in field effect sensing applications.

[1] G. Dubey, G.P. Lopinski, and F. Rosei, *Appl. Phys. Lett.* **91**, 232111 (2007).

[2] G. Dubey, F. Rosei, and G.P. Lopinski, *Small* **6**, 2892 (2010).

[3] S. Cristoloveanu, and S. Williams, *IEEE Elec. Dev. Lett.* **13**, 102 (1992).

[4] B.J. Eves, and G.P. Lopinski, *Langmuir* **22**, 3180 (2006).

3:00pm **TF+EM+SS-ThA4 Micrometer- and Nanometer-Scale Patterning of Azide-Functionalized Self-assembled Monolayers on Gold and Aluminum Oxide Surfaces**, *O. El Zubir*, *I. Barlow*, *G. Leggett*, *N. Williams*, University of Sheffield, UK

Self-assembled monolayers (SAMs) have been prepared by the adsorption of [11-(4-azido-benzoylamino)-undecyl] phosphonic acid on aluminum oxide and by the adsorption of 11-(4-azido-benzoylamino)-undecylthiol. Exposure to near UV radiation causes elimination of nitrogen and the creation of a reactive nitrene species. Quantitative studies by X-ray photoelectron spectroscopy (XPS) and contact angle measurement show that the reaction is complete after an exposure of 20 J  $\text{cm}^{-2}$ . The reaction enables selective introduction of primary amines to the surface. By exposure of the azide under a solution of the amine, derivatization may be carried out with high efficiency, providing a simple pathway for the creation of a variety of multiple-component surface chemical patterns.

Micropatterned surfaces were fabricated by exposure the SAMs to UV-laser ( $\lambda=325$  nm) through a mask in presence of amines. Photopatterning was carried out at the nanometer scale by using scanning near-field photolithography (SNP) in which a scanning near-field optical microscope (SNOM) coupled to a UV laser ( $\lambda=325$  nm) is utilized as the light source. Selective modification of azide terminated monolayers on aluminum oxide by protein-resistant molecules enabled the fabrication of protein nanopatterns that could be imaged by fluorescence microscopy.

**3:40pm TF+EM+SS-ThA6 Free-standing, SAM-based, Hybrid Biocompatible Nanomembranes for Biological Applications, N. Meyerbröker, W. Eck, M. Zharnikov, Universität Heidelberg, Germany**

Functional monomolecular films - so-called self-assembled monolayers (SAMs) - represent a broad platform for nanofabrication, sensor design, and molecular electronics, as well as a framework for Chemical Lithography, and a model system for organic interfaces and molecular, macromolecular and biological assemblies. These films can be prepared on different substrates which provide necessary support and guarantee the persistence of the 2D molecular assembly. Since the intermolecular interaction within the SAMs is relatively weak, such films cannot exist without support, dissipating into the individual constituents upon the separation from the substrate. However, as far as the individual molecules within a SAM can be cross-linked extensively by physical means such as electron irradiation, the resulting quasi-polymer film can be separated from the substrate and exist as a free-standing monomolecular membrane on its own. In this presentation we describe the formation of such free-standing membranes on the basis of aromatic SAMs. In contrast to the previous work, we used not only non-substituted but nitro- and nitrile-substituted SAM constituents which, due to either nitro-to-amine or nitrile-to-amine transformation, become chemically reactive after the irradiation treatment and can be subsequently coupled to further species. As such species we used oligo(ethylene glycol)-based molecules with a specific anchor group providing the coupling to the amine groups of the monomolecular template. After the attachment, these templates and respective hybrid membranes become protein-repelling and as such can be used as a non-disruptive and highly transparent support for proteins and cells in transmission electron microscopy (TEM) experiments. Whereas the ultimate thinness of this support guarantees a high imaging quality, protein-repelling ensures the lack of protein denaturing, which extends essentially the possibilities of TEM experiments in their specific application to sensitive biological targets.

**4:00pm TF+EM+SS-ThA7 Development of Nanoscale Heterostructures: From Single Component Nanostructures to Multicomponent Nanosystems, N. Chopra, The University of Alabama, Tuscaloosa**

**INVITED**

Chemical vapor deposition (CVD) and solution synthesis was coupled to realize a unique surfactant-free approach for the direct nucleation of nanoparticles on 1-D nanostructures. Towards this end, skeleton nanostructures such as carbon nanotubes and oxide nanowires were successfully utilized as a selective nucleation sites for nanoparticles. Carbon nanotubes (CNTs)-Ni/NiO nanoparticles and oxide nanowires -(Au or  $\text{Co}_3\text{O}_4$ ) nanoparticles were synthesized. Morphological evolution of nanoparticles as a function of various growth parameters was studied using TEM, SEM, and XRD. New kinds of lattice relationships, interfaces, and morphologies were established. For example, CuO nanowire- $\text{Co}_3\text{O}_4$  nanoparticles showed unique optical characteristics leading to enhanced absorbance in visible light. Growth mechanisms of heterostructures revealed various competing phenomena at nanoscale including thermodynamic stability and chemical potential, and surface migration of nanoparticles on high curvature 1-D nanostructures as opposed to flat surface. These heterostructures also hold great promise as novel sensors and energy technologies.

**4:40pm TF+EM+SS-ThA9 Physical and Electrical Characterization of Metal Incorporated SAM-based Molecular Electronic Junctions, S. Pookpanratana, M.A. Walsh, C.A. Richter, C.A. Hacker, National Institute of Standards and Technology**

Molecular electronics is attractive for next-generation applications because of the flexibility in tailoring the organic functionality and the facile formation of uniform monolayers by using thiol-Au chemistry for self-assembly. Added functionality can be achieved by using thiol self-assembled monolayers (SAMs) containing terminal carboxylic acid functional groups to chelate with metal ions [1], and thus can incorporate d-orbital transition metals with the SAMs. One challenge in molecular electronics has been the reliable formation of a top contact to the organic layer. Fabrication techniques involving metal evaporation of the top contact often result in penetration to the substrate [2] or into the SAM [3], either of which influences the measured electrical properties across the junction.

Here, we utilize flip chip lamination (FCL), a soft metallization technique by nanotransfer printing, to form a top contact onto SAMs on Au [4].

Based on previous work by Ulman et al. [5] and Allara et al. [6], we have incorporated metal ions (Cu and Ni) with mercaptohexadecanoic acid (MHA) and formed a molecular junction by FCL. SAMs of MHA were prepared on Au on Si and Au on polyethylene terephthalate (PET) substrates. The MHA/Au/Si was exposed to metal ion (M) containing solution. The M-MHA/Au/Si samples were then laminated to MHA/Au/PET to create a 'molecular sandwich' which resulted in the following structure: PET/Au/MHA-M-MHA/Au/Si where the PET substrate is removable.

The SAMs on Au were investigated by using X-ray photoelectron spectroscopy (XPS) and p-polarized reflection absorption infrared spectroscopy (p-RAIRS), and both methods confirm the initial presence of carboxylic acid on the (pre-FCL) surface. Successful incorporation of metal ions into the SAM were directly confirmed by XPS (occupying 30-50% of the -COOH sites), and indirectly by p-RAIRS with the appearance of C=O bands in an acid salt environment. Electrical and physical characterization (using backside p-RAIRS and near edge X-ray absorption fine structure (NEXAFS)) measurements to investigate the monolayer after FCL are currently ongoing. With these results, we are able to obtain a thorough picture linking electrical properties with physical characterization of the buried molecular junctions.

- [1] A. C. Templeton et al., *Langmuir*, 2000, 16, 6682-6688.
- [2] A. V. Walker et al., *J. Am. Chem. Soc.*, 2004, 126, 3954-3963.
- [3] C. A. Richter et al., *Solid-State Electron.*, 2006, 50, 1088-1096.
- [4] M. Coll et al., *J. Am. Chem. Soc.* 2009, 131, 12451-12457.
- [5] S. D. Evans et al., *J. Am. Chem. Soc.*, 1991, 113, 5866-5868.
- [6] T. A. Daniel et al., *Langmuir*, 2007, 23, 638-648.

**5:00pm TF+EM+SS-ThA10 Examining the Role of Laminin-Derived Peptides in Neuronal Attachment, N.A. LaFranzo, J.A. Maurer, Washington University in St. Louis**

Laminin-1 is a 900kD glycoprotein that is a major component of the extracellular matrix (ECM). Laminin is known to be involved in many cellular processes including cell adhesion, migration and differentiation *in vivo* and is often used in *in vitro* experiments to encourage neuronal attachment. While laminin contains some integrin-receptor binding sites, multiple domains on the protein including the peptide sequences IKVAV, YIGSR and RGD have also been shown to bind to non-integrin neuronal receptors, encourage cell adhesion, and encourage neurite outgrowth in the absence of the full protein structure. However, previous experiments performed using these peptides as substrates for neuronal culture fail to consider the effects of excretion of the cells own ECM proteins onto the surface, which we have shown can occur on surfaces with high peptide concentrations. By utilizing self-assembled monolayers (SAMs), we have created a substrate that prevents the non-specific adsorption of proteins excreted by neurons, while introducing a low-concentration of the peptide sequences to encourage neuronal attachment.

A pair of alkane-thiol monomers for assembly on a gold substrate have been designed which contain a tetra-ethylene glycol moiety at the tail to prevent the non-specific adsorption of proteins. One of the monomers is terminated with an azide moiety that can be used to specifically attach molecules with an alkyne group by a copper-mediated azide-alkyne cycloaddition (CuAAC) reaction, also known as the "click" reaction. By introducing 5-pentynoic acid at the N-terminus of each of the peptides during synthesis, we have introduced a bioorthogonal attachment point for reaction with the azide-terminated monomers on the surface. Once prepared, these surfaces have been confirmed to be resistant to adsorption of proteins by quartz-crystal microbalance (QCM) experiments. Primary culture neurons dissected from embryonic mice have been cultured on the surface and the effects of the peptides on neurite outgrowth have been quantified. To better understand the role of these peptides in cell adhesion, neurons transfected with a plasmid encoding EGFP-vinculin or EGFP-paxillin have been cultured on the surface and the focal adhesion morphologies have been observed in live-cell imaging experiments. These results are compared to those observed for a surface where the full laminin protein has been adsorbed. Together, these experiments help to design a surface resistant to non-specific protein adsorption that allows for neuronal adhesion, sheds light on laminin-mediated attachment, and aids in developing better small-molecule mimics of receptor-mediated cellular adhesion.

5:20pm TF+EM+SS-ThA11 **Contact-Free Electrical Characterization of Molecular Layers using CREM**, *H. Cohen*, Weizmann Inst. of Science, Israel

While generally recognized as a powerful analytical tool, XPS is insensitive to hydrogen atoms and, in many cases, to fine variations in the environment of carbon atoms. As such, XPS characterization of organic molecular layers is rather limited, in particular under demands for high overlayer quality. On the other hand, a recent XPS-based technique for chemically resolved electrical measurements (CREM) proposes high sensitivity to even small amounts of defects or organization imperfections [1,2].

Here, CREM application to monolayers self-assembled on metallic or semiconducting substrates is overviewed, demonstrating some of the unique capabilities offered by this non-contact probe. Damage evolution under irradiation is specifically discussed; two of its extreme limits being modeled, yielding the effect of corresponding defect sites on the CREM-derived I-V curves. Potential applications to molecular electronics, approaching *atomic* resolution in the electrical data, will be discussed.

#### References

I. Doron Mor et al., *Nature* **406**, 382 (2000).

H. Cohen, *Applied Physics Letters* **85**, 1271 (2004).

# Friday Morning, November 4, 2011

## Electronic Materials and Processing Division

Room: 210 - Session EM+SS-FrM

### Surfaces and Materials for Next Generation Electronics

**Moderator:** E.X. Zhang, Vanderbilt University, L. Porter, Carnegie Mellon University

8:20am **EM+SS-FrM1 Growth of 3C-SiC Epitaxial Layers on 4H-SiC Step-Free Mesas.** *R.L. Myers-Ward, E.A. Imhoff, J.D. Caldwell, L.O. Nyakiti, V.D. Wheeler, K.D. Hobart, C.R. Eddy, Jr., D.K. Gaskill*, Naval Research Laboratory (NRL)

To avoid defects such as polytype inclusions or dislocations, the epitaxial growth of 3C-SiC requires a lattice-matched, perfect substrate. One solution to this problem is to use step-free mesas of 4H-SiC as 3C-SiC lattice templates [1]. In this work, we describe the formation of large area step-free mesas and the subsequent nucleation and growth of 3C-SiC layers. A powerful array of tools were utilized to characterize the properties of these layers including Nomarski microscopy, secondary electron microscopy (SEM), atomic force microscopy and X-Ray diffractometry. Micro-photoluminescence ( $\mu$ -PL) was employed to investigate the presence of electronic defects and identification of polytype, enabling us to obtain information about the structural and electronic properties on a micron-sized length scale.

On-axis 4H-SiC substrates were initially patterned and reactive ion etched to produce hexagonal and square shaped mesas with varying widths ranging from 40 to 400  $\mu\text{m}$  (400% greater area than previous reports), and heights from 2 to 5  $\mu\text{m}$ . Homoepitaxial layers were grown on the mesas in an Aixtron VP508 horizontal hot-wall chemical vapor deposition reactor using the standard chemistry of silane and propane in order to grow out the steps on the mesas. The homoepitaxial layers were terminated at the mesa step edge and further growth is prohibited. The films were grown at 2 $\mu\text{m/hr}$  and the pressure and temperature were 100 mbar and 1580 $^{\circ}\text{C}$ , respectively. The yields of 200  $\mu\text{m}$  width 4H-SiC step-free mesas was ~95%. Heteroepitaxial 3C-SiC was grown 2  $\mu\text{m}$  thick on the homoepitaxy (4H-SiC) by means of reducing the growth temperature to 1450 $^{\circ}\text{C}$ , while maintaining 100mbar.

Under Nomarski evaluation, ~ 18% of the 200  $\mu\text{m}$  wide 3C-SiC mesas appeared to be step-free. Micro-PL maps were used to confirm the presence of 3C-SiC, where uniform 3C-SiC was detected across the entire mesas. X-ray rocking curves also indicated 3C-SiC, with the FWHM of the SiC (111) being ~21", indicating good quality material.

Yield maps for the 200 and 400  $\mu\text{m}$  mesas will be presented. In addition, real color PL imaging will be used to determine the types of defects within the mesas which displayed lower PL intensity regions of 3C-SiC. Lastly, initial results of Schottky rectifiers performance made on the layers will given.

#### References

[1] J. A. Powell, *et al.*, Appl. Phys. Lett. 77, 1449 (2009).

8:40am **EM+SS-FrM2 Growth of Epitaxial Rare Earth Nanostructures in III-V Semiconductors.** *B.D. Schultz, J.K. Kawasaki, C.J. Palmstrom*, University of California, Santa Barbara

Highly ordered embedded nanostructures of rare-earth monpnictides can be formed within III-V semiconductor heterostructures providing a new degree of control over the structural and transport properties of the heterostructures. Materials such as ErAs and ErSb are thermodynamically stable with GaAs and GaSb respectively, and in both cases a common group-V sublattice is maintained throughout the heterostructures. In both the arsenides and antimonides, co-deposition at concentrations above a few atomic percent results in the formation of nanoparticles and nanorods. The shape of the nanostructures is strongly dependent of the growth surface including reconstructions, stoichiometry, temperature, and crystallographic orientation. Codeposition of Er with GaAs can produce nanoparticles or ordered nanorods oriented along either the [111] or [211] directions depending on aforementioned conditions[1]. While codeposition of Er with GaSb produces either particles or nanorods oriented primarily along the [100] direction. STM of the GaAs(311)A and B surfaces during the initial stages of nucleation show that following the deposition of a fractional monolayer of ErAs, embedded growth of ErAs particles are observed on the B surface, while the A surface shows primarily surface cluster formation. MBE growth of GaAs on (311)A and B orientations produces relatively flat surfaces with uniquely different (8 $\times$ 1) reconstructions. Codeposition of Er with GaAs results in significant roughening of the surface during growth due to anisotropic diffusion of Ga and Er along the <233> and <011> directions and the general tendency of GaAs not to wet ErAs(100) surfaces.

The [211] orientation of the ErAs nanorods on the surface is found to result from preferential growth along the (1 -1 -1) plane on Ga-polar A surfaces. While the angle between the (1 -1 -1) and surface normal remains less than or equal to 90 $^{\circ}$ , the [211] orientated growth is supported. The {111} surface of the rocksalt ErAs is typically a high-energy surface; however, the Ga-rich (1 -1 -1) plane provides a flux mediated epitaxial growth surface for the ErAs analogous to a vapor-liquid-solid type of growth. *In-situ* RHEED, LEED and STM surface studies will be presented along with a detailed growth model to explain differences in the growth process and in nanorod formation for different substrates and substrate orientations.

Supported by AFOSR FA9550-10-1-0119 and ARO W911NF-07-1-0547. [1] T.E. Buehl, C.J. Palmström, and A.C. Gossard, J. Vac. Sci. Technol. B 29, 03C108-1, 2011.

9:00am **EM+SS-FrM3 Bulk Topological Insulators and Superconductors: Discovery and the Frontier.** *M.Z. Hasan*, Princeton University **INVITED**

While most known phases of matter are characterized by broken symmetries, the discovery of quantum Hall effects (1980s) revealed that there exists an organizational principle based on topology rather than broken symmetry. In the past few years, theory and experiments have suggested that new types of topological states of matter exist in certain insulators without any applied magnetic field. These topological insulators are characterized by a full band gap in their bulk and gap-less conducting edge or surface states protected by time-reversal symmetry. Unlike the quantum Hall systems, the topological insulators can be doped into superconductors and magnets revealing the interplay between topological order and broken symmetry order. In this talk, I will briefly review the basic theory and highlight the experimental developments in topological insulators. I will then conclude by drawing connections between the emergent novel physics and their potential applications.

10:20am **EM+SS-FrM7 Inter-band GaN/InGaN/GaN Tunnel Diodes.** *S. Krishnamoorthy, D.N. Nath, S. Bajaj, S. Rajan*, Ohio State University

The III-Nitride material system has demonstrated its potential for a broad range of optoelectronic and electronic applications. However there are no reports of efficient III-Nitride tunnel junctions due to the large band gaps in this material system. In this work, we show that with unique properties such as the polarization, tunneling can be enhanced using band bending over smaller distances in nitride heterostructures, leading to record reverse and forward tunneling current density for the III-nitride material system.

We have designed and demonstrated GaN/InGaN/GaN tunnel junction with a record high current density of 118 A/cm $^2$  at a reverse bias of 1 V by utilizing a 6.4 nm thin In $_{0.33}$ Ga $_{0.67}$ N barrier material. N-polar p-GaN/In $_{0.33}$ Ga $_{0.67}$ N/n-GaN heterostructure designed for tunneling close to zero bias was grown by plasma assisted molecular beam epitaxy by choosing the critical thickness of InGaN barrier appropriately. The tunnel junction sample shows five orders of magnitude higher current at a reverse bias of 1 V as compared to a standard p+/n+ GaN sample indicating efficient tunneling across the InGaN barrier. The tunneling turn-on close to zero bias, and maximum current density of 9.1 kA/cm $^2$  achieved in this work demonstrates the potential of polarization-engineered tunnel junctions.

Two distinct regimes of transport are identified based on the temperature dependent I-V measurements. At lower reverse bias, defect assisted tunneling with strong temperature dependence is found to dominate. In this regime, a plot of  $\ln(J/E)$  vs  $E^{1/2}$  shows a linear behavior suggesting a Frenkel-Poole emission mechanism due to the high field in the InGaN quantum well. A direct band to band tunneling regime resulting in weak temperature dependence that arises from band gap variation with temperature is observed from a reverse bias of 1 V. A decrease in current density is observed with increase in temperature in the range of 77- 150 K and this can be attributed to the presence of band tail states which has been observed previously in In face InGaN.

We discuss the design of these quantum well tunnel junctions. Although higher indium compositions yield higher band to band tunneling probability, calculations using a simplified Kane model reveal that the wider depletion region in n GaN due to higher band offset considerably reduces the net tunneling probability. Calculations also reveal the need for very high doping in the n GaN layer so as to minimize the depletion region thickness in order to achieve very high current densities in such polarization charge assisted tunnel junctions. These calculations can guide future tunnel junctions with better performance characteristics.

10:40am **EM+SS-FrM8 Probing Surface-Induced Fluctuations in Organic Materials using an Atomic Force Microscope**, *N.C. Hoepker, S. Lekkala, R.F. Loring, J.A. Marohn*, Cornell University

The development of organic electronics calls for new tools to study organic thin films. By measuring the frequency noise experienced by a cantilever near a surface, we are able to microscopically probe organic materials. In previous work, we used an Atomic Force Microscope to measure frequency noise due to dielectric fluctuations as a function of cantilever height and voltage over a thin film of polyvinyl acetate. In parallel, we have developed a zero-free parameter linear-response theory of thermally induced dielectric fluctuations that successfully describes our observations.<sup>1</sup>

Having understood dielectric fluctuations, we are now investigating fluctuations induced by carrier motion in polymeric semiconductors. Charge transport in these devices is not well understood. Previous work indicates that the ratio of diffusion constant to mobility in these materials violates what is predicted by the Einstein relation. In addition, there is an ongoing controversy on the charge density and electric field dependence of mobility. While the correlated-disorder model correctly predicts the electric field dependence of mobility, models that predict a density dependence of mobility rely on uncorrelated site-to-site energies.

A resolution of these controversies calls for new tools to study carrier motion in organic semiconductors. By measuring the frequency fluctuations experienced by a cantilever near a surface, we are able to microscopically probe carrier motion in organic materials. Comparing our observations over a poly(3-hexylthiophene) transistor to a calculation based on free diffusion, we find that while theory overestimates the observed fluctuations, it predicts the correct spectral shape and distance dependence of the fluctuations. Even at high gate bias, the observed cantilever frequency fluctuations differ from what we expect based on free diffusion and on the measured carrier mobility. This discrepancy indicates a breakdown of the Einstein relation. Further we present a number of different charge hopping models. We find that the predicted cantilever frequency noise is very sensitive to the details of the model, indicating that frequency noise spectra are a vital tool for selecting appropriate charge transport models.

[1] Nikolas Hoepker, Swapna Lekkala, Roger F. Loring, John A. Marohn (manuscript in preparation). *Quantifying Dielectric Fluctuations over Polymer Films Using an Atomic Force Microscope*.

11:00am **EM+SS-FrM9 2011 AVS Albert Nerken Award Lecture - Electron Spectroscopy of Reconstructed Surfaces: From Silicon to Graphene**, *J.E. Rowe\**, North Carolina State University **INVITED**  
Surface reconstruction of silicon (and other materials) refers to the process by which atoms at the surface of a crystal assume a different structure than that of the bulk and has been extensively discussed and reported at a number of AVS meetings from the early 1960's until present time. In the 1970's a number of electron spectroscopy methods were applied to study this effect and many atomic models were proposed. Early 1970's experiments using electron energy loss spectroscopy and photoemission spectroscopy are described which along with modern theory methods led to the now accepted dimer model (later confirmed by STM) for the Si(100)2x1 and most other reconstructed (100) semiconductor surfaces. Additional core-level synchrotron spectra are described along with very recent studies which include adsorbate-induced surface reconstruction and the role of interface reconstruction of SiC(0001) used for the growth of graphene and studied by STM and STS. Spectroscopy has continued to play an important role even during the past 25 years after the discovery of atomic-scale imaging by STM of the Si(111)7x7 reconstruction. Both early and more recent studies of reconstruction by the author are reviewed.

11:40am **EM+SS-FrM11 Molecular Motion Confined to Self-Assembled Quantum Corrals**, *E. Yitamben, R.A. Rosenberg, N.P. Guisinger*, Argonne National Laboratory

Engineering molecular superstructures on metals opens great possibilities for the control and exploration of complex nanosystems for technological applications. Of particular interest is the use of chiral molecules, such as alanine, to build self-assembled nanoscale structures for the trapping of the two-dimensional free electron gas of a metal. In the present work, molecules of D- or L-alanine were deposited on Cu(111). Scanning tunneling microscopy and spectroscopy revealed the formation of a uniform network of hexagonal pores of average diameter ~1.2 nm. Each pore acts as a quantum corral by confining the two-dimensional electron gas of the Cu(111) surface state. Furthermore, excess alanine molecules were trapped at the inner perimeter of the hexagonal pore, and were observed as rotating or immobile spatial states. This study demonstrates the engineering of one of the smallest quantum confined structures, and the dynamics of molecular motion within these potential wells.

\* Albert Nerken Award Winner

Acknowledgements: This work was supported by the U.S. Department of Energy, Office of Science, Office of Basic Energy Sciences, under Contract No. DE-AC02-06CH11357

## Surface Science Division Room: 107 - Session SS-FrM

### Surface Science on Graphene

Moderator: I.I. Oleynik, University of South Florida

8:20am **SS-FrM1 Towards Controlled Growth of a Single-Layer of MoS<sub>2</sub>**, *D. Sun, W. Lu, D. Kim, J. Mann, L. Bartels*, University of California, Riverside

MoS<sub>2</sub> is a semiconducting material consisting of sulfur-molybdenum-sulfur tripledecker layers loosely bound by van der Waals interactions. MoS<sub>2</sub> has been used technologically for a long time, for instance as lubricant, where similar to graphite its layered character was employed. Recently, its electronic characteristics have attracted increased attention with the finding that it transitions from an indirect bandgap semiconductor at 1.6eV gap to a direct bandgap one at 1.9eV gap at the transition from multilayers to a single layer. A transistor has been constructed from a MoS<sub>2</sub> and shown appreciable properties. The increased bandgap and high fluorescence yield may also suggest applications of the material for photonic or photocatalytic applications.

MoS<sub>2</sub> can be exfoliated mechanically similar to graphene. While this method is simple, it is hard to control and not amendable to mass production of thin films. Solution-based processes have been proposed and may provide a scalable source of a mixture of single and multilayer material. Here we show an alternative avenue for the fabrication of MoS<sub>2</sub> monolayers: growth of MoS<sub>2</sub> on a sulfur-preloaded copper surface. In contrast to all other methods, this route has the potential of providing exclusively monolayer material, as the sulfur source is only available until the substrate is covered. Practically, this approach is related to the growth of graphene monolayers on copper or ruthenium films, where segregation of carbon to the surface is employed in aggregating a carbonaceous layer that transforms into graphene under the correct conditions.

Small MoS<sub>2</sub> triangles of a few nanometers in size have been grown previously on gold in a dilute H<sub>2</sub>S atmosphere. Here we show significantly larger patches, tens of nanometers in size. In contrast to gold, copper forms a multitude of sulfur surface coverages and also readily absorbs sulfur into the bulk. Thus, we can preload the substrate with a specific amount of sulfur using an easy to handle liquid precursor, benzenethiol. In previous work we have shown that heating to below 400K removes the phenyl group of benzenethiol reliably from copper leaving sulfur coverages behind.

8:40am **SS-FrM2 Oxygen Adsorption on Electronically Modified Graphite Surfaces Studied by Molecular Beam Scattering**, *J.P. Oh, T. Kondo, K. Arakawa, Y. Saito, J. Nakamura*, University of Tsukuba, Japan

The graphite surface consists of  $\pi$  conjugated system. When the  $\pi$  conjugated system is broken, the non-bonding  $\pi$  electronic states are known to form on the surface. Recently, the non-bonding  $\pi$  electronic states at the Fermi level of the graphite-related materials are expected to be the active sites for the specific chemical reaction such as oxygen-reduction reaction in the fuel cell [1]. It is thus important to understand the interaction between an oxygen molecule and the graphite surface for the efficient usage of the graphite-related materials. We have reported previously that the defects induced by Ar<sup>+</sup> ion bombardment on the graphite surface significantly affects the gas-graphite interaction based on the measurements of the angular intensity distributions of He and Ar beam scattered from the pristine and the defect induced graphite surfaces [2]. The difference in the gas-surface interaction has been ascribed to the local breaking of the  $\pi$  conjugated system of graphite by defect formation. To further investigate the effect of the modification of the graphite electronic states on the gas-surface interaction, especially for the oxygen adsorption, we have measured angular intensity distributions of O<sub>2</sub> from electronically modified graphite surfaces, namely potassium intercalated graphite, nitrogen-doped graphite (graphite bombarded by N<sub>2</sub><sup>+</sup> ion) and defective graphite (graphite bombarded by Ar<sup>+</sup> ion). The detail of scattering features as well as the effects of the electronic modification of graphite on the oxygen adsorption will be discussed in detail with our recent STM and STS results.

\*E-mail: nakamura@ims.tsukuba.ac.jp  
[mailto:nakamura@ims.tsukuba.ac.jp]

[1] S.F. Huang, K. Terakura, T. Ozaki, T. Ikeda, M. Boero, M. Oshima, J. Ozaki and S. Miyata, *Phys. Rev. B*, **80**, 235410 (2009).

[2] J. Oh, T. Kondo, D. Hatake, Y. Honma, K. Arakawa, T. Machida, J. Nakamura, *J. Phys.: Condens. Matter*, **22**, 304008 (2010).

9:00am **SS-FrM3 Interaction and Thermal Stability of Oxygen Species in Graphene Oxide and Graphene Defects**, *M. Acik, C. Gong, G. Lee, K. Cho, C. Mattevi, M. Chhowalla, Y.J. Chabal*, University of Texas at Dallas  
**INVITED**

Graphene devices are based on finite size flakes (e.g. nanoribbons) in contact with dielectrics or other materials, and therefore require control of edges and depend on the control of processing methods (often involving vapor or wet chemistry). Graphene oxide (GO) represents an interesting system from which much can be learned about oxygen interaction with graphene. Furthermore, studying the reduction of GO provides a powerful way to understand the stability of oxygen species and the role of trapped molecules. We have studied both the thermal and chemical reduction of single- and multi-layer GO using *in situ* infrared (IR) absorption spectroscopy under a variety of conditions. For the commonly used as-synthesized GO, we find that water molecules play an important role in both defect formation (evident from CO<sub>2</sub> evolution)<sup>1</sup> and carbonyl-termination of defect edges at intermediate annealing temperatures (150-250 C).<sup>2</sup> We also find that a very stable edge configuration appears after high temperature anneals (> 850C), involving edge-ether termination of atomically straight zigzag edges and characterized by an anomalously strong IR absorption.<sup>3</sup> The situation is dramatically different when water is replaced by alcohols or more complex molecules (e.g. ionic liquids). In general, defect formation is greatly suppressed (no CO<sub>2</sub> evolution) with less carbonyl formation and a reduced density of atomically straight, edge-ether terminated edges. This talk will summarize the current understanding of the mechanisms involved in thermal reduction and suggest pathways for developing stable graphene nanostructures with reasonable electrical properties.

1. Acik et al., Generation and capture of CO<sub>2</sub> and CO in graphite oxide stacks during thermal reduction Mater. Res. Soc. Symp. Proc., **1205E**, 1205 (2010).
2. Acik et al., The Role of Intercalated Water in Multilayered Graphene Oxide. ACS Nano **4**, 5861 (2010).
3. Acik et al., Unusual infrared-absorption mechanism in thermally reduced GO. Nature Materials **9**, 840 (2010).

9:40am **SS-FrM5 Graphene on Pt(111) as a Template for Pt Nanocluster Formation**, *Z. Liang, H. Khosravian, A. Uhl, R. Meyer, M. Trenary*, University of Illinois at Chicago

Graphene on transition metal substrates often forms superlattices that are manifested as Moiré patterns in scanning tunneling microscopy (STM) images. Such graphene superlattices can serve as templates for the formation of periodic arrays of metal nanoclusters with a uniform size distribution, a situation that is ideal for model catalyst studies. We have used an ultra high vacuum (UHV) STM to investigate graphene growth on Pt(111) from precursor hydrocarbon species. Different periodicities in the Moiré patterns are observed corresponding to different orientations of the graphene layer with respect to the Pt(111) lattice. Various graphene orientations are possible because of a relatively weak graphene-Pt interaction. Following Pt deposition onto the graphene-covered areas of the surface, small Pt nanoclusters were observed. While graphene on Pt(111) only weakly interacts with the substrate, which leads to a weak corrugation in the superlattice compared to other transition metals, such as Ru, our results show that even this weak corrugation is sufficient to serve as a template for the formation of mono-dispersed Pt nanoclusters. These Pt nanoclusters are relatively stable and only undergo agglomeration for annealing temperatures above 600 K.

10:00am **SS-FrM6 Ripening Behavior of Pt Clusters on Monolayer Graphene Supported by Ru(0001) and the System's Thermal Stability**, *C.U. Lorenz, A.K. Engstfeld*, Ulm University, Germany, *H.E. Hoster*, Technische Universität München, Germany, *R.J. Behm*, Ulm University, Germany

The Moiré-type nm-scale patterns of graphene monolayers supported by metal single crystals were recently used for the fabrication of ordered arrays metal nanoclusters by metal vapor deposition under ultrahigh vacuum UHV conditions [1-3]. The corrugation within the adsorption potential of the graphene layer result in virtually monodisperse clusters. These are important for model (electro-)catalysis studies investigating the size dependency of Pt clusters on carbon support.

In this study we analyze the ripening behavior of Pt clusters (formed at room temperature) on monolayer graphene supported by Ru(0001) at temperatures above 450 K by means of STM. The size distribution change of the clusters gives insight into the rate determining step and into the mechanism of the ripening process. Two different annealing step methods (i: a single sample was successively heated to higher temperatures and ii:

individual samples reproducibly prepared in the same manner annealed to certain temperatures; both methods using the same heating period of 10 min) bring us to the conclusion that Pt cluster ripening between 450 K and 725 K occurs via a mechanism proposed by M. Smoluchowski. Above 725 K we observe indications for a change in the ripening mechanism, where Smoluchowski ripening is likely in competition with Ostwald ripening. Also above 725 K, we observed an adverse influence of the Pt on the stability of the monolayer graphene. Single defects in the otherwise well ordered graphene appeared, which were absent after annealing to lower temperatures.

[1] A.T. N'Diaye et al., New J. Phys. **11**, 2009, 103045. [2] Yi Pan et al., Appl. Phys. Lett. **95**, 2009, 093106. [3] K. Donner and P. Jakob, J. Chem. Phys. **131**, 2009, 164701.

10:20am **SS-FrM7 Mechanisms of Graphene Growth on Metals**, *N.C. Bartelt*, Sandia National Laboratories  
**INVITED**

Growth on metal substrates is a promising route for synthesizing high-quality graphene films. In addition, moving electronic applications into the real world requires understanding and controlling the properties of graphene in contact with metals. This talk will focus on the properties and growth mechanisms on several metals distinguished by varying binding strengths to graphene sheets. Mechanistic insight comes from observing growth directly using low-energy electron microscopy (LEEM). On the relatively strongly interacting substrate Ru(0001), graphene grows with a single in-plane orientation from a highly supersaturated sea of C adatoms. On the less interacting substrates Ir(111) and Pd(111), graphene forms several but discrete in-plane orientations. Small but significant differences in graphene's electronic properties (i.e., band structure and work function) result from changes in orientation. On Cu foils, graphene islands nucleate with a large range of orientation. Thus, the weak film-Cu interaction leads to a high defect density. Finally, the mechanism of bilayer graphene growth has been explored. Diffraction analysis reveals that the second graphene layer on Ir(111) grows next to the substrate, not on top of the first layer. This "underlayer" growth mechanism occurs when the carbon source is either segregation from the substrate or deposition on top of the first layer. How this unusual mechanism affects thickness uniformity will be discussed.

This work was supported by the Office of Basic Energy Sciences, Division of Materials and Engineering Sciences of the U.S. Department of Energy under Contract No. DE-AC04-94AL85000.

11:00am **SS-FrM9 Graphene Moiré Polymorphism on Hydrogenated Ruthenium Surfaces**, *B. Diaconescu*, University of New Hampshire, *F. Hagelberg*, East Tennessee State University, *K. Pohl*, University of New Hampshire

Graphene has aroused tremendous interest due to its remarkable electronic and mechanical properties. The lack of a band-gap, however, causes a serious challenge for implementing graphene as a material for electrical switches and therefore creative ways of inducing this band-gap are needed. We will present a STM/LEED/DFT study of the monolayer graphene on Ru(0001) system in the presence of hydrogen. STM reveals a diverse array of Moiré superlattice sizes ranging from 0.9 to 2.4 nm in the presence of hydrogen adlayer structures, as confirmed by LEED. Density functional theory calculations show a correlation between the Moiré superstructure sizes and the hydrogen coverage and the opening of a band-gap in the graphene/H/Ru(0001) system for some of the Moiré/hydrogen adlayer coverages.

This work was supported by the Nanoscale Science and Engineering Center for High-rate Nanomanufacturing (NSF NSEC-425826) and NSF DMR-1006863.

11:20am **SS-FrM10 Modifying Ni(111)/Graphene Interfaces by Sn-Ni Interface Alloy Formation**, *R.Q. Addou, A. Dahal, L. Adamska, I.I. Oleynik, M. Bazill*, University of South Florida

Graphene growth on metal surfaces (Ni, Pt, Ir, Rh and Cu) has been studied extensively [1]. Ni(111) is special among these metals because it is closely lattice matched with graphene ( $a_{\text{graphene}} = 0.246$  nm vs.  $a_{\text{Ni(111)}} = 0.249$  nm) allowing the growth of graphene with a single domain and in registry with the substrate [2]. However, compared to most other metal substrates the interaction between Ni and graphene is rather large, resulting in a small metal-carbon distance and a large shift of the graphene  $\pi$ -band compared to freestanding graphene. In order to de-couple graphene from the Ni-substrate other weaker interacting metals such as Cu and Au have been successfully intercalated between the graphene and Ni-substrate [3]. These metals have, however, a different lattice parameter and consequently the registry between the substrate and graphene is lost. Here we demonstrate a new approach that

weakens the metal-graphene interaction without destroying the lattice registry. By intercalating Sn-atoms an ordered  $\sqrt{3} \times \sqrt{3}$  R30° Sn-Ni alloy is formed at the interface. The Sn intercalation process is characterized by Auger electron spectroscopy (AES) and low energy electron diffraction (LEED). In this alloy Sn substitutes for surface Ni atoms without changing the lattice parameter of the substrate and consequently the registry between the metal substrate and graphene is maintained. DFT simulations indicate that Sn alloying with Ni weakens the interaction of graphene with the metal substrate and consequently increasing the graphene-substrate distance and restoring the graphene  $\pi$ -band close to the position of free-standing graphene. Atomic-resolution scanning tunneling microscopy (STM) imaging reveals that the alloy periodicity is reproduced in the graphene layer, i.e. a  $\sqrt{3} \times \sqrt{3}$  R30° superstructure is imposed on the graphene by the alloy substrate. This indicates a variation of the local density of states for C-atoms located on top of Sn-substrate sites compared to Ni-sites. Further experimental and theoretical characterization of the influence of the substrate on the electronic and structural properties of graphene is ongoing.

[1] J. Winterlin and M.-L. Bocquet, *Surf. Sci.* **603**, 1841-1852 (2009)

[2] J. Lahiri et al., *Nano Lett.* **11**, 518-522 (2010)

[3] A. Varykhalov et al., *Phys. Rev. Lett.*, **101**, 157601 (2008)

11:40am **SS-FrM11 Silicene Epitaxial Sheets: Silicon New Start**, P. Vogt, Aix Marseille Univ, CNRS-CINaM, France and Technische Universität Berlin, Germany, P. De Padova, C. Quaresima, CNR-ISM, Italy, J. Avila, E. Frantzeskakis, M.C. Asensio, Synchrotron SOLEIL, France, B. Ealet, Aix Marseille Univ, CNRS-CINaM, France, G. Le Lay, Aix Marseille Univ, CNRS-CINaM, France and CNR-ISM, Italy

We have just synthesized in Marseille silicene sheets [1], i.e., atom-thin two-dimensional graphene-like silicon layers with an in-plane Si-Si interatomic distance of 0.23 nm [2], upon in-situ epitaxial growth on silver (111) surfaces. The honeycomb atomic structure is revealed in Scanning Tunneling Microscopy, while the long-range epitaxial order is confirmed by sharp 4x4 Low Energy Electron Diffraction patterns. Dirac cones at the K and K' points of the silicene Brillouin zone, evidenced in High-Resolution Synchrotron Radiation Angle-Resolved PhotoElectron Spectroscopy measurements, point to massless relativistic fermions with a Fermi velocity of 1.3E6 m/s, as theoretically predicted [3], quite the same as graphene, and four times higher than previously obtained on a one-dimensional grating of silicene nano-ribbons [4]. Density Functional Theory calculations including the Ag(111) substrate confirm the stability of the epitaxial arrangement. The demonstration that silicon can form sheets of silicene, a two dimensional honeycomb structure, which does not exist in Nature, is tantalizing for new Physics. Silicon being the workhorse of electronics industry, this synthesis could have a major impact for novel devices because of the compatibility with existing Si technologies.

[1] P. Vogt, P. De Padova, C. Quaresima, J. Avila, E. Frantzeskakis, M.C. Asensio and G. Le Lay, submitted

[2] G. G. Guzman-Verri and L.C. Lew Yan Voon, *Phys. Rev. B* **76**, 75132 (2007).

[3] M. Houssa, G. Pourtois, M. Heyns, V.V. Afanas'ev, and A. Stesmans, *J. Electrochem. Soc.* **158**, H107 (2011)

[4] P. De Padova et al., *Appl. Phys. Lett.*, **96**, 261905 (2010)



# Authors Index

**Bold page numbers indicate the presenter**

## — A —

Abb, S.: SS2-MoA2, 10  
Abdulgalil, A.: SS1-MoM1, 4  
Acharya, D.: SS1-TuM11, **16**; SS2-WeM11, 37  
Achim, C.: SS2-TuM11, 18  
Acik, M.: SS-FrM3, **55**; SS-TuP3, **25**  
Adamiv, V.: SS-ThA10, 50  
Adamska, L.: SS-FrM10, 55  
Addou, R.Q.: SS-FrM10, **55**  
Afonso, C.R.M.: SS-TuA1, 20  
Aksoy, F.: IS+AS+SS-TuM9, 14  
Allen, S.A.: SS2-TuM5, **17**  
Altfeder, I.: SE+SS-WeM4, 33  
Altman, E.I.: SS-ThA1, **49**  
Aminpour, M.: SS2-TuM6, 17  
Andersen, J.N.: IS+AS+SS-MoM4, 2; IS+AS+SS-MoM6, 3; IS+AS+SS-MoM9, 3  
Anderson, E.V.: TR+AS+SS-ThM11, 48  
Arahara, S.: SS-TuP27, **29**  
Arakawa, I.: SS1-MoA10, **10**  
Arakawa, K.: SS-FrM2, 54  
Armbrust, N.: SS-TuP12, 27  
Asensio, M.C.: SS-FrM11, 56  
Assaf, E.M.: SS-TuA1, 20  
Avila, J.: SS-FrM11, 56  
Azamoum, Y.: PS+SS-WeM9, 32  
Aznárez, J.A.: SS-TuP29, 29

## — B —

Baddorf, A.: ET+EM+SS-MoM3, **1**  
Baer, M.: SS1-MoM6, 4  
Baglin, V.: VT+MN+NS+SS+AS-TuA12, 23  
Bagus, P.S.: AC+SS-ThM1, **42**; IS+AS+SS-MoM5, 3  
Bajaj, S.: EM+SS-FrM7, 53  
Balaeff, A.: SS2-TuM11, 18  
Bałkowiec, A.: SS1-WeM12, 35  
Ballard, J.: IS+AS+SS-MoM10, 3  
Balmes, O.: IS+AS+SS-MoM6, 3  
Baraket, M.: GR+NS+PS+SS-ThM12, 45  
Barlow, I.: TF+EM+SS-ThA4, 50  
Bartels, L.: SS2-MoA4, **10**; SS-FrM1, 54  
Bartelt, N.C.: SS-FrM7, **55**  
Bartynski, R.A.: SS1-WeM5, 34; SS-TuA2, **20**; SS-TuP22, 28; SS-WeA4, 40  
Barybin, M.: SS2-MoA3, 10  
Baski, A.A.: SS-ThA9, 49  
Batzill, M.: SS-FrM10, 55; SS-WeA3, 40  
Beckers, M.: IS+AS+SS-TuM6, 13  
Beckford, S.: TR+AS+SS-ThM2, 47  
Beerbom, M.M.: SS2-TuM11, 18  
Behafarid, F.: SS-TuP28, **29**  
Behm, R.J.: SS1-WeM4, 34; SS-FrM6, 55  
Belianinov, A.: SS1-WeM6, **34**  
Bennett-Kennett, R.B.: SS1-MoA11, 10  
Bennewitz, R.: TR+AS+SS-ThM1, 47  
Bent, S.F.: SS1-MoA8, 9  
Beratan, D.N.: SS2-TuM11, 18  
Beringer, D.: VT+MN+NS+SS+AS-TuA9, 23  
Berman, D.: VT+MN+NS+SS+AS-TuA3, **22**  
Berrie, C.L.: SS2-MoA3, **10**  
Besenbacher, F.: SS2-WeM2, 35; SS-ThM10, 46  
Beye, M.: SS2-MoM2, 5  
Beyer, A.: GR+NS+PS+SS-ThM4, 44  
Bezer, S.: SS2-TuM11, 18  
Biegalski, M.D.: SS-WeA8, 40  
Blechle, J.M.: PS+SS-WeM5, **31**  
Blomberg, S.: IS+AS+SS-MoM4, 2  
Bluhm, H.: IS+AS+SS-TuM9, 14; SS-ThM9, 46  
Bollmann, T.R.J.: IS+AS+SS-MoA7, 7  
Bonnell, D.A.: SS-ThA3, 49; SS-ThA4, 49  
Booth, J.-P.: PS+SS-WeM9, **32**  
Borg, A.: IS+AS+SS-MoM4, 2  
Bouchoule, S.: PS+SS-WeM1, **31**  
Boyle, T.J.: SS-WeA12, 41  
Bradley, J.D.: SS1-MoA11, 10

Bradley, Q.X.: SS1-MoA11, 10  
Brauer, J.L.: SS1-WeM11, **35**  
Braunstein, P.: SS+EM-TuA4, 19  
Bregliozzi, G.: VT+MN+NS+SS+AS-TuA12, 23  
Broach, A.L.: AC+SS-ThM3, 42  
Brown, A.: SS2-TuM12, 18  
Brown, R.D.: SS2-MoM4, **5**  
Brueck, S.: BI+AS+NS+SS-WeA9, 39  
Bruix, A.: IS+AS+SS-MoM3, 2  
Brumbach, M.T.: SS-WeA12, **41**  
Buchholz, M.: SS-WeA2, **39**  
Bucholz, E.W.: TR+AS+SS-ThM10, **48**  
Bultman, J.: SE+SS-WeM9, 33  
Burak, Ya.: SS-ThA10, 50  
Burghaus, U.: SS2-MoM9, 6; SS-ThM1, 45  
Burnham, N.A.: TR+AS+SS-ThM11, **48**

## — C —

Cabailh, G.: SS-ThM5, 45  
Cagg, B.A.: SS-TuA9, 21; SS-TuP5, 26  
Calaza, F.C.: SS1-TuM12, **16**; SS2-WeM9, 36; SS-WeA8, 40  
Caldwell, J.D.: EM+SS-FrM1, 53  
Calley, W.L.: IS+AS+SS-MoA6, 7  
Calvey, J.: VT+MN+NS+SS+AS-TuA11, 23  
Camillone III, N.: SS2-WeM11, 37  
Campbell, C.T.: SS1-TuM2, 15; SS-ThM6, 46  
Canova, F.F.: SS-ThM10, 46  
Carlsson, P.-A.: IS+AS+SS-MoM6, 3  
Carpick, R.W.: TR+AS+SS-ThM12, 48; TR+AS+SS-ThM6, 47  
Caruso, A.N.: SS-TuP17, 28  
Castner, D.G.: SS1-MoA9, 9  
Chabal, Y.J.: IS+AS+SS-MoM10, 3; SS1-TuM4, 15; SS-FrM3, **55**; SS-TuP3, 25  
Chabert, P.: PS+SS-WeM9, 32  
Chagarov, E.A.: SS-ThA6, 49  
Chakradhar, A.: SS-ThM1, **45**  
Chambers, S.A.: IS+AS+SS-MoM5, 3  
Chang, J.P.: AC+SS-ThM10, 43; PS+SS-WeM2, 31  
Chaudhuri, S.: SS1-TuM4, 15  
Chen, D.: IS+AS+SS-MoA8, 8  
Chen, D.A.: SS1-TuM3, 15; SS-TuA9, **21**; SS-TuP5, 26  
Chen, G.: SE+SS-WeM2, **33**  
Chen, N.: SS2-MoM8, 6  
Chen, W.: SS1-WeM5, 34; SS-TuA2, 20  
Cheng, M.: SS-ThM9, 46  
Cheng, Z.: SS2-MoA4, 10  
Chhowalla, M.: SS-FrM3, 55  
Chiggiato, P.: VT+MN+NS+SS+AS-TuA12, **23**  
Chitre, K.: SS-WeA4, 40  
Cho, E.K.: SS2-TuM12, **18**  
Cho, K.: SS-FrM3, 55  
Choi, J.H.: AC+SS-ThM10, 43  
Chopra, I.: SS1-TuM4, **15**  
Chopra, N.: TF+EM+SS-ThA7, **51**  
Christen, H.M.: SS-WeA8, 40  
Christophis, C.: IS+AS+SS-TuM6, 13  
Clavero, C.: VT+MN+NS+SS+AS-TuA8, **23**; VT+MN+NS+SS+AS-TuA9, 23  
Clemens, J.B.: SS-ThA6, 49  
Coffee, R.: SS2-MoM2, 5  
Coh, S.: SS-WeA4, 40  
Cohen, H.: TF+EM+SS-ThA11, **52**  
Collings, M.: SS1-MoM1, 4  
Conway, J.: VT+MN+NS+SS+AS-TuA11, 23  
Cook, B.: ET+EM+SS-MoM11, 2  
Costa Pinto, P.: VT+MN+NS+SS+AS-TuA12, 23  
Cox, D.F.: SS-ThM2, 45  
Crittenden, J.A.: VT+MN+NS+SS+AS-TuA11, 23  
Crowhurst, J.C.: AC+SS-ThM5, **42**  
Croy, J.R.: SS-TuA10, 21  
Cruguel, H.: SS-ThM5, 45  
Culbertson, R.J.: SS1-MoA11, 10

## — D —

Dahal, A.: SS-FrM10, 55  
Dai, Z.: AC+SS-ThM5, 42  
Dassenoy, F.: TR+AS+SS-ThM10, 48  
De Alwis, A.: SS1-MoA3, 8  
De Graeve, I.: SS1-WeM12, 35  
De Jonge, N.: IS+AS+SS-TuM3, **13**; IS+AS+SS-TuM5, 13  
De Padova, P.: SS-FrM11, 56  
Dela Rosa, A.: SS2-MoA3, 10  
Dell'Angela, M.: SS2-MoM2, 5  
DelSesto, D.: SS2-MoM10, 6  
Demers-Carpentier, V.: SS1-MoA1, 8  
Deng, X.: SS1-TuM10, 16; SS-ThM11, **46**  
Deppert, N.: IS+AS+SS-MoM4, 2  
DeRose, J.A.: SS1-WeM12, **35**  
Desai, T.V.: IS+AS+SS-TuM12, 14  
DeSisto, W.J.: SS1-TuM1, 14  
Deskinds, N.A.: SS2-WeM12, 37  
Deslippe, J.: SS-TuP2, 25  
Devine, B.: GR+NS+PS+SS-ThM10, 45  
Diaconescu, B.: SS-FrM9, **55**  
Dignard, P.: ET+EM+SS-MoM11, 2  
Dobrin, S.: SS1-WeM9, 35  
Dohnalek, Z.: SS2-WeM12, 37; SS-WeA10, 41  
Dohnálek, Z.: SS1-MoA4, 9; SS1-TuM11, 16; SS-WeA1, 39  
Dombrowski, E.: SS2-MoM10, 6  
Dong, Y.: SS-ThM2, **45**; TR+AS+SS-ThM12, **48**  
Donnelly, V.M.: PS+SS-WeM11, 32; PS+SS-WeM6, 32  
Doolittle, W.A.: IS+AS+SS-MoA6, 7  
Dorman, J.A.: AC+SS-ThM10, **43**  
Doudin, B.: SS+EM-TuA4, 19  
Dowben, P.A.: SS+EM-TuA4, 19; SS-ThA10, **50**  
Drews, S.N.: SS1-MoA11, 10  
Driver, M.S.: SS-TuP17, **28**  
Droopad, R.: SS-ThA6, 49  
Droubay, T.: IS+AS+SS-MoM5, 3  
Du, Y.G.: SS2-WeM12, 37; SS-WeA1, 39  
Dubey, G.: TF+EM+SS-ThA3, **50**  
Dupuis, M.: SS2-WeM12, 37  
Duran, A.: SS-TuP23, 28  
Durr, M.: SS-TuP12, 27

## — E —

Ealet, B.: SS-FrM11, 56  
Eck, W.: TF+EM+SS-ThA6, 51  
Economou, D.J.: PS+SS-WeM6, 32  
Eddy, Jr., C.R.: EM+SS-FrM1, 53  
Einstein, T.L.: SS2-MoA4, 10  
El Zubir, O.: TF+EM+SS-ThA4, **50**  
Ellis-Terrell, C.: TR+AS+SS-ThM2, **47**  
El-Zubir, O.: BI+AS+NS+SS-WeA9, 39  
Engstfeld, A.K.: SS1-WeM4, **34**; SS-FrM6, 55  
Engstrom, J.R.: IS+AS+SS-TuM12, 14  
Eralp, T.: IS+AS+SS-TuM9, 14  
Erkens, I.J.M.: IS+AS+SS-MoA9, 8  
Ermanoski, I.: SS-ThM12, **46**  
Escamilla, R.: SS-TuP23, 28  
Escano, M.C.: SS-TuP8, 26  
Escobar, C.A.: BI+AS+NS+SS-WeA11, **39**  
Escudero, C.: IS+AS+SS-TuM1, **13**  
Esfarjani, K.: SE+SS-WeM2, 33

## — F —

Fairbrother, H.: SS1-MoA7, **9**  
Falconi, R.: SS-TuP23, 28  
Falk, M.L.: TR+AS+SS-ThM4, **47**  
Faubel, M.: IS+AS+SS-TuM11, 14; SS1-MoM5, 4  
Fedorov, A.V.: SS-TuP2, 25  
Feici, R.: IS+AS+SS-MoM6, 3  
Feng, X.: GR+NS+PS+SS-ThM3, **44**; IS+AS+SS-MoA8, 8  
Fischer, D.A.: SS-WeA4, 40  
Fisher, E.R.: PS+SS-WeM5, 31

Flake, J.: SS-WeA11, 41  
 Flood, A.H.: SS-TuP15, 28  
 Flores, M.: SS-TuP23, 28  
 Foehlich, A.: SS2-MoM2, 5  
 Foster, A.S.: SS-ThM10, 46  
 Foussekis, M.: SS-ThA9, 49  
 Frantzeskakis, E.: SS-FrM11, 56  
 Frederick, B.G.: SS1-TuM1, 14  
 Frenkel, A.I.: IS+AS+SS-MoM1, 2  
 Freund, H.-J.: SS2-WeM10, 36  
 Friend, C.M.: SS2-MoM3, 5; SS-TuA8, 21; SS-TuP1, 25  
 Fujikawa, S.: SS-TuP9, 27  
 Fujiyama, H.: IS-TuP1, 25  
 Fukasawa, M.: PS+SS-WeM12, 32

— **G** —

Galhenage, R.P.: SS-TuP5, 26  
 Galoppini, E.: SS-WeA4, 40  
 Garcia Flores, H.G.: AC+SS-ThM3, 42  
 Garra, J.: SS-ThA4, 49  
 Garvey, M.: TR+AS+SS-ThM9, 47  
 Gaskill, D.K.: EM+SS-FrM1, 53  
 Gatilova, L.: PS+SS-WeM1, 31  
 Gellman, A.J.: SS1-MoA3, 8; SS2-WeM6, 36; SS-TuA11, 21  
 Gengler, J.: SE+SS-WeM5, 33; SE+SS-WeM9, 33  
 Ghampon, I.T.: SS1-TuM1, 14  
 Gibson, K.D.: SS1-MoM2, 4  
 Giewekemeyer, K.: IS+AS+SS-TuM6, 13  
 Gladh, J.: SS2-MoM2, 5  
 Goebel, H.: SS2-WeM2, 35  
 Gölzhäuser, A.: GR+NS+PS+SS-ThM4, 44; SS2-TuM2, 16  
 Gong, C.: SS-FrM3, 55  
 González González, A.: SS-TuP29, 29  
 Goodman, D.W.: SS2-WeM5, 36; SS-TuA3, 21  
 Gorai, P.: SS-ThA8, 49  
 Gord, J.R.: SE+SS-WeM5, 33  
 Gorniak, T.: IS+AS+SS-TuM6, 13  
 Gousvami, N.N.: TR+AS+SS-ThM1, 47  
 Goundie, B.M.: SS1-TuM1, 14  
 Grass, M.E.: IS+AS+SS-MoM4, 2; IS+AS+SS-TuM9, 14  
 Greene, G.W.: SS2-MoA9, 11  
 Greenlee, J.D.: IS+AS+SS-MoA6, 7  
 Grierson, D.S.: TR+AS+SS-ThM6, 47  
 Grönbeck, H.: IS+AS+SS-MoM4, 2; IS+AS+SS-MoM6, 3  
 Grundmeier, G.: SS-TuP10, 27  
 Grunze, M.: IS+AS+SS-TuM6, 13  
 Guilet, S.: PS+SS-WeM1, 31  
 Guisinger, N.P.: EM+SS-FrM11, 54; VT+MN+NS+SS+AS-TuA8, 23  
 Gumuslu, G.: SS2-WeM6, 36  
 Guo, Q.: SS2-MoA11, 11; SS2-WeM5, 36  
 Gustafson, J.: IS+AS+SS-MoM4, 2; IS+AS+SS-MoM6, 3  
 Gutmann, S.: SS2-TuM11, 18  
 Gyenge, E.: SS-TuP8, 26

— **H** —

Hacker, C.A.: TF+EM+SS-ThA9, 51  
 Hagelberg, F.: SS-FrM9, 55  
 Hagen, C.: SS1-MoA7, 9  
 Ham, H.C.: SS1-TuM9, 16; SS-TuA12, 22; SS-TuP14, 28  
 Hamaguchi, S.: PS+SS-WeM10, 32; PS+SS-WeM12, 32  
 Hamers, R.J.: BI+AS+NS+SS-WeA3, 38  
 Hammer, B.: SS1-MoA1, 8  
 Hanson, J.A.: SS2-MoA8, 11  
 Happel, M.: IS+AS+SS-MoM3, 2  
 Hara, K.: IS-TuP1, 25  
 Harl, R.R.: BI+AS+NS+SS-WeA10, 39  
 Harrison, J.A.: TR+AS+SS-ThM6, 47  
 Hart, M.A.: SS1-MoA11, 10  
 Hasan, M.Z.: EM+SS-FrM3, 53  
 Hasegawa, S.: ET+EM+SS-MoM1, 1  
 Hatton, G.: TR+AS+SS-ThM2, 47

Hausen, F.: TR+AS+SS-ThM1, 47  
 Hayden, B.E.: SS-TuA1, 20  
 He, W.: SS-TuP5, 26  
 Heilemann, M.: GR+NS+PS+SS-ThM4, 44  
 Heinrich, H.: SS-TuA10, 21  
 Held, G.: IS+AS+SS-TuM9, 14  
 Hellman, A.: IS+AS+SS-MoM6, 3  
 Helveg, S.: SS-ThM10, 46  
 Hemminger, J.C.: IS+AS+SS-TuM11, 14; SS1-MoM3, 4; SS1-MoM5, 4; SS-ThM9, 46  
 Henderson, W.E.: IS+AS+SS-MoA6, 7  
 Hennies, F.: IS+AS+SS-MoM9, 3  
 Herbots, N.X.: SS1-MoA11, 10  
 Hernandez, S.C.: GR+NS+PS+SS-ThM12, 45  
 Hersam, M.C.: GR+NS+PS+SS-ThM11, 45  
 Hess, R.F.: SS-WeA12, 41  
 Hinnemann, B.: SS-ThM10, 46  
 Hirahara, T.: ET+EM+SS-MoM1, 1  
 Hirsch, B.E.: SS-TuP15, 28  
 Hobart, K.D.: EM+SS-FrM1, 53  
 Hoepker, N.C.: EM+SS-FrM8, 54  
 Hofer, U.: SS-TuP12, 27  
 Holbrook, R.D.: BI+AS+NS+SS-WeA3, 38  
 Hollister, A.: SS-ThA8, 49  
 Holsclaw, B.: SS1-MoA3, 8  
 Hong, S.: SS1-TuM3, 15; SS-TuA9, 21  
 Hossain, Md.Z.: GR+NS+PS+SS-ThM11, 45  
 Hoster, H.E.: SS-FrM6, 55  
 Hu, J.: SE+SS-WeM4, 33; SE+SS-WeM9, 33  
 Hu, S.: IS+AS+SS-MoA8, 8  
 Hu, W.: SS-TuP9, 27  
 Huang, Y.: SS2-MoM8, 6  
 Huerta, L.: SS-TuP23, 28  
 Hutcheon, I.D.: AC+SS-ThM5, 42  
 Hwang, C.G.: SS-TuP2, 25  
 Hwang, G.S.: SS1-TuM9, 16; SS-TuA12, 22; SS-TuP14, 28

— **I** —

Ibrahim, S.: SS-TuP25, 29  
 Illas, F.: IS+AS+SS-MoM3, 2  
 Ilton, E.S.: AC+SS-ThM1, 42  
 Ilyas, N.: SS+EM-TuA3, 19  
 Imhoff, E.A.: EM+SS-FrM1, 53  
 Isobe, M.: PS+SS-WeM12, 32  
 Israelachvili, J.N.: SS2-MoA9, 11  
 Ito, T.: PS+SS-WeM10, 32

— **J** —

Jantschner, O.: SE+SS-WeM6, 33  
 Jaye, C.: SS-WeA4, 40  
 Jennings, G.K.: BI+AS+NS+SS-WeA11, 39  
 Jimenez, J.M.: VT+MN+NS+SS+AS-TuA12, 23  
 Johansson, N.: IS+AS+SS-MoM9, 3  
 Johns, J.E.: GR+NS+PS+SS-ThM11, 45  
 Johnson, J.: IS-TuP3, 25  
 Joshi, A.: AC+SS-ThM10, 43  
 Jung, S.J.: IS+AS+SS-TuM10, 14  
 Junkermeier, C.E.: GR+NS+PS+SS-ThM12, 45  
 Jupille, J.: SS-ThM5, 45

— **K** —

Kacher, J.: IS+AS+SS-MoA1, 7  
 Kang, S.-Y.: PS+SS-WeM10, 32  
 Karahashi, K.: PS+SS-WeM10, 32  
 Karakoti, A.S.: SS-WeA7, 40  
 Karki, S.: SS-TuP17, 28  
 Karp, E.M.: SS1-TuM2, 15  
 Kasai, H.: SS-TuP8, 26  
 Kaspar, T.C.: IS+AS+SS-MoM5, 3  
 Katayama, T.: SS2-MoM2, 5  
 Kaufman-Osborn, T.: SS-ThA6, 49  
 Kaur, S.: SE+SS-WeM11, 34  
 Kawasaki, J.K.: EM+SS-FrM2, 53  
 Kay, B.D.: SS1-MoA4, 9; SS1-MoM10, 4; SS1-TuM11, 16; SS-WeA10, 41  
 Kaya, S.: SS2-MoM2, 5  
 Kayani, A.: AC+SS-ThM11, 43  
 Keating, P.L.: TR+AS+SS-ThM6, 47  
 Kelley, M.: VT+MN+NS+SS+AS-TuA4, 22  
 Kellogg, G.L.: SS-ThM12, 46

Kelly, L.L.: SS+EM-TuA3, 19  
 Kemper, T.: SS1-MoA6, 9  
 Kent, T.: SS+EM-TuA9, 19; SS-ThA6, 49  
 Kershis, M.D.: SS-TuP30, 30  
 Kessels, W.M.M.: IS+AS+SS-MoA9, 8  
 Ketsman, I.: SS-ThA10, 50  
 Khare, R.: PS+SS-WeM11, 32  
 Khosravian, H.: SS-FrM5, 55  
 Kiejna, A.: SS2-TuM6, 17  
 Killelea, D.R.: SS1-MoM2, 4  
 Kim, B.I.: SS2-MoA8, 11  
 Kim, D.: SS2-MoA4, 10; SS-FrM1, 54  
 Kim, D.H.: IS+AS+SS-TuM10, 14  
 Kim, K.-J.: SS-TuP13, 27  
 Kim, S.: IS+AS+SS-TuM10, 14  
 Kim, T.H.: ET+EM+SS-MoM8, 1  
 Kim, W.K.: TR+AS+SS-ThM4, 47  
 Kim, Y.K.: SS1-MoA4, 9  
 Kimmel, G.A.: SS1-MoM6, 4; SS-WeA9, 41  
 Kish, E.R.: IS+AS+SS-TuM12, 14  
 Kitajima, T.: PS+SS-WeM3, 31  
 Kizilkaya, O.: SS+EM-TuA4, 19  
 Knight, K.B.: AC+SS-ThM5, 42  
 Knoops, H.C.M.: IS+AS+SS-MoA9, 8  
 Knudsen, J.: IS+AS+SS-MoM9, 3; SS-ThM10, 46  
 Koel, B.E.: SS1-WeM5, 34; SS-TuP4, 26  
 Komarneni, M.: SS2-MoM9, 6  
 Komiya, A.: SE+SS-WeM10, 34  
 Kondo, T.: SS2-MoM11, 6; SS-FrM2, 54  
 Kondratyuk, P.: SS1-MoA3, 8; SS2-WeM6, 36; SS-TuA11, 21  
 Korolkov, V.V.: SS2-TuM5, 17  
 Kreil, J.: SS+EM-TuA10, 20  
 Krim, J.: VT+MN+NS+SS+AS-TuA3, 22  
 Krishnamoorthy, S.: EM+SS-FrM7, 53  
 Kristiansen, K.: SS2-MoA9, 11  
 Krupin, O.: SS2-MoM2, 5  
 Kruse, P.: SS-TuP6, 26  
 Kuchibhatla, S.V.N.T.: AC+SS-ThM11, 43; SS-WeA7, 40  
 Kuech, T.F.: SS2-TuM12, 18  
 Kummel, A.C.: SS+EM-TuA9, 19; SS-ThA6, 49  
 Kurosu, M.: SS-TuP26, 29  
 Kurtz, R.: SS-WeA11, 41  
 Kurzydowski, K.J.: SS1-WeM12, 35  
 Kuzmanich, G.: AC+SS-ThM10, 43

— **L** —

Labuda, A.: TR+AS+SS-ThM1, 47  
 LaFranzo, N.A.: TF+EM+SS-ThA10, 51  
 Lahouij, L.: TR+AS+SS-ThM10, 48  
 Laibinis, P.: BI+AS+NS+SS-WeA10, 39  
 Landheer, K.: SS1-MoA7, 9  
 Langhammer, C.B.: BI+AS+NS+SS-WeA4, 38  
 Lanza, G.: VT+MN+NS+SS+AS-TuA12, 23  
 Lanzara, A.: SS-TuP2, 25  
 Larsson, E.M.K.: BI+AS+NS+SS-WeA4, 38  
 Lauritsen, J.V.: SS2-WeM2, 35; SS-ThM10, 46  
 Lawrie, J.: BI+AS+NS+SS-WeA10, 39  
 Lazzari, R.: SS-ThM5, 45  
 Le Gratiet, L.: PS+SS-WeM1, 31  
 Le Lay, G.: SS-FrM11, 56  
 Le, D.: SS2-TuM6, 17  
 Le, M.: SS-WeA11, 41  
 LeClair, P.: SS+EM-TuA10, 20  
 Lee, D.: SS1-MoA6, 9  
 Lee, G.: SS-FrM3, 55  
 Lee, J.: SS1-TuM10, 16; SS-ThM11, 46; SS-TuP13, 27  
 Lee, J.S.: SS-ThA6, 49  
 Lee, S.: SS+EM-TuA9, 19  
 Lee, W.K.: GR+NS+PS+SS-ThM12, 45  
 Lee, Y.: SS-TuP13, 27  
 Leggett, G.: BI+AS+NS+SS-WeA9, 39; TF+EM+SS-ThA4, 50  
 Lekkala, S.: EM+SS-FrM8, 54  
 Levine, M.S.: SS-TuA9, 21; SS-TuP5, 26  
 Lewis, T.: IS+AS+SS-TuM11, 14; SS1-MoM5, 4  
 Li, F.: SS2-MoA11, 11  
 Li, M.: SS2-WeM9, 36

Li, Q.: TR+AS+SS-ThM12, 48  
 Li, Y.: VT+MN+NS+SS+AS-TuA11, **23**  
 Li, Z.J.: SS1-MoA4, **9**  
 Liang, T.: GR+NS+PS+SS-ThM10, **45**  
 Liang, Z.: SS-FrM5, **55**  
 Libuda, J.: IS+AS+SS-MoM3, 2  
 Lidzey, D.: BI+AS+NS+SS-WeA9, 39  
 Lim, H.: SS2-MoA1, **10**  
 Lin, X.: SS1-TuM11, 16; SS-WeA10, **41**  
 Linderoth, T.R.: SS2-TuM9, **17**  
 Lipponer, M.A.: SS-TuP12, **27**  
 Liu, D.-J.: SS1-WeM3, 34; SS2-MoA10, **11**  
 Liu, G.: IS+AS+SS-MoA1, 7  
 Liu, J.: TR+AS+SS-ThM6, 47  
 Liu, L.: SS2-WeM5, **36**  
 Liu, X.: VT+MN+NS+SS+AS-TuA11, 23  
 Liu, Y.: SS-ThM9, **46**  
 Liu, Z.: IS+AS+SS-MoM4, 2; IS+AS+SS-TuM9, **14**  
 Lofaro, Jr., J.C.: SS2-WeM1, **35**  
 Lopez, G.P.: BI+AS+NS+SS-WeA9, 39  
 Lopinski, G.P.: TF+EM+SS-ThA3, 50  
 Lorenz, C.U.: SS-FrM6, **55**  
 Loring, R.F.: EM+SS-FrM8, 54  
 Losovyj, Ya.: SS-ThA10, 50  
 Losvyj, Y.B.: SS+EM-TuA4, 19  
 Louie, S.G.: SS-TuP2, 25  
 Louis, K.: BI+AS+NS+SS-WeA3, 38  
 Lowder, J.E.: IS+AS+SS-MoA6, 7  
 Lu, W.: SS-FrM1, 54  
 Lukaszew, R.A.: VT+MN+NS+SS+AS-TuA8, 23;  
 VT+MN+NS+SS+AS-TuA9, 23  
 Lundgren, E.: IS+AS+SS-MoM4, 2; IS+AS+SS-  
 MoM6, 3; SS-ThM10, 46  
 Lundwall, Matt: SS-TuA3, **21**  
 Luttrell, T.: SS-WeA3, 40  
 Lykhach, Y.: IS+AS+SS-MoM3, 2  
 Lyubinsky, I.: SS2-WeM12, **37**; SS-WeA1, 39;  
 SS-WeA10, 41

— **M** —  
 Mackus, A.J.M.: IS+AS+SS-MoA9, 8  
 Madix, R.J.: SS2-MoM3, 5; SS-TuA8, 21; SS-  
 TuP1, 25  
 Maehashi, K.: GR+NS+PS+SS-ThM9, **44**  
 Maier, S.: GR+NS+PS+SS-ThM3, 44  
 Maluf, S.S.: SS-TuA1, **20**  
 Mann, J.: SS-FrM1, 54  
 Marchack, N.: PS+SS-WeM2, **31**  
 Margarella, A.: SS1-MoM5, 4  
 Marohn, J.A.: EM+SS-FrM8, 54  
 Mårtensson, N.: IS+AS+SS-MoM9, 3  
 Martin, J.M.: TR+AS+SS-ThM10, 48  
 Martin, N.M.: IS+AS+SS-MoM4, 2; IS+AS+SS-  
 MoM6, 3; SS-ThM10, 46  
 Martini, A.: TR+AS+SS-ThM12, 48  
 Matolin, V.: IS+AS+SS-MoM3, 2  
 Matranga, C.: SS-ThM11, 46  
 Matsuda, Y.: IS-TuP1, 25  
 Matsumoto, D.: SS1-MoA10, 10  
 Matsumoto, K.: GR+NS+PS+SS-ThM9, 44  
 Matsumoto, S.: SE+SS-WeM10, 34  
 Matsuoka, D.: SS-TuP11, 27  
 Mattevi, C.: SS-FrM3, 55  
 Maurer, J.A.: TF+EM+SS-ThA10, 51  
 Mavrikakis, M.: SS1-TuM5, **15**  
 Mavrokefalos, A.: SE+SS-WeM2, 33  
 May, R.A.: SS1-MoM10, 4  
 McBreen, P.H.: SS1-MoA1, 8  
 McCarthy, J.: BI+AS+NS+SS-WeA3, 38  
 McClory, J.: SS-ThA10, 50  
 McCoustra, M.: SS1-MoM1, 4  
 McDonald, K.P.: SS-TuP15, 28  
 McDonnell, S.: IS+AS+SS-MoM10, **3**  
 Mei, W.-N.: SS-ThA10, 50  
 Meinander, K.: SS-ThM10, **46**  
 Melitz, W.: SS-ThA6, 49  
 Messing, M.E.: IS+AS+SS-MoM4, 2  
 Meulenbergh, R.W.: SS1-TuM1, 14  
 Meyer, R.: SS-FrM5, 55

Meyerbröker, N.: TF+EM+SS-ThA6, **51**  
 Michalski, J.: SS1-WeM12, 35  
 Migani, A.: IS+AS+SS-MoM3, 2  
 Miller, G.: AC+SS-ThM9, 43  
 Miller, J.B.: SS2-WeM6, 36; SS-TuA11, 21  
 Miller, M.: TR+AS+SS-ThM2, 47  
 Min, Y.H.: IS+AS+SS-TuM10, **14**  
 Mitterer, C.: SE+SS-WeM6, **33**  
 Miura, T.: SS1-MoA10, 10  
 Mizotani, K.: PS+SS-WeM12, **32**  
 Monti, O.L.A.: SS+EM-TuA3, **19**  
 Moore, D.P.: AC+SS-ThM3, 42  
 Moorman, M.W.: SS-WeA12, 41  
 Morales, E.H.: SS-ThA3, **49**; SS-ThA4, 49  
 Morgenstern, K.: SS2-MoM5, 5  
 Morreale, B.D.: SS2-WeM6, 36; SS-TuA11, 21  
 Moseley, M.W.: IS+AS+SS-MoA6, 7  
 Mullins, D.R.: SS1-TuM12, 16; SS-WeA8, **40**  
 Mullins, D.R.: SS2-WeM9, 36  
 Mundy, C.J.: SS1-MoM6, 4  
 Muratore, C.: SE+SS-WeM5, 33; SE+SS-WeM6,  
 33; SE+SS-WeM9, 33  
 Muzik, H.: SS2-TuM2, 16  
 Myers-Ward, R.L.: EM+SS-FrM1, **53**

— **N** —  
 Naboka, M.: SS2-TuM2, 16  
 Nachimuthu, P.: SS-WeA7, 40  
 Nakamura, J.: SS2-MoM11, 6; SS-FrM2, 54  
 Nakanishi, H.: SS-TuP8, 26  
 Nandasiri, M.I.: AC+SS-ThM11, **43**; SS-WeA7, 40  
 Nascente, P.A.P.: SS-TuA1, 20  
 Nath, D.N.: EM+SS-FrM7, 53  
 Neal, B.: SS2-MoA3, 10  
 Nefedov, A.: SS2-TuM2, **16**; SS-WeA2, 39  
 Nelin, C.J.: AC+SS-ThM1, 42  
 Nelson, A.J.: AC+SS-ThM5, 42  
 Neyman, K.M.: IS+AS+SS-MoM3, 2  
 Nilius, N.: SS2-WeM10, 36  
 Nilsson, A.: SS2-MoM2, 5  
 Nogami, J.: SS1-WeM9, **35**  
 Nordlund, D.: SS2-MoM2, 5  
 Nottbohm, C.T.: GR+NS+PS+SS-ThM4, 44  
 Nyakiti, L.O.: EM+SS-FrM1, 53

— **O** —  
 Oberg, H.: SS2-MoM2, 5  
 Ogasawara, H.: SS2-MoM2, 5  
 Ogletree, D.F.: SE+SS-WeM11, **34**  
 Oh, J.P.: SS-FrM2, **54**  
 Ohno, Y.: GR+NS+PS+SS-ThM9, 44  
 Oleynik, I.I.: SS-FrM10, 55  
 Olsson, A.: IS+AS+SS-MoM9, 3  
 Ono, L.K.: SS-TuA10, **21**  
 Orzelli, A.: SS-ThM5, 45  
 Osgood, R.M.: SS2-MoM1, 5  
 Ostrom, H.: SS2-MoM2, 5  
 Overbury, S.H.: SS1-TuM12, 16; SS2-WeM9, **36**;  
 SS-WeA8, 40  
 Owen, J.H.G.: IS+AS+SS-MoM10, 3  
 Ozkaya, B.: SS-TuP10, **27**

— **P** —  
 Palmer, M.A.: VT+MN+NS+SS+AS-TuA11, 23  
 Palmstrøm, C.J.: EM+SS-FrM2, 53  
 Pangan-Okimoto, K.: SS-ThA8, 49  
 Pantelides, S.T.: GR+NS+PS+SS-ThM6, 44  
 Park, C.H.: SS-TuP2, 25  
 Park, E.H.: IS+AS+SS-TuM10, 14  
 Park, J.H.: SS+EM-TuA9, **19**  
 Patriarche, G.: PS+SS-WeM1, 31  
 Paucic, A.D.: SS-TuP6, **26**  
 Peckys, D.B.: IS+AS+SS-TuM3, 13; IS+AS+SS-  
 TuM5, **13**  
 Peterson, E.: SS2-MoM10, 6  
 Petrik, N.G.: SS1-MoM6, 4; SS-WeA9, **41**  
 Petrosky, J.: SS-ThA10, 50  
 Petrova, G.P.: IS+AS+SS-MoM3, 2  
 Petterson, L.G.M.: SS2-MoM2, 5  
 Pham, C.D.: PS+SS-WeM2, 31  
 Phillipot, S.R.: GR+NS+PS+SS-ThM10, 45

Phillipot, S.R.: SS1-MoA6, 9; TR+AS+SS-ThM3,  
 47  
 Pietzsch, A.: IS+AS+SS-MoM9, 3  
 Poelsema, B.: IS+AS+SS-MoA7, 7  
 Pohl, K.: SS-FrM9, 55  
 Pookpanratana, S.: TF+EM+SS-ThA9, **51**  
 Porsgaard, S.: SS2-WeM2, 35  
 Potapenko, D.V.: SS2-MoM1, **5**  
 Prince, K.C.: IS+AS+SS-MoM3, 2  
 Priyadarshini, D.: SS-TuA11, 21  
 Pugmire, D.L.: AC+SS-ThM3, **42**  
 Pushkarev, V.: SS1-MoA3, 8

— **Q** —  
 Qin, X.: SS-TuP7, 26  
 Quang, N.T.: SS-TuP8, **26**  
 Quaresima, C.: SS-FrM11, 56

— **R** —  
 Racke, D.A.: SS+EM-TuA3, 19  
 Rahman, T.S.: SS1-TuM3, 15; SS2-TuM6, 17; SS-  
 TuA9, 21  
 Rajan, S.: EM+SS-FrM7, 53  
 Randall, J.N.: IS+AS+SS-MoM10, 3  
 Rangan, S.: SS-WeA4, **40**  
 Raravikar, N.: SE+SS-WeM11, 34  
 Rasmussen, M.K.: SS-ThM10, 46  
 Reece, C.: VT+MN+NS+SS+AS-TuA9, 23  
 Reed, A.: SE+SS-WeM9, 33  
 Reeder, L.J.: SS2-MoA8, 11  
 Reinecke, T.L.: GR+NS+PS+SS-ThM12, 45  
 Reinicker, A.: SS1-MoA3, 8  
 Ren, M.: SS-WeA11, 41  
 Reshchikov, M.A.: SS-ThA9, 49  
 Resta, A.: IS+AS+SS-MoM6, 3  
 Reutt-Robey, J.E.: SS+EM-TuA7, **19**; SS+EM-  
 TuA8, 19  
 Rhoades, R.L.: SS1-MoA11, 10  
 Richter, C.A.: TF+EM+SS-ThA9, 51  
 Rijnders, G.: IS+AS+SS-MoA3, 7  
 Roach, W.M.: VT+MN+NS+SS+AS-TuA9, **23**  
 Roberts, C.J.: SS2-TuM5, 17  
 Robertson, I.M.: IS+AS+SS-MoA1, 7  
 Robinson, J.T.: GR+NS+PS+SS-ThM1, **43**;  
 GR+NS+PS+SS-ThM12, 45; GR+NS+PS+SS-  
 ThM5, 44  
 Rocca, M.: SS-ThM5, 45  
 Rochford, J.: SS-WeA4, 40  
 Rodríguez Cañas, E.: SS-TuP29, 29  
 Rodríguez-Reyes, J.C.: SS2-MoM3, 5  
 Rogers, B.R.: BI+AS+NS+SS-WeA10, 39  
 Roldan Cuenya, B.: SS-TuA10, 21; SS-TuP28, 29  
 Roldán Cuenya, B.: SS-TuA7, **21**  
 Roozeboom, F.: IS+AS+SS-MoA9, 8  
 Rosa, L.G.: SS+EM-TuA4, 19  
 Rosei, F.: TF+EM+SS-ThA3, 50  
 Rosenberg, R.A.: EM+SS-FrM11, 54  
 Rosenberg, S.: SS1-MoA7, 9  
 Rosenhahn, A.: IS+AS+SS-TuM6, 13  
 Rousseau, R.J.: SS1-MoA4, 9; SS1-MoM6, 4  
 Roussel, P.: AC+SS-ThM3, 42  
 Routaboul, L.: SS+EM-TuA4, **19**  
 Rowe, J.E.: EM+SS-FrM9, **54**  
 Roy, A.: SE+SS-WeM4, 33  
 Roy, S.: SE+SS-WeM5, 33  
 Royer, J.: SS+EM-TuA9, 19  
 Russell, S.M.: SS1-WeM3, **34**  
 Ryan, K.E.: TR+AS+SS-ThM6, 47

— **S** —  
 Sacedón, J.L.: SS-TuP29, **29**  
 Saito, Y.: SS-FrM2, 54  
 Sakurai, M.: SS2-MoM11, 6  
 Salditt, T.: IS+AS+SS-TuM6, 13  
 Salmeron, M.: GR+NS+PS+SS-ThM3, 44;  
 IS+AS+SS-TuM1, 13  
 Sambegoro, P.: SE+SS-WeM2, 33  
 Sanghavi, S.P.: AC+SS-ThM11, 43; SS-WeA7, **40**  
 Santis, S.De.: VT+MN+NS+SS+AS-TuA11, 23  
 Sato, M.: SS-TuP24, 28; SS-TuP27, 29  
 Sauer, M.: GR+NS+PS+SS-ThM4, 44

Savio, L.: SS-ThM5, 45  
 Schildbach, M.A.: AC+SS-ThM6, 42  
 Schlaf, R.: SS2-TuM11, 18  
 Schlotter, W.F.: SS2-MoM2, 5  
 Schmutz, P.: SS1-WeM12, 35  
 Schnadt, J.: IS+AS+SS-MoM9, 3  
 Schnietz, M.: GR+NS+PS+SS-ThM4, 44  
 Schönherr, H.: BI+AS+NS+SS-WeA7, 38  
 Schultz, B.D.: EM+SS-FrM2, 53  
 Schweikert, E.A.: BI+AS+NS+SS-WeA1, 38  
 Scott, S.L.: SS-ThM3, 45  
 Seebauer, E.G.: SS-ThA8, 49  
 Sell, D.A.: SS1-MoA11, 10  
 Sellberg, J.A.: SS2-MoM2, 5  
 Semidey-Flecha, L.: SS2-WeM5, 36  
 Senkbeil, T.: IS+AS+SS-TuM6, 13  
 Shan, T.-R.: TR+AS+SS-ThM3, 47  
 Shao, Q.: SS+EM-TuA8, 19  
 Sharp, J.C.: SS-ThM6, 46  
 Shavorskiy, A.: IS+AS+SS-TuM9, 14  
 Sheehan, P.E.: GR+NS+PS+SS-ThM12, 45;  
 GR+NS+PS+SS-ThM5, 44  
 Shen, J.: SS-ThA6, 49  
 Shen, M.: SS1-WeM3, 34  
 Shen, Q.: SS-TuA2, 20  
 Shenogin, S.: SE+SS-WeM9, 33  
 Shin, H.: PS+SS-WeM6, 32  
 Shinohara, M.: IS-TuP1, 25  
 Shukur, A.: SS-TuP24, 28  
 Shukur, H.: SS-TuP24, 28; SS-TuP25, 29; SS-  
 TuP27, 29  
 Shutthanandan, V.: AC+SS-ThM11, 43  
 Sibener, S.J.: SS1-MoM2, 4; SS2-MoM4, 5  
 Siegbahn, H.: IS+AS+SS-MoM9, 3  
 Siegel, D.A.: SS-TuP2, 25  
 Siekhaus, W.J.: AC+SS-ThM5, 42; AC+SS-ThM6,  
 42  
 Sikora, J.P.: VT+MN+NS+SS+AS-TuA11, 23  
 Silbaugh, T.L.: SS1-TuM2, 15  
 Simonson, R.J.: SS-WeA12, 41  
 Sinnott, S.B.: GR+NS+PS+SS-ThM10, 45; SS1-  
 MoA6, 9; TR+AS+SS-ThM10, 48;  
 TR+AS+SS-ThM3, 47  
 Sirse, N.: PS+SS-WeM9, 32  
 Skála, T.: IS+AS+SS-MoM3, 2  
 Skomski, D.: SS2-MoA2, 10  
 Smerieri, M.: SS-ThM5, 45  
 Smith, R.S.: SS1-MoM10, 4  
 Smith, T.: SE+SS-WeM9, 33  
 Song, S.-H.: SS1-MoA9, 9  
 Sorescu, D.: SS1-TuM10, 16  
 Sorgenfrei, F.: SS2-MoM2, 5  
 Sprunger, P.: SS-WeA11, 41  
 Srivastava, A.: PS+SS-WeM11, 32  
 Staib, P.G.: IS+AS+SS-MoA6, 7  
 Staudt, T.: IS+AS+SS-MoM3, 2  
 Stavale, F.: SS2-WeM10, 36  
 Steele, M.P.: SS+EM-TuA3, 19  
 Stellacci, F.: SS+EM-TuA1, 19  
 Stephens, J.A.: SS1-TuM9, 16; SS-TuA12, 22; SS-  
 TuP14, 28  
 Sterrer, M.: SS2-WeM3, 36  
 Stierle, A.: SS-ThM10, 46  
 Stine, R.: GR+NS+PS+SS-ThM12, 45;  
 GR+NS+PS+SS-ThM5, 44  
 Stroschio, J.A.: VT+MN+NS+SS+AS-TuA1, 22  
 Sun, D.: SS2-MoA4, 10; SS-FrM1, 54  
 Sun, H.: SS-TuP7, 26  
 Sun, X.: TR+AS+SS-ThM3, 47  
 Suter, T.: SS1-WeM12, 35  
 Sutter, P.: SS2-WeM11, 37  
 Suzer, S.: SS+EM-TuA12, 20  
 Suzuki, H.: SS-TuP25, 29  
 Szakal, C.: BI+AS+NS+SS-WeA3, 38  
 Szulcowski, G.J.: SS+EM-TuA10, 20; SS1-  
 WeM11, 35

## — T —

Taborelli, M.: VT+MN+NS+SS+AS-TuA12, 23  
 Taing, J.: SS-ThM9, 46  
 Tait, S.L.: SS2-MoA1, 10; SS2-MoA2, 10; SS2-  
 TuM3, 17; SS-TuP15, 28  
 Tajiri, H.: SS-TuP9, 27  
 Takahasi, M.: SS-TuP9, 27  
 Takaki, Y.: IS-TuP1, 25  
 Takami, Y.: IS-TuP1, 25  
 Takano, I.: SS-TuP24, 28; SS-TuP25, 29; SS-  
 TuP26, 29; SS-TuP27, 29  
 Takekuma, S.: SS1-MoA10, 10  
 Tamanaha, C.R.: GR+NS+PS+SS-ThM12, 45;  
 GR+NS+PS+SS-ThM5, 44  
 Tamura, R.: SS1-MoA10, 10  
 Tang, L.: SS2-MoA11, 11  
 Tao, J.: SS-WeA3, 40  
 Tatsumi, T.: PS+SS-WeM12, 32  
 Tendler, S.J.B.: SS2-TuM5, 17  
 Tenney, S.A.: SS-TuA9, 21; SS-TuP5, 26  
 Terryn, H.: SS1-WeM12, 35  
 Thevuthasan, S.: AC+SS-ThM11, 43; SS-WeA7,  
 40  
 Thiel, P.A.: AC+SS-ThM9, 43; SS1-WeM3, 34  
 Thissen, A.: IS+AS+SS-MoA10, 8  
 Tizazu, G.: BI+AS+NS+SS-WeA9, 39  
 To, N.: SS1-WeM9, 35  
 Trenary, M.: SS-FrM5, 55  
 Trincherro, A.: IS+AS+SS-MoM6, 3  
 Trogler, W.: SS+EM-TuA9, 19  
 Tskipuri, L.: SS+EM-TuA8, 19  
 Tsud, N.: IS+AS+SS-MoM3, 2  
 Turchanin, A.: GR+NS+PS+SS-ThM4, 44; SS2-  
 TuM2, 16  
 Turner, J.J.: SS2-MoM2, 5  
 Turner, K.T.: TR+AS+SS-ThM6, 47  
 Turner, M.W.: SS2-MoA8, 11  
 Tuxen, A.: SS2-WeM2, 35  
 Tysoe, W.T.: TR+AS+SS-ThM9, 47  
 — U —  
 Uhl, A.: SS-FrM5, 55  
 Utz, A.: SS2-MoM10, 6; SS2-MoM8, 6  
 — V —  
 Valente-Feliciano, A.-M.: VT+MN+NS+SS+AS-  
 TuA10, 23  
 Vallier, L.: PS+SS-WeM1, 31  
 Valtiner, M.: SS2-MoA9, 11  
 van Gastel, R.: IS+AS+SS-MoA7, 7  
 vanDorp, W.: SS1-MoA7, 9  
 Varga, K.: ET+EM+SS-MoM11, 2  
 Varga, T.: AC+SS-ThM11, 43  
 Varshney, V.: SE+SS-WeM4, 33  
 Vasco, E.: SS-TuP29, 29  
 Vattuone, L.: SS-ThM5, 45  
 Vayssilov, G.N.: IS+AS+SS-MoM3, 2  
 Veyan, J.F.: IS+AS+SS-MoM10, 3; SS1-TuM4, 15  
 Vlad, A.: SS-ThM10, 46  
 Voevodin, A.A.: SE+SS-WeM4, 33; SE+SS-  
 WeM6, 33; SE+SS-WeM9, 33  
 Vogt, P.: SS-FrM11, 56  
 Vohs, J.M.: SS-ThA4, 49  
 — W —  
 Wagner, M.S.: SS1-MoA9, 9  
 Waite, A.: SE+SS-WeM9, 33  
 Waldeck, D.H.: SS2-TuM11, 18  
 Walker, M.J.: VT+MN+NS+SS+AS-TuA3, 22  
 Wallace, R.M.: IS+AS+SS-MoM10, 3  
 Walle, L.E.: IS+AS+SS-MoM4, 2  
 Walsh, M.A.: TF+EM+SS-ThA9, 51  
 Walter, C.: SE+SS-WeM6, 33  
 Walton, S.G.: GR+NS+PS+SS-ThM12, 45  
 Wandelt, K.R.: SS2-MoA6, 11  
 Wang, B.: GR+NS+PS+SS-ThM6, 44  
 Wang, F.: SS-WeA11, 41

Wang, H.: SS1-WeM5, 34  
 Wang, L.: SS-ThA10, 50  
 Wang, P.: SS+EM-TuA11, 20  
 Wang, W.: SS-WeA7, 40  
 Wang, Y.M.: SS-WeA2, 39  
 Wang, Z.T.: SS-WeA1, 39; SS-WeA10, 41  
 Wei, R.: TR+AS+SS-ThM2, 47  
 Wei, Y.: SS+EM-TuA7, 19  
 Weidner, T.: SS1-MoA9, 9  
 Weinert, M.: TR+AS+SS-ThM9, 47  
 Weiss, S.M.: BI+AS+NS+SS-WeA10, 39  
 Weitering, H.H.: ET+EM+SS-MoM5, 1  
 Whaley, S.D.: SS1-MoA11, 10  
 Wheeler, M.C.: SS1-TuM1, 14  
 Wheeler, V.D.: EM+SS-FrM1, 53  
 White, M.G.: SS2-WeM1, 35; SS-TuP30, 30  
 Wierzbinski, E.: SS2-TuM11, 18  
 Williams, N.: TF+EM+SS-ThA4, 50  
 Wilson, D.P.: SS-TuP30, 30  
 Winter, B.: IS+AS+SS-TuM11, 14; SS1-MoM5, 4  
 Wnuk, J.: SS1-MoA7, 9  
 Wolak, M.A.: SS2-TuM11, 18  
 Wolf, M.: SS2-MoM2, 5  
 Woll, A.R.: IS+AS+SS-TuM12, 14  
 Wöll, C.: SS2-TuM2, 16; SS-WeA2, 39  
 Wong, K.T.: SS1-MoA8, 9  
 Wooten, D.: SS-ThA10, 50  
 Wu, A.T.: VT+MN+NS+SS+AS-TuA7, 22  
 Wu, C.L.: SS+EM-TuA11, 20  
 Wu, I.: SS+EM-TuA11, 20  
 Wu, Z.: SS2-WeM9, 36  
 Wurth, W.: SS2-MoM2, 5  
 Wyrick, J.: SS2-MoA4, 10

## — X —

Xiang, T.: ET+EM+SS-MoM10, 2  
 Xiao, J.: SS+EM-TuA4, 19  
 Xu, B.: SS-TuA8, 21; SS-TuP1, 25  
 Xu, M.C.: SS-WeA2, 39  
 Xu, Q.: IS+AS+SS-MoA8, 8  
 Xu, Y.: SS1-TuM12, 16; SS2-WeM5, 36

## — Y —

Yakshinskiy, B.V.: SS-TuP22, 28  
 Yan, Z.: SS2-WeM5, 36  
 Yang, P.: SS-WeA7, 40  
 Yang, X.F.: SS1-WeM5, 34; SS-TuP4, 26  
 Yao, Y.: SS2-WeM5, 36  
 Yao, Y.X.: SS-ThM6, 46  
 Yin Vallgren, C.: VT+MN+NS+SS+AS-TuA12,  
 23  
 Yitamben, E.: EM+SS-FrM11, 54  
 Yoda, S.: SE+SS-WeM10, 34  
 Yoshimura, M.: SS-TuP11, 27  
 Youn, Y.-S.: IS+AS+SS-TuM10, 14  
 Yuan, H.: SS1-MoM2, 4  
 Yuen, C.: AC+SS-ThM9, 43

## — Z —

Zaera, F.: SS-TuP7, 26  
 Zandvliet, H.: IS+AS+SS-MoA7, 7  
 Zaug, J.M.: AC+SS-ThM5, 42  
 Zhang, X.-G.: ET+EM+SS-MoM10, 2  
 Zhang, Z.: SS+EM-TuA4, 19; SS1-TuM11, 16;  
 SS2-WeM12, 37; SS-WeA11, 41  
 Zhao, M.: SS-ThA4, 49  
 Zharnikov, M.: TF+EM+SS-ThA6, 51  
 Zhdanov, V.P.: BI+AS+NS+SS-WeA4, 38  
 Zheng, Z.: GR+NS+PS+SS-ThM4, 44  
 Zhou, W.: SS2-MoA11, 11  
 Zhou, Z.: SS2-WeM5, 36  
 Zhu, J.F.: IS+AS+SS-MoA8, 8  
 Zhu, W.: PS+SS-WeM6, 32  
 Zoric, I.L.: BI+AS+NS+SS-WeA4, 38  
 Zou, M.: TR+AS+SS-ThM2, 47  
 Zuilhof, H.: TF+EM+SS-ThA1, 50  
 Zulkifli, A.R.: BI+AS+NS+SS-WeA11, 39